Physicochemical Problems
of Mineral Processing

Fizykochemiczne Problemy
Mineralurgii

35

2001

Instructions for preparation of manuscripts
It is recommended that the following guidelines be followed by the authors of the manuscripts:
- Original papers dealing with the principles of mineral processing and papers on technological aspects of mineral processing will be published in the journal which appears once a year.
- The manuscript should be sent to the Editor for reviewing before February 15 each year.
- The manuscript should be written in English. For publishing in other languages on approval of the editor is necessary.
- Contributors whose first language is not the language of the manuscript are urged to have their manuscript competently edited prior to submission.
- The manuscript should not exceed 10 pages.
- Two copies of the manuscript along with an electronic should be submitted for publication before April 15.
- There is a 80 USD fee for printing the paper. No fee is required for the authors participating in the Annual Symposium on Physicochemical Problems on Mineral Processing.
- Manuscripts and all correspondence regarding the symposium and journal should be sent to the editor.

Physicochemical Problems of Mineral Processing 35 (2001)

Z. SADOWSKI
(EDITOR)

WROCŁAW 2001

SPIS TREŚCI

M. NIEWIADOMSKI[*], J. HUPKA[**], J. NALASKOWSKI[*], J. D. MILLER[*]

DISPERSED OIL IMPACT ON FROTH STABILITY IN FLOTATION

Foam stability in flotation has been studied for more than half of the last century, however, the mechanisms responsible for the defoaming action of many presently used reagents are not completely understood. This research presents oil flotation data, which may be used in the evaluation of aqueous methods for oily soil treatment. MIBC (isobutylcarbinol, 4-methyl-2-pentanol) and $C_{12}E_{10}$ (polyoxyethylene 10 lauryl ether) were used as surfactants. Dynamic and static froth stability in the presence of emulsified paraffin oil was determined as a function of the surfactant concentration. The froth stability was examined for the O/W emulsion only and combined with silica particles (-38μm) suspension. The entry, spreading and bridging coefficients were determined to elucidate the mechanism of oil interaction in the froth phase.

Key words: froth control, foam control, oil flotation, polyoxyethylene 10 lauryl ether ($C_{12}E_{10}$), isobutylcarbinol (MIBC)

INTRODUCTION

Froth stability is an important matter, which determines the performance of flotation machines, particularly when an oil dispersion is being separated. This is especially true for the flotation column and the air sparged hydrocyclone. The principles of operation of both units can be found elsewhere (Pondstabodee et al. 1998, Schultz et al. 1991, Luttrell et al. 1991, Falutsu 1994, Miller et al. 1982, Miller and Hupka 1983, Miller and Kinneberg 1985, Miller and Das 1995, 1996). Soil cleaning systems involve both dispersed oil and solid particles. Solid particles can exhibit various degrees of hydrophobicity/hydrophilicity depending on the presence of a stable film and surfactant adsorption. Hydrophobic particles in a mixture with non-polar liquids typically constitute effective defoaming agents (Denkov et al. 1999,

---
[*]Department of Metallurgical Engineering, University of Utah, Salt Lake City, Utah 84112, USA.
[**]Department of Chemical Technology, Technical University of Gdansk, 80-952 Gdansk, Poland.

Denkov 1999). Thus froth control may be a difficult task in oil flotation systems such as are encountered in many soil cleaning applications.

In the present paper, dispersed oil and hydrophobic particles were considered separately and in combination.

FROTH STABILITY FUNDAMENTALS

INFLUENCE OF DISPERSED OIL

Dispersed oil can stabilize or destabilize the froth phase, depending on the relative significance of three interfacial phenomena 1) aqueous film thinning rate during oil droplet entry to the gas phase, 2) oil spreading on the water surface, and 3) thin water film bridging. It has been indicated in the literature that the destabilizing effect was observed only when oil droplets were able to enter the surface of the aqueous phase (Garret 1993, Denkov et al. 1999, Basheva et al. 2000, Bergeron et al. 1997). In order to describe conditions controlling oil droplet entry to the aqueous surface, Harkins (1941) defined the entering (or the rupture) coefficient $E_{o/w}$:

$$E_{o/w} = \gamma_{wg} + \gamma_{ow} - \gamma_{og} \tag{1}$$

where γ corresponds to the surface or interfacial tension, and the subscripts w, g, o pertain to water, gas and oil. Positive values of the entering coefficient mean that oil droplet enters the water/gas interface. For negative values the oil droplet remains in the aqueous phase without contact with the gas phase. The interfacial and surface tensions are not only dependent on the surfactant concentration but also on mutual saturation of all phases. The original entering coefficient accommodates three partial values, the initial $E_{o/w}$, the semi-initial $E'_{o/w}$ and the final or equilibrium $E''_{o/w}$ (Ross 1950). The initial coefficient describes the system, when an oil droplet is newly added to the aqueous solution and both phases are not yet saturated with each other. The semi-initial coefficient defines a system when one of the phases is already saturated and the final coefficient describes a system with all phases saturated.

It turns out that this classical approach does not predict the real behavior of dispersed oil very well. The entering coefficient is calculated considering each of the involved phases separately. It does not take into account surface interaction forces in the system during approach of the oil droplet to the surface of the aqueous solution. In this regard a generalized entering coefficient for an oil droplet in an aqueous environment was discussed (Kruglyakov and Vilkova 1999, Bergeron et al. 1997, Aronson et al. 1994, Bergeron et al. 1993). In the modified equation the oil/gas surface tension is replaced with the tension of the aqueous film, which includes interfacial forces and is regarded as the disjoining pressure, Π:

$$E_{g,o/w} = -\int_{\Pi(h=\infty)=0}^{\Pi(h)} h_w \, d\Pi_{g/w/o} \tag{2}$$

where $E_{g,o/w}$ determines the generalized entry coefficient, Π denotes disjoining pressure and h the film thickness. The integration is performed from disjoining pressure of an infinitely thick film h=∞, for which $\Pi = 0$, to the disjoining pressure of an actual film of thickness h, $\Pi(h)$. The subscripts w and g/w/o mean respectively water film and water film between gas and oil phases.

An oil droplet entering a gas bubble, shown in Fig. 1, is separated by a thin aqueous film, also called a pseudoemulsion film. Measurements of the disjoining pressure are difficult and elaborate, and may be found from the dependence of capillary pressure on the film thickness function. The situation becomes complicated when the pseudoemulsion film is curved. However, when the interfaces are assumed flat the system simplifies, and the capillary pressure, P_c, can be found as a difference between the pressure in the meniscus and in the gas bubble:

$$P_c = P_g - P_w \tag{3}$$

The film reaches equilibrium thickness when the capillary pressure P_c is equal to the disjoining pressure of the film, which ensures that water is not flowing between the meniscus and the pseudoemulsion film. The important aspect is that the capillary pressure can control pseudoemulsion film stability, which is graphically presented in Figure 2. When the capillary pressure is small, as presented in Figure 2a, a thicker film reaches equilibrium. According to terminology proposed by Bergeron (Bergeron 1993) such a film can be called the common film (CF). Further film thinning is prevented by the energy barrier. Increasing the capillary pressure above maximum, as shown in Figure 2b, the thinning phenomenon continues until a new thickness, h_0, behind the energy barrier is reached. This new thickness is on the order of several nanometers, and referred to as the Newton film (NF) (Bergeron 1993). The generalized entering coefficient is represented by the shaded area. In Figure 2a the shaded area corresponds to positive pressure values, therefore yields negative E_g (in equation 2). At an elevated capillary pressure, see Figure 2b, the overall entering coefficient depends on the ratio of areas A to the area B. When B exceeds the sum of A areas, the entering coefficient is positive.
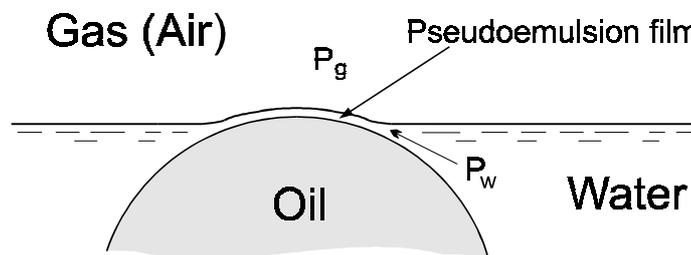
Fig. 1. Oil/water/gas system, oil droplet entering aqueous solution surface, modified from (Bergeron et al. 1993)

Besides the capillary pressure, the kinetic energy - when able to overcome the energy barrier - is another determining factor for the film thickness. The kinetic energy level allows for the entering or non-entering behavior of oil droplets to be understood, but still there are other phenomena, which must be answered. One of the recent research directions has been the study film thinning. Stratified foam film thinning was observed very early in the beginning of the 20th century. Nikolov and Wasan (1989) investigated this phenomenon using an anionic surfactant as the foaming agent. They found that micelles had an ordered structure in the thinning film. The stratification in the thinning process corresponded very well to the Debye atmosphere diameters of the micelles. The ionic strength of the solution could influence the stratification thickness by decreasing the Debye atmosphere and by lowering the electrostatic repulsion. Ordered surfactant micelles hinder film drainage. Bergeron and Radke (1992) measured the disjoining pressure isotherm for a single, isolated foam film. They found oscillations for films 50 nm thick. Step-wise thinning creates an additional energy barrier to the oil drop entry.
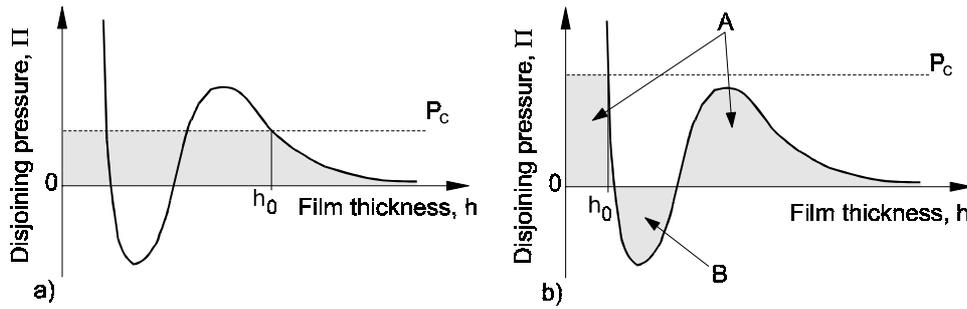
Figure 2. Disjoining and capillary pressures. a) equilibrium film thickness at common black film b) equilibrium film thickness at Newton black film

Similarly to the entry coefficient, the classical spreading coefficient $S_{o/w}$ was defined (Harkins 1941, Ross 1950):

$$S_{o/w} = \gamma_{wg} - \gamma_{ow} - \gamma_{og} \qquad (4)$$

The initial, semi-initial and final coefficients were also proposed.

Including the disjoining pressure into the definition, a generalized spreading coefficient $S_{g,o/w}$ was obtained (Kruglyakow et al. 1999, Bergeron et al. 1997, Jha et al. 2000):

$$S_{g,o/w} = \int_{\Pi(h=\infty)=0}^{\Pi(h)} h_{oil} d\Pi_{g/o/w} \qquad (5)$$

where Π determines the disjoining pressure, h - the film thickness, and subscripts g/o/w mean oil films between the gas and water phases, respectively. The integral in equation (5) is very similar to that describing the generalized entry coefficient in equation (2) but the water film is replaced by the oil film. As entry of an oil droplet is crucial for foam destabilization, spreading of oil was reported as an unnecessary phenomenon (Garret 1993, Denkov et al. 1999, Jha 2000). Mechanisms of foam destruction either include or do not include oil spreading.

Bridging of aqueous foam films by oil was investigated theoretically by Garret (Garret 1980). Assuming that the liquid bridge obeys the Neumann's triangle rule of three phase contact, and that the thin water film is planar, he determined conditions for an oil bridge stability. Figure 3 presents two states for oil bridges. As indicated by Garret, a mathematical proof exists that bridges for which the oil-water contact angle $\Theta_{ow} \leq \pi/2$ cannot be stable. For the contact angle $\Theta_{ow} > \pi/2$, a stable bridge can exist with equilibrium film thickness h_{eq}. On the basis of these findings, the bridging coefficient (B) was defined (Garret 1980, Aveyard et al. 1993, Bonfillon-Collin and Langevin 1997, Denkov 1999):

$$B = \gamma_{wg}^2 + \gamma_{ow}^2 - \gamma_{og}^2 \qquad (6)$$

Positive and zero values of B mean an unstable film, while negative values of B allow for an equilibrium film thickness, h_{eq} at which the film is mechanically stable. The system presented in Figure 3 refers to a planar water film. Other shapes were investigated in detail by Denkov (1999). He found that in some cases small droplets can yield a stable bridge even if the bridging coefficient is positive. This observation was explained by the existence of the so-called perturbed zone of the water film in the vicinity of an oil bridge. Minimal water flow from the vicinity of the bridge, which could be practically neglected, still yields stable bridge for positive B. Large oil droplet bridges were found to be always unstable for positive B.
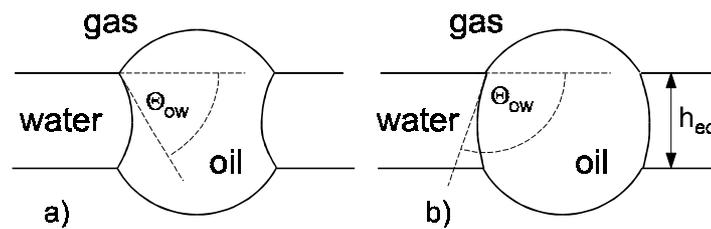
Figure 3. Oil bridging. a) unstable bridge, $\Theta_{ow} \leq \pi/2$, b) stable bridge, $\Theta_{ow} > \pi/2$, adopted from (Denkov 1999)

Three main mechanisms of foam film collapse due to the dispersed oil presence were proposed (Basheva et al. 2000, Denkov et al. 1999, Aveyard et al. 1994),see Figure 4. All of them require oil droplet entry. In spreading - fluid entrainment oil

causes Marangoni-driven flow of liquid in the foam film (fluid entrainment), which results in local film thinning and rupture. The other two mechanisms require formation of an oil bridge between the gas phases. Lack of oil wetting by water in the first case or stretching of the oil film in the latter case leads to the rupture.
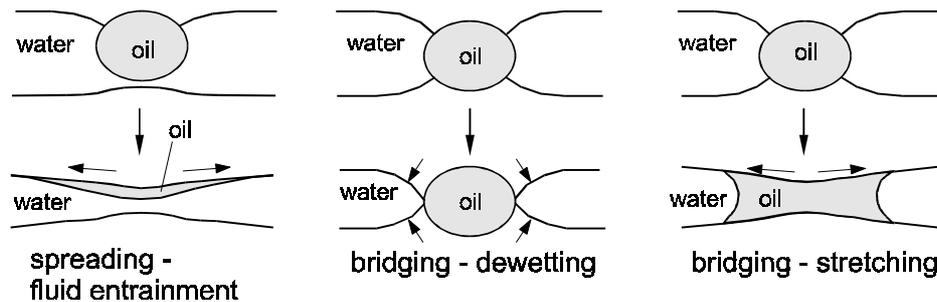
Figure 4. Three possible mechanisms of foam film destruction by an oil droplet, adopted from (Denkov et al. 1999)

Regarding the initiation of breakage of the foam film, the most probable hypothesis states that Gibbs-Plateau borders play a role. The Gibbs-Plateau borders are aqueous solution regions where three or four thin films meet. As indicated by Schramm and Novosad, emulsified oil cannot flow through foam lamellae when the droplet diameter is too large (Schramm and Novosad 1990). Koczo et al. observed that foam collapse occurs in the Gibbs-Plateau borders (Koczo et al 1994). The hydrophobic particles resided in lamellae 1 - 2 seconds to return to the Gibbs-Plateau borders immediately afterwards. It can be expected, based on observations of Shramm and Novosad, that oil droplets behave in the same way. According to Koczo, thin foam films forced oil droplets to move from lamellae to the Plateau borders, where they were able to bridge the aqueous films. Foam can collapse in the dynamic conditions for sufficiently thick lamellae allowing oil droplet holdup and entry. The Plateau-border mechanism was confirmed by an investigation of the antifoam effective droplet size. Bergeron et al. had shown that oil droplets smaller than 6 μm were not able to destabilize the froth regardless the solution chemistry. This size is relatively large and suggests that these oil droplets were hidden in the Plateau-borders, where they were not able to bridge the foam films (Bergeron et al. 1997).

There are also reports of foam stabilization by the dispersed oil (Koczo et al. 1992, 1994). This phenomenon was found for the non-entering oil droplets when the emulsion accumulated in Plateau-borders and inhibited foam drainage.

HYDROPHOBIC PARTICLES

Dippenaar (1982) investigated the mechanism of froth destabilization by fine solids. Hydrophobic particles destabilized the aqueous film when its thickness was smaller than the particle diameter. Single hydrophobic particles ruptured the film, while with multiple particles the film was stabilized. Johansson and Pugh (1992) found that the froth stability was uneffected by hydrophilic particles (contact angles less than 40°). When the hydrophobicity increased (contact angle 65°), froth stability reached a maximum and then decreased for particles with contact angle more than 80°.

The bridging-dewetting mechanism is responsible for the film rupture here (Garret 1993, Aveyard et al. 1994, Frye and Berg 1989, Aronson 1986). Another mechanism was also indicated by Garret (1993). He proposed that the solid particle can cause film thinning by the Marangoni effect when it is in contact with one air/water surface. Solid particles are regarded as better defoamers than dispersed liquids, which is believed to be related to roughness.

SYNERGISM OF OIL AND HYDROPHOBIC PARTICLES

A synergistic effect of hydrophobic particles and non-polar oils was discovered and patented in early 1950s. A list of twenty six patents was given by Garret (Garret 1993). However, studies on the controlling mechanisms were reported twenty years later (Povich 1975, Kulkarni et al. 1977). Particle size of effective liquid-solid defoamers range from 1 nm to 1 µm, and the particle concentration from 1 % to 30 % by weight. The pseudoemulsion film rupture and enhancement of the oil droplet entry is today the accepted antifoaming mechanism (Aveyard et al. 1993, 1994, Koczo et al. 1994, Frye and Berg 1989). Active are hydrophobic solid particles protruding from the oil droplets, and facilitating the pseudoemulsion film rupture.
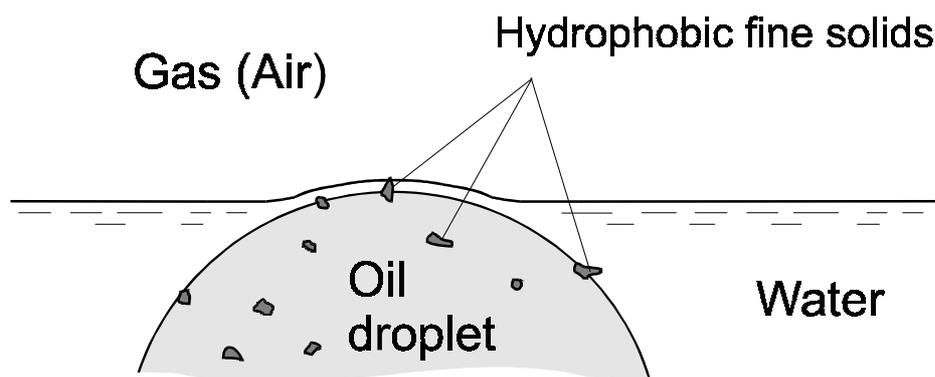
Figure 5. The pin-effect of fine protruding hydrophobic particles

EXPERIMENTAL PROCEDURE

MATERIALS

Two surface active compounds from Sigma and Aldrich were used, Polyoxyethylene 10 lauryl ether ($C_{12}E_{10}$), and 4-methyl-2-pentanol (isobutylcarbinol, MIBC), 99% purity. $C_{12}E_{10}$ is known as a good detergent, exhibiting strong foaming action (Porter, 1991), which can be effective in oily soil clean-up. Paraffin white, light oil was obtained from Mallinckrodt. Experiments with solid particles were performed using fine (minus 38 μm) silica sand from US Silica. In all experiments deionized water was used.

TECHNIQUES

The froth stability was evaluated using 60 cm long and 3 cm diameter glass tube with a porous glass frit (medium size) at the bottom. Oil-in-water emulsion was prepared using a homogenizer. The dispersion stability was evaluated based on determination of coalescence in a cylinder at 1 cm height from the bottom. The estimated rate of oil content decrease ranged from 8.5×10^{-3} s^{-1} at $C_{12}E_{10}$ concentration of 1×10^{-5} M to 1×10^{-4} s^{-1} at a $C_{12}E_{10}$ concentration 5×10^{-4} M. Oil droplet size distribution indicated presence of both numerous oil droplets below 1 μm in diameter and droplets as large as 20 to 60 μm depending on the $C_{12}E_{10}$ or MIBC concentration. 40 cm^3 of surfactant solution were poured into the tube and simultaneously air was blown at a rate of 0.54 dm^3/min. Considering the very stable froth created from $C_{12}E_{10}$ solutions, the dynamic froth stability was evaluated from the ratio of the froth volume to the air volume introduced to the tube:

$$\text{Dynamic Froth Stability} = \frac{\text{Volume of froth created in a unit time}}{\text{Volume of air introduced in a unit time}} \cdot 100\% \quad (7)$$

Static froth stability was evaluated as the collapse rate of the froth given in centimeters per second. The dynamic surface and interfacial tension measurements were performed by the pendant bubble method using a Rame-Hart goniometer.

RESULTS AND DISCUSSION

The dynamic froth stability and the collapse rate of $C_{12}E_{10}$ aqueous solutions without oil and with 1% by weight of paraffin oil-in-water emulsion are presented in Figure 6. Almost no froth was generated below 1×10^{-5} M concentration, in the dynamic conditions. The froth reached 100 % dynamic stability at concentration 5×10^{-5} M, and the collapse rate dropped significantly to 0.017 cm/s. Both very high dynamic stability and very low collapse rate were observed for the same

concentration. The dispersed oil shifted the dynamic stability 100 % point beyond 1×10^{-4} M. The collapse rate turned out to be relatively high even at this concentration, and was equal to 0.33 cm/s. A low collapse rate of 0.025 cm/s was observed at 5×10^{-4} M. It is evident that in the presence of paraffin oil there is a 1×10^{-4} to 5×10^{-4} M concentration range which yields a stable dynamic froth but still a weak static froth.

The presented froth stabilities can be related to the classical entry, spreading and bridging coefficients, see data in Figure 7, which were calculated for 30 seconds contact and equilibrated system. The dynamic surface and interfacial tension measurements indicate that surfactant adsorption attained equilibrium only after 10 minutes, see Figure 8. Therefore the flotation system did not reach chemical equilibrium. Hence a 30 seconds time of contact was arbitrarily chosen to represent the interfacial conditions during the dynamic stability tests. The difference between coefficient values for 30 seconds and for an equilibrated system results from the progressive adsorption of surfactant at the interfaces. The entry coefficient after 30 seconds is much larger than for an equilibrated system, therefore it has a positive value, and according to the theory, represents non-entering oil droplets.
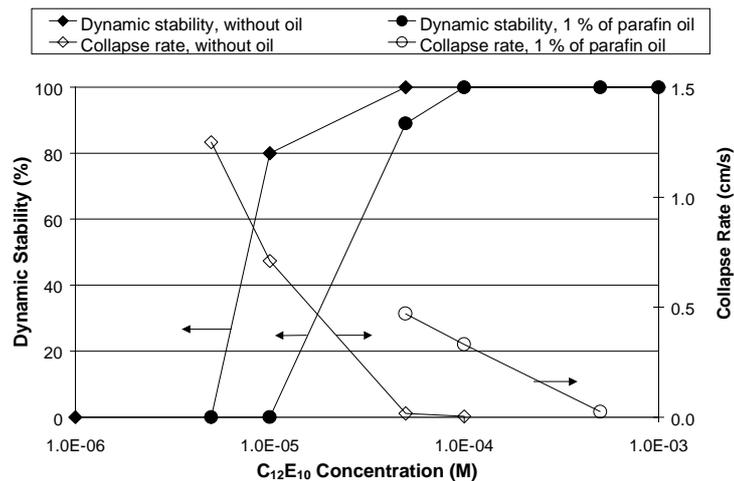
Figure 6. Dynamic froth stability and collapse rate for $C_{12}E_{10}$ aqueous solutions

Nevertheless, a defoaming action of the oil was observed. It can be concluded that the effective entry coefficient is in fact smaller due to the disjoining pressure, which was not taken into account in the above calculations. Most probably at 1×10^{-4} M the effective entry coefficient is already negative, therefore very stable (dynamically) froth is observed, as shown in Figure 6. The classical spreading coefficient reaches values close to zero beginning at concentrations 5×10^{-5} M in the case of an equilibrated system and 1×10^{-4} M in the case of the system after 30 seconds contact time. Nevertheless the role of spreading is not clear. Negative values for concentrations lower than 5×10^{-5} M may indicate that it is not a satisfactory condition

for froth destabilization. Similarly, as in the case of the entry coefficient, the intermolecular forces are not considered in the classical approach and calculated small negative values of the spreading coefficient can be in fact positive.

The bridging coefficient is positive over the entire range of concentrations investigated, which indicates unstable bridges. Paraffin oil caused a decrease in the dynamic stability for the concentration range from 5×10^{-6} to 1×10^{-4} M. Relatively large positive values of the entry and bridging coefficients suggest that formation of unstable bridges (bridging-dewetting or bridging-stretching) is the most probable mechanism of froth colapse and spreading appears to play a minor role. Low static stability in the concentration range from 5×10^{-5} to 5×10^{-4} M can be explained by both mechanisms, bridging-dewetting and spreading-fluid entrainment, since the spreading coefficient approaches zero in this concentration range.
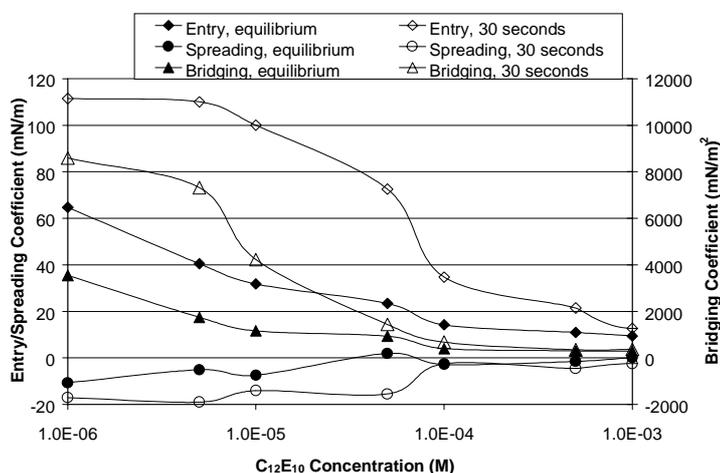
Figure 7. Entry, spreading and bridging coefficients of the system: $C_{12}E_{10}$ aqueous solution and dispersed paraffin oil

The difference between dynamic and static stabilities in the presence of paraffin oil is unclear. According to Manlowe and Radke (1990) froth can be metastable under some dynamic conditions. They explained such a behavior by short contact times between the gas and oil phases under dynamic conditions. It can be assumed that dynamic conditions inhibit foam destabilization. This supposition, however, requires further investigation.

The dynamic froth stability and the collapse rate of MIBC aqueous solutions without oil and with 1% of paraffin oil are presented in Figure 9. The dynamic stability of MIBC shows that the impact of paraffin oil is similar to that of $C_{12}E_{10}$. An order of magnitude greater frother concentration was required for achieving 100% dynamic froth stability. However, the static stability was practically not influenced by the presence of oil.

The influence of fine solid particles (- 38 μm) is presented in Table 1. Silica particles were added as hydrophilic particles and as hydrophobilized by exposure to oil for 24 hours prior to the experiment. The dynamic stability in 1×10^{-4} M $C_{12}E_{10}$ solution was not affected. The collapse rate, however, increased when oil exposed silica particles (24 hours) were used, the static froth stability turned out to be much lower, and the collapse rate increased from 0.33 to 0.44 cm/min.
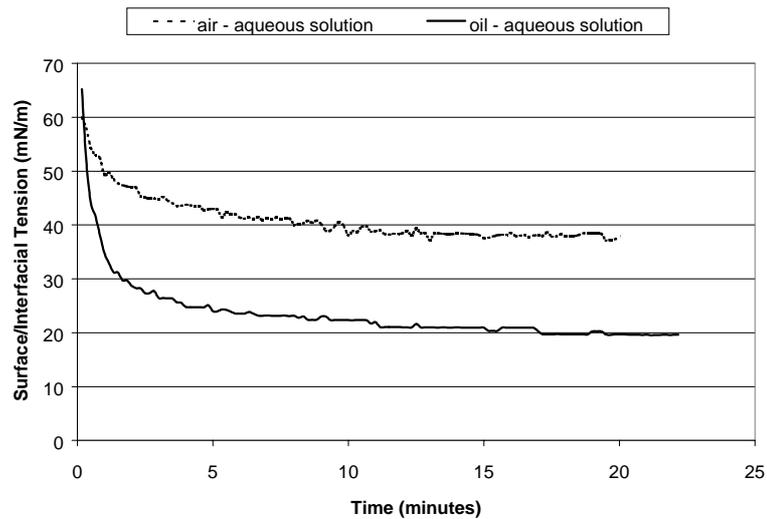
Figure 8. Surface/interface tension of 1×10^{-5} M $C_{12}E_{10}$ as a function of time
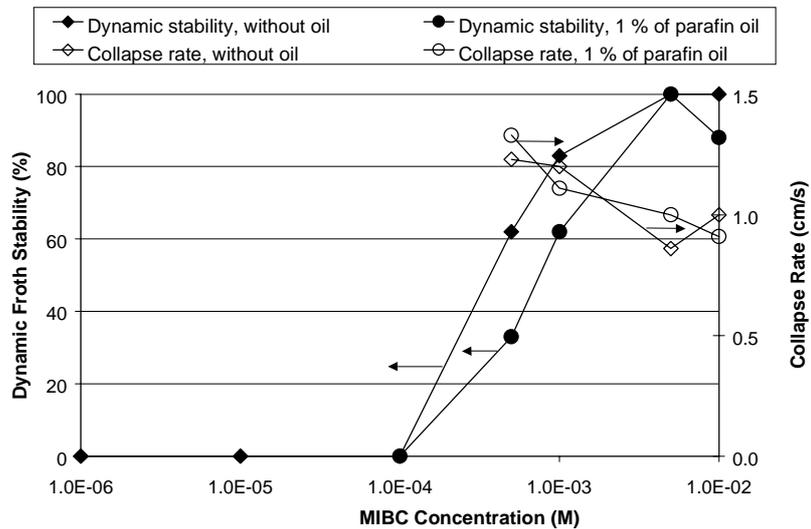
Figure 9. Dynamic stability and collapse rate of MIBC aqueous solutions

Table 1. The influence of solid particles on the froth stability. 1×10^{-4} M $C_{12}E_{10}$ aqueous solution containing 1 % by weight of emulsified oil

Presence of Solid Particles	Dynamic Stability (%)	Collapse Rate (cm/sec.)
None	100	0.33
Hydrophilic silica, 1 wt. %	100	0.32
Silica particles wetted by oil for 24 hours prior to the experiment	100	0.44

CONCLUSIONS

1. The frothing ability of aqueous solutions of polyoxyethylene 10 lauryl ether ($C_{12}E_{10}$) was determined. Experimental results indicated excellent frothing properties of this compound.
2. The presence of paraffin oil deteriorated the froth dynamic stability for $C_{12}E_{10}$ only slightly. For 1 wt. % oil in the concentration range of $C_{12}E_{10}$ from 1×10^{-5} to 5×10^{-4} M it was possible to obtain a dynamically stable froth, which simultaneously had low static stability. It appears that dynamic conditions inhibit defoaming action.
3. The equilibrium interfacial and surface tensions were achieved after 10 minutes, while the dynamic froth stability was evaluated during the initial 30 seconds. Therefore a non-equilibrated system was considered for calculation of the oil-controlled foam stability coefficients.
4. The entry, spreading and bridging coefficients calculated based on classical assumptions did not correlate with the experiments, which is confirmed by previous reports in the literature.
5. Comparison of the dynamic and static froth stability obtained with $C_{12}E_{10}$ and MIBC showed that ethoxylated compound provided for better froth stability at lower concentrations.
6. Hydrophobic silica particles, conditioned for 24 hours in paraffin oil decreased the static froth stability to some extent without deterioration the dynamic stability.
7. The froth behavior results are usefull in the analysis of flotation, particularly air-sparged hydrocyclone flotation, because a stable dynamic froth is essential for high recovery. On the other hand an unstable static froth facilitates natural transport after the separation process. Small soil particles which are expected to be entrained in the flotation concentrate during oil flotation from soil should not influence the dynamic stability and may help destabilize the froth after flotation.

LIST OF SYMBOLS

B	-	Bridging coefficient
$E_{g,o/w}$	-	Entry coefficient, generalized, for an oil droplet entering an aqueous solution surface
$E_{o/w}$	-	Entry coefficient, classical, for an oil droplet entering an aqueous solution surface
h	-	Film thickness
h_0	-	Equilibrium film thickness under the condition of the capillary pressure equal to the disjoining pressure
h_{eq}	-	Equilibrium film thickness of an oil bridged aqueous film
h_{oil}	-	Oil film thickness
h_w	-	Water film thickness
P_c	-	Capillary pressure
P_g	-	Gas pressure
P_w	-	Water or aqueous phase pressure
$S_{g,o/w}$	-	Spreading coefficient, generalized, for an oil phase spreading on an aqueous phase
$S_{o/w}$	-	Spreading coefficient, classical, for the oil phase spreading on an aqueous phase
γ_{og}	-	Interfacial tension, oil - gas
γ_{ow}	-	Interfacial tension, oil - aqueous solution
γ_{wg}	-	Surface tension of an aqueous solution
Π	-	Disjoining pressure
$\Pi_{g/o/w}$	-	Disjoining pressure of a gas/oil/water film
$\Pi_{g/w/o}$	-	Disjoining pressure of a gas/water/oil film
$\Pi(h)$	-	Disjoining pressure of a film of thickness h
$\Pi(h=\infty)=0$	-	Disjoining pressure of an infinitely thick film, which is essentially zero
$\Theta_{o/w}$	-	Contact angle of an oil droplet on water

REFERENCES

ARONSON M.P., 1986, *Influence of Hydrophobic Particles on the Foaming of Aqueous Surfactant Solutions,* Langmuir, 2, 653-659.

ARONSON A.S., BERGERON V., FAGAN M.E., RADKE C. J., 1994*, The influence of disjoining pressure on foam stability and flow in porous media,* Colloids and Surfaces A, 83, 109-120.

AVEYARD R., COOPER P., FLETCHER P.D.I., RUTHERFORD C. E., 1993*, Foam Breakdown by Hydrophobic Particles and Nonpolar Oil,* Langmuir, 9, 604-613.

AVEYARD R., BINKS B. P., FLETCHER P.D.I., PECK T. G., RUTHERFORD C. E., 1994, *Aspects of Aqueous Foam Stability in the Presence of Hydrocarbon Oils and Solid Particles,* Advances in Colloid and Interface Science, 48, 93-120.

BASHEVA S.E, GANCHEV D., DENKOV N.D., KASUGA K., SATOH N., TSUJII K., 2000, *Role of Betaine as Foam Booster in the Presence of Silicone Oil,* Langmuir, 16, 1000-1013.

BERGERON V., RADKE C. J., 1992, *Equilibrium measurements of oscillatory disjoining pressure in aqueous foam films,* Langmuir, 8, 3020-3026.

BERGERON V., FAGAN M. E., RADKE C. J., 1993, *Generalized Entering Coefficients: A Criterion for Foam Stability against Oil in Porous Media,* Langmuir, 9, 1704-1713.

BERGERON V., COOPER P., FISHER C., GIERMANSKA-KAHN J., LANGEVIN D., POUCHELON A., 1997, *Polydimethylsiloxane (PDMS)-based antifoams,* Colloids and Surfaces A: 122, 103-120.

BONFILLON-COLIN A., LANGEVIN D., 1997*, Why Do Ethoxylated Nonionic Surfactants Not Foam at High Temperature?,* Langmuir, 13, no. 4, letters, 599-601.

DENKOV N.D., COPER P., MARTIN J-Y., 1999, *Mechanism of action of Mixed Solid-Liquid Antifoams. 1. Dynamics of Foam Film Rupture,* Langmuir, 15, 8514-8529.

DENKOV N.D., 1999, *Mechanism of Action of Mixed Solid-Liquid Antifoams. 2. Stability of Oil Bridges in Foam Films,* Langmuir, 15, 8530-8542.

DIPPENAAR A., 1982, *The destabilization of froth by solids. I. The Mechanism of film rupture,* International Journal of Mineral Processing, v. 9, 1-14.

DIPPENAAR A., 1982, *The destabilization of froth by solids. II. The Rate Determining Step,* International Journal of Mineral Processing, 9, 15-22.

FALUTSU M., 1994, *Column Flotation Froth Characteristics - Stability of the Bubble-particle System,* International Journal of Mineral Processing, 40, 225-243.

FRYE G.C., BERG J.C., 1989, *Antifoam Action by Solid Particles,* Journal of Colloid and Interface Science, vol. 127, (1), 222-238.

GARRETT P. R., 1980, *Preliminary Considerations Concerning the Stability of a Liquid Heterogeneity in a Plane-Parallel Liquid Film,* Journal of colloid and interface science, 76, (2), 587-590.

GARRET P. R., Ed., 1993, *Defoaming, Theory and Applications,* Marcel Dekker, Inc., New York, pp. 13,

HARKINS, W. D., 1941, *A general Thermodynamic Theory of the spreading of liquids to form duplex films and of liquids or solids for form monolayers.* J. Chem. Phys., 9 ,552-568.

JHA B.K., CHRISTIANO S. P., SHAH D.O., 2000, *Silicone Antifoam Performance: Correlation with Spreading and Surfactant Monolayer Packing,* Langmuir, 16, (26), 9947-9954.

JOHANNSON G., PUGH R. J., 1992, *The influence of particle size and hydrophobicity on the stability of mineralized froths,* International Journal of Mineral Processing, 34, 1-21.

KOCZO K., LOBO L. A., WASAN T., *Effect of oil on Foam Stability: Aqueous Foams Stabilized by Emulsions,* Journal of Colloid and Interface Science, 150, (2), 1992, 492-506.

KOCZO K., KOCZONE J.K., WASAN D. T., 1994, *Mechanisms for Antifoaming Action in Aqueous Systems by Hydrophobic Particles and Insoluble Liquids,* Journal of Colloids and Interface Science, 166, 225-238.

KRUGLYAKOV P. M., VILKOVA N. G., 1999, *The relation between stability of asymmetric films of the liquid/liquid/gas type, spreading coefficient and surface pressure,* Colloids and surfaces A, 156 () 475-487.

KULKARNI R. D., GODDARD E. D., KANNER B., Ind. Eng. Chem., Fundam, 16(4): 472, 1977

LUTTRELL G. H., TAO D. P., YOON R. H., 1991, *Effects of froth behavior on the column flotation of fine coal,* Preprints of SME 91-152.

MANLOWE D. J., RADKE C. J., 1992, *Pore-level investigation of foam/oil interactions in porous media,* SPE Reservoir Engineering, 5, (4), 495-502.

MILLER J. D., KINNEBERG D. J., VAN CAMP M. C., 1982, *Principles of Swirl Flotation in a Centrifugal Field with an Air-Sparged Hydrocyclone,* Preprint - Society of Mining Engineers of AIME, SME-AIME Annual Meeting, Dallas, TX, USA. Prepr. n. 82-167.

MILLER J. D., HUPKA J., 1983, *Water De-oiling in an Air-Sparged Hydrocyclone,* Filtration and Separation, v. 20 (4), 279-282.

MILLER J. D., KINNEBERG D. J., 1985, *Fast Flotation with an Air-Sparged Hydrocyclone,* Proceedings of MINTEK 50: International Conference on Mineral Science and Technology, v. 1, 373-383.

MILLER J. D., DAS A., 1995, *Flow Phenomena and its Impact on Air-Sparged Hydrocyclone Flotation of Quartz,* Minerals and Metallurgical Processing, February, 51-63.

MILLER J. D., DAS A., 1996, *Swirl Flow Characteristics and Froth Phase Features in Air-Sparged Hydrocyclone Flotation as Revealed by X-ray CT Analysis.* International Journal of Mineral Processing, 47, 251-274.

NIKOLOV A. D., WASAN D. T., 1989, (a) *Ordered Micelle Structuring in Thin Films Formed from Anionic Surfactant Solutions. I. Experimental,* Journal of colloid and interface science, 133, (1), 1-12.

NIKOLOV A. D., WASAN D. T., 1989, (b) *Ordered Micelle Structuring in Thin Films Formed from Anionic Surfactant Solutions. II. Model Development,* Journal of colloid and interface science, 133, (1), 13-22.

PONDSTABODEE S., SCAMEHORN J. F., CHAVEDEJ S., HARWELL J. H., 1998, *Cleanup of Oily Wastewater by Froth Flotation: Effect of Microemulsion Formation,* Separation Science and Technology, 33, (4), 591-609.

PORTER M.R., 1991, Handbook of Surfactants, Blackie & Son Ltd., Glasgow, 130-134.

POVICH M. J., A. I. Ch. E. J. 21(5): 1016, 1975.

ROSS S., 1950, *Inhibition of foaming. II A Mechanism for the Rupture of Liquid Films by Antifoaming Agents,* J. Pchys., Colloid Chem., 54, 429-436

SCHRAMM L.L., NOVOSAD J.J., *Micro-Visualization of Foam Interactions with a Crude Oil,* Colloids and Surfaces, 46, 1990, 21-43.

SCHULTZ, C. W., MEHTA R. K., BATES, J. B., 1991, *The Flotation Column as a Froth Separator,* Mining Engineering, 43, (12), 1449-1451.

YARAR B., SPOTTISWOOD D. J., Ed., 1981, Franklin Pierce College, Ridge, New Hampshire, August 2-7, 287-301.

Niewiadomski M., Hupka J., Nalaskowski J., Miller J. D., *Wpływ emulsji olejowej na stabilność piany podczas flotacji,* Fizykochemiczne Problemy Mineralurgii, 35, 2001, 5-19 (w języku angielskim).

Stabilność piany była badana od pierwszej połowy zeszłego wieku, jednak mechanism jej destabilizacji przez środki przeciwpianowe nie został dotychczas całkowicie poznany. W przedstawionej publikacji określono stabilność piany wodnych roztworów surfaktantów w obecności emulsji oleju parafinowego, jako modelowego układu spotykanego podczas oczyszczania zaolejonej ziemi przez flotację pianową. Zastosowano dwa powierzchniowo czynne związki: $C_{12}E_{10}$ oraz MIBC. Określono również wpływ obecnosci piasku o wielkości ziaren poniżej 38 μm.

Pierwszy zastosowany związek, $C_{12}E_{10}$ wykazał znacznie silniejsze działanie pianotwórcze niż MIBC. Powstawanie stabilnej piany zaobserwowano przy stężeniach powyżej 5×10^{-6} mol/dm^3, przy czym 100 % stabilności piany otrzymano powyżej stężenia 5×10^{-5} mol/dm^3. Obecność emulsji olejowej spowodowała, że porównywalną stabilność dynamiczną obserwowano przy stężeniach kilkakrotnie większych. MIBC pozwalił na osiągnięcie stabilnej piany przy stężeniach powyżej 1×10^{-4} mol/dm^3, przy czym 100 % stabilności piany otrzymano dla stężenia MIBC 5×10^{-3} mol/dm^3 jedynie w początkowym etapie jej tworzenia. Po początkowych kilku sekundach od rozpoczęcia doświadczenia szybkość gaśnięcia piany zwiekszła się i dorównywała szybkości tworzenia, co prowadziło do osiągnięcia równowagowej wysokości piany w warunkach dynamicznych. Obecność oleju parafinowego podobnie jak w prypadku $C_{12}E_{10}$ spowodowała, że kilkakrotnie większe steżenia surfaktanta były wymagane do osiągnięcia podobnych stabilności dynamicznych.

Stabilność statyczna piany przy zastosowaniu $C_{12}E_{10}$ korelowała ze stabilnością dynamiczną w układzie bez emulsji olejowej. Przy zastosowaniu oleju parafinowego zaobserwowano brak korelacji pomiędzy dynamiczną i statyczną stabilnością w zakresie stężeń od 1×10^{-4} mol/dm^3 do 5×10^{-4} mol/dm^3. Stabilność statyczna roztworów MIBC była bardzo niska w całym badanym zakresie stężeń.

Hydrofilowe ziarna krzemionki w roztworrze $C_{12}E_{10}$ o stężeniu 1×10^{-4} mol/dm^3 nie wykazały wyraźnego wpływu na stabilność piany, w przeciwieństwie do ziaren krzemionki hydrofobizowanej przez zaadsorbowanie oleju parafinowego, które znacząco obniżyły statyczną stabilność piany. Stabilność dynamiczna, która wynosiła 100 %, pozostała nie zmieniona.

Małgorzata ULEWICZ[**], Władysław WALKOWIAK[**], Cezary KOZŁOWSKI[***]

SELECTIVE FLOTATION OF ZINC(II) AND CADMIUM(II) IONS FROM DILUTE AQUEOUS SOLUTIONS IN THE PRESENCES OF HALIDES

An experimental investigation is presented of the batch ion flotation of zinc(II) and cadmium(II) ions from dilute aqueous solutions with sodium dodecylbenzenesulfonate (DBSNa) as an anionic surfactant and cetylpyridinium chloride (CPCl) as a cationic surfactant. The effect of halides, i.e. fluorides, chlorides, bromides, and iodides, on the selectivity of cadmium(II) over zinc(II) is established. Separation of Cd(II) and Zn(II) ions by DBSNa is not occurred. The separation of Cd(II)/Zn(II) by CPCl in presence of halides at concentration range of 0.001 M to 1.0 M increases in sequence: $F^- < Cl^- < Br^- < I^-$.

INTRODUCTION

Zinc and cadmium are removed from dilute aqueous solutions with different methods such as solvent extraction, ionic exchange, ion flotation, sorption or liquid membranes. Among these methods, ion flotation has special position for the removal of ions from very dilute solutions, i.e. at the concentration below $1.0 \cdot 10^{-4}$M. Ion flotation involves the removal of surface inactive ions from aqueous solutions by the introduction of a surfactant and the subsequent passage of gas bubble through the solution.

The ion flotation selectivity for inorganic cations has been presented in several papers. Jurkiewicz (1984-85) investigated foam separation of Cd(II) ions by lauryl sulfate and sodium dodecanoate from aqueous solutions. The presence of electrolyte in the solutions has a negative influence on Cd^{2+} foam separation. Also, Jurkiewicz (1985) investigated separation of thiocyanate and iodide complexes of cadmium(II) in

---

   * Department of Chemistry, Technical University of Częstochowa,
     42-200 Częstochowa, Armii Krajowej 19 Street, e-mail: ulewicz@mim.pcz.czest.pl
  ** Institute of Inorganic Chemistry and Metallurgy of Rare Elements, Wrocław University of Technology,
     50-370 Wrocław, Wybrzeże Wyspiańskiego 27 Street, e-mail: Walkowiak@ichn.ch.pwr.wroc.pl
*** Institute of Chemistry and Environment Protection Pedagogical University of Czestochowa,
     Armii Krajowej 13, 42-201 Czestochowa.

acidic aqueous solutions using cetylotrimethylamonium bromide (CTMABr). In the presence of acids, the zinc thiocyanate complex removal increases in following sequence: $HClO_4 < HI < HNO_3 < H_2SO_4 < H_3PO_4 < CH_3COOH$. The influence of chloride, bromide, iodide and thiocyanate ions on the separation of zinc(II) and cadmium(II) ions with CTMABr Jurkiewicz (1990) also conducted. For anionic surfactants (sodium dodecylbenzenesulfonate and sodium dodecylsulfonate) Walkowiak (1991) found the following cations foam separation selectivity sequences toward: $Mn^{2+} < Zn^{2+} < Co^{2+} < Fe^{3+} < Cr^{3+}$, and $Ag^+ < Cd^{2+} < In^{3+}$. For the flotation of cations where no sublate was formed in the bulk solution, the good correlation between selectivity sequences of studied metal ions with anionic surfactant and the ionic potentials of those cations was found. The selective flotation of zinc(II), cadmium(II), mercury(II) and gold(III) ions using of cetyltrimethylamonium chloride in presence of chlorides and cyanides was also investigated by Walkowiak et al. (1976, 1979, 1992). The selectivity order of foam fractionation was as follows: $Au(CN)_4^- > Hg(CN)_4^{2-} > Cd(CN)_4^{2-} > Zn(CN)_4^{2-}$ (Walkowiak and Grieves 1976). The effect of inorganic ligands, i.e. thiosulfates, thiocyanates, and cyanides on the selectivity of ion flotation of Zn(II) and Ag(I) was investigated by Charewicz et al. (1999). The affinity of cyanide complexes to cetylpyridinium chloride follows the order: $[Ag(CN)_2]^- < [Zn(CN)_4]^{2-} + [Zn(CN)_3]^-$. The influence of zinc and cadmium ion concentrations on the effectiveness of flotation removal with potassium oleate was studied by Sinkova (1998). Zinc(II) and cadmium(II) ions are removed effectively from aqueous solution using this collector. Also, Scorcelli et al. (1999) was studied the removal of cadmium(II) using sodium dodecylsulfate as a collector. The best removal (99 %) was obtained for a metal cations to collector ratio equal to 1:3. Preliminary research of cadmium(II) over zinc(II) ions separation by cetyltrimethylamonium chloride was conducted by Kozłowski et al. (2000).

This paper concerns the selective removal of zinc(II) and cadmium(II) ions from dilute aqueous solutions in competitive ion flotation. Anionic complexes of Zn(II) and Cd(II) from aqueous solutions were floated with cetylpyridinium chloride. The competitive ion flotation of Zn^{2+} and Cd^{2+} by sodium dodecylbenzenesulfonate was also studied.

<div align="center">EXPERIMENTAL</div>

The flotation experiments were carried out in a glass column 45.7 cm high and 2.4 cm in diameter. The nitrogen gas was saturated with water, and the flow rate was maintained at 12 ml/minute through a sintered glass sparger of 20-30 μm, of nominal porosity. The initial volume of each feed solution was 100 ml. The temperature was maintained at 20 ± 2 ^oC. The concentration of zinc(II) and cadmium(II) was $1.0 \cdot 10^{-5}$M. All aqueous solutions were prepared by using double distilled water of conductivity 0.1 μS/m at 25 ^OC. Inorganic ligands, i.e. F^-, Cl^-, Br^-, and I^- were investigated in range of the concentrations of $5.0 \cdot 10^{-5} \div 1.0$ M. Reagent grade inorganic chemical: NaF, NaCl, NaBr, NaI, $ZnSO_4$, $CdSO_4$, NaOH and H_2SO_4 were obtained from POCh

(Gliwice, Poland). Typical ionic surfactants were applied, i.e. sodium dodecylbenzenesulfonate (DBSNa, BHD reagent) as an anionic surfactant, and cetylpyridinium chloride (CPCl, Loba-Chemie reagent) as a cationic surfactant. Both surfactants were purified by recrystalization from ethanol. The concentration of surfactants in the aqueous solutions was $2.0 \cdot 10^{-4}$ M.

The dependence of metal ions concentration versus time of each metal in the bulk solution (c) was recorded continuously during an ion flotation experiment by means of radioactive analytical tracers and gamma radiation spectrometry following a procedure described previously by Charewicz and Niemiec (1969) and improved by Walkowiak and Ulewicz (1999). A single channel, gamma radiation spectrometer was used as the detector of radiation intensity of specific energy. The gamma radioactive isotopes, i.e., Zn-65 and Cd-115m, were from the Atomic Energy Institute „POLATOM" (Świerk near Otwock, Poland). They were of sufficiently high specific activity to neglect the effect of carrier concentration (9.2 MBq/mg for Zn-65 and 2.26 MBq/mg for Cd-115m).

The maximal percent removal (M) is described by an equation:

$$M = 1 - c_r / c_i \tag{1}$$

where c_i – the initial ion concentration,
      c_r – metal ion concentration in the residual solution after foam ceased.
Selectivity coefficient (S) is described by an equation:

$$S_{Me1/Me2} = \frac{M_{Me1}}{M_{Me2}} \tag{2}$$

where M_{Me1} – the maximal percent removal of the first metal,
      M_{Me2} – the maximal percent removal of the second metal.
The first order equation describing the dependence of floated ion concentration vs. time is applied to the flotation kinetics studies (Walkowiak and Ulewicz 1999):

$$\frac{dc}{dt} = - \frac{c_i}{c_i - c_r} k(c - c_r) \tag{3}$$

where   k – kinetic rate constant,
      t – time of flotation process,
      c – metal ion concentration at a given time.
The Statistica Program (Version 5.0) was applied to calculate values of *k*. The program also allows to find the determination coefficient (r^2), which is from 0.0000 to 1.0000 and can be treated as a measure of data fitting to a first order kinetic equation (3).

The total concentration of metal in solutions can be described by an equation (4) and the formation ratio of metal complexes was calculated by an equation (5). In table 1 are given values of the stability constants of halide complexes of Zn(II) and Cd(II).

$$c_M = [M] + [ML] + [ML_2] + \ldots\ldots + [ML_n] \tag{4}$$

$$\alpha_n = \frac{\beta_n [L]^n}{1 + \beta_1 [L] + \beta_2 [L]^2 + \ldots\ldots + \beta_n [L]^n} \tag{5}$$

where [L] – ligand concentration not complexed by a metal,
β_n – overall stability constants of metal complex.

Table 1. Stability constants of zinc(II) and cadmium(II) for halide complexes (Stability constants, 1982)
Tabela 1. Stałe trwałości jonów kompleksowych Zn(II) i Cd(II) z halogenkami

System		$\log\beta_1$	$\log\beta_2$	$\log\beta_3$	$\log\beta_4$
F⁻	Zn(II)	0.95	-	-	-
	Cd(II)	0.76	0.60	-	-
Cl⁻	Zn(II)	0.72	0.49	-0.19	0.18
	Cd(II)	1.32	2.22	2.31	1.86
Br⁻	Zn(II)	-1.46	0.47	-2.24	-
	Cd(II)	1.57	2.26	2.93	-
I⁻	Zn(II)	0.70	1.18	-	-
	Cd(II)	1.91	3.34	4.65	5.86

RESULTS AND DISCUSSION

The study of batch ion flotation first involved the flotations of zinc(II) and cadmium(II) ions from aqueous solutions containing single metal ions, at the concentrations of metals equal to $1.0 \cdot 10^{-5}$ and $2.0 \cdot 10^{-5}$ M. The flotations of zinc(II) and cadmium(II) ions from equimolar mixture of both metals were also conducted. The kinetic curves for flotation of the studied Zn^{2+} and Cd^{2+} cations with DBSNa as the anionic surfactant are shown in Fig. 1. The maximal flotation percent of Zn(II) and Cd(II) cations was 92.1 and 89.0, respectively. Zinc(II) ions are removed better than cadmium(II) ions from solutions containing single metals and from equimolar mixture. However, comparing process rate, i.e. values of *k*, the cadmium(II) ions are removed faster then zinc(II) ions. The results of the kinetic calculations for these flotations are shown in table 2. The determination coefficients were high, i.e. from 0.9789 to 0.9963, respectively. This means that the fitting of experimental points to the equation (3) is statistically very good.
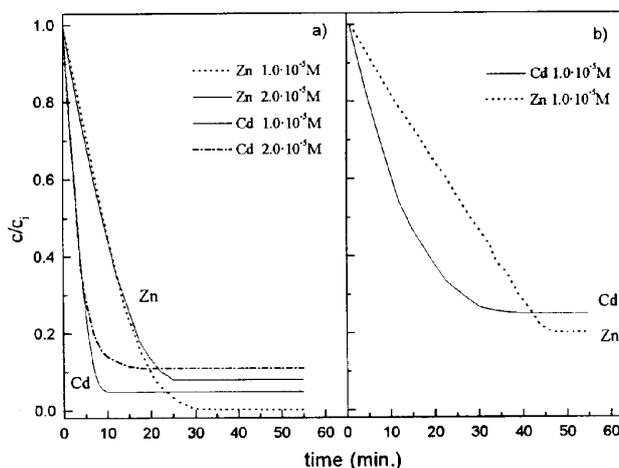
Fig. 1. Flotation curves for the Zn(II) and Cd(II) ions from solutions containing single metal (a) and equimolar metal mixture (b) by $2.0 \cdot 10^{-4}$ M DBSNa

Table 2. The maximum percent removal of zinc(II) and cadmium(II) ions and results of the kinetic calculations

Concentration of ions, [mol/dm³]		The maximal flotation percent	Rate constant, [min⁻¹]	Determination coefficients
Zn²⁺	$1.0 \cdot 10^{-5}$	0.993	0.369	0.9928
	$2.0 \cdot 10^{-5}$	0.921	0.369	0.9939
Cd²⁺	$1.0 \cdot 10^{-5}$	0.951	0.481	0.9963
	$2.0 \cdot 10^{-5}$	0.890	0.488	0.9925
Zn²⁺ + Cd²⁺	$1.0 \cdot 10^{-5}$	0.800	0.329	0.9789
Cd²⁺ + Zn²⁺	$1.0 \cdot 10^{-5}$	0.752	0.356	0.9907

The influence of inorganic ligands, i.e. F^-, Cl^-, Br^-, and I^- on the separation of zinc(II) and cadmium(II) ions was examined. The removal of zinc(II) and cadmium(II) ions decreases with increasing of ligands concentration in aqueous solution using anionic collector, i.e. DBSNa. The separation of Zn(II) and Cd(II) in of fluorides, chlorides, bromides and iodides media aqueous solution with DBSNa is not possible, since the removal of both metals was comparable (Ulewicz, 2000). The separation of both metals occurs when a cationic collector, i.e. CPCl, was applied. In Fig. 2 flotation kinetics curves of Zn(II) and Cd(II) for competitive ion flotation of those metal from 1.0 M bromide (a) and iodide (b) aqueous solutions with CPCl is presented. As can be seen from this figure cadmium(II) is floated much better than zinc(II).

The maximal percent removal of Zn(II) and Cd(II) ions in presence of chloride, bromide and iodide ions are shown in Fig. 3. In this figure, the calculated percent formation of metal complexes for chlorides, bromides and iodides is also shown. Floatation of Zn(II) and Cd(II) in with cationic collector does not occur. Using this collector it is possible to remove of Zn(II) and Cd(II) existing in anionic forms from

aqueous solutions. The differences of predomination range for anionic forms of Zn(II) and Cd(II) allow to separate cadmium(II) over zinc(II). With the increase of halides concentration a removal of Cd(II) ions increase, whereas the removal of Zn(II) is not excited of 10 %. The maximal percent removal of Cd(II) and Zn(II) is comparable with the halides complex anions of the investigated metals.
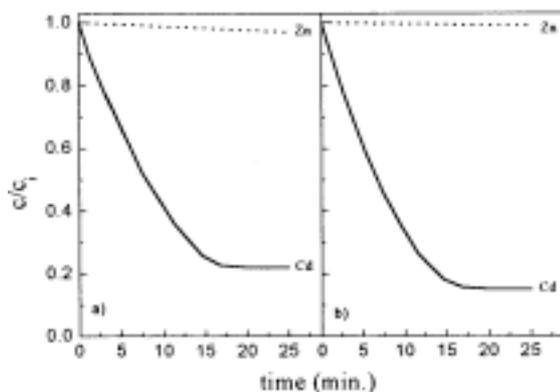
Fig. 2. Kinetic curves of the Zn(II) and Cd(II) ions from aqueous solutions containing 1.0 M bromide (a) and 1.0 M iodide (b) ions in solution by CPCl, $[Zn^{2+}] = [Cd^{2+}] = 1.0 \cdot 10^{-5}$ M, $[CPCl] = 2.0 \cdot 10^{-4}$ M, pH = 4.0
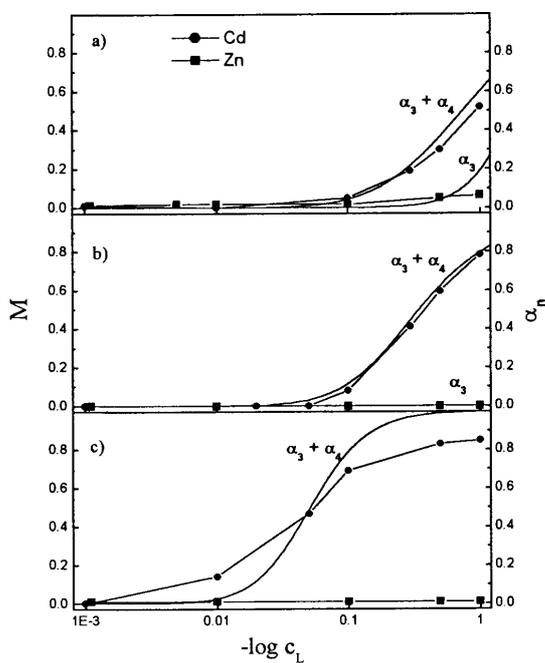
Fig. 3. Influence of analytical concentration of chloride (a), bromide (b) and iodide (c) on removal of Zn(II) and Cd(II) ions with CPCl, and molar fractions of anionic metal complexes, pH = 4.0

The selectivity coefficients of cadmium(II) over zinc(II) separation in presence of investigated ligands are shown in Fig. 4. The selectivity separation of investigation metals by CPCl in halides media aqueous solution at the concentration range of 0.01 to 1.0 M increases in the following sequence: Cl^- « Br^- < I^-. The selectivity coefficients of Cd(II)/Zn(II) at the concentration of 0.5 and 1.0 M for chloride, bromide and iodide are: 7.3; 59.2; 82.0 and 6.0; 67.3, 85.0, respectively. Separation of Cd(II) and Zn(II) ions using CPCl is the best in the presence of iodides and bromides. In the presence of chlorides we observed only a partial separation of Cd(II)/Zn(II) from aqueous solutions. The values of rate constants increase with halides concentration increasing, when CPCl was used (Table 3). As can be seen from this table, the kinetic rate constants for cadmium(II) are much higher than for zinc(II). The rate constant ratios of Cd(II)/Zn(II) for Cl^-, Br^-, and I^- are equal: 1.95; 18.7 and 19.2, respectively.
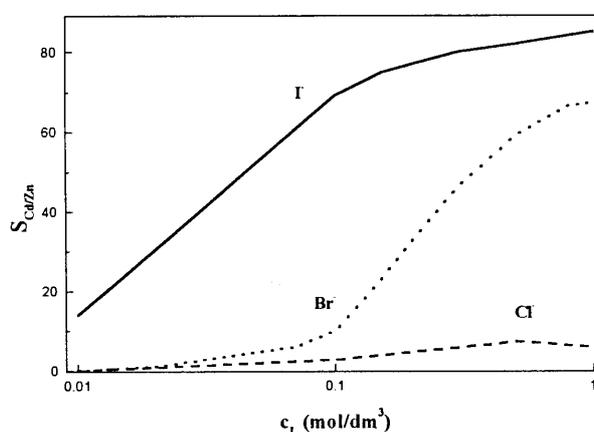
Fig. 4. Selectivity coefficients ($S_{Cd/Zn}$) vs. concentration of ligands, [CPCl] $=2.0 \cdot 10^{-4}$ M

Table 3. Rate constant of Zn(II) and Cd(II) by CPCl in presence of halides at concentration of 1.0 M

Lignads	k [min^{-1}] Zn(II)	r^2	k [min^{-1}] Cd(II)	r^2
Cl^-	0.040	0.9907	0.078	0.9972
Br^-	0.010	0.9914	0.187	0.9893
I^-	0.005	0.9897	0.096	0.9924

CONCLUSIONS

Separation of Cd(II) and Zn(II) ions using anionic collector, i.e. DBSNa, in halides media aqueous solution at the concentrations range of $5.0 \cdot 10^{-5} \div 1.0$ M is not possible, since the removal of both metals is comparable. This is caused by the fact, that zinc(II) and cadmium(II) form cation complexes possess comparable values of stability

constants. In the presence of chlorides, bromides, and iodides in the range of concentrations of $5.0 \cdot 10^{-5}$ to 1.0 M the separation of Cd(II) over Zn(II) using a cationic collector, i.e. CPCl, is possible. The selectivity coefficient of Cd(II)/Zn(II) in the presence of studied ligands at the range concentrations of 0.5 to 1.0 M increases in the sequence: $F^- < Cl^- << Br^- < I^-$. The separation-ability for Cd over Zn are the highest at halides concentration range of 0.5 to 1.0 M. Selectivity coefficients of Cd/Zn reaches the values of: 67.3 and 85.0 for 1.0 M aqueous solutions of Br^- and I^-, respectively.

REFERENCES

CHAREWICZ W. A., HOLOWIECKA B. A., WALKOWIAK W., (1999), *Selective flotation of zinc(II) and silver (I) ions from dilute aqueous solutions,* Sep. Sci. Technol., Vol. 34, No 12, 2447-2460.
CHAREWICZ W., NIEMIEC J., (1969), *Flotation of anions using cationic surfactants, I. Flotation of molibdates*, Nukleonika, Vol. 14, 17-27.
GRIVES R. B., WALKOWIAK W., BHATTACHARYYA D., (1979), *Foam fractionation selectivity sequence of quaternary ammonium surfactant for simple and complex anions:* A review, In: *Recent development in Separation Science, CRC Press Inc.*, Florida, 5, 55-65.
JURKIEWICZ K. (1984-85), *Study on the separation of Cd from solutions by foam separation. I. Foam separation of cadmium cations*, Sep. Sci. Technol., Vol. 19, 1039-1050.
JURKIEWICZ K. (1985), *Study on the separation of Cd from solutions by foam separation. III. Foam separation of complex cadmium anions,* Sep. Sci. Technol., Vol. 20, 179 –192.
JURKIEWICZ K. (1990), *The removal of zinc from solutions by foam separation. I. Foam separation of complex zinc anions,* Int. J. Miner. Process., Vol. 28, 173 – 187.
KOZŁOWSKI C., ULEWICZ M., WALKOWIAK W., (2000), *Separation of zinc and cadmium ions from chlorides by ion flotation and liquid membranes,* Physicochemical Problems of Mineral Processing, No. 34, 141-151.
SCORZELLI I. B., FRAGOMENI A. L., TOREM M. L., (1999), *Removal of cadmium from a liquid effluent by ion flotation*, Minerals Engineering, Vol. 12, 905-917.
SINKOVA L. A. (1998), Influence of zinc and cadmium ions concentration on effectiveness of flotation removal from aqueous solutions with potassium oleate, Ukr. Kim. Zhrn. Vol. 64 , 94-99.
Stability Constants of Metal-Ion Complex; Part A: Inorganic Ligands, Pergamon Press, New York, 1982.
ULEWICZ M., (2001), *Flotation of ions from aqueous solutions in hydrometallurgical process of removal and separation of cadmium and zinc,* Doctoral dissertation, Technical University of Częstochowa.
WALKOWIAK W. (1991), Mechanism *of selective ion flotation. 1. Selective flotation of transmission metal cations.* Sep. Sci. Technol., Vol. 26, 559 – 568.
WALKOWIAK W., (1992), *Mechanism of selective ion flotation technology", In: Innovation in flotation technology,* Edited by P. Mavros, K. A. Matis, *NATO ASI Series, Kluwer Academic Publishers, London,* Vol. 208, 455-473.
WALKOWIAK W., BHATTACHARYYA D., GRIEVES R. B., (1976), *Selective foam fractionation of chloride complex of Zn(II), Cd(II), Hg(II), and Au(III),* Anal. Chem., Vol. 48, 975-979.
WALKOWIAK W., GRIEVES R. B. (1976), *Foam fractionation of cyanide complex of zinc(II), cadmium(II), mercury(II), and gold(III),* J. Inorg. Nucl. Chem., Vol. 38, 1351-1356.

WALKOWIAK W., ULEWICZ M., (1999), *Kinetics studies of ions flotation,* Physicochemical Problems of Mineral Processing, No. 33, 201-214.

M. Ulewicz, W. Walkowiak, C. Kozłowski, *Selektywna flotacja jonów Zn(II) i Cd(II) z rozcieńczonych roztworów wodnych w obecności halogenków*, Fizykochemiczne Problemy Mineralurgii, 35*,* 2001, 21-29, (w jęz. ang.)

Zbadano wydzielanie oraz selektywne rozdzielanie jonów cynku i kadmu w postaci Zn^{2+} i Cd^{2+} oraz jako aniony kompleksowe z wybranymi ligandami nieorganicznymi z roztworów wodnych zawierających zarówno pojedyncze metale jak i z roztworów zawierających równomolową mieszaninę obu metali przy użyciu kolektora kationowego - chlorku cetylopirydyniowego (CPCl) oraz kolektora anionowego - dodecylobenzenosulfonianu sodu (DBSNa). Ponieważ cynk i kadm tworzą kationowe formy kompleksowe o podobnych wartościach stałych trwałości rozdzielenie jonów Zn(II) i Cd(II) przy użyciu kolektora anionowego nie jest możliwe. Separacja jonów kadmu(II) od cynku(II) jest natomiast możliwa przy zastosowaniu kolektora kationowego, tj. chlorku cetylopirydyniowego. Separacja badanych jonów metali przy użyciu CPCl w obecności halogenków o stężeniu 0,5 i 1,0 M wzrasta w szeregu: $F^- < Cl^- << Br^- < I^-$. Współczynniki selektywności Cd(II)/Zn(II) dla stężenia ligandów równego 0,5 M wynoszą odpowiednio: 7,3; 59,2; 82,0 i dla stężenia 1,0 M odpowiednio: 6,0; 67,0; 85,0. Tak więc, niezależnie od stężenia halogenków, najlepsze rozdzielenie jonów Cd(II) od Zn(II) uzyskano w obecności jonów jodkowych i bromkowych w roztworze wodnym.

Władysław JANUSZ, Anna GAŁGAN[*]

ELECTRICAL DOUBLE LAYER AT MANGANESE OXIDES/1:1 ELECTROLYTE SOLUTION INTERFACE

Results of the investigations of the electrical double layer (edl) at manganese oxides/ aqueous solution of alkali metal chlorides interface are presented. The solid phase in the experiments consists of Mn_2O_3 or MnO_2. Dzeta potential (ζ) and surface charge (σ_0) measurements for the mentioned oxides were performed in 0.1- 0.001M solutions of LiCl, NaCl and CsCl. On the basis of surface charge density as a function of pH and ionic strength data the ionization and complexation constants of surface hydroxyl groups were calculated. The surface charge measurements and cation adsorption data indicated that the sequence of the adsorption of alkali metal cations is Li> Na>Cs.

INTRODUCTION

Dispersions of manganese dioxide are present in environment as *pyrolusite*. Manganese hydroxy (oxides) form mineral component of soil. Manganese dioxide may be found in form of nodules on the bottom of the oceans. It finds vide application in numerous branches of industry. For example, it is common oxidant, and in ceramic, textile and rubber industry it is applied as a mineral dye. It is used also as a depolarizer of dry batteries in electronics (Surowce Mineralne Świata 1981). Recently, MnO aroused great interest as a promoter of Fe/Si-2 catalyst for olefin production (Xu et al. 1998), improving its activity and selectivity.

A stability of the dispersion and its rheologic properties are connected with the structure of the electrical double layer at the interface: metal oxide/aqueous solution of electrolyte. The electric charge at such interface is formed as a result of some reactions of acid-base hydroxyl group of metal oxide with electrolyte solution ions (Wiese et al. 1976, James and Parks 1982).

*Department of Radiochemistry and Colloid Chemistry, Maria Curie Skłodowska University,
 pl. M.C. Skłodowskiej 3, 20-031 Lublin, Poland

$$\equiv SOH_2^+ \leftrightarrow \equiv SOH + H^+ \tag{1}$$

$$\equiv SOH \leftrightarrow \equiv SO^- + H^+ \tag{2}$$

The another determinant, influencing the charge magnitude and the structure of the double layer is concentration of the background electrolyte. The ions of this electrolyte take part in, so called, complexation reactions of the surface hydroxyl groups of the oxide, resulting in the increase of the surface charge density, on the other hand compensating the surface charge (James et al. 1978).

$$\equiv SOH_2^+ An^- \leftrightarrow \equiv SOH + An^- + H^+ \tag{3}$$

$$\equiv SOH + Ct \leftrightarrow \equiv SO^- Ct^+ + H^+ \tag{4}$$

Reactions (1-4) are described by thermodynamic constants defined as follows:

$$K_{a_1} = \frac{[H^+][\equiv SOH]}{[\equiv SOH_2^+]} \cdot \frac{\gamma_H \gamma_0}{\gamma_+} \cdot \exp\left(\frac{-e\Psi_0}{kT}\right) \tag{5}$$

$$K_{a_2} = \frac{[H^+][\equiv SO^-]}{[\equiv SOH]} \cdot \frac{\gamma_H \gamma_-}{\gamma_0} \cdot \exp\left(\frac{-e\Psi_0}{kT}\right) \tag{6}$$

$$K_{An} = \frac{[H^+][An^-][\equiv SOH]}{[\equiv SOH_2^+ An^-]} \cdot \frac{\gamma_H \gamma_{An} \gamma_0}{\gamma_\pm} \cdot \exp\left(\frac{-e(\Psi_0 - \Psi_\beta)}{kT}\right) \tag{7}$$

$$K_{Ct} = \frac{[H^+][\equiv SO^- Ct^+]}{[\equiv SOH][Ct^+]} \cdot \frac{\gamma_H \gamma_\mp}{\gamma_0 \gamma_{Ct}} \cdot \exp\left(\frac{-e(\Psi_0 - \Psi_\beta)}{kT}\right) \tag{8}$$

where:

K_{a_1} - dissociation constant of surface group $\equiv SOH_2^+$; K_{a_2} - dissociation constant of surface group $\equiv SO^-$; K_{An} - anion complexation constant; K_{Ct} - cation complexation constant; [.] - concentrations of specific surface forms or ions in the solution; Ψ_0 -surface potential; Ψ_β - potential of Inner Helmholtz Plane (IHP); T- temperature; k-Boltzman constant ($1.38 \cdot 10^{-23}$ J·K^{-1}), e- electron charge, γ_H - activity coefficient of H$^+$ ions, γ_0 - activity coefficient of $\equiv SOH$ groups, γ_+ - activity coefficient of $\equiv SOH_2^+$ groups, γ_- - activity coefficient of $\equiv SO^-$ groups, γ_{An} activity coefficient of anions, γ_{Ct} - activity coefficient of cations, $\gamma_\pm$ - activity coefficient of $\equiv SOH_2^+ An^-$ groups, $\gamma_\mp$ - activity coefficient of $\equiv SO^- Ct^+$ groups.

Equilibrium constants of ionization and complexation reactions allow, according to „site binding" theory, calculation of the concentrations of specific forms, bearing electric charge on the surface of the oxide and determination of the structure of the electrical double layer at metal oxide- electrolyte solution interface. These constants may be determined from the dependencies: surface charge density versus pH and concentration of the electrolyte solution (James et al. 1978, Janusz 1991, Janusz and Szczypa 1998).

It is well known from studies on the stability of dispersed system, that even monovalent ions of alkali metals reveal some differences in coagulation capacity, that is reflected in so called Hofmeister's lyotropic series ($Cs^+ > Rb^+ > K^+ > Na^+ > Li^+$). Examinations of edl structure in metal oxide-electrolyte solution system and following studies on dispersion stability showed that for some system for example α-Fe_2O_3, γ-Al_2O_3 this series may be reversed (Lyklema 1995). What is more, even for the same oxide TiO_2 and alkali metal salt solutions the classic lyotropic series or reversed series may be noticed, depending on the preparation method of the solid. (Dumont 1987).

Ardizzone and Trassatti 1996 summarized information concerning the electrical double layer of the manganese oxides/electrolyte properties of manganese dioxides. From their review one can noticed those pzc and iep values scatter, even for the same crystallographic structure of the sample. They cited data of Tamura et al., for the γ-MnO_2/solution of $NaNO_3$, which indicated the dependence of the pzc on the concentration of background electrolyte.

In present paper the results of experiments on the structure of electrical double layer for manganese dioxide and Mn_2O_3 in LiCl, NaCl and CsCl solutions are presented. The investigations included following measurements: surface charge by potentiometric titrations, adsorption of alkali metal cations with application of radioactive isotopes and dzeta potential by electrophoresis. Obtained results were used to calculation of equilibrium constants of ionization and complexation of surface hydroxyl groups of metal oxides.

EXPERIMENTAL

MATERIALS

Aldrich, Milwakee, USA delivered manganese dioxide. Specific surface of the sample, determined by BET method (adsorption and desorption of nitrogen) was $38.14 m^2/g$ and porosity analysis proved existence of micropores (total volume of pores from desorption 1,7nm $<d<$ 300nm by BJH method was 0,046 cm^3/g and their average pore radius from desorption was 4.9nm). Grain size distribution of the sample determined by PCS method (Photo Correlation Spectroscopy) reveals relatively broad diameter, 150-550 nm, of grains.

Manganese oxide (III) was obtained following Ul Hag and E. Matijevic (1997) method. A mixture of carbamide (30.0279 g/l) and $MnSO_4$ (15.099g/l) solutions was heated in 85^oC during two hours, then cooled to room temperature. Next the obtained

suspension was centrifuged; sediment was washed out with double distilled water and dried. Dry $MnCO_3$ was calcinated in 700^oC during one hour in air. According to BET measurements, the specific surface of the obtained sample was 9.22 m^2/g and such as MnO_2 sample it was microporous (total volume of pores from desorption 1,7nm <d< 300nm by BJH method was 0,0184 cm^3/g and their average pore radius from desorption was 7.8nm). Grain size distribution of this sample demonstrated also broad range of the particle diameter (100-750 nm).

METHOD

Potentiometric titration was performed in Teflon vessel. Temperature of measurements, equal to 25^oC was maintained by Julabo F10UC thermostat. Carbon dioxide, dissolved in solutions was removed from the system by flowing nitrogen. Such method provides neutral atmosphere during titration of the solutions and suspensions. The content of the titration vessel was stirred by propeller mixer. A pH measurement was carried out with Radiometer Copenhagen PHM 85 Precision pH Meter. A titrant (base solution) was added with Metrohm Dosimat 665 burette. Both the pH meter and the burette were connected to a computer for acquisition data (pH and titrant volume) and to control the addition of titrant. From obtained data the surface charge density values were computed.

The adsorption of Na^+ or Cs^+ was determined by the isotope technique, by measurement of the ^{22}Na or ^{137}Cs activity uptake from the solution. Details of this procedure were described by Janusz 1996. The adsorption of Li^+ was calculated from uptake of the concentration of Li^+ ions from solution. The concentration of Li^+ was determined by means of AAS method.

Dzeta potential was determined by electrophoretic method with Zetasizer 3000 by Malvern.

RESULTS AND DISCUSSION

ELECTRICAL DOUBLE LAYER AT MnO_2/ ALKALI METAL IONS SOLUTIONS

As was mentioned earlier electrical charge at the interface of metal oxide/ electrolyte solution is formed as a result of the reactions of acid-base hydroxyl groups (Reactions 1 and 2) and due to complexation reactions of surface hydroxyl group with the background electrolyte ions (Reactions 3 and 4). In the case of specific adsorption of the electrolyte ions the increase of the electrolyte concentration results in the increase of the charge density.

Surface charge density versus pH and concentration of the electrolytes (LiCl, NaCl, and CsCl) dependencies are presented on Figures 1, 2 and 3 respectively. It can be noticed that pH_{pzc} equals nearly 4. For the MnO_2/CsCl solution system the pH_{pzc} is the same for all concentration of background electrolyte. Small shift of pH_{pzc} with electrolyte concentration was noticed for LiCl solution. Unexpectedly high shift of

pH_{pzc} was observed for NaCl solutions; for 0.001M solution it moves to pH=5.5. Such shift of pH_{pzc} is characteristic for specifically adsorbing cations. These results confirm results of Tamura et al. (Ardizzone and Trasatti 1996). On the other hand, a comparison of surface charge for the greatest concentrations of the electrolyte suggests that adsorption sequence should be as follows:

Li> Na > Cs
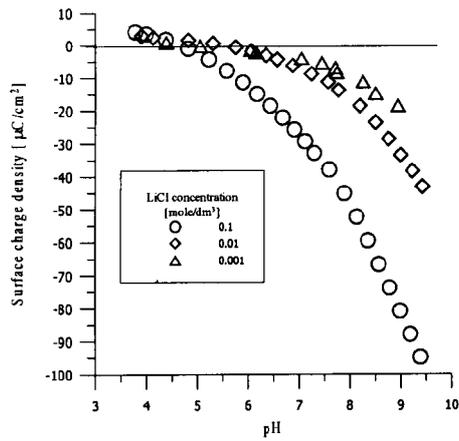
Fig. 1. Surface charge density as a function of pH and electrolyte concentration for the MnO_2/LiCl solution system
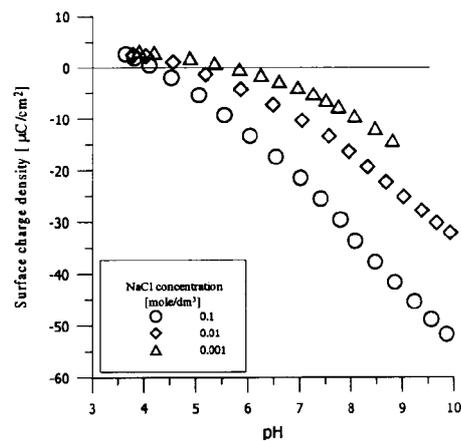
Fig. 2. Surface charge density as a function of pH and electrolyte concentration for the MnO_2/NaCl solution system
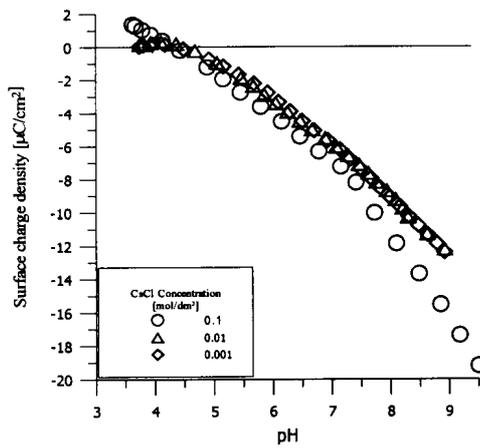
Fig. 3. Surface charge density as a function of pH and electrolyte concentration for the MnO_2/CsCl solution system
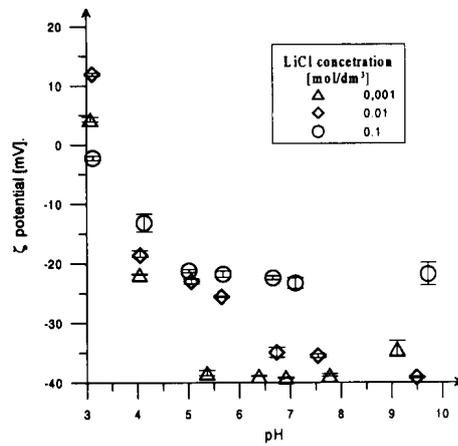
Fig. 4. Zeta potential as a function of pH and electrolyte concentration for th MnO_2/LiCl solution system

This sequence is in good agreement with observation for many oxides, for example TiO_2, Fe_2O_3 (Lyklema 1995) nevertheless it should be noticed that for lithium the charge density at pH=9 is two times higher than for sodium which is also higher than for cesium.

In presented sequence of electrolytes the decrease of the influence of the electrolyte concentration on the charge density is well visible. Considering above it seems that titration by NaOH and CsOH leads, beside acid base reactions also to neutralization of some substances that contaminate the surface. LiOH as week base does not take part in such type reactions.

Potential dzeta versus pH dependence for discussed electrolytes is presented on Fig 4, 5 and 6 for LiCl, NaCl and CsCl solutions, respectively. For all studied systems pH_{iep} is lower than 4.
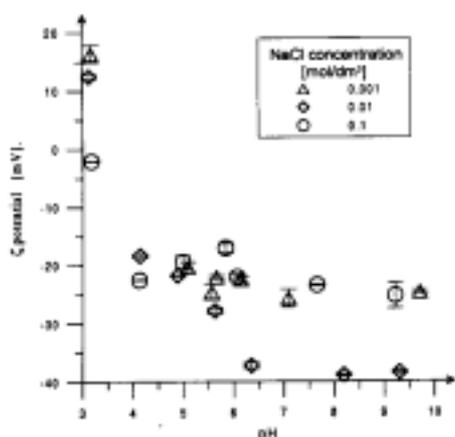
Fig. 5. Zeta potential as a function of pH and electrolyte concentration for the MnO_2/NaCl solution system
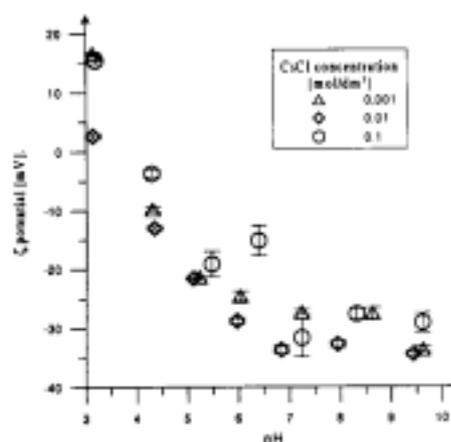
Fig. 6. Zeta potential as a function of pH and electrolyte concentration for the MnO_2/CsCl solution system.

Only for MnO_2/LiCl system the relationship of the ζ potential as a function of background electrolyte concentration is typical for oxide systems relation. Dzeta decreases when the electrolyte concentration increases. The less pronounced dependence is observed for MnO_2/CsCl. For MnO_2/NaCl system the highest ζ is observed for concentration 0.01M. This effect seems to be difficult to explain and may be caused by porosity of the solid.

Figure 7 demonstrates dependence of the adsorption of alkali cation on pH of the 0.001M solutions. A plot of these dependencies is in agreement with reaction 4 that is adsorption increases with the pH increase, however observed increase of the adsorption as a function of pH is not uniform. For Na^+ and Li^+ sharp increase of the adsorption is observed at pH=7 whereas for Cs^+ the increase of the adsorption starts at pH_{iep}. The greatest adsorption is noticed for sodium ions. It may be explained by low value of dzeta potential in the case of MnO_2/NaCl system.
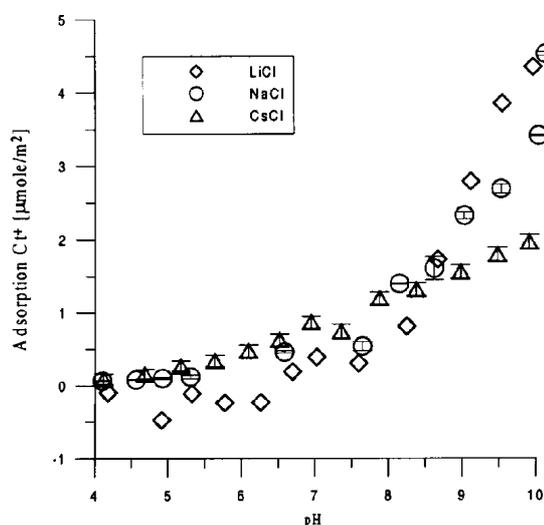
Fig 7. Adsoption of cations (Ct = Li, Na, Cs) vs pH at the MnO$_2$/0,001 M. CtCl electrolyte interface

Equilibrium constants for ionization and complexation of surface hydroxyl groups were calculated according to Davies et al. 1978 method, basing on potentiometric titration data. Obtained constants for LiCl, NaCl and CsCl solutions are listed in Table 1. It may be noticed that values of the constants of positively charged groups are similar. Only for NaCl the higher stability of ionized, positively charged groups is observed. Considered cations arrange in the following sequence: the lowest ionization tendency reveals CsCl solutions and the highest LiCl.

Table 1. Ionization and complexation constants of surface hydroxyl groups for MnO$_2$/Ct
(Ct = Li, Na, Cs)Cl system.

Constants	Elektrolyte		
	LiCl	NaCl	CsCl
pK$_{a1}$	2.93±0.65	4.12±0.97	3.02±1.34
pK$_{a2}$	8.70±0.07	8.38±0.82	7.62±0.30
pK$_{Cl}$	2.62±1.14	1.20±0.66	0.26±1.09
PK$_{Ct}$	6.20±1.03	5.44±0.42	5.96±1.06

Analysis of the value of the cation complexation constants indicates that the strongest complexes are formed by sodium ions, weaker for cesium and the weakest for lithium ions in observed system. These results are in agreement with ion adsorption studies – Fig. 7. It may be concluded from the above that in lithium chloride solutions the ionization reactions has the greatest share in the charge formation whereas complexation reactions does the same in MnO$_2$/NaCl system.

ELECTRICAL DOUBLE LAYER AT Mn_2O_3/ALKALI METAL IONS SOLUTIONS

Surface charge density versus pH dependence for Mn_2O_3/LiCl solution system is presented on Figure 8, Mn_2O_3/NaCl solution system on Figure 9 and for Mn_2O_3/CsCl solution system on Figure 10. For Mn_2O_3/LiCl and Mn_2O_3/NaCl systems pH_{pzc} equals to 6 whereas for Mn_2O_3/CsCl small shift to pH=6.4 was noticed. On Figure 8 small dependence of charge density on the concentration of the background electrolyte may be noticed. For the remaining two cases (Figs 9 and 10) this dependence is typical for the oxides, although its character is different for each system. For Mn_2O_3/NaCl solution system pronounced dependence of surface charge density on electrolyte concentration is visible up to pH=7, whereas for Mn_2O_3/CsCl system this dependence is relatively higher below pH_{pzc}. In the first example the higher influence of the cation adsorption on the charge density is visible.
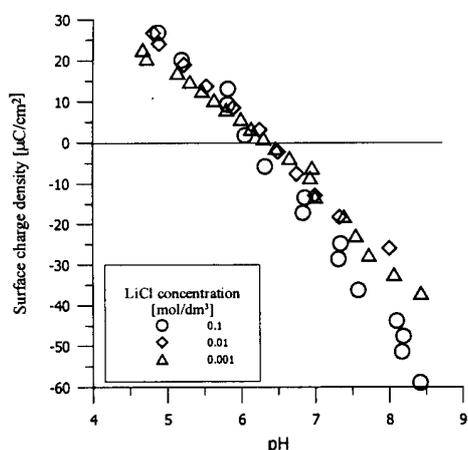
Fig. 8. Surface charge density as a function of pH and electrolyte concentration for the Mn_2O_3/LiCl solution system
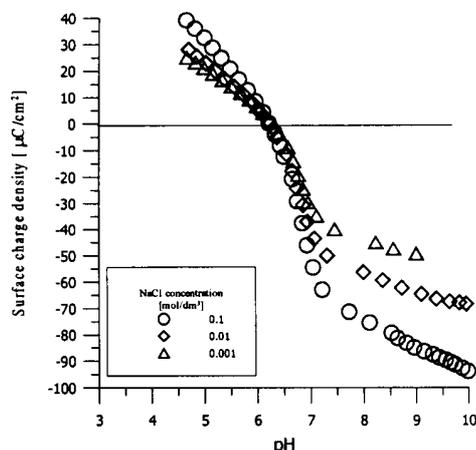
Fig. 9. Surface charge densit as a function of pH and electrolyte concentration for the Mn_2O_3/NaCl solution system

Dzeta potential versus pH dependences for three concentrations of the background electrolyte for systems Mn_2O_3/LiCl Mn_2O_3/NaCl and Mn_2O_3/CsCl are presented in Figures 11, 12 and 13 respectively. It may be noticed that pH_{iep} value for Mn_2O_3/LiCl and Mn_2O_3/NaCl systems equal to 3.2 whereas for Mn_2O_3/CsCl it is 3.5. A comparison of both values, pH_{pzc} and pH_{iep}, reveals difference in all systems bigger than three units. The reason for such difference may be significant adsorption of the anion, which shifts pH_{pzc} towards higher values, presence of contamination or porosity of the solid.

Examination of the structure of the solid by BET method (adsorption and desorption of the nitrogen) can not exclude the latter factor in principle. The lack of this shift for higher ionic strengths proves the same adsorption of the electrolyte ions at pH_{pzc} vicinity, so for any noticed shift alkali contamination such as NaOH or KOH should be responsible. On the other hand, the process of the sediment preparation

excludes their presence. The precipitation of $MnCO_3$ is performed in the presence of carbamide and obtained sediment is washed with doubly distilled water until the conductivity of supernatant was constant. A difference between pH_{pzc} and pH_{iep} may results from neglecting the sediment solubility. Titration of the sediment with various weighed portion of the solid, to take the solubility into account, gave shift towards lower values about 0.5 pH unit. Because mentioned difference between pH_{pzc} and pH_{iep} was too big the washing out the solid with acid is necessary.
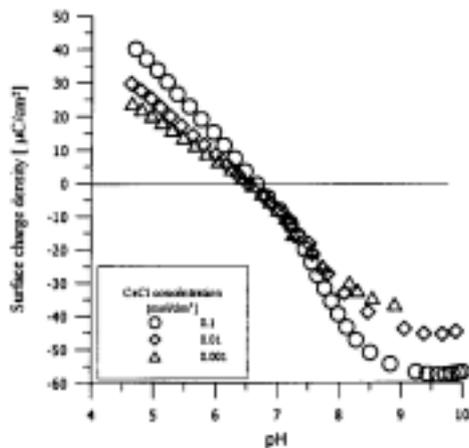
Fig. 10. Surface charge density as a function of pH and electrolyte concentration for the Mn_2O_3/CsCl solution system
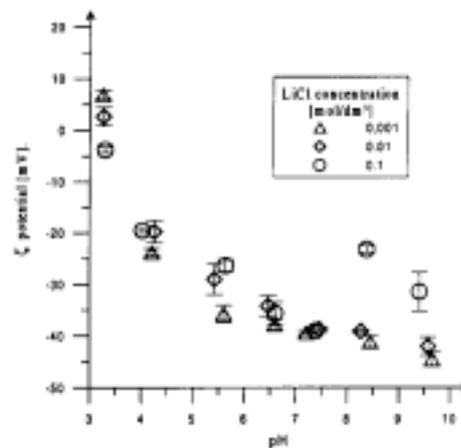
Fig. 11. Zeta potential as a function of pH and electrolyte concentration for the Mn_2O_3/LiCl solution system
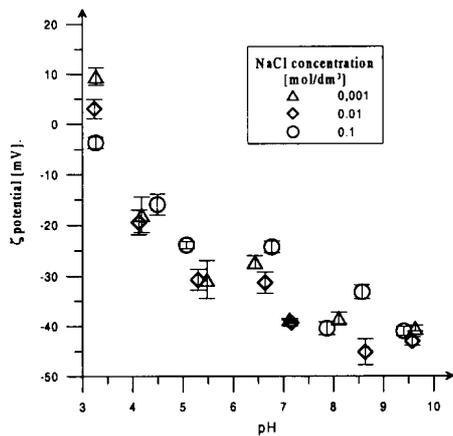
Fig. 12. Zeta potential as a function of pH and electrolyte concentration for the Mn_2O_3/NaCl solution system
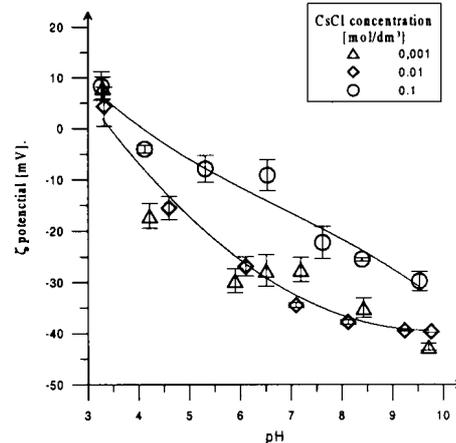
Fig. 13. Zeta potential as a function of pH and electrolyte concentration for the Mn_2O_3/CsCl solution system

W. Janusz, A. Gałgan

Ionization and complexation constants of surface hydroxyl groups were determined from the dependence - surface charge density versus pH, according to Davies et al. These constants are listed in Table 2, for studied electrolytes.

Table 2. Ionization and complexation constants of surface hydroxyl groups
for Mn_2O_3/Ct (Ct=Li, Na, Cs)Cl system

Constant	Electrolyte		
	LiCl	NaCl	CCl
pK_{a1}	4.77±0.01	5.02±0.20	4.97±0.07
pK_{a2}	7.85±0.08	7.80±0.22	8.28±0.08
pK_{Cl}	4.99±0.06	5.02±0.35	5.54±0.32
pK_{Ct}	7.50±0.01	7.52±0.28	8.15±0.09

For this oxide, some small differences of ionization constants are connected with positively charged groups (0.2 pH units) and a little bigger with negatively charged (0.4 pH units). The greatest differences are visible for cations. From the above data it may be concluded that lithium cations are the stronger complexing agent whereas cesium cations are the weakest one. This sequence is different than that of for previously mentioned MnO_2 and may result from ordered state of water layer at the surface of the oxide. For oxides with firmly hydrated surface the adsorption of hydrated ions is favored, whereas for the oxides with poorly hydrated surface the adsorption of ions hydration shield for example cesium. To prove above assumption the calculation of hydration degree of both oxides seems to be very helpful.

CONCLUSIONS

The following conclusions may be drawn from calculations based on potentiometric titrations, ion adsorption and dzeta potential measurements of the systems manganese oxide/ alkali metal chlorides:
1. pH_{pzc} and pH_{iep} of MnO_2 in solutions of alkali metal chlorides is lower than 4.
2. Obtained sequence of the adsorption of alkali metal cations is Li> Na>Cs. It should be noticed that the highest charge density was obtained for LiCl and the smallest one for CsCl solution. It is caused by a considerable contribution of the ionization of surface hydroxyl groups in LiCl solution.
3. Examination of the systems with Mn_2O_3 revealed big difference between pH_{pzc} (6.5) and pH_{iep} (3.8), which is difficult to explain on the base of the performed experiments.
4. Sequence of cations adsorption on Mn_2O_3 surface is Li> Na>Cs.

REFERENCES

ARDIZZONE S., TRASATTI S. (1996), *Interfacial properties of Oxides with Technological Imapct in Electrochemistry*, Adv. Colloid Interface Sci., 64, 173-251.

DAVIS, J.; JAMES, ROBERT O.; LECKIE J., (1978), *Surface Ionization and Complexation at the Oxide/Water Interface. I. Computation of Electrical Double Layer Properties in Simple Electrolytes*. J. Colloid Interface Sci., 63, pp 480-499.

DUMONT F., WALRUS J., WATILLON A., J. O. (1987), *Influence of the Point Zero of Charge of Titanium Dioxide Hydrosols on the Ionic Adsorption Sequences,* J. Colloid Interface Sci. 138, pp. 543.

JAMES, R.O., PARKS, G.A. (1982) *Surface and Colloid Science*, Matijevic,E., Ed, Wiley-Interscience, New York, vol.12, pp. 119-216.

JANUSZ, W. (1991), *Determination of Surface Ionization and Complexation Constants from Potentiometric Titration Data*, Polish J. Chem. 65, pp. 799-807.

JANUSZ W., (1996), *The Structure of Electrical Double Layer at the LiChrosphere type adsorbent/Aqueous Electrolyte Solution Interface* Ads, Sci. Technol., 14(3), 151-161.

JANUSZ W., SZCZYPA J., (1998*), Determination of the Ionization and Complexation Constants in the Metal Oxide/ Electrolyte System*, J. Dispersion Sci. Technol., 19, 267-292.

SUROWCE MINERALNE ŚWIATA, Mangan-Mn; Chrom Cr, Wydawnictwa Geologiczne, Warszawa 1981,

LYKLEMA, J. (1995), *Fundamentals of Interface and Colloid Science*. Academic Press. New York vol II, 4.1-4.120

XU, L., WANG, Q., LIANG, D., WANG, X., LIN, L., CUI, W., XU, Y. (1998), *The Promotions of the MnO and K_2O to fe/Silicate-2 catalyst for the production alkanes from CO_2 hydrogenation,* Applied Catalysis 173, pp. 19-25.

UL HAG, I., MATIJEVIC, E. (1997), *Preparation and properties of uniform coated inorganic colloidal particles. 11. Nickel and its compounds on manganese compounds,* Chem. Mater. vol. 9, no. 12.

WIESE, G.R., JAMES, R.O., YATES,D.E., HEALY, T.W. (1976), *Electrochemistry of the Colloid-Water Interface*, Int. Rev. Sci., Phys. Chem. Ser. 2, Bockris, J.O'M., Ed, Butterworths London, pp. 53-102.

Janusz W., Gałgan W., *Podwójna warstwa elektryczna na granicy faz tlenki manganu/roztwór elektrolitu 1:1,* Fizykochemiczne Problemy Mineralurgii, 35, 2001, 31-41 (w jęz. ang.).

Przedstawiono wyniki badań podwójnej warstwy elektrycznej na granicy faz tlenki manganu/wodny roztwór chlorków metali alkalicznych. Badania prowadzono nad właściwościami granicy faz w których fazę stałą stanowiły tlenki manganu; Mn_2O_3 i MnO_2. Pomiary ζ i ładunku powierzchniowego (σ_0) dla wyżej wymienionych tlenków przeprowadzono w 0.1-0.001M roztworach LiCl, NaCl, CsCl. W oparciu o zależności gęstości ładunku powierzchniowego, potencjału ζ od pH i stężenia elektrolitu obliczono stałe jonizacji i kompleksowania powierzchniowych grup hydroksylowych tlenków. Na podstawie pomiarów ładunku powierzchniowego oraz przez bezpośredni pomiar adsorpcji kationów określono następującą sekwencję adsorpcji kationów Li>Na>Cs.

Robert OGONOWSKI, Wiesław WÓJCIK and Bronisław JAŃCZUK[*]

THE EFFECT OF LIQUIDS ON THE INTERACTION BETWEEN COAL PARTICLES

Taking into account the published earlier values of the destruction time of the coal column structure formed from the four fractions of coal particles having the average diameter 1.5×10^{-4} m, 2.5×10^{-4} m, 3.5×10^{-4} m and 4.5×10^{-4} m in the homologous series of alkanes and alcohols, the correlation between destruction time and bulk properties of coal and liquids as well as the liquid-air, coal-air and coal-liquid interfacial properties was studied. On the basis of this study the linear relationship between the reciprocal destruction time and average diameter of the coal fractions, work of alkane and alcohol cohesion, their density, the difference between liquids and coal density, and free energy of interactions per one molecule of the liquid was found. From these relationships, the critical values of the particles diameter, work of cohesion, density, difference between coal and liquid density, and free energy of interactions for infinitely long destruction time were determined. It was stated that for systems having critical values of these parameters, the detachment force is equal to the attachment one. From study it also results that the attachment forces between coal particles depend on the work of cohesion of liquid and work of adhesion of coal to liquid, and that the destruction of the structure of the sediment column take place as a result of the interruption of the film of the liquid between two coal particles.

Key words: adhesion, coal particles, alkanes, alcohols, interfacial interactions, attachment and detachment forces

INTRODUCTION

Interactions among particles of solid through a liquid play an important role in many technological processes such as: froth flotation, oil agglomeration, shear flocculation, carrier flotation, precipitate flotation, coagulation flocculation (Leja 1982), (Warren 1975), (Sadowski 1993) and (Wójcik et. al. 1978). In these processes an aqueous suspension of mineral particles is mixed with a collector or an immiscible

[*]Department of Interfacial Phenomena, Faculty of Chemistry, Maria Curie-Skłodowska University, Maria Curie-Skłodowska Sq. 3, 20-031 Lublin, Poland

liquid, such as kerosene or diesel oil, which consist of different kinds of hydrocarbons. Adsorption or spreading of the collector on the surface of a mineral causes its hydrophobization. Hydrophobic or hydrophobized particles of an ore can be preferentially wetted by an apolar liquid, which forms capillary bridges between the particles, causing thus their aggregation or agglomeration.

Knowledge of the values of the interparticle interactions through a liquid can be helpful to explain more exactly the mechanism of these processes.

Different apparatuses and methods are used to determine adhesive interaction as well as the perimeter of the contact plane between a soft solid sphere and a flat rigid solid surface, or between a hard solid sphere and a flat soft solid surface (Johnson et al. 1971), (Maugis 1992), Derjaguin et al. 1961) and (Derjaguin et al. 1975). The obtained results are discussed on the basis of two main approaches commonly called as Johnson, Kendall and Roberts (JKR) (1971) or Derjaguin, Muller and Toporow (DMT) (1975) theories. In our laboratory in the sixties, a simple device was used to measure the destruction time of the sediment coal structure (Waksmundzki et al. 1965) and (Waksmundzki et al. 1965a).

Using this device the destruction time of the sediment column structure of coal particles was measured in two homologous series of liquids: n-alkanes (Wójcik et al. 2000) and n-alcohols (Wójcik et al. 2000a). The obtained results were interesting, but not explained enough so far. Therefore, the purpose of our paper is to find the correlation between the destruction time and bulk properties of the n-alkanes, n-alcohols, and coal as well as the n-alkanes (n-alcohols)-air, coal-air and coal-n-alkanes (n-alcohols) interfacial properties.

EXPERIMENTAL

METHOD

A schematic diagram of the device for measurements of the destruction time of the sediment column structure (Waksmundzki et al. 1965), (Waksmundzki et al. 1965a), (Wójcik et al. 2000), (Wójcik et al. 2000a) and (Wójcik et al. 2000b) is presented in Fig. 1. It consists of a glass tube (1) -0.4m long and a $3 \ 10^{-3}$m in inner diameter, and a glass vessel $3 \ 10^{-5}$m^3 in volume (2) connected with the glass tube by a rubber plug (3) so as to move the tube up and down. The glass vessel is closed by a stopper (4). The other end of the tube is closed by a silicone plastics seal tightened by a screw (5).

MEASUREMENTS

The destruction time of the coal sediment column structure was measured for four size fractions of coal particles whose average diameters were: $1.5 \ 10^{-4}$m, $2.5 \ 10^{-4}$m, $3.5 \ 10^{-4}$m and $4.5 \ 10^{-4}$m, respectively. The measurements were carried out in n-alkanes, from hexane to hexadecane, and in n-alcohols from methanol to decanol (Wójcik et al. 2000) and (Wójcik et al. 2000a).

Fig. 1
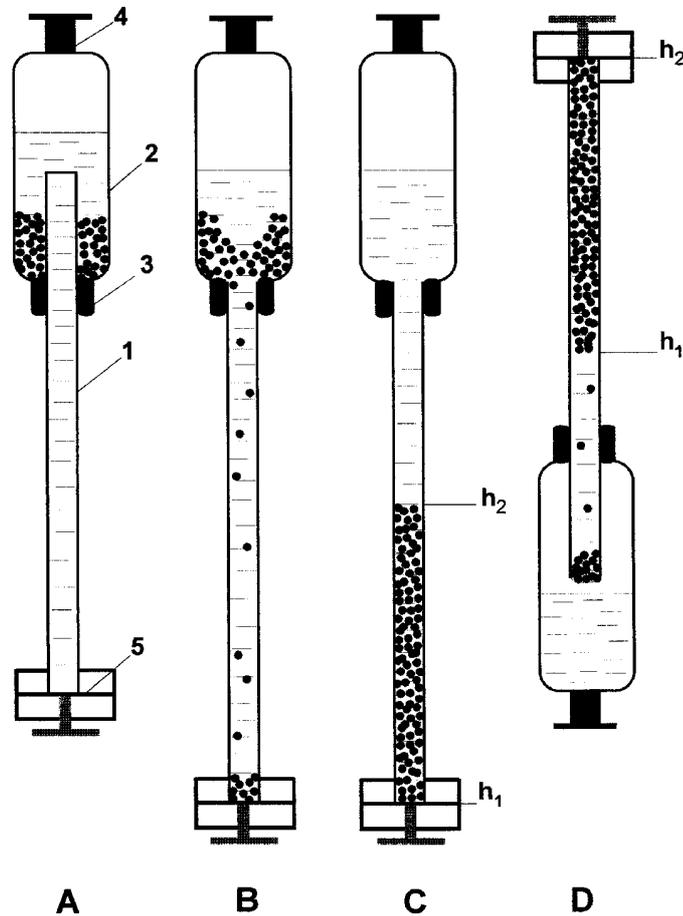
Fig. 1. Schematic diagram of the device for the destruction time measurements: (1) glass tube; (2) glass vessel; (3) rubber plug; (4) stopper; and (5) sealing system. (A) The device filled with the studied suspension; (B) formation of the sediment column; (C) the sediment column formed; (D) destruction sediment column structure. h_1 and h_2 are the bottom and upper levels of the of the sediment column

    The sediment column of coal particles was formed in the glass tube by pouring $2,5 \ 10^{-5} m^3$ of the liquid in the glass vessel and tube and adding $2 \times 10^{-3} kg$ sample of a given fraction of coal particles (Fig.1A). The tube was moved down, as shown in Fig. 1B, and the particles falling into the tube formed a sediment column, the length of which was ca. 0.3 m between the level h_1 and h_2 (Fig. 1C). Next, the tube was moved up over the level of alkane, and the column structure was established in 10 min. After

that the device was quickly inverted, as shown in Fig. 1D, and the particles detached from the sediment column and dropped to the end of the tube, forming a new sediment column (Fig. 1D).

The destruction time of the coal sediment column structure was measured by a stop-watch, starting when the first coal particle detached from the column at the level h_1 (Fig. 1D), and stopping when the last coal particle started to drop at the level h_2 (Fig. 1D). The procedure of the destruction time measurements was repeated several times for each coal fraction and each liquid used.

DISCUSSION

We have found that the destruction time increases with increasing length of the hydrocarbon chain of the studied liquids and decreases with increasing diameter of coal particles. This means that the difference between the force of a coal particle attachment to a coal particle through the liquid and the force of a coal particle detachment from a coal particle increases with increasing number of carbon atoms in a molecule of the liquid and decreases with increasing average diameters of coal particles. These findings suggest that the difference between the attachment and detachment forces go to zero as the average diameter of coal particles decreases. Therefore, for certain size of coal particles the destruction time is infinitely long and the particles do not detach from those of the column. The diameter of such particles is called the critical diameter (Waksmundzki et al. 1965), (Waksmundzki et al. 1965a), (Wójcik et al. 2000), (Wójcik et al. 2000a) and (Wójcik et al. 2000b).

We have found linear relationship between the reciprocal of the destruction time and: 1) the average diameter of coal particles fractions, 2) work of cohesion of the liquids, 3) density of the liquids, 4) difference between densities of coal and a studied liquid, 5) reciprocal of the free energy of interaction per molecule of the liquid. These relationships satisfy the equation:

$$1/t = a + bX \tag{1}$$

where: t is the destruction time, a and b are the constants and X the parameters mentioned above.

The parameters determined from Eq. (1) for the destruction time equal to infinity ($1/t = 0$) were called critical. The critical diameter of coal particles did not depend on length of the hydrocarbon chain of the liquids and average values in alkanes and alcohols is $9.4 \cdot 10^{-5}$ m and $9.8 \cdot 10^{-5}$ m, respectively.

The critical work of cohesion of the liquids and their critical density difference practically did not depend on the average diameter of coal particle fractions (Tab. I).

For each studied liquid if the coal particles diameter has critical value, then the detachment force is equal to the attachment one. The same case takes place for all studied fractions of coal particles if the liquid (alkane or alcohol) would have the critical work of cohesion. In these cases coal particles do not detach from one another and the sediment column is stable.

Table I. Critical work of cohesion of alkanes and alcohols and the critical density differences between coal and the liquids

Liquids		Coal size fractions x10^{4}m	Critical work of cohesion in mN/m	Critical density differences $\Delta\rho$ in kg/m^3
A				
Alkanes	1.5		57.1	556.5
	2.5		57.3	551.3
	3.5		57.5	549.8
	4.5		57.5	549.9
	Average		57.3	551.9
B				
Alcohols	1.5		58.2	505.5
	2.5		58.3	504.3
	3.5		58.5	503.2
	4.5		58.4	503.5
	Average		58.4	504.1

Assuming that coal particles are spheres, the detachment force was calculated from equation (Wójcik et al. 2000) and (Wójcik et al. 2000a)

$$F_D = \frac{1}{6}\Pi d_{cr}^3 g\left(\rho_C - \rho_L\right) \tag{2}$$

where d_{cr} is the critical diameter of coal particles, g is the acceleration due to gravity; ρ_C and ρ_L are the density of coal and liquid, respectively. The calculated F_D values in alkanes (from hexane to hexadecane) and alcohols (from methanol to decanol) were in the range from $29.1 \cdot 10^{-10}$ N/particles to $24.2 \cdot 10^{-10}$ N/particles and from $26.6 \cdot 10^{-10}$ N/particles to $24.7 \cdot 10^{-10}$ N/particles (Tab. II), respectively (Wójcik et al. 2000) and (Wójcik et al. 2000a).

Taking into account the critical density difference, the detachment force was calculated from Eq. (2) for alkanes and alcohols and was $23.5 \cdot 10^{-10}$ N/particle and $24.4 \cdot 10^{-10}$ N/particle, respectively.

For coal particles having the critical diameter the detachment force can be expressed by the equation

$$F_D = W_{Coh.cr} \cdot L = W_{Coh.cr} \cdot 2\pi R \tag{3}$$

where $W_{Coh.cr}$ is the critical work of cohesion of the alkane or alcohol, L is the parameter of the contact plane between two coal particles in the liquid and R is the radius of the contact plane.

Table II. Detachment (F_D) and attachment (F_A) forces between two coal particles (in N/particle and in N/m), radius of the contact plane between coal particles (R), and the difference between attachment and detachment forces (F_D - F_A) .

Liquid	$F_D \cdot 10^{10}$ N/particle	$F_D \cdot 10^3$ N/m	$R \cdot 10^{10}$ M	$F_A \cdot 10^{10}$ N/particle	$(F_D-F_A) \cdot 10^{10}$ N/m	$F_A \cdot 10^3$ N/m
A.						
1.Hexane	29.1	57.3	80.9	18.7	10.4	37.6
2.Heptane	28.0	57.3	77.8	19.7	8.3	41.2
3.Octane	27.2	57.3	75.6	20.5	6.7	44.0
4.Nonane	26.9	57.3	74.8	21.5	5.4	46.6
5.Decane	26.1	57.3	72.5	21.7	4.4	48.6
6.Undecane	25.6	57.3	71.1	22.0	3.6	50.2
7.Dodecan	25.2	57.3	70.0	22.4	2.8	51.9
8.Tridecane	24.9	57.3	69.2	22.6	2.3	53.0
9.Tetradecane	24.7	57.3	68.6	22.8	1.9	54.9
10.Pentadecane	24.3	57.3	67.5	22.9	1.4	55.0
11.Hexadecane	24.2	57.3	67.3	23.2	1.0	55.9
12.Average	23.5	57.3	65.3	23.5	0	57.3
B.						
1.Methanol	26.6	58.4	72.6	20.4	6.2	45.1
2.Ethanol	26.7	58.3	72.9	20.5	6.2	45.1
3.Propanol	26.0	58.4	70.9	20.8	5.2	47.1
4.Butanol	25.7	58.4	70.1	21.5	4.2	49.2
5.Pentanol	25.5	58.4	69.6	22.5	3.0	51.8
6.Hexanol	25.2	58.3	68.8	22.6	2.6	52.7
7. Heptanol	25.1	58.4	68.5	23.1	2.0	54.1
8.Octanol	25.0	58.4	68.2	23.4	1.6	55.0
9.Nonanol	24.8	58.3	67.8	23.7	1.1	56.0
10.Decanol	24.7	58.4	67.4	24.0	0.7	57.1
11.Average	24.6	58.4	67.1	24.6	0	58.4

The radius of the contact plane between two coal particles in the studied liquids was calculated from Eq. (3), using the detachment force and critical work of cohesion of alkane and alcohol taken from literature (Wójcik et al. 1978), (Wójcik et al. 2000a) and (Wójcik et al. 2000b). The values of the radius of the contact plane are listed in Tab. II A and B and they decrease with increasing length of the hydrocarbon chain of alkanes from $80.9 \cdot 10^{-10}$ m to $67.3 \cdot 10^{-10}$ m and alcohols from $72.6 \cdot 10^{-10}$ m to $67.4 \cdot 10^{-10}$ m.

Knowing the detachment force in Newton per particle and the perimeter of the contact plane between two coal particles in the liquid, detachment force in Newton per unit of length was calculated from Eq. (3) and listed in Tab. II. As it is seen the values of the detachment force, for both homologous series of liquids, do not depend on the length of hydrocarbon chain of alkanes and alcohols. The average values for these series of liquids are $57.3 \cdot 10^{-10}$ N/m and $58.4 \cdot 10^{-10}$ N/m, respectively. These values are equal to the critical cohesion of alkane and alcohol determined from linear

relationship of the reciprocal of the destruction time as a function of the work of cohesion of the liquid.

The changes of the radius of the contact plane were unexpected to us because the work of cohesion of the studied liquids and their work of adhesion to coal increased with increasing length of the hydrocarbon chain of the liquids. Only the interfacial free energy of the coal–liquid system decreased as a function of the length of hydrocarbon chain of alkanes and alcohols. Therefore, we previously calculated the attachment force of two coal particles through a liquid assuming that the contact plane between them was formed by a constant number of molecules of the studied alkanes or alcohols (Wójcik et al. 2000) and (Wójcik et al. 200a). The values of the attachment force obtained in this way were bigger than those of the detachment force, which would mean that coal particle were not disrupted from the sediment column. To explain this problem the attachment force between two coal particles through the studied liquid was calculated from the equation

$$F_A = W_{Coh} \cdot 2\pi R \qquad (4)$$

where W_{Coh} is the work of the cohesion of the studied liquid, R is the radius of the contact plane between two coal particles.

The attachment force for the homologous series of alkanes from hexane to hexadecane and alcohols from methanol to decanol is in the range from $18.6 \cdot 10^{-10}$ N/particle to $23.1 \cdot 10^{-10}$ N/particle and from $20.4 \cdot 10^{-10}$ N/particle to $24.0 \cdot 10^{-10}$ N/particle, respectively as listed in Tab. II A and B, respectively. The attachment force increases with increasing length of the hydrocarbon chain of the liquids which is clearly seen in Fig. 2 A and B where, the attachment and detachment forces as a function of the number of carbon atoms in alkane and alcohol molecules are presented. It appeared that the maximal attachment force was equal to the minimal force (Fig. 2 A and B, Tab. II A and B).

As it is seen in Fig. 2 the difference between the detachment and attachment forces which values are also listed in Tab. I decreases with increasing length of the hydrocarbon chain of the liquids, reaching zero for alkane and alcohol whose work of cohesion is critical. In Fig. 3 A and B the relationship of the reciprocal of the destruction time as a function of the difference between the detachment and attachment forces is plotted. The reciprocal of the destruction time of the coal sediment column structure decreased linearly (Fig. 3) with decreasing difference between the detachment and attachment forces *(ΔF)*.

The curves presented in Fig. 3 should be started from the beginning of the co-ordinate system because for *ΔF = 0* the reciprocal of the destruction time should be zero. As it is seen in Fig. 3 for *1/t = 0* the difference between the detachment and attachment forces is smaller than zero. It is evident that the attachment force results not only from the work of cohesion of the liquid but also from the work of adhesion of coal-liquid.

R. Ogonowski, W. Wójcik , B. Jańczuk
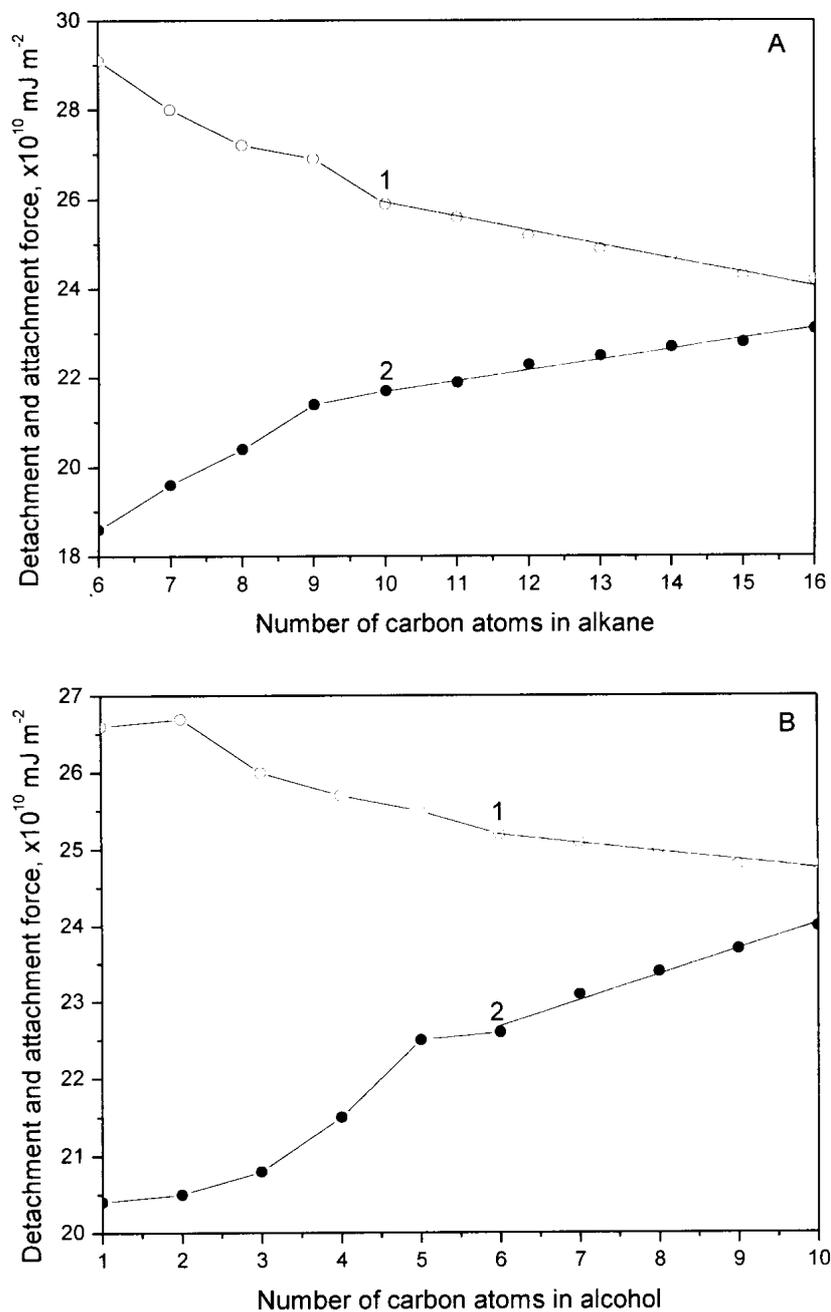
Fig. 2. The detachment (curve 1) and attachment (curve 2) forces as a function of the number of carbon atoms in molecule of alkanes (Fig. 2A) and alcohols (Fig. 2B)
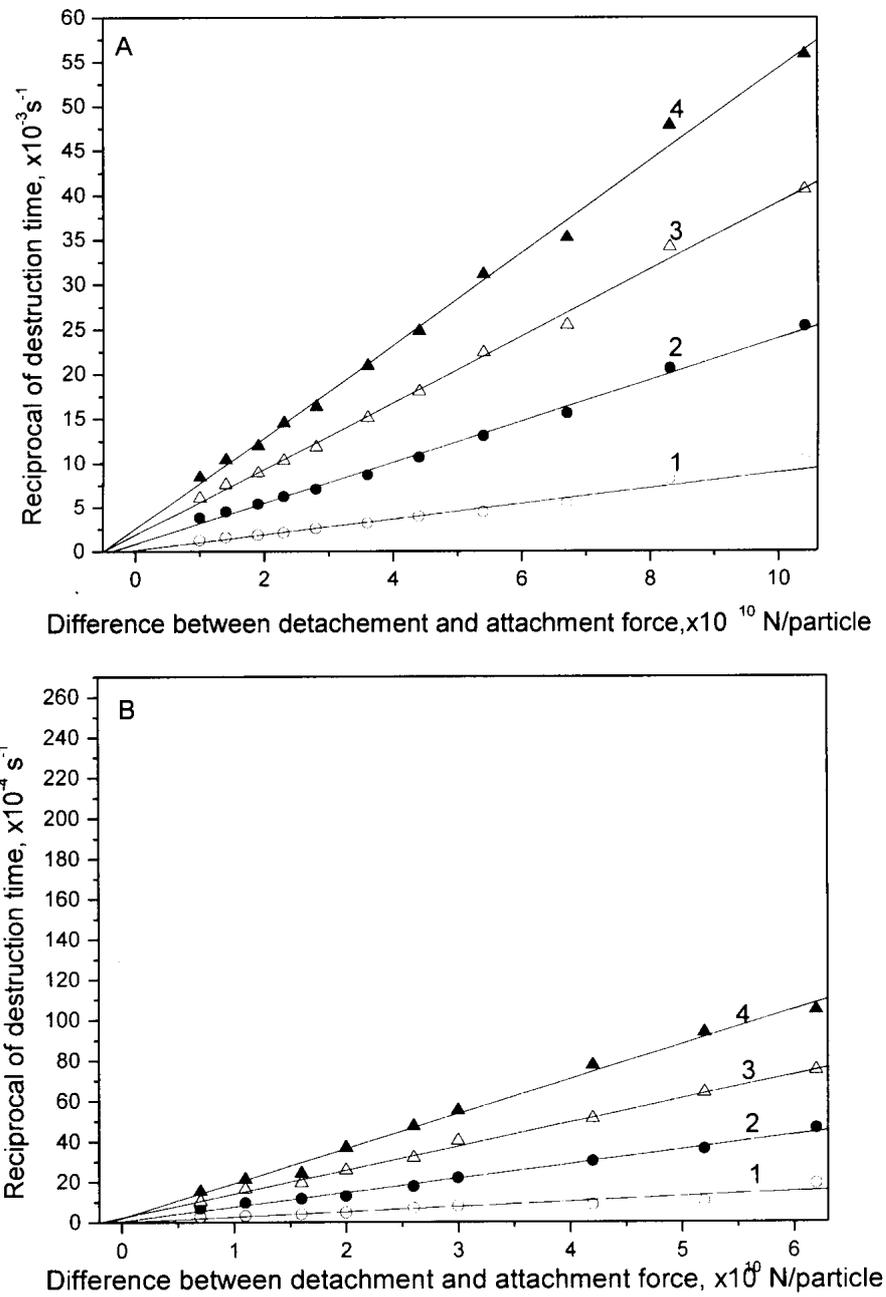
Fig. 3. Relationship of the reciprocal of the destruction time of coal sediment column structure as a function of the density differences between coal and alkanes (Fig. 3A), and coal and alcohols (Fig. 3B)

It is seen from the results presented in Fig. 3 that the curves would start from the beginning of the co-ordinate system if the values of ΔF (Tab. II) were smaller by about $0.4 \cdot 10^{-10}$ N/particle and $0.13 \cdot 10^{-10}$ N/particle for alkanes and alcohols, respectively. To obtain these smaller values of ΔF, the attachment force should be enhanced by $0.4 \cdot 10^{-10}$ N/particle and $0.15 \cdot 10^{-10}$ N/particle for alkanes and alcohols, respectively. Thus the attachment force for alkanes and alcohols is in the range from $19.1 \cdot 10^{-10}$ N/m to $23.6 \cdot 10^{-10}$ N/particle and from $20.55 \cdot 10^{-10}$ N/particle to $23.85 \cdot 10^{-10}$ N/particle, respectively. Then the values of the attachment force per unit of the perimeter length of the contact plane were calculated and listed in Tab. II. As it is seen the value of the attachment force is bigger by 1 mN/m than the work of cohesion of alcohols. It is evident that the detachment of coal particles from the sediment column occurred by disruption of the liquid film present between them. The attachment force between coal particles in alkanes and alcohols is a little bigger than the work of cohesion of the liquid. It means that the origin of the attachment force is the work of cohesion of the liquid and work of adhesion coal-liquid.

CONCLUSION

The presented analysis and discussion of the results of the detachment experiments has clearly shown that detachment of coal particle from one another in the studied liquids occurs by disruption of the liquid film present between them.

The perimeter of the contact plane between two coal particles decreases with increasing length of the hydrocarbon chain of alkanes and alcohols.

Increase of the destruction time of the sediment column structure of coal particles with increasing length of the hydrocarbon chain of the studied liquids results on the one hand from decrease of the detachment force of coal particle and from one another and on other from an increase of the attachment force between them.

The values of the attachment force is determined by the cohesion work of alkane or alcohol and by the adhesion work of coal – studied liquid.

REFERENCES

DERJAGUIN B. V. and ZIMON D. (1961), *Исследование прилипания частиц порошков к плоским поверхностям,* Коллоидный Журнал, Vol. 23, No. 5, 544-551.

DERJAGUIN B. V., MULLER V. M. and TOPOROV Yu. P. (1975), *Effect of contact deformations on the adhesion of particles*, Journal of Colloid and Interface Science, Vol. 53, No. 2, 314-325.

JOHNSON K. L., KENDALL K. and ROBERTS A. D. (1971), *Surface energy and contact of elastic solids*, Proceeding Royal Society London, Ser A, Vol. 324, 301-313.

LEJA J. (1982), *Surface Chemistry of Forth Flotation*, Plenum Press, New York, pp. 571-596.

MAUGIS D. (1992), *Adhesion of spheres: the JKR-DMT transition using a dugdale model*, Journal of Colloid and Interface Science, Vol. 150, No. 1, 243-269.

WAKSMUNDZKI A. and SZYMAŃSKI E. (1965), *Niszczenie struktury słupka sedymentu jako metoda badania wielkości sił zlepienia pomiędzy ziarnami suspensji mineralnych*, Roczniki Chemii, Vol. 39, No. 5, 731-736.

WAKSMUNDZKI A., SZYMAŃSKI E. and CHOJNACKA G. (1965a), *Czynniki wpływające na wielkość sił zlepienia ziaren mineralnych w suspensjach wodnych*, Roczniki Chemii, Vol. 39, No. 5, 895-900.

WARREN L. J. (1975), *Shear-flocculation of ultrafine scheelite in sodium oleate solutions*, Journal of Colloid and Interface Science, Vol. 50, No. 2, 307-318.

WÓJCIK W. and WAKSMUNDZKI A. (1978), *Flokulacyjna flotacja siarki*, Przemysł Chemiczny, Vol. 57, No. 5, 263-266.

WÓJCIK W., JAŃCZUK B. and OGONOWSKI R. (2000), *Interparticle interaction between coal grains through an alkane*, Journal of Adhesion Science and Technology, Vol. 14, No. 8, 1021-1033.

WÓJCIK W., JAŃCZUK B. and OGONOWSKI R. (2000a), *Adhesion of a coal grain to a coal grain in an alcohol*, Journal of Adhesion Science and Technology, Vol. 14, No. 13, 1665-1676.

WÓJCIK W., JAŃCZUK B. and BRUQUE J. M. (2000b), *The destruction time of the sediment column structure as a method for studying the dispersion system,* Powder Technology, Vol. 113, No. 1-2, 1-8.

SADOWSKI Z. (1993), *Selective spherical agglomeration of fine salt-type mineral particles in aqueous solution*, Colloids and Surfaces A:, Vol. 80, No. 2, 147-152.

Ogonowski R, Wójcik W., Jańczuk B., *Wpływ cieczy na oddziaływanie między ziarnami w*ęgla, Fizykochemiczne Problemy Mineralurgii, 35, 33-43, (w jęz. ang.)

Wykorzystując opublikowane wartości czasu destrukcji struktury słupka sedymentu w rurce szklanej dla frakcji ziaren węgla o średniej średnicy 1.5×10^{-4}m, 2.5×10^{-4}m, 3.5×10^{-4}m i 4.5×10^{-4}m, w węglowodorach od heksanu do heksadekanu i alkoholach od metanolu do dekanolu, przeprowadzono badania nad korelacją pomiędzy czasem destrukcji a właściwościami objętościowymi badanych cieczy i węgla oraz międzyfazowymi ciecz-powietrze, węgiel-powietrze i węgiel-ciecz. Na podstawie przeprowadzonych badań stwierdzono, że czas destrukcji rośnie ze wzrostem długości łańcucha węglowodorowego alkanów i alkoholi a maleje ze wzrostem średniej średnicy ziaren węgla. Zmiany czasu destrukcji wynikają z różnicy pomiędzy siłami odrywającymi ziarno węgla od ziarna węgla a siłami adhezyjnymi (zlepienia), które odpowiednio zależą od oddziaływań grawitacyjnych i międzyfazowych. Obliczone siły odrywające, przy założeniu, że ziarna węgla są kulkami, maleją ze wzrostem długości łańcucha węglowodorowego badanych cieczy.

Dla obu badanych szeregów homologicznych stwierdzono liniową zależność pomiędzy odwrotnością czasu destrukcji słupka sedymentu i średnią średnicą badanych frakcji ziaren węgla, pracą kohezji alkanów i alkoholi, ich gęstością, różnicą gęstości węgla i badanych cieczy oraz swobodną energią oddziaływań w przeliczeniu na jedną cząsteczkę cieczy.

Prostoliniowe zależności pozwoliły na wyznaczenie tzw. „krytycznych wartości" takich parametrów jak: średnica ziaren, praca kohezji, gęstość, różnica gęstości i swobodna energia oddziaływań dla nieskończenie długiego czasu destrukcji (1/t=0). Dla układów o krytycznych wartościach wymienionych parametrów siły odrywania równe są siłom zlepienia. Biorąc to pod uwagę obliczono promień płaszczyzny kontaktu oraz wielkość sił zlepienia pomiędzy ziarnami węgla w badanych cieczach. Przeprowadzone obliczenia wykazały, że siły zlepienia pomiędzy ziarnami węgla są nieco wyższe od pracy kohezji badanej cieczy. Wynika z tego, że o wielkości sił zlepienia pomiędzy ziarnami węgla w badanych cieczach decyduje nie tylko wielkość pracy kohezji danej cieczy ale również wielkość pracy adhezji węgiel-badana ciecz. Ponieważ praca adhezji jest większa od pracy kohezji, zatem niszczenie struktury słupka sedymentu ziaren węgla zachodzi w wyniku przerwania ciekłego filmu pomiędzy dwoma ziarnami węgla.

Witold A. CHAREWICZ[*], Zhu CHAOYIN[**], Tomasz CHMIELEWSKI[*]

THE LEACHING BEHAVIOR
OF OCEAN POLYMETALLIC NODULES
IN CHLORIDE SOLUTIONS

Laboratory investigations have been undertaken in order to determine the influence of major parameters on the process of leaching of metal values from ocean nodules by means of model "sea-water", that is - acidified chloride solutions. The effect of leaching conditions, i.e. time, temperature, stirring rate, liquid/solid ratio and HCl concentration was examined on leaching efficiency. It was found that concentration of hydrochloric acid greatly influences leaching of metals from ocean nodules. At HCl concentration exceeding 4.0 M and at 30 ^{o}C of temperature all valuable metals were almost completely leached out from the feed. Elevation of the leaching temperature allowed for reduction of the initial HCl concentration. Deep-sea nodules studied in this work exhibited somewhat different leaching behavior that reported in the literature.

INTRODUCTION

Since the 1960's manganese nodules have been recognized as a prospective source of metals and their investigation is stimulated by the progressive depletion of land-based mineral resources (Agarwal et al., 1976). These nodules are an unique and complex deposit requiring an equally unique extraction process suitable to their specific properties. Manganese and iron oxides are the major components of nodules while copper, cobalt and nickel - finely disseminated in the oxide matrix - make their economic value (Sridhar et al., 1976; Agarwal et al., 1976; Fuerstenau et al., 1973). Unfortunatelly, nickel, copper and cobalt are not present in separate mineral phases and therefore they cannot be liberated and beneficiated by means of widespread physical methods. Unique chemical compositions as well as dissemination of Cu, Ni, Co and heavy metals in Fe/Mn oxide phase require the application of chemical reductants to decompose the oxide matrix and to liberate the colloidal particles of metallic compounds for leaching.

*Division of Hydrometallurgy, Institute of Inorganic Chemistry and Metallurgy of Rare Elements, Wrocław University of Technology, 50-370 Wrocław, Poland.
**Mineral and Metallurgical Institute of Changsha, Division of Mineral Processing, Changsha, P.R.China.

Numerous metallurgical processes for recovering of metals from nodules have been investigated in recent thirty years (Han et al, 1974, Han and Fuerstenau, 1975; Han and Fuerstenau, 1980; Fuerstenau and Han, 1983; Jana, 1993; Kohga et al, 1995; Acharya, 1999. High moisture content (30 - 40 %), high porosity (about 60 %), and inability for common physical beneficiation eliminate the application of simple and economically feasible smelting processes for ocean nodules. Hydrometallurgy remains the only rational route of metals recovering from this specific raw material. In rational selection of the most effective hydrometallurgical process, we look for the lowest consumption of reagent and for the best recovery of metals in a relatively simple process. However, processes considered for the commercial application must strictly involve a reducing step of insoluble MnO_2 matrix to soluble $Mn(II)$ ions and releasing the valuable metals for further recovering (Han and Fuerstenau, 1980; Shinn et al., 1984; Kawahara and Mitsuo, 1993; Chen, 1996). Hydrogen chloride, $Fe(II)$ ions, sulfur dioxide and some organic compounds are frequently used as reductans.

The hydrometallurgical processes can be divided into several types with respect to leaching reagents used. For example, hydrochloric acid (Jana, 1993) is comparatively cheap leaching agent and can be obtained from the sea water and reused. Both ammonia (Chen, 1996, Acharya, 1999); and elevated temperature/elevated pressure leaching processes (Han and Fuerstenau, 1975) can selectively extract nickel, copper and cobalt from the feed nodules and therefore, reduce the consumption of leaching reagents.

We now report experimental results on hydrochloric acid leaching, ammonia leaching and elevated temperature, elevated pressure leaching processes of the Pacific's polymetallic nodules. Leaching behavior of these nodules in hydrochloric acid acidified model "sea water " has been studied in detail.

EXPERIMENTAL

A sample of polymetallic nodules was taken from northeastern Pacific's subequatorial part of Clarion/Clipperton Fracture Zone (CCZ). Particularly, nodules from eastern nodule-bearing area of CCZ within the Interoceanmetal (IOM) pioneer investor claim. The air-dried nodules, which density was 2.53 g/cm^{3} and bulk density of 1.23 g/cm^{3}, were crushed with a hammer and subsequently ground in the ball mill for about 1 hour. The particle size distribution of ground nodules used as a feed in the leaching experiments is given in Table 1.

Table 1. Particle size distribution of deep-sea nodules

Size fraction	Weight %
-0.045	10.06
-0.071+0.045	38.7
-0.160+0.071	29.27
-0.300+0.160	13.26
+0.300	8.71

Thermal analysis revealed 13.06 % of the moisture content in the examined nodules. Feed material for leaching experiments was the mixture of all particle fractions. Chemical composition of the feed is given in Table 2. Leaching experiments were carried out in a three-necked, round-bottomed glass reactor with the reflux condenser and a stirrer of adjustable stirring rate. Samples of 30 g of nodules were leached in 300 ml of solution. Reagent grade chemicals dissolved in distilled water were utilized during the examinations. The temperature was kept constant using thermostat throughout each test.

Table 2. Chemical composition of polymetallic deep-sea nodules

Element	Cu	Mn	Fe	Ni	Co
Content, % wt.	1.05	22.51	3.82	1.12	0.13

Additional preliminary tests were performed in 0.6 M $NH_3 \cdot H_2O$ + 0.6 M $(NH_4)_2CO_3$ in the presence of SO_2 at temperature – 90 ^{o}C and at liquid/solid ratio - 10:1. A sample of nodules was also leached at 120 ^{o}C and 0.7 MPa of O_2 pressure with liquid/solid ratio of 10:1 and H_2SO_4 added in amount of 0.75 kg/kg of nodules.

After each leaching experiment and after periodical sampling, a solid-liquid separation was performed. The filtered aqueous phase was colorimetrically analyzed for cobalt with 0.20 % of Nitroso-R-Salt and 25 % of CH_3COONa solutions while manganese was determined colorimetrically as MnO_4^- due to oxidation with KIO_4. Moreover, selected solid residues after leaching were digested and analyzed with AAS for nickel, copper, cobalt, manganese and iron to verify the results of leaching.

RESULTS AND DISCUSSION

PRELIMINARY EXPERIMENTS

In order to determine the leaching behavior of examined nodules at conditions previously reported in the literature (Agarwal, 1976; Fuerstenau et al., 1973; Han and Fuerstenau, 1980; Jana, 1993, Sridhar et al., 1976; Kohga, 1995), several checking experiments were performed. The experiments involved hydrochloric acid and sodium chloride leaching, ammonia-SO_2 leaching and high temperature, high pressure sulfuric acid leaching.

Figure 1 shows the recovery versus leaching time plot for cobalt and manganese during the leaching of nodules with hydrochloric acid - sodium chloride aqueous solutions at 30 ^{o}C. The relationships in Figure 1 indicate that about 80% of cobalt and nearly 70% of manganese were extracted after 1.5 hours of leaching of nodules with aqueous HCl + NaCl. The results based on the chemical analysis of the solid residue (9.6 g) after leaching for 3 hours are shown in table 3. The reported results of similar leaching: 99% of copper, 99% of nickel, 93% of cobalt, 92% of iron and 96% of manganese recovery (Jana, 1993), were better than these of above experiment.

Table 3. Leaching recovery of metals in HCl – NaCl solution at 30 ^{o}C

Element	Cu	Fe	Mn	Ni	Co
Assay of residue , %	0.135	3.37	16.69	0.293	0.068
Recovery , %	96.19	71.77	76.27	91.63	83.26
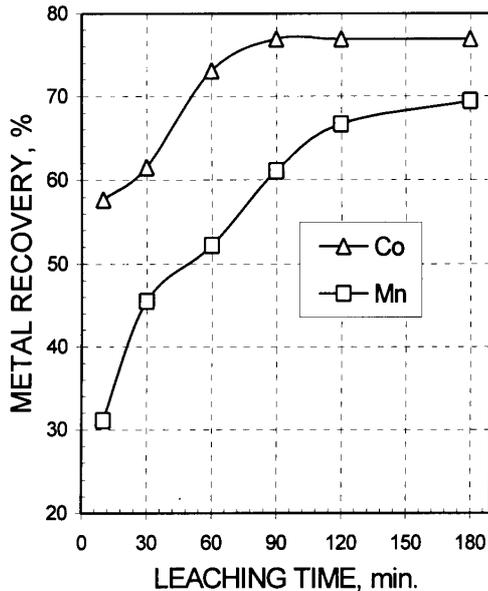
Fig. 1. The recovery – time relationship for HCl - NaCl leaching of nodules
(NaCl - 4.0 M, HCl - 2.75 M, temperature – 30 ^{o}C, stirring rate - 900 rpm, liquid/solid ratio - 10:1)
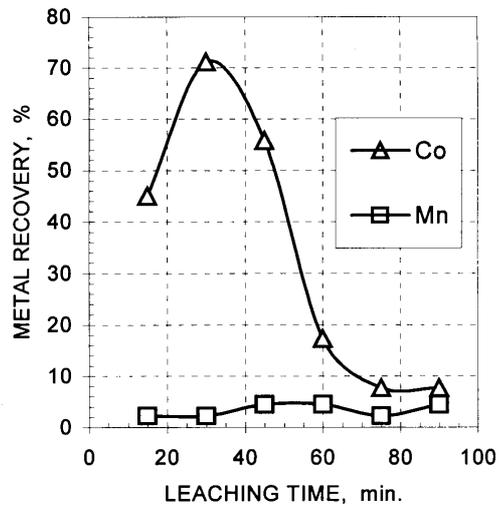
Figure 2. Recovery of Co and Mn during the leaching of nodules in NH$_3$ - SO$_2$ solution.
(NH$_3 \cdot$ H$_2$O - 0.6 M, (NH$_4$)$_2$CO$_3$ - 0.6M, flow rate of SO$_2$ -100 ml/min., temperature – 90 ^{o}C, stirring rate – 900 rpm, liquid/solid ratio - 10:1)

Figure 2 shows the Mn and Co recovery - time plots for ammonia - SO$_2$ leaching of nodules at 90 ^{o}C. The observed relationships evidently show that cobalt was greatly extracted in half an hour while the most of manganese reminded in the solid after leaching. The results based on the analysis of the residue (29.26 g) after leaching for 30 minutes are given in Table 4.

Table 4. Leaching recovery of metals in NH$_3$ – SO$_2$ solution at 90 ^{o}C

Element	Cu	Fe	Mn	Ni	Co
Assay of residue , %	0.638	3.46	21.85	0.821	0.064
Recovery , %	41.30	11.66	5.33	28.50	51.98

Literature data (Kawahara and Mitsuo, 1993) reported different results of nodules' leaching with NH_3 -SO_2 solutions. Recovery of metals increased with the time of leaching and 99% of copper, 98% of nickel, 95% of cobalt, 3% of manganese and 1% of iron was leached after 1.5 hour. Figure 3 reveals that recovery of cobalt increases with the leaching time up to 30 minutes, but thereafter remarkably decreased.

Literature reported recoveries (Kawahara and Mitsuo, 1993) were higher than these in Figure 2. The reason for this discrepancy may originate from cobalt precipitation or adsorption on precipitated Fe and Mn solid compounds (Osseo-Assare and Fuerstenau, 1979) since the final pH observed was as high as 4.8. Moreover, liquid to solid ratio applied in the literature (Kawahara and Mitsuo, 1993) was much higher. Therefore, a different leaching tendency was observed in presented examinations.

The results of leaching of nodules with oxygenated sulfuric acid at elevated temperature and pressure (120 °C and 0.7 MPa of O_2 pressure) based on analysis of the solid residue (71.58 g) after leaching of 100 g of nodules for 3 hours, are given in table 5.

Table 5. Recovery of metals during the elevated temperature and pressure leaching of nodules

Element	Cu	Fe	Mn	Ni	Co
Assay of residue , %	0.289	4.12	24.08	0.532	0.128
Recovery , %	80.30	22.80	23.43	66.00	29.52

Table 6. Leaching recovery of metals in 6 M HCl at 30 °C

Element	Cu	Fe	Mn	Ni	Co
Assay of residue, %	0.03	4.12	0.09	0.009	0.0013
Recovery ,%	99.58	84.25	99.94	99.88	99.85

These leaching results differ from those reported in the literature (Han and Fuerstenau, 1975) where 80 % of nickel, 90 % of copper, 30 % of cobalt, 3.2 % of manganese and 2.0 % of iron was extracted from the feed nodules at 195 C, 0.7 MPa (7 atm) of O_2 and 10 g H_2SO_4/kg of nodules.

The results of preliminary leaching tests reveal that the examined nodules exhibited somewhat different leaching behavior than other nodules described in the literature. Particularly, low metal recoveries were achieved with studied nodules at similar leaching conditions. Nevertheless, general tendencies in metal leachability were similar.

LEACHING WITH HYDROCHLORIC ACID

The leaching systems using hydrochloric acid were systematically examined since their essential practical meaning. Figure 3 shows the concentration versus time relationships for leaching of Co and Mn from nodules with aqueous 6.0 M HCl. It can be observed that recovery of cobalt and manganese slightly increases with leaching

time. Over 95 % of cobalt and 98 % of manganese was extracted after leaching in 6.0 M hydrochloric acid for half an hour at 30 ^{o}C. Table 6 provides the results of leaching based on analysis of the solid residue (4.38 g) after leaching for 2 hours.

The results presented in Table 6 indicate that even at temperature as low as 30 ^{o}C the leaching with 6.0 M solutions of hydrochloric acid resulted in recovering of almost all nickel, copper, cobalt, manganese and the most of iron from the feed nodules.
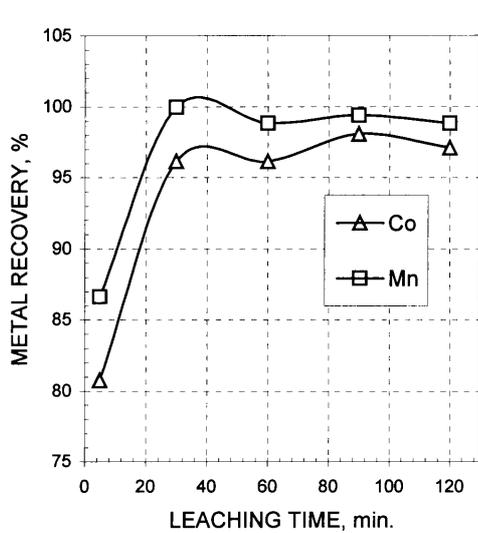
Fig. 3. Recovery of Co and Mn during the leaching of nodules with hydrochloric acid solution.(HCl – 6.0 M, temperature – 30 ^{o}C, stirring rate - 900 rpm, liquid/solid ratio - 10:1)
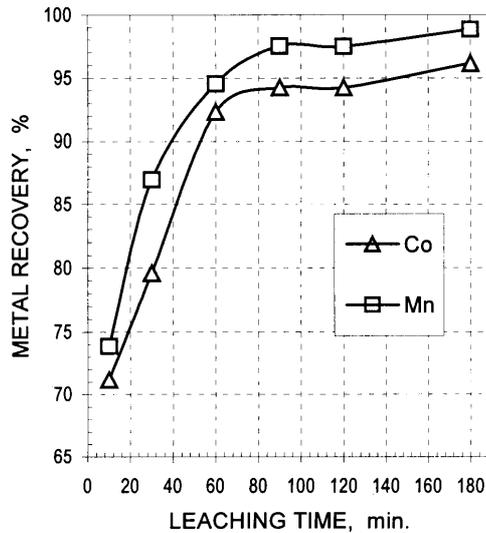
Fig. 4. Recovery of Co and Mn from nodules during the leaching in HCl +NaCl solution. (NaCl 0.55 M, HCl 5M, stirring rate 900 r/min., temperature 30°C, liquid to solid ratio 10:1

Based on the idea that leaching of nodules would be performed on a ship fixed at the spot where the ocean polymetallic nodules are mined, the leaching behavior of nodules in acidified with HCl model "sea water" has been studied in detail. Since the content of Cl^{-} in the ocean water from CCZ is 19.6 g/L, the model " sea water " used in the subsequent tests contained 0.55 M of NaCl.

EFFECT OF LEACHING TIME

The metal recovery vs. leaching time plots for extraction of nodules with a model "sea water" containing 5.0 M HCl is showed in Figure 4. It is well seen that leaching for only 5 minutes leads to more than 70 % of cobalt and manganese recovery. Observed recovery of both cobalt and manganese was therefore high and further increased with leaching time. After 1.5 hour of the process, almost all manganese and

about 95 % of cobalt was leached out from the feed nodules. Extension of the leaching time over 2 hours resulted in additional increasa of the recovery of Co and Mn to about 95 % and 98 %, respectively.

The results of leaching of nodules with model "sea water" containing varying concentrations of HCl are shown in Figure 5. The recovery of cobalt and manganese from nodules increased with the increase of hydrochloric acid concentration at 30 °C. However, this dependence is rather complex. At hydrochloric acid concentration less than 3.0 M recovery of cobalt and manganese was very low. The reason for this was to low concentration of hydrochloric acid required to reduce insoluble Mn(IV) to Mn(II) ions. This reduction step was necessary for cobalt, copper and nickel (associated with iron- and manganese-containing minerals) to be leached.

EFFECT OF HYDROCHLORIC ACID CONCENTRATION

The leaching recovery of cobalt and manganese rose sharply with hydrochloric acid concentration between 3.0 M and 5.0 M and reached above 93 % for Co and above 98 % for Mn in 5.) M HCl.

EFFECT OF STIRRING RATE

Experiments have been performed at stirring rates within the range of 300 - 1100 rpm and the results were presented in Figure 6.
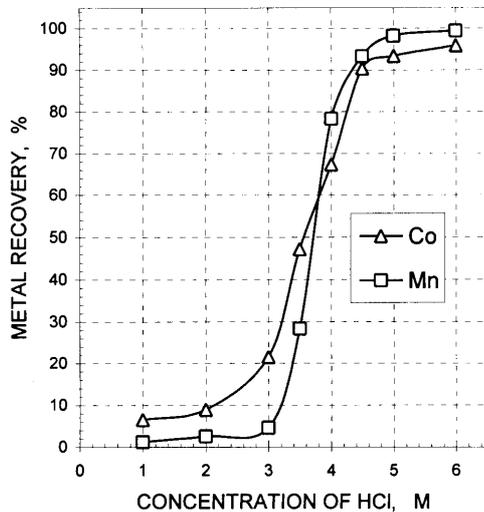
Fig. 5. Effect of concentration of hydrochloric acid on leaching recovery for Co and Mn.. (NaCl - 0.55 M, tem. – 30 °C, stirring rate 900 rpm, liquid/solid ratio - 10:1, leaching time - 1.5 hour)
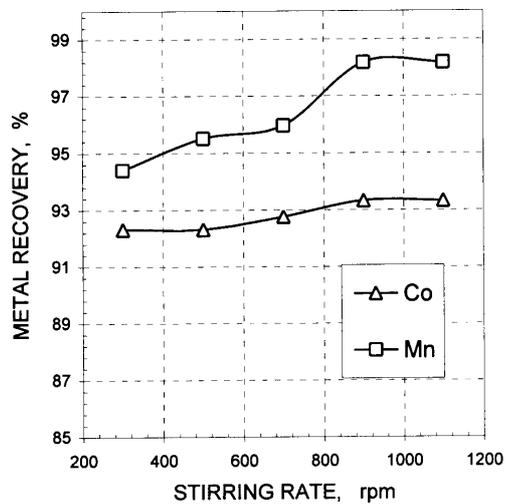
Fig. 6. Effect of stirring rate on recovery of Mn and Co from nodules (HCl + NaCl solution). (NaCl - 0.55 M, HCl – 5.0 M, temperature – 30 °C, liquid/solid ratio - 10:1, leaching time - 1.5 hour)

It was found that recoveries of cobalt and manganese are barely influenced by stirring rate. At 300 rpm more than 90 % of cobalt and manganese was leached out. These recoveries increased gradually with the stirring rate and almost all metals were transferred to the solution at stirring rate 1100 rpm under studied experimental conditions.

EFFECT OF LIQUID TO SOLID RATIO

Liquid to solid ratio in the leaching system was studied within the range from 2:1 to 10:1 (Figure 8). The experimental results revealed that liquid to solid ratio remarkably influenced the observed recoveries of metals from nodules leached with acidified "sea water". The decrease of liquid to solid ratio resulted in remarkable decrease of the recovery of cobalt and manganese. Only about 30 % of cobalt and manganese was recovered from nodules during the leaching when liquid to solid ratio was 2:1 (100 g nodules were leached in 200 ml of solution). There are two possible reasons for the observed effects:
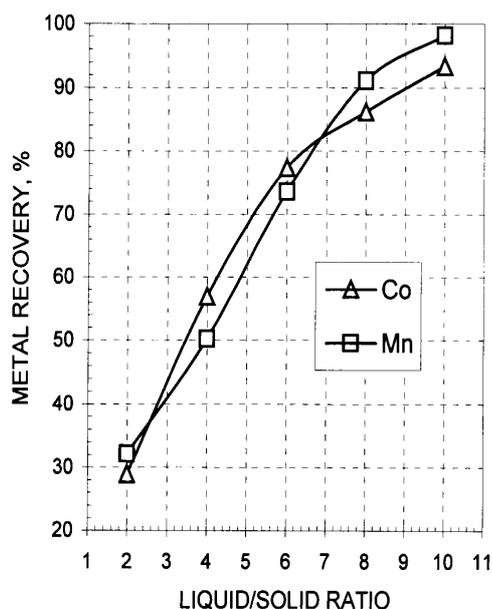
Fig. 7. Effect of liquid/solid ratio on recovery of Co and Mn.(NaCl - 0.55 M, HCl – 5.0 M, temperature – 30 °C, stirring rate - 900 rpm, leaching time - 1.5 hour
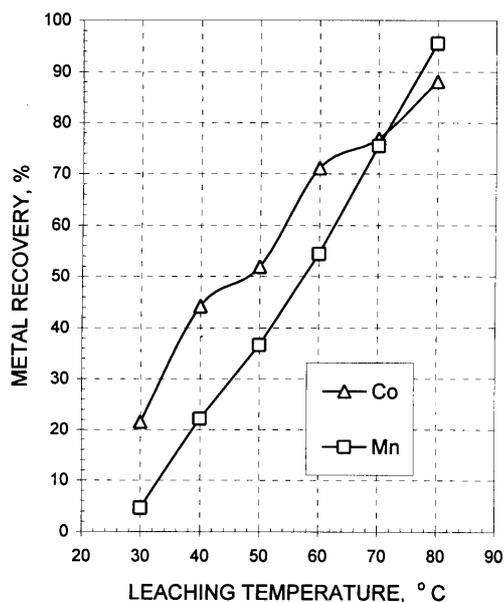
Fig. 8. Effect of leaching temperature on recovery of Co and Mn from nodules. (NaCl - 0.55 M, HCl – 3.0 M, leaching time - 1.5 hour, stirring rate - 900 rpm, liquid/solid ratio - 10:1)

- In a hydrochloric acid solution, insoluble Mn(IV) being in the form of MnO_2, must first be reduced to Mn(II). Then, remaining metals can be leached (there are 0.41 moles of manganese, 0.07 moles of iron, 0.002 moles of cobalt, 0.02 moles of nickel and 0.016 moles of copper in 100 g of nodules). To leach out the entire amount of these metals, 1.92 mol of Cl^- is theoretically required. At liquid to solid ratio 2:1, the amount of Cl^- available was 1.11 mol. This is only a half of Cl^- required to reduce Mn(IV) to Mn(II) and to leach all metals.).
- The Mn(IV) begins to be reduced to Mn(II) only at certain hydrochloric acid concentration. If concentration of hydrochloric acid is lower than this level, the Mn(IV) is hardly reduced to Mn(II). Consequently, copper, cobalt and nickel associated with manganese-containing minerals can not be extracted, except some copper, cobalt, and nickel from the surface of iron- and manganese- containing minerals.

On the other hand, at liquid to solid ratio of 10:1, the recovery of both Mn and Co from the feed nodules has reached 98 % and 93 %, respectively.

EFFECT OF LEACHING TEMPERATURE

The effect of leaching temperature on recoveries of Co and Mn from nodules is given in Figure 8. The observed relationships revealed that leaching temperature substantially influences the leaching of nodules. At temperatures ranging from 30 to 80 ^{o}C and with 3 M HCl in the model "sea water", the recovery of cobalt varied from 21.55 % to about 90 % while the recovery of manganese varied from 4.66 % to 95 %. These results based on the analysis of leaching residue (7.4 g) after leaching for 1.5 hour at 80 ^{o}C are given in table 7.

Table 7. Leaching recovery of metals in 3 M HCl at 80 ^{o}C.

Element	Cu	Fe	Mn	Ni	Co
Assay of residue, %	0.086	2.75	16.16	0.155	0.044
Recovery, %	97.98	82.24	82.36	96.56	91.65

From the experimental results it comes that concentration of hydrochloric acid in the leaching solution could be greatly reduced by means of raising the temperature of leaching. Based on above data, we have examined both two stage counter-current and multiple fresh solid leaching systems under following conditions: leaching temperature – 30 ^{o}C, stirring rate - 900 rpm, leaching time - 1.5 hours, 30 g of nodules, 300 ml of 0.55 M NaCl and 5.0 M HCl aqueous solution.

Semi two-stage countercurrent leaching of nodules reveals that analyses of the final liquid gave recoveries of 43.1 % for Co and 59.6 % for manganese. The results of these experiments, based on the analysis of final solid residue (28.39 g), are given in table 8 .

Table 8. Leaching recovery of metals in HCl – NaCl at 30 ^{o}C during two-step process.

Element	Cu	Fe	Mn	Ni	Co
Assay of Residue, %	0.23	3.08	19.47	0.48	0.07
Recovery, %	91.71	69.48	67.26	83.78	79.62

The multiple, four-stage leaching of fresh solid gave the final solution containing 0.22 g/L of cobalt and 33.5 g/L of manganese. Table 8 shows the weights of feed nodules and volumes of leaching liquid at each stage of the multiple-stage leaching experiment.

Table 9. Weight of feed nodule and volume of leaching liquid during the multiple-stage experiments

Stage number	I	II	III	IV
Feed nodule weight, g	30	29	28	27
Liquid volume, ml	300	290	280	270

CONCLUSIONS

- Concentration of hydrochloric acid greatly influences leaching recovery of metals from ocean nodules. At temperature of 30 ^{o}C, high recovery of metals from raw deep sea polymetallic nodules can be obtained by leaching them with hydrochloric acid solution of concentration exceeding 4.0 M.
- Concentration of hydrochloric acid in the leaching solution can be substantially reduced by raising the temperature or by adding sodium chloride.
- Leaching recovery of metals from raw nodules was barely influenced by stirring rate ranging from 300 rpm to 1100 rpm under experimental conditions.
- Copper, cobalt and nickel can be selectively leached from raw deep-sea polymetallic nodules with ammonia-SO_2 solutions or with H_2SO_4 under high temperature and high pressure. Both manganese and iron remain in the solid residue.
- Studied polymetallic nodules taken from Clarion/Clipperton Fracture Zone at northwestern Pacific exhibit somewhat different leaching behavior than the nodules reported in the literature. Though, general tendencies in metal leachability were similar.

REFERENCES

ACHARYA R., et al., (1999*), Leaching of metals from Indian ocean nodules in SO_2-H_2O-$(NH_4)_2SO_4$ medium, Hydrometallurgy* 53, 169-175.

AGARWAL J.C. et al., (1976), *Processing of ocean nodules: a technical and economic review*, J.Metals, 284, 24-31.

CHEN H. (1996), *Reduction leaching of ocean nodules with waste residue in ammonia-amonium solutions*, Erzmetall, 49(3), 204-206.

FUERSTENAU D.W., HERRING A.P., HOOVER M., (1973), *Characterization and extraction of metals from sea floor manganese nodules*, Trans.Soc.Min.Eng. AIME, 254, 205-211.

FUESRTENAU D.W., HAN K.N., (1983), *Metallurgy processing of marine manganese nodules*, Min.Process.Techn.Rev., 1, 1-83.

HAN K.N., FUERSTENAU D.W., (1980), *Extraction behavior of metal elements from deep-sea manganese nodules in reducing media*, Mar.Min., 2(3), 155-169.

HAN K.N., HOOVER M., FUERSTENAU D.W., (1974), *Ammonia-ammonium leaching of deep-sea manganese nodules*, Int.J.Min.Process., 1, 215-230.

HAN K.N., FUERSTENAU D.W., (1975), *Acid leaching ocean manganese nodules at elevated temperatures*, Int. J.Miner. Process., 2(2), 163-71.

HUBRED G.L., *Manganese nodule extractive metallurgy review 1973-1978*, Marine Min., 2(3) (1980) 191-212.

JANA R.K., (1993), *Leaching of sea nodules in acidic chloride-sulphide media*, Trans.Inst.Min.Metall., Sec.C, 102, C191-194.

KAWAHARA M., MITSUO T., (1993), *Selective leaching of manganese nodules using sulfur dioxide as a reductant*, 1st Int.Conf.Process.Mater.Properties, (Henein H and Oki T. – Editors.), The Min.Metal and Mater.Soc., 471-474.

KOHGA T. et al., (1995) *Recovering iron, manganese, copper, cobalt, and high-purity nickel from sea odules*, J. Metals, (December 1995) 40-43.

OSSEO-ASSARE K., FUERSTENAU D. W., (1979), *Adsorption phenomena in hydrometallurgy. 1. The uptake of copper, nickel and cobalt by oxide adsorbents in aqueous ammoniacal solutions*, Int.J.Min.Process., 6, 85-104.

SHINN D.W., SEDWICK P.N., ZEITLIN H., (1984), *The hydometallurgical behavior of sulfated ferro-manganese nodules*, Mar. Min., 5(1), 57-73.

SRIDHAR R., JONES W.E., WARNER J.S., (1976), *Extraction of copper, nickel and cobalt from sea nodules*, J. Metals, 284, 32-37.

Charewicz W., Zhu Chaoyin, Chmielewski T., *Ługowanie polimetalicznych konkrecji oceanicznych w roztworach chlorkowych*, Fizykochemiczne Problemy Mineralurgii, 35, 2001, 55-66, (w jęz. ang.)

Przeprowadzono badania laboratoryjne nad wpływem najważniejszych parametrów na proces ługowania metali z rozdrobnionych, polimetalicznych konkrecji oceanicznych, pobranych z pola Clarion-Clipperton na Pacyfiku. Konkrecje te zawierają mangan i żelazo jako składniki główne zaś miedź, nikiel i kobalt stanowiły cenne do odzysku metale. Jako czynnik ługujący zastosowano tzw. „modelową wodę morską", tj. zakwaszone roztwory chlorkowe. Określono wpływ warunków ługowania: czasu, temperatury, szybkości mieszania zawiesiny, stosunku masowego fazy ciekłej do stałej (l/s) oraz stężenia HCl na wydajność szybkość ługowania.

Przeprowadzone badania wykazały, że stężenie kwasu solnego jest parametrem, który najbardziej wpływa zarówno na szybkość jak i na wydajność ługowania metali z badanych konkrecji oceanicznych. Dla stężenia HCl powyżej 4.0 M i w temperaturze 30 °C obserwowano prawie całkowite przeprowadzenie metali z surowca do roztworu po ok. 30 minutach ługowania. Podwyższenie

temperatury ługowania do 80 ºC pozwalało uzyskać znaczne podniesienie szybkości procesu i istotnie zredukować stężenie kwasu solnego w roztworze. Zaobserwowano, że zmiana stosunku fazy ciekłej do stałej w zakresie od 3 do 10 prowadziła do wzrostu wyługowania z 30 do 93-97 %. Porównanie uzyskanych wyników z danymi literaturowymi pozwoliło stwierdzić, że choć badane konkrecje oceaniczne zachowywały się podczas ługowania chlorkowego nieco odmiennie w porównaniu z konkrecjami opisywanymi w literaturze, to ich podatność na ługowanie w badanych warunkach daje możliwość odzyskania zawartych w nich metali.

Władysława MULAK[*], Maria CHOJNACKA[*], Dorota WAWRZAK[**]

MECHANISM OF CATALYTIC ACTION OF CUPRIC IONS IN FERRIC SALTS LEACHING OF MILLERITE

Based on experimental leaching results of millerite as well as changes in the composition and microstructure of solid residue surface after leaching with ferric salts acid solutions the mechanism of catalytic action of cupric ions has been proposed. The solid residues were examined using a scanning microscope (SEM), X-ray diffraction, electron microprobe and chemical analyses. It was found that cupric ions added to the ferric chloride solution oxidizes catalitically the sulphide ions on the surface of millerite to the elemental sulphur. During the ferric sulphate leaching of millerite a sulphurrich sulphide layer passivating the surface of the mineral was found, and addition of cupric ions has no influence on the leaching rate.

INTRODUCTION

It has been shown by several investigators that the addition of cupric ions to acidic oxidizing leach solution significantly accelerates the rate of dissolution of sphalerite (Dutrizac, MacDonald 1978; Crundwell 1987), chalcopyrite (Dutrizac 1978) and heazlewoodite (Mulak 1985; Mulak 1987, Mulak 1996).

Dutrizac and MacDonald (1978) studied the effect of $CuCl_2$ addition on dissolution rate of sphalerite disc in ferric chloride solution to which various amounts of $CuCl_2$ has been added. Although the rate increases steadily with copper concentration, the greatest influence was noted in going from 0 to 8 g/dcm^3 of $CuCl_2$. When copper was present in the solution, the surface of the disc became covered with a black film consisting of sphalerite and copper sulphides. Crundwell (1987) found that dissolution of sphalerite in ferric solutions with $CuSO_4$ addition resulted in diminished rate of the leaching.

[*] Institute of Inorganic Chemistry and Metallurgy of Rare Elements, Wrocław University of Technology, Wyb. Wyspiańskiego 27, 50-370 Wrocław, Poland
[**] Institute of Chemistry, Academy of Pedagogy, 42-200, Częstochowa, Poland

Mulak (1985, 1987, 1996) examined the addition of cupric ions on dissolution of heazlewoodite in nitric acid solutions. It was found that in the presence of cupric ions dissolution of Ni_3S_2 in dilute nitric acid solutions is controlled by surface mechanism. There is a suggestion that in moderate acidic oxidative conditions without cupric ions the hydrogen sulphide gas evolved in the first step produces some polysulphides which are more stable thermodynamically than the dissolved Ni_3S_2. Cupric ions eliminate the evolution of H_2S and oxodize it directly on the surface of dissolving sulphide by forming intermediate products which are oxidized faster in the leaching solution than hydrogen sulphide. A catalytic effect of cupric ions was also noticed during the bioleaching of metal sulphides (Ballaster et al. 1989; Ballaster et al. 1990).

The principal aim of presented work was to investigate the mechanism of millerite leaching in acid solutions of ferric chloride or ferric sulphate with cupric ions addition.

EXPERIMENTAL

Preparation of synthetic β-NiS, the equipment used, and this work procedure were described in our previous paper (Mulak 1983). Metal ions concentration in the solution was determined by atomic absorbtion spectroscopy method. Iron ions concentration in the ferric salts leaching was found by dichromate titration. The elemental sulphur content was measured by CS_2 extraction of washed and dried samples. In addition, the reaction residues at various levels of nickel extraction were examined by SEM, X-ray diffraction, electron microprobe and chemical analyses.

RESULTS AND DISCUSSION

FERRIC CHLORIDE LEACHING

Ferric chloride leaching of millerite was tested in 0.2M $FeCl_3$ – 1.0M HCl – 2.0 M NaCl solution at 95°C. After 5 hours leaching 21% of nickel was extracted. The addition of 0.2M cupric chloride to the leaching solution increases the nickel extraction from 21 to 51%. It was found that after the 1 hour leaching with cupric ions addition the fraction of nickel extracted vs. time obeys a linear law (Mulak, Wawrzak 1997). The constant dissolution rate seems to indicate that the reaction area remains constant during the leaching. Similar results have been obtained in catalytic action of cupric and ferric ions in nitric acid leaching of heazlewoodite (Mulak 1987).

Optical observation of the solid residues of millerite after the ferric chloride leaching with addition of cupric chloride shows that the characteristic colour of β-NiS (grey with metallic lustre) changes during the process to that of cupric sulphide, which is black. Due to the extreme thinness of the layer no measurable change in the cupric ions concentration can be detected.

Figure 1 shows some particles of solid residues after the reaction in the ferric chloride solution with the cupric ions addition at $95^{\circ}C$. Two types of elemental sulphur particles are visible in the leached regions: small, discrete granules of $0.5 \div 1$ μm and much more globules of $5 \div 7$ μm in diameter. Many such sulphur particles occur preferentially in certain chosen regions. This may indicate a selective dissolution in isolated active areas. The development of large, well formed, sulphur crystals during the process suggests that sulphur is deposited rather from species dissolved in the leaching solution and it is not formed directly by the immediate attack of millerite.
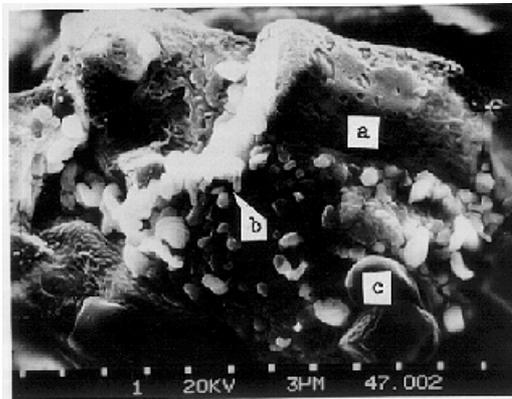
Fig. 1. SEM photograph of millerite leach residue after 5 hours leaching in
$0.2M$ FeCl$_3$ - $0.2M$ CuCl$_2$ – $1.0M$ HCl – $2.0M$ NaCl solution at $95^{\circ}C$;
(a) – leached millerite, (b) – small sulphur granules, (c) – large sulphur granules

We presume the following mechanism:

- step I: acid attack of millerite

$$NiS + 2H^{+} = Ni^{2+} + H_2S(aq) \tag{a}$$

Hydrogen sulphide formed according to eq.(a) dissolves in the leaching solution at the millerite surface and then it is oxidized by cupric ions to the elemental sulphur.

- step II: intermediate products formation

$$2H_2S(aq) + 2Cu^{2+} = Cu_2S + S + 4H^{+} \tag{b}$$

- step III: intermediate products oxidation

$$Cu_2S + 2Fe^{3+} = CuS + 2Fe^{2+} + Cu^{2+} \tag{c}$$

$$CuS + 2Fe^{3+} = Cu^{2+} + 2Fe^{2+} + S \tag{d}$$

It is worth mentioning that the elemental sulphur is formed in two stages: (b) and (d).

During the ferric chloride leaching in the case of absence of cupric ions hydrogen sulphide arising at the millerite surface is oxidized directly by ferric chloride:

$$2H_2S(aq) + 4FeCl_3 = 4FeCl_2 + 4HCl + 2S \qquad\qquad (e)$$

Evidently, the leaching rate in the presence of cupric chloride in the leaching solution is markedly increased. The explanation of this fact seems to be apparent: chloride system consisting of three ions (Fe^{3+}, Cu^{2+}, Fe^{2+}) is more effective than this consisting of two ones (Fe^{3+}, Fe^{2+}). Ferric chloride quickly oxidizes the intermediate cuprous ions and maintains a high activity of cupric ions. This is the way in which the cupric ions act as catalyst in ferric chloride leaching.

FERRIC SULPHATE LEACHING

The leaching was tested in 0.2M $Fe_2(SO_4)_3$ − 1.0M H_2SO_4 solution at 95°C. It was found that after 30 min leaching only 2.5% of nickel dissolved . Unfortunately, an extension of the leaching time from 30 to 300 min increases the nickel extraction from 2.5 to 3.6% only. Similarly, any increasing the sulphuric acid concentration from 1 to 5M has no noticeable effect on the rate of the process. Varying the ferric sulphate concentration from 0.1 to 3 M has no influence on leaching rate of millerite too. Thus, the process is ineffective.
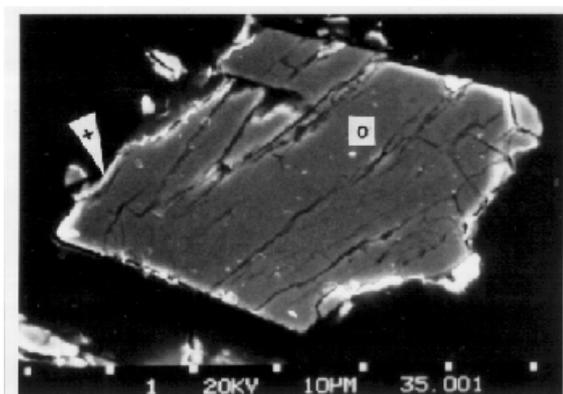
Fig. 2. SEM photograph of millerite particle cross-section after 5 hours leaching in 0.2M $Fe_2(SO_4)_3$ − 1.0M H_2SO_4 solution at 95°C; two different phases – grey and white – are denoted by o and +, respectively.

The residue from the leaching experiments after drying was washed with carbon disulphide. No elemental sulphur was detected. Figure 2 shows a SEM photograph of cross-section of solid residue after 5 hours leaching in 0.2M $Fe_2(SO_4)_3$ − 1.0M H_2SO_4 solution at 95°C. Two different phases are visible – a grey and a white one. The results of electron microprobe analysis of both the phases are shown in Figure 3a and 3b.

The grey part of the particle (marked by a circle in Figure 3a) is characterized by two distinct nickel and sulphur peaks of the same intensity. On the other hand, for the white part (indicated by a cross in Figure 3b) the sulphur peaks dominates indicating a sulphur-rich sulphide phase.
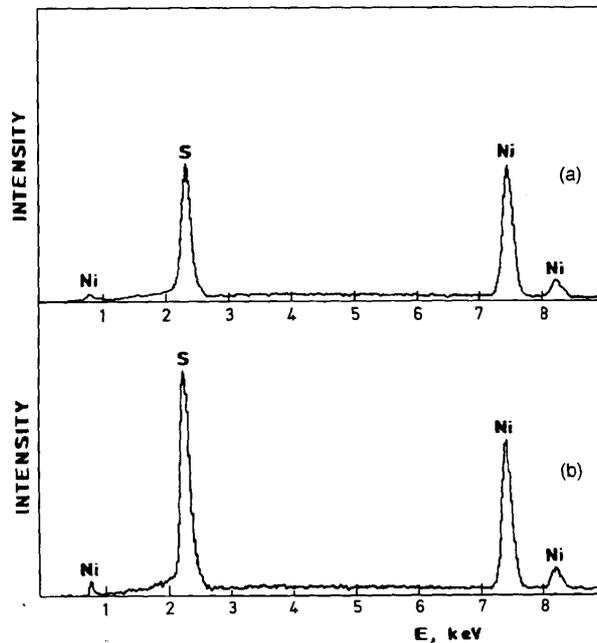
Fig. 3. Microprobe diagrams of the particle shown in Figure 2 for: grey phase (indicated by a circle), white phase (indicated by a cross)

The results of microprobe analyses suggest that the passivating layer is a sulphur-rich one. It is found as a result of modifications inside the solid phase that this layer occurs on the millerite surface during the leaching. The presence of the sulphur-rich sulphide layer passivating the surface of nickel sulphide was also demonstrated by Power (1981) during its anodic dissolution in acid solution within the potential range from 0 to 0.8V. The addition of cupric ions to the ferric sulphate solution has no influence on leaching rate of millerite.

CONCLUSIONS

Based on experimental leaching results of millerite as well as changes in composition and microstructure of surface of solid residue after leaching with ferric salts acid solutions the mechanism of catalytic action of cupric ions has been proposed. The solid residues were examined using a scanning microscope (SEM), X-ray diffraction, electron microprobe and chemical analyses. It was found that cupric ions added to the ferric chloride solution eliminate the evolution of hydrogen sulphide oxidizing it directly on the surface of dissolving millerite by forming intermediate products which are oxidized faster by ferric ions than hydrogen sulphide. Leaching of millerite in ferric sulphate solution produces a sulphur–rich sulphide layer passivating the millerite surface and the addition of cupric ions has no influence on the leaching

rate. The main requirement for metal ion to exhibit the catalytic activity appears to be the formation of such intermediate products, which are oxidized by the leaching solution in consequence of which the catalytic ion is reproduced.

REFERENCES

DUTRIZAC, J.E. and MACDONALD, R.J.C.: *The dissolution of sphalerite in ferric chloride solutions*, Metal. Trans., 9B, 543-551, 1978

CRUNDWELL, P.K.: *Kinetics and mechanism of the oxidative dissolution of a zinc sulphide concentrate in ferric sulphate solutions*, Hydrometallurgy, 19, 227-242, 1987

DUTRIZAC, J.E.: *The kinetics of dissolution of chalcopyrite in ferric ion media*, Metal. Trans., 9B, 431-438, 1978

MULAK, W.: *Kinetics of dissolution of synthetic heazlewoodite (Ni_3S_2) in nitric acid solutions*, Hydrometallurgy, 14, 67-87, 1985

MULAK, W.: *The catalytic action of cupric and ferric ions in nitric acid leaching of Ni_3S_2*, Hydrometallurgy, 17, 201-214, 1987

MULAK, W.: *Metal ions catalysis in acidic leaching of metal sulphides*. In: Changing Scopes in Mineral Processing, M. Kemal, V. Arslan, A. Akar, M. Canbazoğlu (eds), A.A. Balkema, Rotterdam, 1996, pp.495-498

BALLASTER, A., BLÁZGUEZ, M.L., GONZÁLES, F.: *Kinetic study of bioleaching of mineral sulphides: sphalerite and complex sulphide*, Erzmetall, 42, 62-65, 1989

BALLASTER, A., GONZÁLES, F., BLÁZGUEZ, M.L., MIER, J.L.: *The influence of various ions in the bioleaching of metal sulphides*, Hydrometallurgy, 23, 221-235, 1990

MULAK, W.: *Kinetics of dissolution of synthetic millerite (β-NiS) in acidic potassium dichromate*, Hydrometallurgy, 11, 79-89, 1983

MULAK, W. and WAWRZAK, D.: *Leaching behaviour of millerite (β–NiS) in moderate oxidizing and reducing media*. In: Proceedings of the XX Intern. Miner. Proc., Achen 1997, H. Hoberg and H. von Blottnitz (eds), GDMB, Clausthal–Zellerfeld 1997, Vol. 4, pp. 189-198

POWER, G.P.: *The electrochemistry of the nickel sulphides*. I. NiS, Austr. J. Chem., 34, 2287-2296, 1981

Mulak W., Chojnacka M, Wawrzak D., Mechanizm katalitycznego działania jonów miedzi w procesie ługowania millerytu, Fizykochemiczne Problemy Mineralurgii, 35, 2001, 67-72, (w jęz. ang.)

W oparciu o wyniki ługowania milerytu jak również nowe dane eksperymentalne dotyczące zmiany składu i mikrostruktury powierzchni faz stałych po ługowaniu w roztworach soli żelaza (III) zaproponowano mechanizm katalitycznego wpływu jonów miedzi (II) na proces ługowania. Fazy stałe po ługowaniu badano mikroskopem skaningowym, mikrosondą rentgenowską, jak również poddano analizie rentgenowskiej i chemicznej. Ługowanie prowadzono w czasie 5 godz. w roztworach zawierających 0.2M $FeCl_3$ – 1.0M HCl – 2.0 M NaCl w temperaturze 95°C. Stwierdzono, że dodatek 0.2 M $CuCl_2$ w powyższych warunkach ługowania zwiększa wyługowanie niklu z 21 do 51%. Zaproponowano mechanizm katalitycznego wpływu jonów miedzi (II) na proces ługowania. Zgodnie z tym mechanizmem jony miedzi (II) biorą bezpośredni udział w utlenieniu wydzielanego siarkowodoru z utworzeniem produktów pośrednich ulegających szybciej utlenianiu przez jony żelaza (III) niż siarkowodór. Wykazano, że podczas ługowania milerytu roztworami siarczanu żelaza (III) następuje tworzenie się pasywnej warstewki polisiarczku niklu na powierzchni milerytu. Dodatek jonów miedzi (II) do roztworu siarczanu żelaza (III) nie wpływa na szybkość ługowania milerytu. Warunkiem koniecznym, aby jony miedzi (II) spełniały rolę katalizatora w procesie ługowania jest powstawanie takich produktów pośrednich z jonami siarczkowymi, z których roztwór ługujący szybko odtwarza jony miedzi (II).

Janina GRODZKA*, Andrzej KRYSZTAFKIEWICZ*, Teofil JESIONOWSKI*

COMPARISON OF CARBONATE-SILICATE FILLERS MODIFIED WITH VARIOUS PROADHESION COMPOUNDS

Studies were performed on the production of highly dispersed carbonate-silicate fillers by the precipitation procedure. The fillers were subjected to surface modification employing for this purpose either the dry or the wet technique. For the modification various acrylic derivatives and silane coupling agents were used. The obtained products showed variable hydrophobic character and particle homogeneity. The modified and the unmodified carbonate-silicate fillers were used in facade acrylic paints and in silicate paints. Application of the fillers promoted production of facade acrylic paints of properties consistent with the norms an of silicate paints of a good density in the formulation system.

Key words: carbonate-silicate fillers, silane coupling agents, acrylic derivatives, acrylic and silicate paints

1. INTRODUCTION

Despite rich deposits of natural chalk and natural limestones, the synthetic calcium carbonate is still a product which is highly required by multiple users. Also in the nature various types of calcium silicates are encountered (e.g., bentonites, montmorillonites, etc.). Co-precipitated calcium carbonate and calcium silicate should exhaust several requirements, among other high extent of dispersity, low bulk density, well developed outer surface, particle homogeneity, surface activity, defined crystallographic structure, etc.

The principal problem which still awaits solution involves selection of optimum parameters of $CaCO_3$ precipitation, which assure that the planned properties of the product are obtained. According to a widespread opinion, selection of raw materials from which carbonate-silicate filler is precipitated by carbonisation with gaseous CO_2

_____

*Poznan University of Technology, Institute of Chemical Technology and Engineering,
 Pl. M. Sklodowskiej-Curie 2, 60-965 Poznan, Poland, e-mail: Teofil.Jesionowski@put.poznan.pl

exerts significant effect on quality of the product. Literature data permit to conclude (Domka 1979, 1995, Trypuć 1990, Sekutowski 1992) that chemical synthesis of calcium carbonate of the quality which is required by the industry is far from easy. Depending upon the precipitation process, calcium carbonate and calcium silicate form gel-like colloid sediments of carbonate-silicate fillers, which gradually transform into crystallic sediments, consisting of the grains of various polymorphic varieties of $CaCO_3$, i.e., calcite, aragonite, or waterite. The type of crystalisation is determined by conditions of the precipitation (Domka 1979, Krysztafkiewicz 1998, Grodzka 1999, Grodzka 2000).

At the second stage of the process, i.e. at the stage of $CaCO_3$ crystal growth, undergoing when the sediment is left in the original medium, either a further increase may take place in the number and the size of grains of a given variety or the transformation of the unstable waterite crystals into thermodynamically stable varieties, i.e. calcite and aragonite (Krysztafkiewicz 1990).

EXPERIMENTAL

MATERIALS

For production of carbonate-silicate fillers, the following substrates were used:
- Sodium metasilicate (10 wt% solution of M=3.3 modulus)
- Calcium hydroxide (10 wt% solution)
- Carbon dioxide (gaseous).

For surface modification of carbonate-silicate fillers the following compounds were used:
- Acrylic derivatives: acrylic acid and methyl acrylate
- Silane coupling agent:
    - 3-ureidoethylaminopropyltrimethoxysilane (U-165),
    - 3-methacryloxypropyltrimethoxysilane (U-511),
    - N-2-aminoethyl-3-aminopropyltrimethoxysilane (U-15D),
    - n-octyltrimethoxysilane (U-222).

METHODS

Carbonate-silicate fillers were precipitated using 10 wt% solution of calcium hydroxide, 10 wt% solution of sodium metasilicate, the modulus of $SiO_2/Na_2O = 3.3$, and gaseous CO_2 with the flow rate equal 300 cm^3/min. On the other hand, modification of carbonate-silicate filler surface was performed by the following two procedures:
- *Modification in the course of precipitation (the "wet" technique)*
The modification was conducted in such a way that various amounts of an appropriate modifier (1 to 7 weight parts per 100 weight parts of the obtained filler) were added to the reactor in the course of precipitation of carbonate-silicate filler. The

reaction was conducted at $60^{o}C$. The substrates included 10% solutions and gaseous CO_2 was dosed at the rate of 300 cm^3/min.

●   *Modification of precipitated carbonate-silicate fillers (the "dry" technique)*

The carbonate-silicate filler, precipitated from solutions of sodium metasilicate and calcium hydroxide in the presence of gaseous CO_2 (Na_2SiO_3:$Ca(OH)_2$=2:1 (v/v), the temperature of precipitation: $60^{o}C$), was placed in a mixer, adding appropriate amounts of the modifier. The mixing was conducted for 1 h. The silanes were added at 1 to 7 weight parts per 100 weight parts of the filler and acrylic derivatives at 0.5, 1, 2, or 3 weight parts per 100 weight parts of the filler.

Selected samples of the precipitated fillers were subjected also to microscopic analysis, mainly in order to characterise the surface morphology of respective particles and their tendency to form agglomerates. For this purpose, the scanning electron microscope, Philips SEM 515 was used. Sample preparation included formation of a suspension of the filler in tertiary butanol, application of the suspension on the microscope table and 10 min coating with gold atoms on an ionisation plate.

Particle size distribution was also examined using a ZetaPlus apparatus (Brookhaven Instruments Co, USA). The particle size was measured using the dynamic light scattering (DLS) technique. The technique involved weighing out of an appropriate sample, placing it in a small amount of water (0.1 g in 200 cm^3 H_2O) and stabilising it in an ultrasonic bath (50 kHz). The prepared sample was placed in a cuvette and size distribution of carbonate-silicate particles was then measured.

The unmodified carbonate-silicate filler was used as a substitute for titanium white and for the carbonate filler (chalk) in the formulation of the facade acrylic paint *AKRYL LAKMA*. In the studied paint, 10 wt% of the titanium white content in the formulation and the total amount of the chalk filler were substituted by the carbonate-silicate filler.

Carbonate-silicate fillers were used also in the anti-corrosion silicate paints. Composition of the silicate paint included:
-   50 g potassium metasilicate solution, modulus 4.0
-   25 g zinc powder
-   0.5 g pyrogenic silica, Cab-O-Sil
-   5 g carbonate-silicate filler, unmodified or modified.

Time of silicate paint densification was measured. Paint samples were observed for one week.

RESULTS AND DISCUSSION

The samples of carbonate-silicate fillers, precipitated from sodium metasilicate and calcium hydroxide solution using gaseous CO_2 at various temperatures, are listed in Table 1.

Carbonate-silicate filler of best parameters was obtained at $60^{o}C$. The product showed the lowest bulk density, the highest paraffin oil and dibutyl phthalate absorbing capacities and a high value of flow-off point.

Table 1. Physicochemical properties of carbonate-silicate fillers precipitated with calcium hydroxide and sodium metasilicate solutions as well as gaseous carbon (Na_2SiO_3:$Ca(OH)_2$ =2:1)

Temperature [^oC]	Bulk density [g/dm^3]	Flow-off point [$cm^3/10g$]	Dibutyl phthalate absorbing capacity [$cm^3/100g$]	Paraffin oil absorbing capacity [$cm^3/100g$]	Water absorbing capacity [$cm^3/100g$]
40	243	26.5	300	400	250
60	235	26.5	300	450	200
80	282	23.0	250	300	200

Modification of carbonate-silicate filler using either the "dry" or the "wet" technique was conducted using various substances in order to obtain various physicochemical properties of the fillers.

At the first stage, acrylic derivatives, methyl acrylate and acrylic acid were used for modification. The derivatives were introduced to the system in the course of precipitation, preserving the remaining conditions of the process. Samples of carbonate-silicate fillers, precipitated in the presence of acrylic derivatives, are listed in Table 2. As compared to acrylic acid, methyl acrylate was less effective in affecting principal physicochemical properties of the carbonate-silicate fillers. Acrylic acid induced higher activity of carbonate-silicate fillers: bulk densities of the fillers decreased and the values of their flow-off point increased. The amounts of acrylic acid used for the modification of carbonate-silicate filler evidently affected parameters of the filler. Following modification of the filler with 3 weight parts of acrylic acid, bulk density decreased by more than 25% and flow-off point increased by almost 75% as compared to the unmodified filler.

Table 2. Physicochemical properties of carbonate-silicate fillers precipitated with calcium hydroxide and sodium metasilicate solutions as well as gaseous carbon in presence of acrylic derivatives

Amount of modifying agent [w/w]	Methyl acrylate		Acrylic acid	
	Bulk density [g/dm^3]	Flow-off point [$cm^3/10g$]	Bulk density [g/dm^3]	Flow-off point [$cm^3/10g$]
0.5	296	28.0	263	26.0
1.0	205	32.0	238	30.0
2.0	224	29.0	174	36.5
3.0	236	29.0	175	36.0

Modification with the silanes was conducted both by the "dry" and the "wet" technique. Principal physicochemical parameters of carbonate-silicate fillers following their modification are presented in Tables 3 and 4.

Table 3. Physicochemical parameters of chose sample of carbonate-silicate fillers modified with silane coupling agents ("wet method")

Amount of modifying agent [w/w]	Bulk density [g/dm³]	Flow-off point [cm³/10g]	Dibutyl phthalate absorbing capacity [cm³/100g]	Paraffin oil absorbing capacity [cm³/100g]	Water absorbing capacity [cm³/100g]
U-165 silane					
1	251	20.5	300	250	350
2	289	20.0	200	200	300
5	248	21.0	250	250	300
U-511 silane					
1	296	18.0	200	200	250
2	305	17.5	200	250	200
5	279	23.5	250	250	250
U-15D silane					
1	217	21.5	336	253	275
3	221	26.0	325	276	306
5	231	28.5	277	280	310
7	245	29.0	223	292	320
U-222 silane					
1	216	*	390	210	*
3	255	*	260	216	*
5	270	*	210	235	*
7	265	*	200	250	*

*non-wettable

Following modification with ureidosilane and with aminosilane in particular the capacity of carbonate-silicate fillers to absorb water increased markedly. The respective value reached even 360 cm³/100g. This proved that the adsorption of silanes with the amino group increased hydrophilic character of the modified fillers. Similar relations could be observed (Tables 3 and 4) whether the "wet" or the "dry" technique of modification was applied. Surface modification of carbonate-silicate fillers with octylsilane was most effective in altering surface of the filler from a typically hydrophilic to a hydrophobic one. This was shown by the measurements both the water absorbing capacity and the flow-off point. The surface was demonstrated to be completely unwettable with water.

Size distribution of agglomerates of carbonate-silicate filler, precipitated at 60°C, at the Na_2SiO_3:$Ca(OH)_2$, v/v ratio = 2:1, is presented in Fig.1. Mean diameter of agglomerates was 1,772.4 nm and the polydispersity value amounted to 0.011. As demonstrated by the presented agglomerate size distribution, the unmodified carbonate-silicate filler was characterised by the presence of two agglomerate bands of various intensities.

J. Grodzka, A. Krysztafkiewicz, T. Jesionowski

Table 4. Physicochemical parameters of chose sample of carbonate-silicate fillers modified with silane coupling agents („dry method")

Amount of modifying agent [w/w]	Bulk density [g/dm³]	Flow-off point [cm³/10g]	Dibutyl phthalate absorbing capacity [cm³/100g]	Paraffin oil absorbing capacity [cm³/100g]	Water absorbing capacity [cm³/100g]
U-165 silane					
1	296	18.0	200	200	250
2	305	17.5	200	250	300
5	279	23.5	250	250	350
U-511 silane					
2	356	19.5	250	320	250
5	367	*	150	300	*
U-15D silane					
1	217	25.5	240	225	290
3	247	29.0	230	243	350
5	267	32.5	203	276	360
7	282	33.0	200	296	360
U-222 silane					
1	215	*	380	200	*
3	239	*	265	193	*
5	267	*	260	156	*
7	296	*	250	136	*

*non-wettable

Aggregates		Agglomerates	
Diameter d (nm)	Intensity G(d)	Diameter d (nm)	Intensity G(d)
1170.9	49	2388.8	56
1211.3	79	2471.1	73
1253.1	100	2556.5	63
1296.4	45	2644.8	19
1341.2	16		

Multimodal Size Distribution
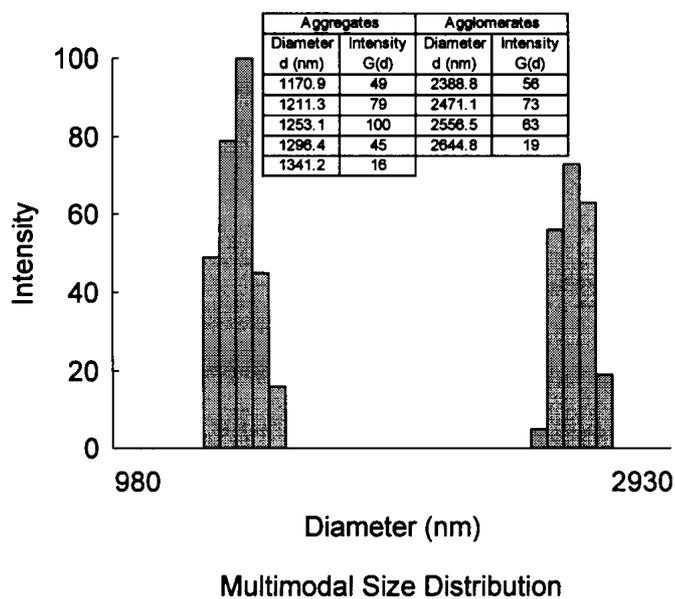
Fig. 1. Particle size distribution of unmodified carbonate-silicate filler

The primary agglomerate (aggregate) band exhibited higher intensity than that shown by the secondary agglomerate band. The primary agglomerate band fitted the agglomerate range of 1,170-1,350 nm (maximum intensity of 100 corresponded to the agglomerate diameter of 1,253.1 nm). On the other hand, the band of secondary agglomerates occupied the diameter range of 2,300 to 2,650 nm (maximum intensity of 73 corresponded to the agglomerate diameter of 2,471.1 nm). Thus, the unmodified sample of carbonate-silicate filler showed low homogeneity.

Following modification with ureidosilane (U-165), conducted in the course of precipitation of the carbonate-silicate filler, more extensive secondary agglomerates formed than those of the unmodified filler. Following modification with 2 weight parts of U-165 silane, mean diameter of agglomerates was 4,878.8 nm and polydispersity value was 0.250. The particle size distributions for the carbonate-silicate filler, modified with 2 weight parts of ureidosilane, is presented in Fig.2. In the distribution, two primary agglomerate bands of lower intensity are present together with a secondary agglomerate band of a higher intensity. The primary agglomerate band is noted within the range of small diameters (340 to 610 nm) and maximum intensity of 80 corresponded to agglomerate diameter of 482.6 nm. On the other hand, the band of secondary agglomerates fitted the range of 7,900 to over 10,000 nm.

Aggregates		Agglomerates	
Diameter d (nm)	Intensity G(d)	Diameter d (nm)	Intensity G(d)
382.2	29	7920.2	99
429.5	51	8899.5	100
482.6	80	10000.0	99
542.3	63		
609.3	44		
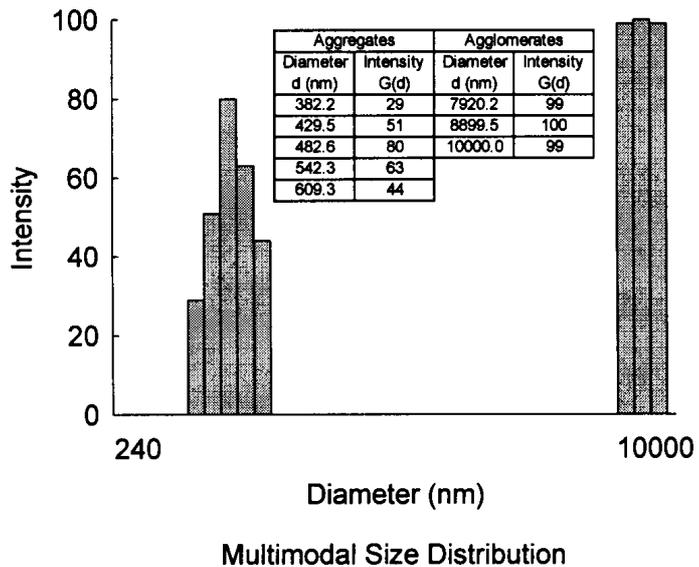
Fig. 2. Particle size distribution of modified carbonate-silicate filler with 2 w/w of U-165 silane

Most important parameters of facade acrylic paints are presented in Table 5. In the table, the parameters of the standard paint were compared with the parameters of the paint in which 10% of titanium white in the formulation and the complete amount of chalk filler were substituted by the precipitated unmodified carbonate-silicate filler (the sample was precipitated at $60^{o}C$ at $Na_2SiO_3:Ca(OH)_2$, v/v ratio = 2:1).

In Table 5, similar parameters were obtained for both studied acrylic paints. Moreover, the acrylic paints containing precipitated carbonate-silicate filler manifested coat quality, coat adherence to the base, water solubility, coating ability and the resistance to flowing off vertical surfaces consistent with appropriate norms.

Effect of modified carbonate-silicate fillers on time of densification of silicate paint. The unmodified and the aminosilane-modified carbonate-silicate fillers were found to form a stable suspension of a silicate paint. This consistency persisted for over a week (in line with expectations).

Table 5. Physicochemical parameters of acrylic paint

Parameter	Norm requarement [PN-C-81914: 1998]	TOP AKRYL LAKMA W	AKRYL LAKMA with modified carbonate-silicate filler
Density, $[g/cm^3]$	1.45-1.55 [$\leq$ 1.6]	1.48	1.48
Viscosity KW10 estimated by time of dripping, [s]	Drips after 10-30″	Drips after 23″	Drips immediately
Viscosity acc. to Brookfield, [cP] (S05, 20RPM)	-	82.5% 16520	16 180
Drying time 1° [min.] 5° [min.]	- [$\leq$ 5h]	(20°C, 58% air humidity) 23′ 28′	20°C, 64% air humidity) 13' 18'
Resistance to wet scrubbing	[$\geq$ 750 advances]	Base exposure after 800 advances	Base exposure after 10,000 advances
Quality coating of white paint	$\leq$ III	I	III

On the other hand, the fillers modified with methacryloxysilane and, first of all, those modified with octylsilane promoted rapid gelation and densification of the paint. Thus, in silicate paints the best effects were obtained using fillers of a hydrophilic character. Following application on metal plates, the obtained silicate paints, containing aminosilane-modified carbonate-silicate fillers, were noted to form ideal coats of the surfaces.

CONCLUSIONS

- Modification of carbonate-silicate filler with acrylic acid promoted increased activity of the surface (flow-off point elevated by 75% as compared to the unmodified filler)
- Following modification with octylsilane (U-222), independently of the applied modification technique, the carbonate-silicate filler exhibited highly hydrophobic character.

- Following modification with ureidosilane (U-165), conducted in the course of precipitation, secondary agglomerates of carbonate-silicate filler were formed and the effect was more pronounced than in the case of the unmodified filler.
- Unmodified and aminosilane-modified carbonate-silicate fillers form stable suspensions of silicate paints.

REFERENCES

DOMKA L., 1979, *Wpływ warunków doświadczalnych na własności fizykochemiczne węglanu wapniowego strącanego*, Wyd. Naukowe UAM, Poznań.

DOMKA L., 1995, *Wpływ parametrów na właściwości fizykochemiczne węglanu wapnia otrzymywanego z kredy naturalnej*, Fizykochemiczne Problemy Mineralurgii, 29, 109.

GRODZKA J., 1999, *Otrzymywanie i modyfikacja napełniaczy węglanowo-krzemianowych*, Fizykochemiczne Problemy Mineralurgii, 33, 45.

GRODZKA J., 2000, *Wpływ silanowych związków wiążących na właściwości napełniaczy węglanowo-krzemianowych*, Fizykochemiczne Problemy Mineralurgii, 88, 95.

KRYSZTAFKIEWICZ A., 1998, *Wpływ warunków doświadczalnych na własności fizykochemiczne napełniaczy węglanowo-krzemianowych*, Fizykochemiczne Problemy Mineralurgii, 35, 89.

KRYSZTAFKIEWICZ A., 1990, *Use of highly dispersed, precipitated carbonate-silicate powders as fillers for elastomers*, Powder Technology, 63, 1.

SEKUTOWSKI D.,1992, Plastic Additives and Modifiers Handbook (ed.: Edenbaum J.), New York, Van Nostrand Reinhold, 450.

TRYPUĆ M. and BUCZKOWSKI R., 1990, *Badania nad otrzymywaniem węglanu wapniowego z płynu podestylacyjnego i wodnego roztworu wodorowęglanu sodowego*, Przemysł Chemiczny, 69, 131.

ACKNOWLEDGEMENTS

J. Grodzka, A. Krysztafkiewicz , T. Jesionowski, *Porównanie napełniaczy węglanowo-krzemianowych modyfikowanych różnymi czynnikami wiążącymi,* Fizykochemiczne Problemy Mineralurgii*, 35, 2001, 73-81, (w jęz. ang.)

Przeprowadzono badania nad otrzymywaniem metodą strącania wysoko zdyspergowanych napełniaczy węglanowo-krzemianowych. Napełniacze te poddawano powierzchniowej modyfikacji, wykorzystując w tym celu metodę „mokrą" i „suchą". Do modyfikacji zastosowano pochodne akrylowe oraz silanowe związki wiążące. Otrzymano produkty o różnym stopniu hydrofobowości oraz jednorodności cząstek. Modyfikowane i niemodyfikowane napełniacze węglanowo-krzemianowe zastosowano w farbach akrylowych fasadowych oraz w farbach krzemianowych. Aplikacja tych napełniaczy przyczynia się do uzyskania farb fasadowych akrylowych o właściwościach zgodnych z normami oraz farb krzemianowych o dobrym stopniu zagęszczenia w układzie recepturowym.

Ludwik DOMKA[*], Lubomira DOMKA[**], Maciej KOZAK[**]

UTILISATION OF ASBESTOS WASTES

The fibrous structure of asbestos, the ubiquitous material in the environment and exhibiting multiple applications, has proven to constitute hazards for human health. For this reason at present utilisation of asbestos has to be stopped, its resources have to be neutralised and reutilised in a safe way. In this paper we shall present studies on asbestos utilisation with the use of selected fluxes in order to alter its fibrous character but preserving fire resistance of the new material.

Key words: asbestos, utilisation, structural change

INTRODUCTION

Asbestos belongs to the dangerous air-polluting agents, ranked third in importance in the list of global scale environment-polluting substances in the Report of the Rome Club on The Limits to Development (World Health Organisation, 1986). The common name of asbestos (from the Greek, asbestos = unextinguished, undestroyable) includes natural silicates of the serpentinite and amphibole groups. The first group include chrysolite ($3MgO \cdot 2SiO_2 \cdot 2H_2O$) while the other contains actinolite ($2CaO \cdot 4MgO \cdot FeO \cdot 8SiO_2 \cdot H_2O$), tremolite ($2CaO \cdot 5MgO \cdot 8SiO_2 \cdot H_2O$), crockidolite ($Na_2O \cdot Fe_2O_3 \cdot 3FeO \cdot 8SiO_2 \cdot H_2O$), antophyllite ($7MgO \cdot 8SiO_2 \cdot H_2O$) and amosite ($5.5FeO \cdot 1.5MgO \cdot 8SiO_2 \cdot H_2O$). All the mentioned varieties differ in respect to physical and chemical traits, which reflects both the type of deposite and conditions which prevailed when the asbestos was formed.

---

 * Technological Centre, Adam Mickiewicz University, Grunwaldzka 6, 60-780 Poznań.
   Asbestos Handler Certificate (04713) New York and (10254) State of New Jersey Department
   of Labor Office of Asbestos Control and Licensing.
 ** Department of Environmental Education, Adam Mickiewicz University, Słowackiego 20,
   60-823 Poznań.
*** Department of Macromolecular Physics, Adam Mickiewicz University, Umultowska 85,
    61-614 Poznań.

Apart from its fibrous structure, all asbestos varieties exhibit extensive resistance to physical forces, mechanical strength, high resistance to tearing, temperature changes and to action of corrosive substances. They exhibit low electrical conductance, high elasticity, specific sorptive and isolating properties. Due to these properties, asbestos finds multiple applications. Its presence can be noted in over 3,000 industrial products (Domka et al 2000; Wachowski and Domka 2000).

In the human environment, asbestos originates, first of all, from:

- natural deposits, from which asbestos is washed off with the outflowing waters (asbestos impurities are encountered in exploited deposits of coal, copper ores, construction stones, etc);
- asbestos processing (e.g., in mines, industrial works, wastes formed in the course of production of articles containing the fibrous material);
- utilised asbestos products (asbestos dust is released to air during corrosion of asbestos-cement or eternit panels, upon abrasion of brake and gear box discs, from heating, ventilation, air-conditioning appliances, from house elevations and isolation).

The mineral fibres may penetrate human organism through the respiratory tract, alimentary tract or through the injured skin. The first of the penetration pathways has received the greatest attention. The stable, chemically resistant fibres of the mineral puncture walls of pulmonary alveoli, lead to inflammatory conditions, tissue hyperplasia and to further, life-threatening conditions. Together with the asbestos fibrils, the organism may be penetrated by fibre surface-adsorbed hazardous aromatic hydrocarbons (e.g., benzo(a)pyrene). Human populations exposed to asbestos manifested numerous clinical signs/symptoms, radiological alterations, impoverished pulmonary function, appraised by the pulmonary function tests. The resulting diseases include asbestosis, lung cancer, pleural or peritoneal mesothelioma, laryngeal tumours and other. The risk of severe disturbances linked to the long-term exposure to asbestos dust corresponds to the size and morphology of incorporated fibrils. Fibres of more than 5 μm in length and of a diameter below 3 μm (according to the norm ISO DP10312, 1995; ISO 13794, 1997; ASTM, 1990) are thought to carry the highest potential to induce malignant tumours in humans and animals. In view of the health and life hazards associated with asbestos exposure, in 1970s many countries have implemented very restrictive regulations, which reduce contact of the material with humans. In the countries regulations have been introduced which forbid utilisation of the fibrous materials. For a long time, air pollution monitoring has been conducted and methods are used to eliminate asbestos-containing materials (mainly using the wet technique with addition of surfactants) by dismantling them, securing all safety precautions, removing them from rooms, installations (central heating, ventilation).

The removed asbestos wastes are secured in such a way as to prevent emission of mineral dusts and fibres to the environment. The so called solid wastes contain below 20% asbestos, strongly fixed in the material. The wastes manifest higher volume

density (exceeding 1,000 kg/m^3) and, due to higher mechanical strength, they present lower risk of asbestos fibre emission, which used to accompany mechanical processing. Product defined as soft asbestos products contain over 20% asbestos and are regarded to be particularly dangerous for health and, as such, they should be removed and utilised in an alternate way. Solid wastes are packed in polyethylene foil of at least 0.2 mm in thickness while the soft wastes, such as asbestos dust or loose asbestos are placed in bags made of a similar foil, hermetically sealed at an elevated temperature or using an appropriate glue. Following the packing, fibrous aerosol content has to be established in the air. The collected waste material should be placed in depositories adjusted for the purpose. Asbestos wastes should be covered by 20 cm thick layer of soil or an inert material. After filling an appropriate chamber, it is additionally covered by HDPE geomembrane of at least 1.5 mm in thickness, which is overlaid by 2 m soil layer.

A new, chemical technique for asbestos utilisation at the site of its manifestation is worth attention, patented and marketed by the American company, Grace (Grace Construction 1999). The applied DMA (Digestion Material for Asbestos) product is based on phosphoric acid, supplemented with fluoride catalyser and surfactants, which induce foaming of the mixture (Mastalski 1999). In order to identify the surfaces subjected to DMA action, a pigment was additionally introduced to the preparation. Surfactant content assures that the deeper layers of the treated material are penetrated and appropriately wetted. The preparation was found to react with chrysotile asbestos and to abolish its fibrous structure while preserving the required characters, like fire-proof property of the new material. Chrysotile asbestos contains alternate layers of silicate and magnesium, oriented according to a cylindrical geometry, which under effect of DMA active component become split. Application of the technique may, to a certain extent, restrict the need for exchange of asbestos-containing elements to new elements which do not contain asbestos. Moreover, the costs associated with utilisation of asbestos wastes and with isolation of the renovated site are lowered (Grace Construction 1999).

In Poland, the health hazards associated with asbestos are particularly grave. Much later than in other countries, the act of 19 June, 1997 (Dz.U. No.101, pos.928), which abolished the use of asbestos-containing products, established the deadline for production of asbestos-cement items at 28 September, 1998. Legal regulations have been worked out which control application and utilisation of asbestos-containing products. In the decision of 17 June, 1998 (Dz.U. No.79, pos.513), the Minister of Labour and of Social Policies established the highest permissible levels and intensities of health-hazardous agents in a work environment. In our country, asbestos-associated hazards are very severe and solution of the problems will probably take several years. For example, in the Szczucin community the total volume of asbestos wastes with the earth masses polluted with the mineral is appraised at 1 million m^3. Volatile asbestos dusts, originating from destruction or modernisation of

buildings constructed of asbestos materials, will continue to present a hazardous source for a long time (Dołegowski, Janczała 1999). In such a situation, the search and design of effective asbestos utilisation techniques is an important and a currently urgent goal. We have attempted to approach the problem in this presentation.

EXPERIMENTAL

The studies were performed on asbestos samples mixed with selected flux. The samples were subjected to elevated temperatures. The zero (standard) sample consisted of asbestos which contained over 95% chrysotile. The asbestos decomposition reaction was conducted in various experimental conditions. The temperature of the reaction varied between 50 ^{o}C to 500 ^{o}C, and the reaction time was 2 to 3 h. Asbestos samples were mixed with selected fluxes, introduced in excess, at the molar ratio of 1.5:1. Two series of experiments were performed.

In the first series, the agents which degraded asbestos structure included the following fluxes: NaF, NH_4F, $Na_2B_4O_7.10H_2O$, H_3BO_3, $H_3PO_4+NH_4F$. The samples were subjected to the temperature of 500 ^{o}C in a muffle furnace.

In the other series of experiments, 4% flux solutions and mineral acids were used, known for their catalytic affect of reactions which take place upon structural alterations in the studied fibrous mineral. In the series, extensively mixed samples in the modifying reagent solutions were left for 24 h at room temperature. Then, the solutions were paper-filtered and the residue on the filter was dried at around 100 ^{o}C. The obtained residue was subjected to a structural analysis. Before microscopic analysis, some of the samples were additionally roasted at 300 ^{o}C.

Morphology of samples was examined by scanning electron microscopy (SEM-515, Philips). The powdered sample, intended for the studies, was dispersed in t-butanol and, following sedimentation on a microscope holder, it was coated with gold using ionisation chamber. The typical magnification ratio was 100-200.

Some asbestos samples were also examined by powder X-ray diffraction analysis using a modified HZG-3 powder diffractometer and CuKa radiation (λ=1.54178 Å). The source of X-ray was X-ray tube mounted on TUR M62 generator operated at 30 kV and 30 mA. Diffraction test were conducted within the t angle of 5-45, at the scanning rate 0.05 ^{o}/s. The identification took advantage of the POWDER data base

RESULTS

Results of morphological analysis of asbestos samples, fused with selected fluxes, are presented in SEM microphotographs (Figs. 1 to 6). As compared to the standard sample (Fig. 1), fusing of asbestos with sodium fluoride (at 500 ^{o}C, Fig. 2) or with boric acid (at 300 ^{o}C, Fig. 3) proved least effective: the fibrous structure of asbestos remained practically unaltered, large chrysotile fibres were seen, of few hundred μm

in length and few to more than ten μm in diameter. Also the fine, particularly dangerous fibres of few to more than ten μm in length and less than 1 μm in diameter remained unchanged. Somewhat better effects were obtained with asbestos samples fused with borax at 300 ºC (Fig. 4). Analysis of morphology of such a sample demonstrated a clearly reduced fine fibrous fraction of asbestos. The best effects were noted for asbestos fused at 500 ºC for 2 and 3 h with borax (Fig. 5) or ammonium fluoride (Fig. 6). The respective SEM microphotograph demonstrated none or sporadic only fine or long asbestos fibres.
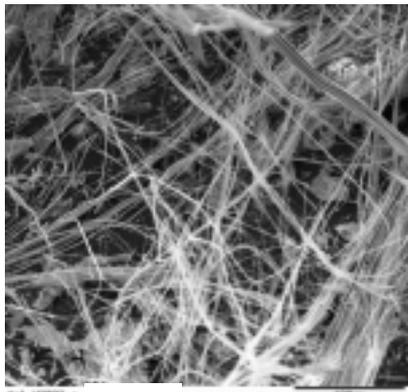
Fig 1. Asbestos (chrysotile) - standard

Fig 2. Asbestos fused with NaF (500 ºC, 2h)

Fig 3. Asbestos fused with H_3BO_3 (300 ºC, 2h)
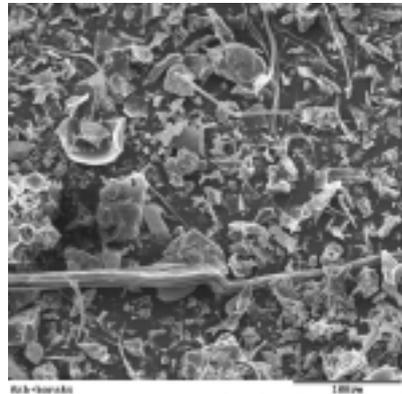
Fig 4. Asbestos fused with borax (300 ºC, 2h)
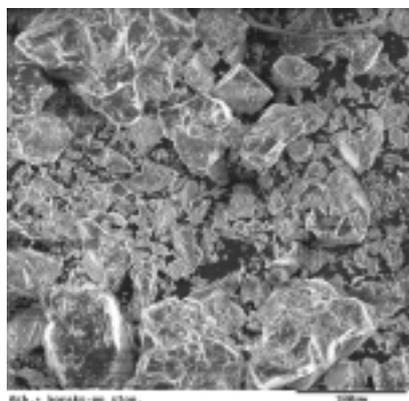
Fig 5. Asbestos fused with borax
(500 ℃, 2h)
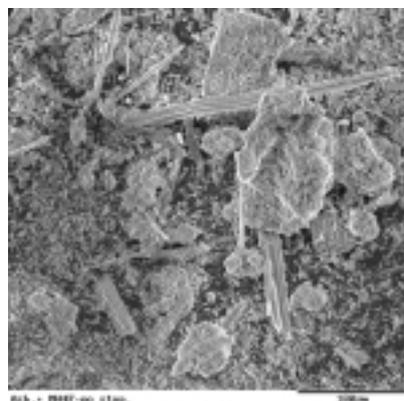
Fig 6. Asbestos fused with NH_4F
(500 ℃, 2h)

Results of microstructure analysis and those on morphology of asbestos samples subjected to degradation in 4% solution of NaF, NH_4F, H_3BO_3 are presented in Figs 7. In most of the samples subjected to degradation process in solution, only weak effects of the modifying agents on asbestos structure could be detected. Both the asbestos fibre structure and content of individual size fractions remained unchanged. The situation did not change when the additional stage of roasting the dried samples was introduced.

The most extensive degradation of asbestos fibrous structure was observed using H_3PO_4 and NH_4F mixture (at the molar ratio of 2:2, respectively, per 3 moles of asbestos). The so degraded sample showed a fully amorphous structure even when no roasting stage was used. (Fig. 8).

The samples of asbestos fused with borax and those fused with phosphoric acid and ammonium fluoride, which showed the most desirable morphology, suggesting transition from the stratified to amorphic structure, were subjected to diffraction studies. The recorded powder diffractograms were compared with the standard data, listed in ASTM files 22-1162, 25-645 and 31-808, characterising diffractive parameters of chrysotile. The course of diffractogram lines and the absence of diffractive peaks comparable of the standard peaks pointed to complete degradation of chrysotile asbestos structure and to amorphic structure of the samples.
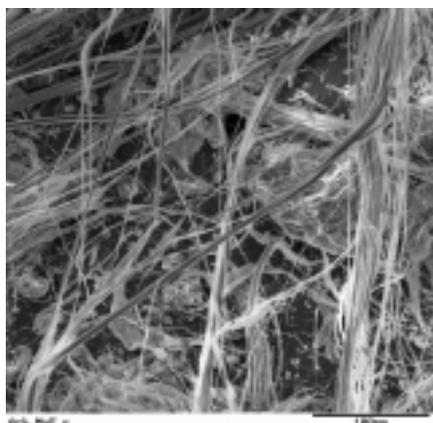
Fig 7. Asbestos after degradation process in solution (NaF)
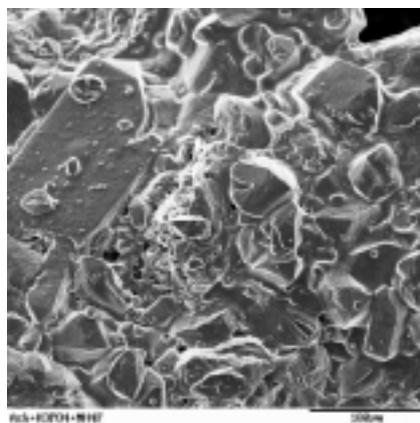
Fig 8. Asbestos after degradation process in solution (NH$_4$F and H$_3$PO$_4$)

CONCLUSIONS

In the conducted series of experiments, effects of selected fluxes were demonstrated on alteration of chrysotile asbestos structure from a fibrous to amorphic one. In asbestos samples with flux supplementation the desired effect was obtained upon roasting at 700 ^{o}C, at lower temperatures the structure was only partially degraded.

Alterations of asbestos structure in samples subjected to action of flux solutions was negligible but was complete in samples subjected to action of a mixture of the flux (NH$_4$F) and phosphoric acid.

REFERENCES

WORLD HEALTH ORGANISATION, (1986), *Environmental Health Criteria 53, Asbestos and other natural fibres*, WHO Press, Geneva.

DOMKA L., KOZAK M., KOZAK A. (2000), *Unieszkodliwianie odpadów azbestowych*. Materiały Ogólnopolskiej Konferencji Szkoleniowej *Unieszkodliwianie i utylizacja komunalnych odpadów niebezpiecznych*. Wisła 11-13 IV 2000", pp. 143-156, Abrys.

WACHOWSKI L., DOMKA L. (2000) *Sources and effects of asbestos and other mineral fibres presence in ambient air*. Pol. J. Environ. Stud. **9(6)**, 443-454.

DOŁĘGOWSKI B., JANCZAŁA S. (1999), *Bhp przy pracy z azbestem,* Gdańsk.

MASTALSKI J. (1999), *Wyroby zawierające azbest - bezpieczne użytkowanie i usuwanie*. Biuletyn Instytutu Gospodarki Odpadami **2**, 3-7.

GRACE CONSTRUCTION PRODUCTS (1999), *DMA^{TM} - Digestion material for asbestos - product information*.

ISO DP10312, (1995) *Ambient air determination of asbestos fibres - direct transfer transmission electron microscopy method*. International Standards Organisation.

ISO 13794, (1997) *Ambient air determination of asbestos fibres - indirect transfer transmission electron microscopy method*. International Standards Organisation.

ASTM, American Society for Testing Materials, (1990), *Standard method for testing for asbestos containing materials by polarized light microscopy*.

Domka L., Domka L., Kozak M., *Utylizacja odpadów azbestowych*. Fizykochemiczne Problemy Mineralurgii, 35, 2001, 83-90 (w jęz. ang.).

Włóknista struktura azbestu, mającego wiele różnorodnych zastosowań co wiąże się z jego wszechobecnością w środowisku, okazała się zagrożeniem dla zdrowia człowieka. W związku z tym obecnie, ważnym problemem jest wycofywanie azbestu z użytkowania, unieszkodliwianie go i utylizacja. W niniejszym opracowaniu zaprezentowano badania nad utylizacją azbestu przy wykorzystaniu wybranych topników celem zmiany jego struktury włóknistej przy zachowaniu cech ognioodporności nowego materiału. Próbkę wzorcową stanowił chryzotyl. Jako topniki zastosowano związki znane z katalitycznego wpływu na przebieg zachodzących reakcji przy zmianie minerału. Były to: NaF, NH_4F, $Na_2B_4O_7 \cdot 10H_2O$, H_3BO_3, $H_3PO_4 + NH_4F$. Najlepszy wynik w postaci zmiany struktury uzyskano dla prób azbestu stapianego w temperaturze 500 ºC w ciągu 2 i 3 godzin z boraksem, kwasem fosforowym oraz mieszaniną kwasu fosforowego i fluorku amonu. Dokumentują to mikrofotografie SEM.

Henryk KUCHA, Renata CICHOWSKA[*]

PRECIOUS METALS IN COPPER SMELTING PRODUCTS

Mineralogical and geochemical research was carried out on shaft slags, converter slags, suspension slags and copper matte from the Legnica-Glogow Copper Region. Silver appears as small metallic inclusions in metallic Cu, metallic Pb is found in both in copper matte as well as metallic and sulphide droplets in slags. Silver occurs also as solid solution in metallic Cu and as Pb-Ag alloys. The main gold carriers are metallic phases: silver, lead and copper. The main carriers of Pd and Pt is metallic silver and metallic copper.

INTRODUCTION

The copper ore-deposit located in the Legnica-Glogow Copper Region is a polimetallic deposit. Copper is associated with following elements: Fe, Pb, Zn, Ni, Co, Mo, Ag, Au, Bi, Ga, Ge, Hg, In, Re, Sb, Se, Sn, Te, Tl, V and platinum group metals (Kucha 1981, 1983, Banaś et al. 1976). In the whole process of metal production they do not have significant importance, but many of them are enriched, mainly during the flotation, metallurgical and refining processes (Rapacz 1998).

Precious metals, which occurs in copper concentrates sometimes form their own minerals or substitutions in others. For example: silver occurs as native silver, Ag-Cu sulphides or substitutions in bornite & chalcocite (Salamon 1979). Gold forms its own minerals or substitutions in arsenides, antimonides, sulphides, organic matter, arsenates and oxysulphides (Kucha 1982, 1990), behave in similar way to the platinum group metals (Kucha 1976, 1982, 1984).

Copper metals is produced in copper smelters, which use two different technologies: multistage smelting - copper smelter in Legnica (HML) and Glogow I (HMG I) (Fig.1); single stage smelting – copper smelter in Glogow II (HMG II) (Fig.2).

*University of Mining and Metallurgy, Faculty of Geology, Geophysics and Environmental Protection,
ul. Mickiewicza 30, 30-059 Cracow, Poland

H. Kucha, R. Cichowska
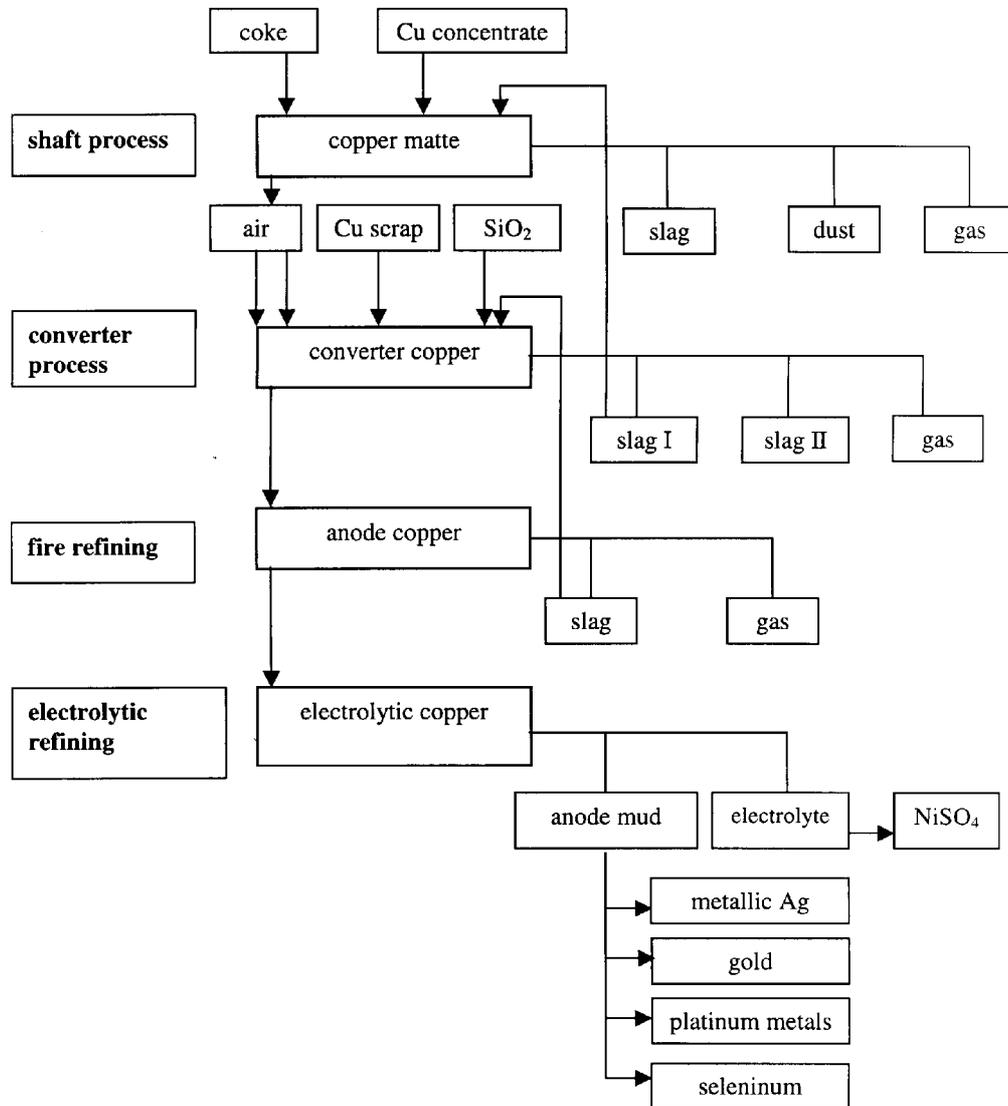
Fig. 1. Schematic diagram of technology in Copper Smelter Legnica and Glogow I
(modified after Karwan et al. 1996)
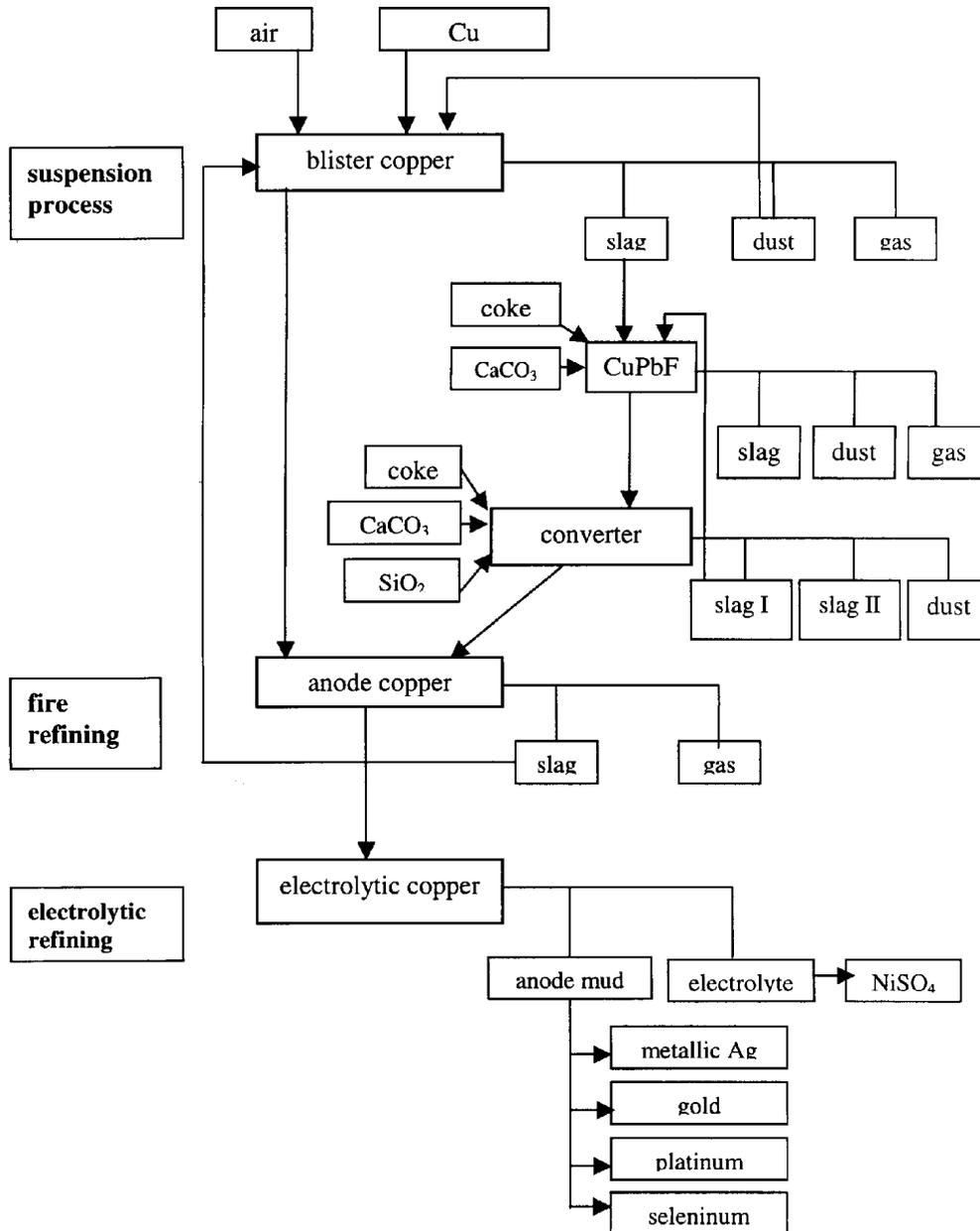
Fig. 2. Schematic diagram of technology in Copper Smelter Glogow II
(modified after Karwan et al. 1996)

During the process of copper concentrate smelting, copper accumulates in the shaft process as a copper matte and converter copper, and in the suspension process as blister and converter copper. Research has shown that part of the copper and other precious elements are lost in the slag by mechanical and physico - chemical ways during these processes (Acuna 2000, Imriś et al. 2000, Sridhar et al. 1997, Simeonov et al. 1996). This causes a loss of precious metals during metallurgical production.

The aim of the study was the mineralogical and geochemical characterisation of the metallurgical slags and copper matte from the Legnica-Glogow Copper Region. Phases hosting precious metals, such as: Ag, Au, Pt and Pd were located and identified, and their chemical composition has been examined.

MATERIALS AND METHODS

Samples of shaft slag from Legnica, converter slag from Legnica and Glogow, suspension slag from Glogow and copper matte from Legnica were studied by reflected light microscopy, scanning electron microscope (SEM), proton induced X-ray emission (PIXE), electron microbe and bulk chemical analysis. Areas for scanning electron microscope (SEM) were selected based on the reflected microscope. The SEM analyses were carried out at AGH using a JEOL ISM 5400 scanning electron microscope. Electron microprobe analyses were carried out at the Institute of Non-ferrous Metals in Gliwice using a JEOL JCXA 733 at 20 kV. The following spectral lines and synthetic standards were used: S K_α, Fe K_α, Co K_α, Cu K_α, Zn K_α, MgO K_α, Ni K_α, Ag L_α, As L_α, Mo L_α, PbF_2 M_α, Au M_α. All analyses were ZAF corrected. The PIXE analyses were carried out at the Institute of Nuclear Physics in Cracow. The proton energy was 2,5 MeV and beam intensity was up to 5μA, time counting was 20 to 30 min. The beam diameter on the target was about 0,5 mm. Analyses were corrected by "Maestro" software package. Bulk chemical analyses were done at Omac Laboratories Ltd., Loughrea, Ireland by inductively coupled plasma (ICP).

SLAGS

The main component of slag is a glass phase that contains abundant small, oval aggregates of metallic copper, sulphides, Fe-Co alloys, Pb-Ag alloys, spinels, sphalerite, arsenate phases and sometimes olivine and pyroxene or amphibole crystals. The proportion of glass phase to crystalline phase changes widely in different slags. Porosity changes from a single pore to structures similar to pumice (Muszer 1996, Kucha et al. 1998).

METALLIC COPPER

Metallic copper from slag creates small, oval aggregates (Fig.3). Analyses in microarea showed that its chemical composition is as follow (%wt): Al 0,05-0,08, V 0,04-0,08, S 0,07-0,21, Mn ≤ 0,02, Fe 0,11-0,67, Co 0,03-0,17, Ni 0,03-0,16, As up to

0,06, Ag 0,05-0,41, Zn 0,05-0,2, Pb 0,09-0,33 (Tab.1). Sometimes metallic Cu from suspension and converter slags (HMG II) contains detectable gold. Gold concentration in suspension slag are from 0,225±0,04 to 0,304±0,03 and in converter slag from 0,016± 0,009 to 0,024±0,009 (Tab.2).

SULPHIDES

Copper sulphides from slags are similar in composition to chalcocite and half-bornite (Kucha et al.1998). Sulphides similar to Cu_2S very often contain inclusions of metallic silver, metallic copper, Fe-Co alloys, and Pb-Ag alloys (Fig.4, 5). Metallic silver from converter slag (HL) contains (%wt.): up to 0,75 S; 1,42-2,44 Fe; up to 0,64 As; 3,66-4,73 Pd; up to 0,41 Sb; up to 0,73 Te; up to 1,01 Au; up to 0,74 Hg and up to 1,88 Bi (Cichowska & Kucha 2000). Fe-Co alloys are reach in Ni, Cu and As. Pb-Ag alloys are very small and difficulty to examine.

ARSENATES

Their chemical composition is close to $CaAsO_4$. They create big crystals and contain from 3,01 to 3,88 %wt. of S; from 28,36 to 29,76 %wt. Ca; from 0,10 to 0,27 % wt. Fe; 0,23 to 0,65 % wt. Cu; from 31,05 to 33,68 %wt. As; from 2,68 to 3,29 %wt Pb; from 30,05 to 34,03 %wt.O. They have sometimes small admixture of Co, Ni, Ag, Sn and La.

The other phases, such as: spinels, pyroxenes, amphiboles and sphalerite do not contain detectable admixtures of precious metals.

Bulk chemical analyses showed that there is 6 ppm Ag, 9 ppb Au, ≤ 2 ppb Pt and Pd in shaft slag from Legnica and about 40 ppm Ag, 8 ppb Au, ≤2 ppb Pt and Pd in converter slag from Legnica.
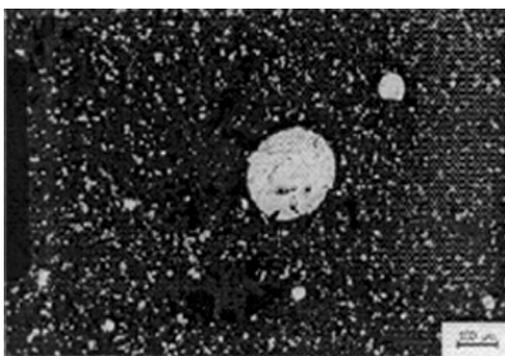
Fig. 3. Microphotograph of suspension slag from HMG II – metallic copper (oval bright) with Fe-Co alloys. Reflected light. Scale bar 100 μm
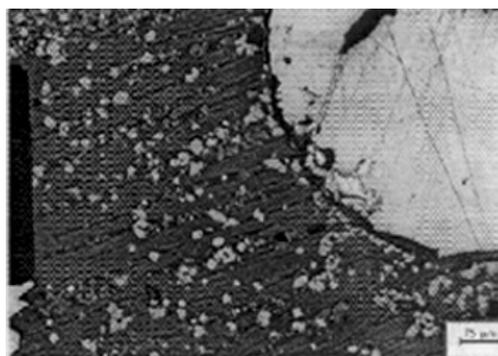
Fig.4. Microphotograph of converter slag from HMG II – chalcocite (oval light-grey) with light metallic copper inclusions. Reflected light. Scale bar 75 μm
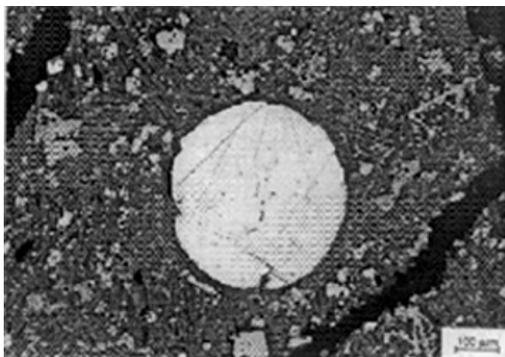
Fig.5. Microphotograph of converter slag from HL – chalcocite (oval light) with light metallic silver inclusions. Reflected light. Scale bar 100 μm

Table 1. Chemical composition of metallic copper from slags (%wt.), electron microprobe analyses
(Not detected: Mn ≤0,02)

Sample	Al.	V	S	Mn	Fe	Co	Ni	Cu	As	Ag	Zn	Pb	Σ
5A/1	0,03	≤0,04	≤0,07	≤0,02	0,39	0,17	0,14	99,41	≤0,06	0,03	≤0,05	0,17	100,34
5A/2	≤0,05	0,05	≤0,07	≤0,02	0,36	0,01	0,08	99,56	≤0,06	0,04	≤0,05	0,24	100,34
5A/3	0,08	0,08	≤0,07	≤0,02	0,67	0,02	0,08	96,82	≤0,06	0,26	≤0,05	0,19	98,2
5A/4	0,06	≤0,04	≤0,07	≤0,02	0,57	≤0,03	0,16	97,03	≤0,06	0,12	≤0,05	0,22	98,16
7B/1b	≤0,05	≤0,04	≤0,07	≤0,02	0,06	0,03	0,07	98,51	≤0,06	0,33	≤0,05	0,33	99,35
7B/2b	≤0,05	≤0,04	≤0,07	≤0,02	0,11	0,04	≤0,03	99,71	≤0,06	0,05	≤0,05	0,11	100,02
6A/3b	≤0,05	≤0,04	0,16	≤0,02	0,36	≤0,03	≤0,03	98,71	0,06	0,41	0,3	≤0,09	100
6A/4b	≤0,05	≤0,04	0,21	≤0,02	0,41	≤0,03	≤0,03	99,11	≤0,06	0,24	0,02	≤0,09	99,99

Table 2. Chemical composition of metallic copper. Suspension slag (X26037G/3**,** X26037H/3, X26037I/3) and converter slag (X26A37P/5, X26037L/7) from HMG II. PIXE analyses [%wt.]

Elements	X26037G/3	X26037H/3	X26037I/3	X26A37P/5	X26037L/7
Ca	0,054 ±0,004	0,078 ±0,007	0,108 ±0,006	0,005 ±0,002	0,012 ±0,003
Cr	0,119 ±0,008	0,053 ±0,010	0,111 ±0,010	0,027 ±0,008	0,026 ±0,005
Fe	12,718 ±0,060	16,368 ±0,081	17,853 ±0,074	6,130 ±0,050	2,713 ±0,030
Ni	≤0,005	≤0,005	≤0,005	0,583 ±0,050	0,120 ±0,020
Cu	32,324 ±0,120	36,294 ±0,152	41,692 ±0,140	60,604 ±0,215	28,236 ±0,080
Br	0,033 ±0,005	0,214 ±0,006	0,304 ±0,031	0,959 ±0,180	0,838 ±0,081
La	≤0,005	≤0,005	≤0,005	0,066 ±0,020	0,023 ±0,009
Au	0,250 ±0,020	0,225 ±0,040	0,304 ±0,031	0,024 ±0,009	0,016 ±0,009
Pb	2,604 ±0,062	3,485 ±0,070	3,519 ±0,083	33,348 ±0,221	6,935 ±0,090

COPPER MATTE

The main component of copper matte are copper sulphides, which constitute 80 – 95 %, metallic copper 5 – 17 % and Fe-Co alloys, metallic silver, galena, Pb-Ag alloys, Pb-Ni alloys, Pb-Cu alloys and arsenides.

COPPER SULPHIDES

Copper sulphides are the main component of copper matte. There are two different sulphides, one is similar in chemical composition to $Cu_{5,75}Fe_{0,25}S_4$ and other to $Cu_{5,5}Fe_{0,5}S_4$ (Kucha et al. 1998).These sulphides contain (%wt.) Al from 0,10 to 2,86; As from 0,10 to 0,83; Ag from 0,10 to 0,20 and Pb from 0,15 to 2,45.

METALLIC COPPER

Metallic Cu forms veins, oval and irregular droplets of variable sizes (Fig.6). Copper aggregates are from single μm to several cm. Metallic copper contains inclusion of Fe-Co alloys, Pb-Ag alloys, metallic silver, metallic lead and copper oxides. Chemical composition of metallic Cu is shown in table 3. Metallic copper contains admixture of gold, which is associated with lead (Fig.7). The Au content is from 0,08 to 0,39 % wt. Tab.3, 4). There is also platinum in amount of up to 0,113±0,004 %wt.
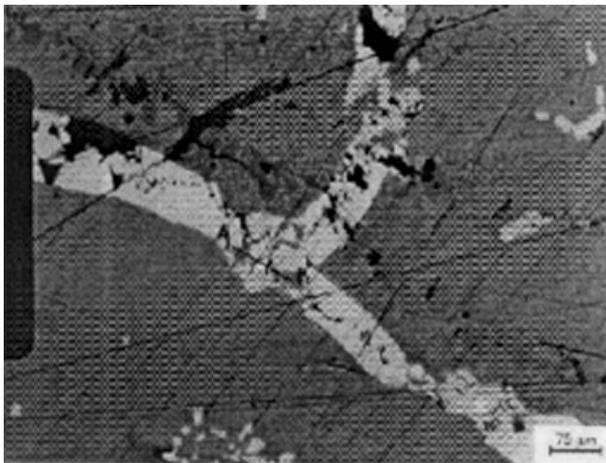
Fig.6. Microphotograph of copper matte from HL –metallic copper. Reflected light. Scale bar 75μm
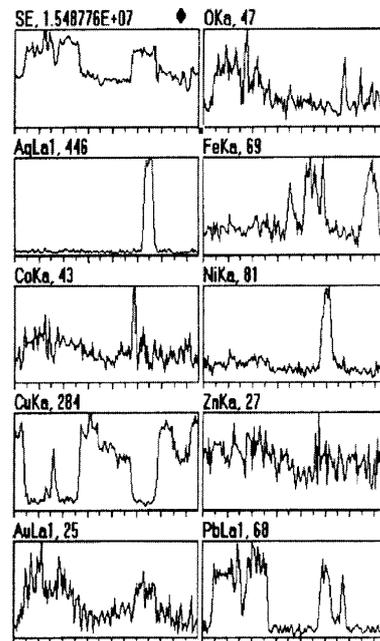
Fig.7. Distribution of O, Ag, Fe, Co, Ni, Cu, Zn, Au, Pb in the copper matte alongside profile A-B marked in fig. 6

METALLIC SILVER

Metallic Ag forms small inclusions in metallic copper. It contains (%wt): Fe 0,26 to 0,57, Co 0,03 to 0,19; Ni 0,03 to 0,15; Cu 2,27 to 5,07, As 0,06 to 0,08 and Pb 0,06 to 6,99 (Tab.5). Metallic silver sometimes has an admixture of gold of up to 0,94 % wt. (Kucha et al. 1998).

ALLOYS

Various metals alloys occur mainly in metallic copper as small droplets. They have small sizes and different chemical composition.
Fe-Co alloys, beside Fe and Co, consist of Ni, Cu, Mo, As and Ag changing from 0,01 to 0,18 % wt.

Pb-Ag alloys have admixtures of Cu, Ni, Co, Fe and sometimes up to 0,48 % wt. Au (Kucha et al. 1998). Pb-Ag alloys like Pb-Ag alloys from slags are very small and difficulty to analyse.

Pb-Cu alloys consist of (%wt.): Pb 26,85 to 72,59; Cu 14,78 to 64,67; Fe 0,91 to 2,29; Co 0,09 to 10,95; Ni 0,15 to 0,81 and Ag up to 0,22. These alloys contain also up to 0,52 %wt. Au, but this problem requires further research.

Pb-Ni alloys consist of (%wt.): Pb 53,61 to 69,79; Ni 21,16 to 26,62; Cu 4,15 to 7,01; Co 0,29 to 2,58; Fe 1,43 to 6,26 and sometimes of up to 7,75 Ag.

METALLIC Pb

Metallic lead creates inclusions in metallic copper. It has small admixtures of Cu, Fe, Cr, Co and up to 0,33 % wt. Ag and up to 0,48 % wt. Au.

Bulk chemical analyses of copper matte showed significant content of: >1000 ppm Ag, 72 ppb Au, 13 ppb Pt and 18 ppb Pd.

Table 3. Chemical composition of metallic copper from copper matte (%wt.),
electron microprobe analyses

Sample	O	Cr	Fe	Co	Ni	Cu	Mo	Ag	Au	Pb	Σ
19A/4	≤0,05	≤0,02	0,30	0,06	1,50	96,28	≤0,06	0,38	≤0,08	≤0,06	98,52
19C/1	≤0,05	≤0,02	0,56	≤0,03	≤0,03	97,14	≤0,06	0,47	≤0,08	≤0,06	98,17
19C/5	≤0,05	≤0,02	1,54	0,45	1,42	94,23	≤0,06	0,54	≤0,08	1,31	99,49
19C/2A	≤0,05	≤0,02	2,12	0,39	0,36	95,87	≤0,06	0,17	≤0,08	≤0,06	98,91
19D/2	2,24	0,91	0,24	≤0,03	≤0,03	96,67	0,23	0,66	≤0,08	≤0,06	100,95
19D/3	1,02	0,22	0,08	≤0,03	≤0,03	94,82	0,16	0,94	≤0,08	≤0,06	97,24
20/4b	≤0,05	≤0,02	0,41	0,08	0,01	98,08	≤0,06	0,30	0,39	0,31	99,58
20/4'b	≤0,05	≤0,02	0,44	0,03	≤0,03	98,03	≤0,06	0,35	0,30	0,20	99,35

Table 4. Chemical composition of metallic copper from copper
matte. PIXE analyses [%wt.]

Elements	X26037S	X26037T	X26037U
Ti	0,014 ±0,005	0,020 ±0,005	0,014 ±0,005
Cr	0,031 ±0,007	0,020 ±0,012	0,012 ±0,008
Mn	0,016 ±0,006	0,017 ±0,007	0,024 ±0,007
Fe	0,030 ±0,009	0,027 ±0,009	0,049 ±0,020
Ni	0,030 ±0,009	0,027 ±0,009	0,049 ±0,020
Cu	87,215 ±0,310	92,586 ±0,320	77,186 ±0,320
Au	≤0,005	0,054 ±0,030	0,112 ±0,020
Pt	0,113 ±0,004	≤0,005	≤0,005
Pb	0,397 ±0,090	0,469 ±0,130	0,498 ±0,061

CONCLUSIONS

The aim of the study was mineralogical and geochemical characterisation of the metallurgical slags and copper matte from the Legnica-Glogow Copper Region. Analyses showed that main carrier of precious metals are metallic copper and metallic lead.

Silver appears as small metallic inclusions in metallic Cu, metallic Pb and in both the copper matte and sulphides droplets in slags. Sometimes metallic Ag contains an increased admixture of gold. In converter slags from Legnica Ag is connected with copper sulphides and contains up to 4,73 %wt. Pd. The presence of Pd in these products suggests that this precious metal escapes to slags. This problem requires father research.

The main carrier of gold is metallic copper, metallic silver, metallic lead and Pb-Ag alloys. The presence of Au is connected with Pb. Gold present in suspension slags is probably entirely recovered. Au-Pb association controls gold behaviour during smelting. Further research on this subject is warranted because the timing and the way of removal of Pb from copper matte may cause significant loss of gold.

Analyses performed so far showed that detectable amounts of Pt occur only in the metallic copper from copper matte. The problem requires further study.

REFERENCES

ACUNA C.M. (2000) *Copper losses and treatment in Chilean smelters.* Metallurgy and Foundry Engineering, vol. 26, no.1, p.9-19

BANAŚ M., KUCHA H., SALAMON W. (1976) *Geochemistry of metals associated with copper mineralization at the Fore-Sudetic Monocline.* Przegląd Geologiczny 5, 240-246

CICHOWSKA R, KUCHA H. (2000) *Metallurgical slags waste from the Legnica-Głogow copper region.* The Fifth International Symposium and Exhibition on Environmental Contamination in Central and Eastern Europe Prague 2000.

IMRIŚ I, REBOLLEDO S, SANCHEZ M, CASTRO G, ACHURRA G, HERNANDEZ F.(2000) *The copper losses in the slag from The El Teniente process.* Canadian Metallurgical Quarterly, vol. 39, no. 3, p.281-290

KARWAN T., KOTARSKI J., PLUCIŃSKI S. (1996) *Hutnictwo cz. VI.* Monografia KGHM Polska Miedź S.A. p. 915 – 1116.

KUCHA H. (1976) *Platinum, palladium, mercury and gold in the Zechstein rocks of the Fore-Sudetic Monocline.* Rudy i Metale, 1, 24-25.

KUCHA H. (1982) *Platinum metals in the Zechstein copper deposits, P*oland. Econ. Geol., 77, 1578-1591.

KUCHA H. (1981) *Precious metal alloys and organic matter in the Zechstein copper deposits, Poland.* Tschermak's Min.Pet.Mitt., 28, 1-16.

KUCHA H. (1983) *Precious metal bearing shale from Zechstein copper deposits, Lower Silesia, Poland.* Trans Instn Min. Metall. (Sect. B: Appl. erth sci.), 92, 72-79.

KUCHA H. (1984) *Palladium minerals in the Zechstein copper deposits in Poland.* Chemie Erde, 43, 27-43.

KUCHA H. (1990) *Geochemistry of Kuperschiefer, Poland.* Geol. Rundschau, 79/2, s.387-399

KUCHA H, PLIMER I, STUMPFL E. (1998) *Geochemistry and mineralogy of gold and PGE's in mesothermal and epithermal deposits and their bearing on the metal recovery.* Fizykochem. Problemy Mineralurgii, 32, s. 7-30.

KUCHA H., PIESTRZYŃSKI A., CICHOWSKA R., RAJCHEL B. (1998) - *Badania nineralogiczne i geochemiczne produktów hutniczych.* Prace specjalne nr.10, s. 201-219

MUSZER A.(1996)- *Charakterystyka petrograficzno -mineralogiczna żużli metalurgicznych z Huty Miedzi Głogów.* Fizykochem. Problemy Mineralurgii 30, 193-205

NAGAMORI M. (1974) *Metal loss to slag: part I. Sulphidic and oxidic dissolution of copper in fayalite slag from low grade matte.* Metallurgical Transactions, vol.5, p.531-538

RAPACZ A.(1998) *Odzyskiwanie metali towarzyszących z koncentratów KGHM.* Prace Specjalne. Zeszyt 10, s.221-239

SALAMON W.(1979) *Ag i Mo w cechsztyńskich osadach monokliny przedsudeckiej.* Prace Miner. O. PAN, s.62

SIMEONOV S.R, SRIDHAR R, TOGURI J.M.(1996) *Relationship between slag sulphur content and slag metal losses in non-ferrous pyrometallurgy.* Canadian Metallurgical Quarterly, vol.35, no.5, p.436-467

SRIDHAR R, TOGURI J.M, SIMEONOV S.R. (1997) *Copper losses and thermodynamic considerations in copper smelting.* Metallurgical and Materials Transactions B, vol. 28B, p.191-200

Kucha H., Cichowska T., *Metale szlachetne w produktach hutniczych miedzi, Fizykochemiczne Problemy Mineralurgii,* 35, 2001, 91-101, (w jęz. ang.)

Celem badań była charakterystyka minralogiczno-geochemiczna żużli i kamienia miedziowego z Legnicko-Głogowskiego Okręgu Miedziowego oraz identyfikacja faz, w których lokują się metale szlachetne.Próbki żużli i kamienia miedziowego były badane przy użyciu mikroskopu do światła odbitego, skaningowego mikroskopu elektronowego (SEM), mikrosondy elektronowej, analizy fluorescencyjnej indukowanej jonami (PIXE) + ICP.

Głównym składnikiem żużli jest faza szklista zawierająca małe, okrągłe wtrącenia miedzi metalicznej, siarczków, stopów Fe-Co, Pb-Ag, spineli, sfalerytu, faz arsenowych, czasem kryształy oliwinu, piroksenów, bądź amfiboli. Głównym składnikiem kamienia miedziowego są siarczki miedzi 80-95%, miedź metaliczna 5-17%, a także stopy Fe-Co, Pb-Ag, Pb-Ni, Pb-Cu i arsenki.

Srebro pojawia się jako małe inkluzje w miedzi i ołowiu metalicznym zarówno w kamieniu miedziowym, jak i w siarczkowych wkropleniach w żużlach. Czasem Ag metaliczne zawiera domieszkę złota. W żużlach konwertorowych z Legnicy srebro związane z siarczkami miedzi zawiera do 4,73 % wag. Pd. Obecność Pd w tych produktach sugeruje ucieczkę tego metalu do żużli. Problem palladu wymaga dalszych badań.

Głównym nośnikiem złota jest miedź metaliczna, srebro metaliczne, ołów metaliczny i stopy Pb-Ag. Obecność Au związana jest z Pb – problem wymaga dalszych badań. Przeprowadzone do tej pory badania wykazały, że Pt związana jest z miedzią metaliczną z kamienia miedziowego. Badania nad obecnością metali szlachetnych w produktach hutniczych miedzi będą kontynuowane.

Tadeusz GLUBA, Andrzej HEIM, Andrzej OBRANIAK[*]

INVESTIGATION OF THE DRUM GRANULATION CONDITIONS FOR MINERAL RAW MATERIAL OF DIFFERENT GRAIN SIZE COMPOSITIONS

Results of investigation on drum granulation of fine-grained materials of different particle size distributions at changing conditions and variable parameters of bed wetting are discussed in the paper. In the experiments fine-grained dolomite flour with different grain size composition and grains < 0.315 mm was used. Changing conditions of bed wetting determined by wetting intensity were applied. The effect of particle size distribution of raw material and wetting of the granulated bed on particle size composition of the obtained product was determined.

Key words: agglomeration, granulation, size distributions, wetting conditions

INTRODUCTION

One of the often applied agglomeration methods is pressure-free granulation carried out in rotary drums with rolling motion of the feed. For most materials a defined amount of wetting or binding liquid is required to be added to the granulated material (Kapur and Fuerstenau 1966, Sastry and Fuerstenau 1973, Newitt and C-Jones 1958). During the rolling motion of a wetted fine-grained bed the solid particles interact with liquid droplets and air. The size and type of forces acting on single material particles and their agglomerates strictly depend on properties of particular media, their relationships and in particular on the particle size distribution of the raw material, the shape of particles and extent of spraying of the wetting liquid.

Research carried out by many authors (Gluba et al. 1990, Pataki et al. 1987, Horvath et al. 1989) proved that properties of the products of wet granulation depend strictly on bed wetting. It was found that in the range of moisture content at which granulation of raw material took place in a proper way, an increase in moisture content of the feed resulted in the formation of a product with larger grain size and

---

*Technical University of Lodz, Department of Process Equipment
 90-924 Lodz, Stefanowskiego 12/16, Poland

more resistant mechanically. It was shown also (Adetayo et al. 1993, Linkson et al. 1973) that properties of the granulated material depend on the grain size and composition of the raw material being granulated.

The conditions of wetting liquid supply to the bed are also very important for the granulation process. During wetting, granulation nuclei are formed and then they grow due to joining subsequent grains of the raw material and also due to combining other nuclei. Thus, the conditions of wetting liquid supply can affect significantly the nucleation process in the bed, and as a result determine properties of the granulated product. Both the time of the wetting liquid supply and the degree of liquid jet split (droplet size) are important. Studies concerning the effect of particle size distribution of the material and wetting conditions on granulated product properties described in the literature do not provide clear explanation because of complexity of the problem. Further studies in this area are required.

Results of the investigation of drum granulation of dolomite flour of different initial grain size compositions at varying conditions of bed wetting in the drum are presented in the paper. The investigation was divided into two parts. In part I an attempt was made to determine the impact of wetting conditions for particular raw materials on the properties of granulated product obtained immediately after supplying of a wetting liquid. Part II included the description of the effect of the amount of liquid supplied to the bed on the properties of granulated product obtained from particular raw materials after a determined granulation period.

EXPERIMENTAL

MATERIAL

The investigated material was dolomite flour with particle diameter < 0.315 mm. On the basis of four initial size groups of this material seven mixtures of different particle size distributions further on denoted by the symbols D1 to D7, were prepared. Each mixture was a starting material for the granulation process. The particle size distribution of the raw materials was determined by a laser size analyzer Analysette 22 (FRITSCH GmbH). A comparison of curves of the total (volumetric) particle size distribution for all raw materials used in the tests is shown in Fig. 1. Basic physical properties of the raw materials used in the tests are summarised in Table 1.

EXPERIMENTAL SET-UP AND METHODS

Granulation was carried out batch-wise in a laboratory drum granulator 0.4 m in diameter and 0.24 m long, at a constant rotational speed of 0.40 s^{-1} and constant mass of raw material in the drum equal 2 kg. The wetting liquid (water) was supplied to the moving bed by a pneumatic nozzle at changing operating parameters which determined liquid jet splitting and wetting duration.
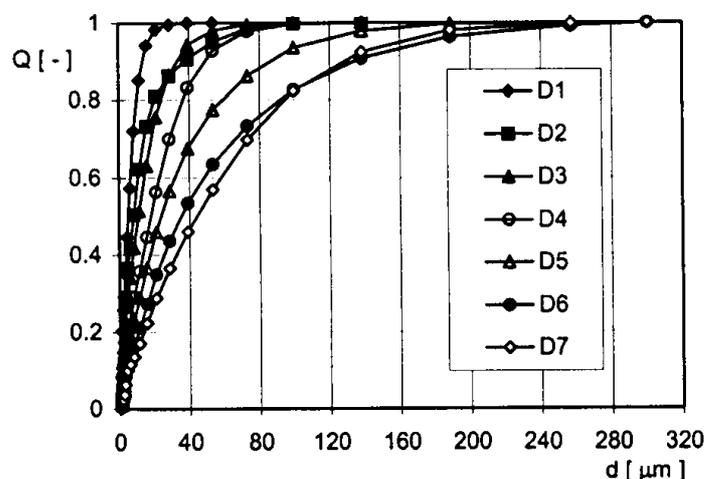
Fig. 1. Comparison of particle size distributions of fine-grained raw materials

Table 1. Physical properties of raw materials

Mater.	ρ_b [kg/m³]	ρ [kg/m³]	ε_m [-]	m_{1m}	M_{2m}	K_{1m}	K_{2m}
D1	916		0,666	6,14	26,4	2,01	1,28
D2	994		0,637	13,7	274,7	5,10	2,20
D3	1153	2741	0,579	14,47	188,8	3,43	1,60
D4	1181		0,569	22,06	366,8	1,80	1,26
D5	1207		0,560	34,37	1186,2	2,90	1,60
D6	1243		0,547	53,08	2906,2	2,47	1,59
D7	1287		0,530	57,49	2437,0	1,21	1,17

The other process parameters applied in the investigation concerned
1. the impact of bed wetting conditions
    − mean moisture content of the bed: 0.14 kg water/kg powder
    − parameters of the pneumatic nozzle:
    − water flow rate $Q_w = 3, 4, 5, 6, 7$ dm³/h,
    − air flow rate $Q_a = 3.5$ m³/h.
2. the impact of the amount of liquid supplied to the bed
    − time of feeding the wetting liquid 132 to 276 s
    − total time of granulation t = 6 min
    − parameters of the pneumatic nozzle:
    − water flow rate $Q_w = 6$ dm³/h,
    − air flow rate $Q_a = 3.5$ m³/h.

In the first part of the investigations, the effect of wetting liquid feed rate to a fine-grained bed on the properties of granulated product obtained from particular raw materials immediately after dosing the wetting liquid was determined. The product

obtained after the wetting had been completed, was distributed into size fractions and dried. The grain size composition was determined on the basis of the mass of each size fraction. In the second part, the effect of the amount of liquid supplied to the granulated feed at constant operating parameters of the wetting nozzle on the grain size composition of the product obtained after a defined granulation period was specified. The amount of wetting liquid was changed by altering the time of its feeding. In the whole experimental cycle a constant total time of granulation t = 6 min was applied. The time was counted from the onset of wetting. When the granulation was completed, the product was divided into size fractions, dried and the particle size distribution was determined.

RESULTS AND DISCUSSION

INVESTIGATION OF THE IMPACT OF BED WETTING CONDITIONS

The process of granulation investigated at the stage of wetting was carried out for seven fine-grained raw materials (dolomite) taking into account five bed wetting parameters. Variable bed wetting conditions were determined by means of wetting intensity calculated from the formula:

$$I_w = \frac{m_w}{m_m \cdot N_w} \tag{1}$$

where: m_w – mass of water fed into the granular bed, kg
  m_m – mass of fine-grained material in the drum, kg
  N_w – number of drum rotations during wetting,
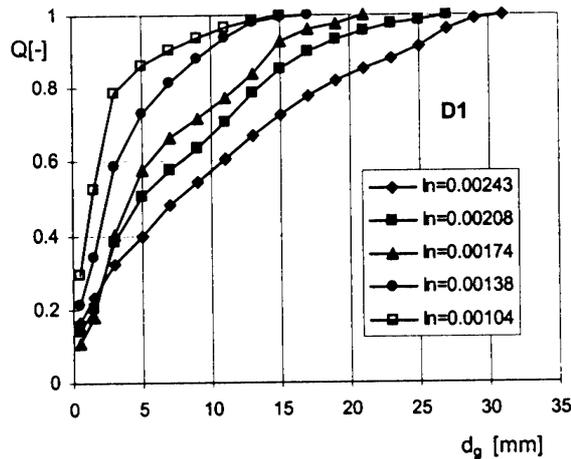
Fig. 2. A comparison of particle size composition of the granulated product obtained from raw material D1 at different values of wetting intensity

Figure 2 shows a comparison of curves for the total grain size composition of the granulated product obtained from raw material D1 at different values of wetting intensity. A similar character and system of grain size composition curves were obtained for other raw materials used in the experiments. It was found on the basis of the curve analysis that an increase of wetting intensity resulted in formation of bigger granules. This relationship is illustrated in Fig. 3 which shows the effect of the bed wetting intensity on the maximum diameter of granules produced from particular raw materials. In the description of particle size distribution of both raw materials and granulated product the theory of moments was applied. Ordinary and central moments of the k-th order were determined on the basis of the distribution function of real particle size distribution:

$$m_k = \sum_{i=1}^{n} d_i^k x_i \qquad (2)$$

$$M_k = \sum_{i=1}^{n} (d_i - m_1)^k x_i \qquad (3)$$

On the basis of central moments the concentration and asymmetry coefficients of the distribution, K_1 and K_2, respectively, were determined from the relationships:

$$K_1 = \frac{M_4}{M_2^2} - 3 \qquad (4)$$

$$K_2 = \frac{M_3}{(M_2)^{3/2}} \qquad (5)$$
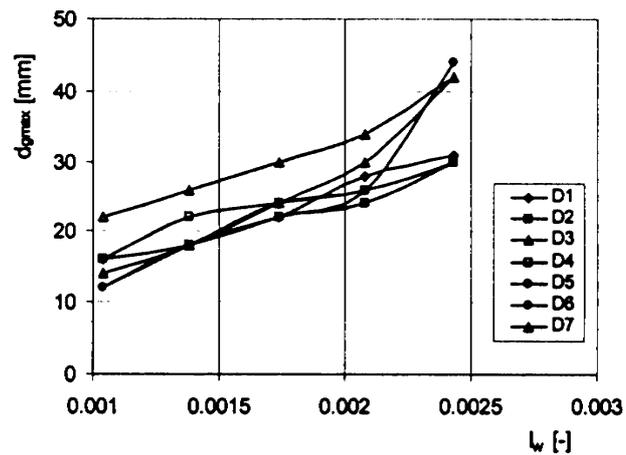
Fig. 3. The effect of wetting intensity on the maximum diameter of granules
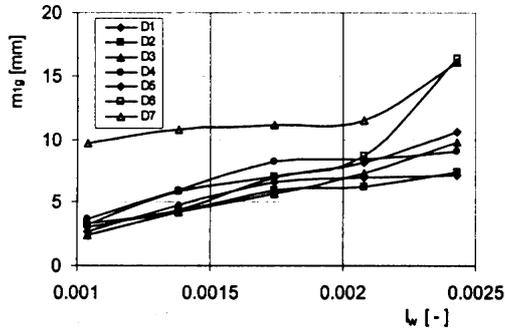
Fig. 4. The effect of wetting intensity during granulation on the value of m_{1g}
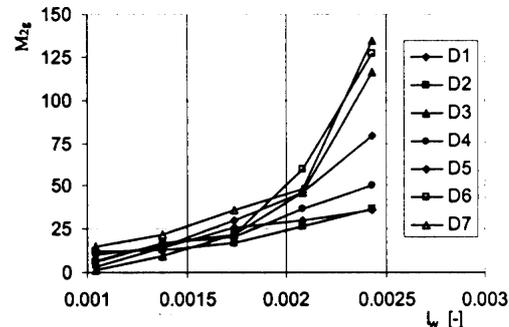
Fig. 5. The effect of wetting intensity during granulation on the value of M_{2g}

The effect of wetting intensity during granulation on the properties of granulated product obtained from particular raw materials, as determined by parameters m_{1g} and M_{2g} is shown in Figs. 4 and 5. It follows from the above graphs that the increase of wetting intensity has an influence on both the mean diameter of granules being formed (m_{1g}) and the increase of M_{2g} value, i.e. on the increase of the range of grain size composition of the final product. These relationships occur in the case of all raw materials tested, however their character is different. This confirms the effect of a parameter which differentiates the raw material, i.e. the grain size composition.

The effect of grain size composition of the raw material described by parameters m_{1m} and M_{2m}, and of wetting intensity on the grain size and composition of granulated product obtained during wetting is defined by the power equations:

$$m_{1g} = A \cdot m_{1m}^{1.4} \cdot M_{2m}^{-0.6} \cdot I_w^{1.2} \tag{6}$$

$$M_{2g} = B \cdot m_{1m}^{1.3} \cdot M_{2m}^{-0.6} \cdot I_w^{2.8} \tag{7}$$

The correlation coefficients for both equations exceeded 0.9.

The above equations prove that the grain size composition of the granulated product obtained during wetting of a fine-grained bed strictly depends on the wetting conditions and grain size composition of the raw material being granulated.

In the range of graining used in the experiments, the grain size of the product after the bed wetting has been completed, is directly proportional to the mean grain diameter of the raw material (m_{1m}) and inversely proportional to the range of grain size composition (M_{2m}). These two parameters of grain size composition of the raw material had a similar influence on the range of grain size composition of the granulated product described by parameter M_{2g}. Hence, it follows that at the stage of wetting, the granulated product with bigger grains and wider range of grain size

composition can be obtained from a raw material with bigger grain but narrower range of grain size composition. Most probably, this conclusion cannot be extended onto arbitrary grain size compositions of granulated materials, and in particular on monodisperse systems. These relationships can hold for distributions which are often encountered in practice and which are close to a normal distribution.

The other parameter which has a significant effect on the nucleation process, and, consequently, on grain size composition of the granulated product obtained during bed wetting, is the rate of wetting liquid supply. An increase of wetting intensity means that the wetting liquid is supplied to the bed in a shorter time. In the case when liquid is supplied by a pneumatic spray nozzle, an increase of liquid flow rate through the nozzle Q_w at constant air flow rate Q_a causes lesser splitting of the jet supplied by the nozzle, which can be characterized by the Q_a/Q_w quotient. The increase of wetting intensity denotes both shortening of the time of wetting liquid supply to the bed and wetting it with less dispersed jet, i.e. with bigger droplets.

As follows from the experiments, the wetting liquid supplied in the form of bigger droplets (higher wetting intensity) provides more advantageous conditions for binding particular grains into nuclei and then attaching subsequent grains to these nuclei. As a result, bigger agglomerates are formed in a shorter time.

INVESTIGATION OF THE IMPACT OF BED WETTING DEGREE

The granulation tests were carried out for 7 fine-grained raw material and for 5 wetting times for each material type. The range of moisture content of the material at which the granulation process was correct, appeared to be different for each raw material. The widest range of changes in the moisture content taken as a mass of water added to 1 kg of dry material was possible for raw materials with the finest particles and decreased with an increase in the size of raw material particles.

Figure 6 shows a comparison of the curves representing total particle size distribution of granulated product obtained from the raw material with the smallest particles (D1) at different wetting of the feed determined by saturation degree S which denotes the filling of intraparticle space in the granulated raw material with the wetting liquid. The system of curves in Fig. 6 proves that with an increase in the saturation degree a product is obtained with bigger particles and a smaller percentage of fraction < 1 mm, which contains also not granulated residue. When a larger amount of the wetting liquid is added, more liquid bridges are formed, next material particles adhere to the already existing granules, and subsequent nuclei of granulation are started.

In the description of particle size distribution of both raw materials and granulated product the theory of moments was applied. The effect of saturation degree of the material on particle size distribution of the granulated product expressed by the moments calculated from eqs. (2) to (5) is shown in Fig. 7.
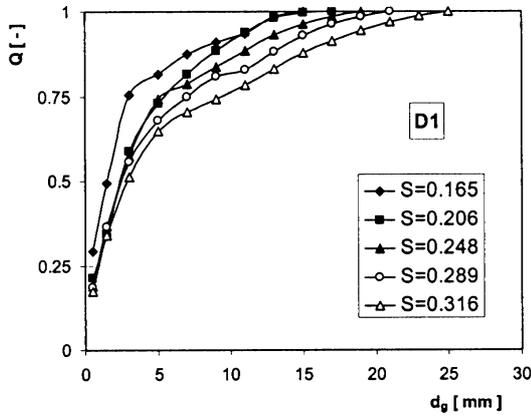
Fig. 6. Comparison of particle size
distribution curves
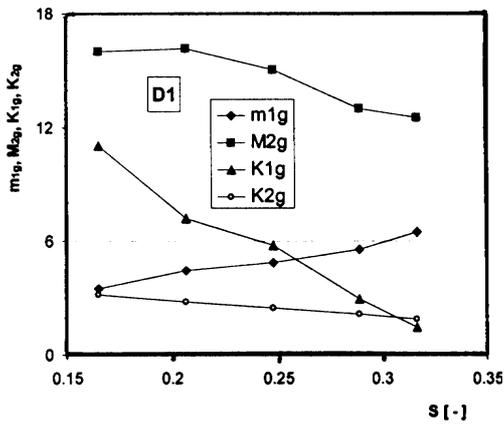
Fig. 7. Dependence of particle size
distribution of the product on saturation
degree of the raw material (D1)
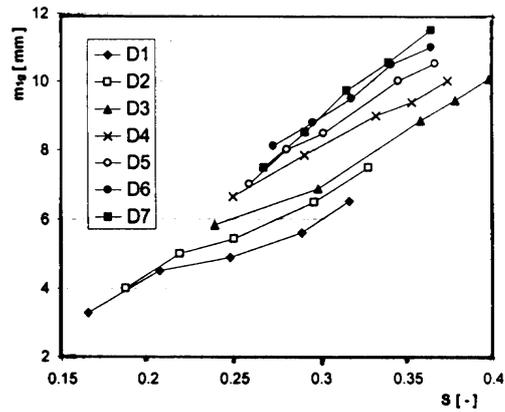
Fig. 8. Dependence of moment m_1 of the granulated
product (m_{1g}) on saturation degree of the raw
material

Basic properties which characterise the granular material, i.e. m_1, M_2, K_1 and K_2 were used to describe the particle size distribution.

It follows from Fig. 7 that an increase in the saturation degree affects changes in parameters of the particle size distribution curves. On the basis of analysis of these values also for other raw materials used in the granulation process, it was found that a similar character of changes could be observed only in the case of moment m_1. Figure 8 shows the dependence of mean particle diameter of the granulated product (m_{1gr}) on the saturation degree for all raw materials tested.

It follows from Fig. 8 that an increase in the saturation degree in each case leads to formation of granulated product with bigger particles. This dependence has approximately linear character for all materials, but the rate of increase of mean

diameter is different for subsequent raw materials. This is related to varying properties of materials, and in particular to different particle size distributions. The effect of particle size distribution of the raw material and its saturation degree on particle size of the granulated product expressed by the moment m_1 is described by eq. (8):

$$m_{1g} = C \cdot m_{1m}^{0,87} \, K_{2m}^{0,3} \, M_{2m}^{-0,37} \, S^{0,7} \qquad (8)$$

where m_{1g} and m_{1m} are the ordinary moments of the first order for granulated product and raw material, respectively, K_{2m} is the asymmetry coefficient of particle size distribution curve, and M_{2m} is the central moment of the second order of particle size distribution curve. The correlation coefficient for eq. (5) was $R = 0.96$.

It follows from eq. (8) that the particle size distribution and the moisture content of the raw material have a significant effect on the particle size of the granulated product. This effect is revealed by both mean particle size of raw material (m_{1m}) and other parameters which characterise particle size distribution curves (K_{2m} and M_{2m}). For raw material used in the experiments, the mean particle diameter of granulated product increases with the growth of m_{1m} and K_{2m}, and is inversely proportional to M_{2m}. Granulated products with bigger particles are obtained from raw material with bigger particles, smaller range of particle size distribution and positive asymmetry of size distribution curves.

CONCLUSIONS

On the basis of the results of our investigations it can be stated that the process of wet granulation, and as a result the grain size composition of a product obtained, is strongly dependent on both the grain size composition of raw material and the method of processing, in particular the amount of wetting liquid supplied and wetting conditions of the bed. The grain size of granulated product can be modified to some extent already during the bed wetting. This can be done by changing the intensity of wetting liquid supply as well as altering the amount of liquid added to the granulated raw material. An increase of wetting intensity usually results in the formation of bigger "green" granules which during further granulation can give a final product with coarser grains. This depends, however, on the mechanisms which occur further during granulation (coalescence, grinding, crushing, etc.) determined by the bridge bonding power of particular grains which is connected with the amount of wetting liquid added to the bed (saturation degree). An increase of the bed wetting in a determined range leads to an increase of the mean diameter of granulated product and a growth of granulation degree of the feed. The grain size composition of the granulated product strictly depends on the grain size composition of the raw material subjected to granulation. In the studied range of grain size distribution, the size of grains of the granulated product appeared to be directly proportional to the grain size of the raw

material. Results of the investigations show that by an appropriate selection of the grain size composition of the raw material and its wetting conditions, it is possible to control to some extent the process of granulation in order to obtain a final product of desired properties.

REFERENCES

ADETAYO A. A., LITSTER J. D. DESAI M., (1993)*, The effect of process parameters on drum granulation of fertilizers with broad size distributions,* Chem. Eng. Sci.48, 23 pp.3951-396.1

GLUBA T., HEIM A., KOCHANSKI B, (1990), *Application of the theory of moments in the estimation of powder granulation of different wettabilities,* Powder handling & processing 2, 4, pp.323-326.

HORVATH E., PATAKI K., ORMOS Z., (1989)*, Effect of the size distribution of the raw material on the physical properties of the granules,* Hungarian Journal of Industrial Chemistry, vol.17*,*

KAPUR P. C., FUERSTENAU D. W., (1966), *Size distributions and kinetic relationships in the nuclei region of wet pelletization,* I & EC Proc. Des. and Dev. 5, 1 pp.5-10.

LINKSON P. B., GLASTONBURY J. R., DUFFY G. J., (1973) *The mechanism of granule growth in wet pelletising,* Trans. Instn Chem. Engrs., Vol. 51.

NEWITT D. M., CONWAY-JONES J. M., (1958), *A contribution to the theory and practice of granulation,* Trans. Instn Chem. Engrs., Vol.36.

PATAKI K., HORVATH E., ORMOS Z., (1987), *Effect of relative amount of granulation liquid on the physical properties of granules using constant rolling time*, Hungarian Journal of Industrial Chemistry, vol.15.

SASTRY K. V. S., FUERSTENAU D. W., (1973), *Mechanisms of agglomerate growth in green pelletization,* Powder Technology, 7, pp.97-106

NOMENCLATURE

A, B, C coefficients
d - particle size, mm
d_g - granule diameter, mm
d_i - i-th class diameter, mm
I_w - wetting intensity, -
K_1 - concentration coefficient, -
K_2 - asymmetry coefficient, -
m_k - ordinary moment of the k-th order,

M_k - central moment of the k-th order,
Q_a - air flow rate, m^3/h
Q_w - water flow rate, m^3/h
S - saturation degree, -,
x_i - percent of mass fraction, -
ε_m - porosity of raw material, -
ρ - density of the raw material, kg/m^3
ρ_b - bulk density of the raw material, kg/m^3

Gluba T., Heim A., Obraniak A., *Badania warunków granulacji surowca mineralnego o różnych składach ziarnowych*, Fizykochemiczne Problemy Mineralurgii, 35, 2001, 103-112, (w jęz. ang.)

Przedstawiono wyniki badań mokrej granulacji bębnowej mączki dolomitowej o różnych składach ziarnowych przy zmiennych warunkach nawilżania złoża. Ciecz zwilżającą (wodę destylowaną) podawano na przesypujące się w bębnie złoże drobnoziarniste za pomocą dyszy pneumatycznej W czasie nawilżania zmieniano natężenie przepływu wody przez dyszę przy stałej wartości natężenia przepływu powietrza, oraz czas dozowania cieczy przy ustalonych parametrach pracy dyszy. Dawało to zmienną szybkość nawilżania złoża, którą określano za pomocą intensywności nawilżania a także zmienną wilgotność wsadu określaną za pomocą stopnia saturacji cieczy. Określono wpływ parametrów składu granulometrycznego surowca i warunków nawilżania złoża (intensywności nawilżania i stopnia saturacji) na skład ziarnowy granulatu uzyskanego tuż po zakończeniu nawilżania a także po określonym czasie granulacji po nawilżaniu.

Tomasz SZYMAŃSKI, Piotr WODZIŃSKI[*]

MEMBRANE SCREENS WITH VIBRATING SIEVES

The subject of this paper are screens with vibrating sieves. These machines differ from other industrial screens by the fact that only a sieve itself vibrates, while the riddle stays immobile. Special attention is given to a screen with a driving frame, which was built in Łódź Technical University. The authors give some results of process investigations of this machine. At present, the research is carried out on the sieve dynamics and amplitude distribution. The construction of the screen enables the implementation of rotating vibrators beside the electromagnetic vibrator, so the screen can be used in a wide range of research and industrial applications. The tested screen is built in an industrial scale and is designed for fine-grained materials.

INTRODUCTION

A characteristic feature of screens with vibrating sieves are vibrations of the sieve itself and of the material being screened, which moves along this sieve. In the classical screens, sieves vibrate along with the riddle whose mass is often bigger than the sieve mass. This is connected with the use of large vibrators which would impart forces high enough. This in turn is related to high power demand necessary to induce vibrations and to high inertia forces which act partly upon the supporting structure. These problems do not occur in the screens with a direct sieve excitation because riddles are immobile in these machines.

Another important feature of the screens with vibrating sieves is an almost unlimited possibility of constructing different variants of these machines. Depending on demand, there can be different arrangements of particular screens, e.g. in a common riddle. Additionally, these machines have a relatively simple construction, they can be made of usual construction materials and they can contain typical elements – sub-assemblies which are taken from other, already existing machines.

---
[*]Łódź Technical University, Faculty of Process and Environmental Engineering, Department of Process Equipment, Chair of Granular Material Classification

Screens with vibrating sieves are designed first of all for screening of fine- and very fine-grained materials. They have relatively high dynamic factors. In the screen described in this paper the maximum value of the dynamic factor was K=15. Therefore, these machines are characterised by good segregation of a layer on the sieve (the process of stratification) and high screening efficiency. In practice, they reach screening efficiency ranging from 0.9 to 1.0.

The features mentioned above cause that these screens can become very useful in screening fine-grained material. Their disadvantage is a reduced sieve durability and more complicated sieve mounting, as compared to the screens with mobile riddles. However, taking into account the fact that modern woven and polyurethane sieves are very fast, these negative features of screens with vibrating sieves become less annoying.
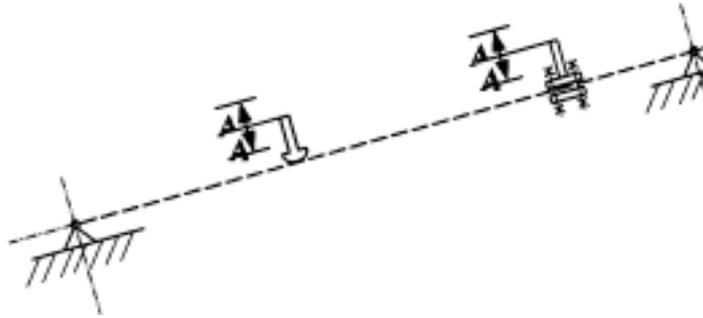
Fig. 1. Principle of vibrating
sieve operation

The principle of vibrating sieve operation is shown in Fig. 1. The sieve vibrations are induced by pushing rods. Depending on the method of excitation, single and double-sided screens are distinguished. A characteristic feature of the first type is that the pushing rods induce vibrations through constant or temporary press on one side. The sieve returns to the state of equilibrium due to its resilience.

The double-sided screens impart full vibrations onto the sieve because they are connected to it rigidly. The advantage of such excitement is shown in Fig. 2. An important role in both single- and double-sided screens is played by mesh tension, both in axial and transverse direction.

Attention should be paid to the fact that in the screens with a direct sieve excitation, due to continual sieve vibrations, the effect of removal of particles hard to screen and blocking the mesh from the sieve surface are achieved. The effect of self-cleaning is a very beneficial phenomenon which does not occur, or occurs to a too small extent, in the classical screens where sieves remain immobile.

Two basic designs of the screens are known. In the first one the sieve is driven by electromagnetic vibrators, each connected separately to the sieve by pushing rods. Such a design is shown in Fig. 3.
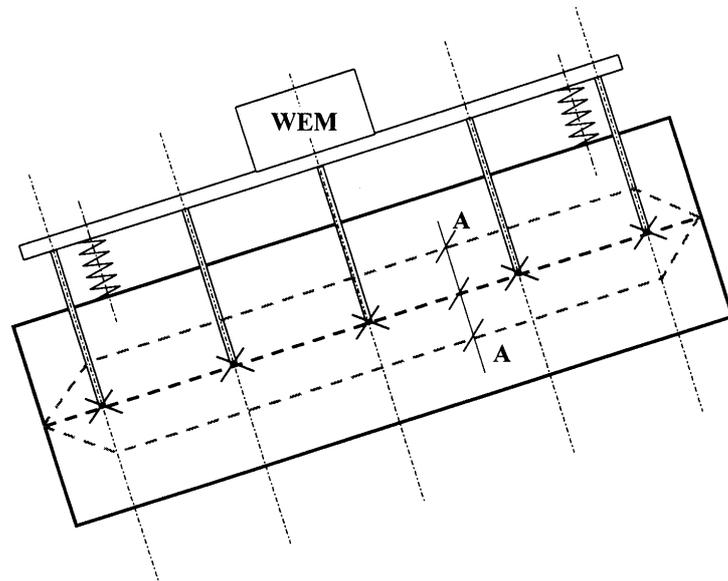
Fig. 2. Advantage of
a double-sided excitement

Fig. 3. Screen with single
vibrators

K_G– oversize,
K_D– undersize
S – sieve,
W– vibrator,
R – riddle
N – feed,
P– pushing rod
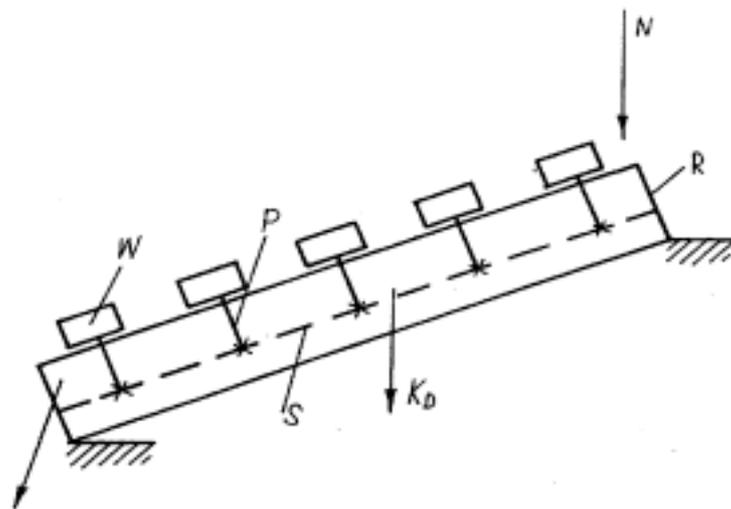
The other basic design solution is a screen with a driving frame illustrated in Fig. 4. Pushing rods are connected to the driving frame which is induced into vibrations by an attachable electromagnetic vibrator. This solution is discussed in the present paper. It is much more advantageous than the one presented earlier because a uniform distribution of amplitudes is obtained for every pushing rod, and additionally, only one electrovibrator can be used. It is also possible to replace the electromagnetic vibrator with rotating vibrators.
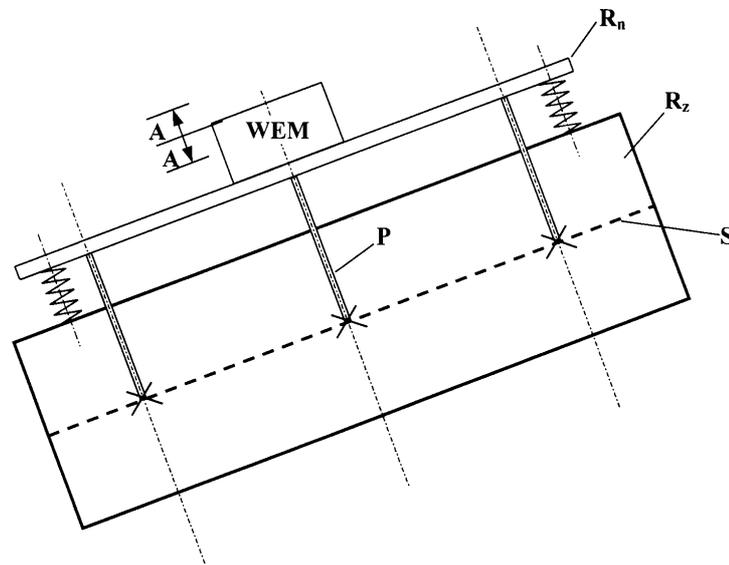
Fig. 4. Screen with
a driving frame
WEM – electromagnetic
vibrator
R_n – driving frame
R_z – riddle
S – sieve
P – pushing rod

   This solution enables also the application of many electromagnetic vibrators to the driving frame drive. This system seems to be the most appropriate. A characteristic feature of electromagnetic vibrators is that they can be easily synchronised in the vibrating motion. There is a simultaneous synchronisation which ensures translatory motion of the whole frame and, consequently, the motion of the entire sieve. When one electromagnetic vibrator placed in the axis of symmetry of the screen is used, a risk of torsional vibrations of the frame around the centre of gravity may appear. This is not advantageous because the centre of the sieve will move at small amplitude, and as a result the screened material will be collected in the central part of the screen.

   Screens with vibrating sieves are characterised by high frequency of vibrations and small amplitudes. In the screen tested by the authors, the frequency was 50 Hz and maximum amplitude was of the order of 1.5 mm. The angle of inclination of the sieve to the level ranged from 0 to 45°, i.e. the inclination was twice as large as in the case of screens with immobile sieves. Such big values of the angles and high accelerations caused significant velocities of material on the sieve amounting to 0.5 to 1.0 m/s.

   A characteristic feature of classification on the screens with vibrating sieves is a thin layer of material on the sieve. Its thickness is equal or twice as large as the stated particle size. This provides very good stratification conditions. High efficiencies reaching 100% can be achieved, which is impossible in the classical screens. The process capacities are also much higher than those obtained in other screens.

   Screens with vibrating sieves are able to self-clean the sieves. Vibrations of the sieve surface cause that blocked particles are removed from the mesh. This feature may be a reason why higher process capacities are achieved and causes that these screens are especially suitable for screening of fine- and very fine-grained materials.

The discussed screens with sieves excited directly, and in particular the screens with driving frames, due to their specific construction, i.e. location of an electrovibrator outside the riddle side walls, are very suitable for wet screening.

FLAT SIEVE GEOMETRY

In the classical screens, i.e. the ones with immobile sieves, the layer on the screen is tossed evenly. In the screens with sieves excited directly, due to specific excitement of vibrations, the tossing of material on the sieve surface is different. To approach this phenomenon quantitatively, a description of the vibrating sieve geometry is proposed in Fig.5.
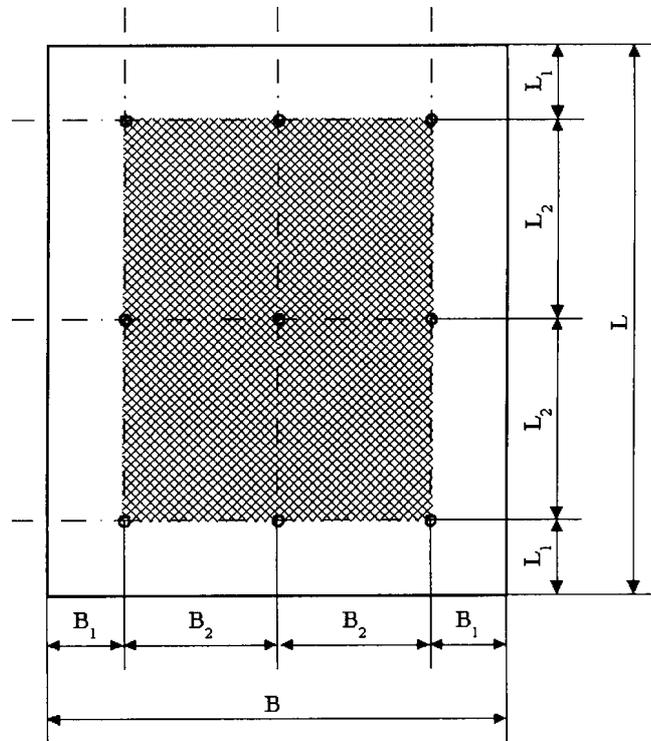
Fig.5. Vibrating sieve geometry

It is obvious that sieves of the screens discussed move only in the plane perpendicular to the sieve surface. However, the amplitude of vibrations is not the same in each point. Because the sieve is mounted on an immobile riddle not the entire sieve surface takes place in the translatory motion. To reflect this phenomenon in model calculations it is necessary to introduce some calculation coefficient.

This role can be played by a surface module m_p. It denotes part of the sieve which performs translatory, linear vibrating motion. This value is a ratio of the surface subjected to full excitement to the overall sieve surface.

$$m_p = \frac{F_d}{F_s} \tag{1}$$

where :

    F_d – vibrating surface
    F_s – total surface

$$m_p = m_l \cdot m_b \tag{2}$$

where:

    m_l – longitudinal module
    m_b – transverse module

Taking into account symbols from Fig. 5, the formulae describing the above values have the form

$$m_l = \frac{(n-1)l_{2l}}{L} \tag{3}$$

$$m_b = \frac{(n_b-1)b_2}{B} \tag{4}$$

where:

    n_l – the number of pushing rods in the longitudinal direction
    n_b – the number of pushing rods in the transverse direction

In conclusion, the surface module of the screen with a vibrating sieve has the form:

$$m_p = \frac{(n_b-1)b_2 \cdot (n_l-1)l_2}{B \cdot L} \tag{5}$$

The values of b_2 and l_2 in the above formula depend on process parameters and in particular on the mesh size and thickness of the layer on the sieve.

CHARAKTERISTIC FEATURES OF SIEVE MOTION IN THE SCREENS WITH VIBRATING SIEVES

As seen in Fig. 6, in the screens with vibrating sieves there are so-called membrane amplitudes A_m at distances between the pushing rods. This follows from the fact that the sieve is flexible and vibrates like a membrane. Besides, because the sieves are mounted on the immobile riddles, the amplitude increases from zero to the value of vibration amplitude of the pushing rods. This is reflected by a surface module discussed in the previous section. The sieve motion was proposed to be described by a membrane equation, however the authors of this paper are of the opinion that typical membrane equations cannot be applied because specific excitement of vibrations occurs in several points on the sieve surface.
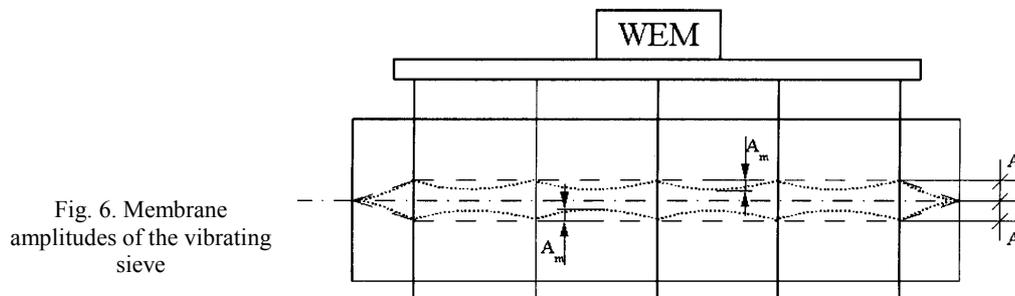
Fig. 6. Membrane amplitudes of the vibrating sieve

In the description of dynamics of the screen with a vibrating sieve we use a dynamic model shown in Fig. 7.

Fig. 7. Dynamic model of a screen with vibrating sieve
m_{R2} – immobile riddle mass
m_R – driving frame mass
m_K – mass of the vibrator anchor
C_1 – flexibility of the driving frame suspension
C_2 – mesh elasticity
C_3 – elasticity of inner elements of the vibrator
P_0 – exciting force induced by the vibrator coil
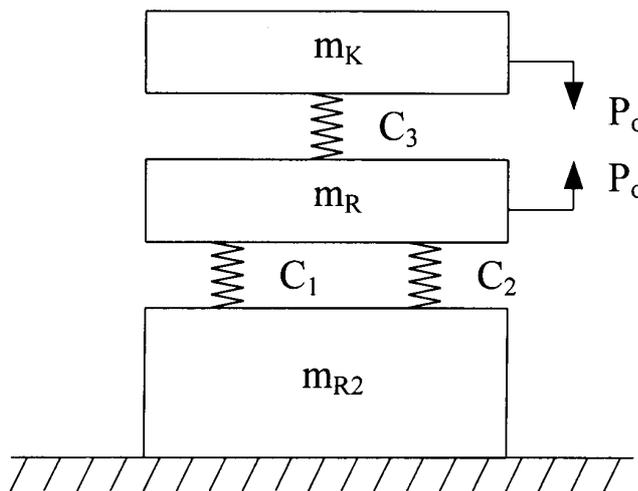
This system is characterised by variable flexibility constant C_2. During the screen operation the sieve is "elongated" (deformed), which leads inevitably to changes in the sieve elasticity. So, to make typical dynamic calculations of the vibrating system is difficult because:

- Rigidity of the sieve mounted on the riddle cannot be determined – each time we can expect a different tension.
- The sieve during operation is deformed which can change significantly rigidity C_2.

So, it is postulated not to consider the parameter C_2 at all, the more that the driving system is usually designed for high exciting forces and the value of C_2 is in this case negligibly small. The screen operation depends first of all on C_1 and C_3, while the effect of the sieve elasticity is negligible as compared to other values and consequently it is omitted.

At present, the research is carried out on the amplitude distribution on the vibrating sieve surface. The measuring devices include piezoelectric sensors, an integrating circuit and a computer with an A/D converter PCL-818 HD. Under the influence of acceleration the sensors produce a voltage signal which is then transmitted to the integrating circuit. The sensor parameters are as follows:

- Acceleration 10 mV/m/s^2
- Velocity 10 mV/mm/s
- Deflection 10 mV/μm.

The voltage signal produced by the sensors is integrated twice, and as a result the value of deflection of the tested point on the sieve is obtained. These signals are acquired by the A/D card and logged in the computer. The system is calibrated by a manual tastograph. The correctness of readings of the whole measuring system must be checked because the signals obtained from the sensors are double-integrated.

After the measurements of amplitude distribution on the whole vibrating sieve surface, the authors tried to describe the phenomenon mathematically and then by relating it to the vibrating sieve geometry, to develop a correlation suitable for model calculations of screens with immediate sieve excitation.

EXPERIMENTAL RIG

In the nearest future also process investigations of the screen with vibrating sieves will be carried out. An experimental rig constructed for this purpose is shown in Fig.8.

Supporting structure 1 is the machine frame. Riddle 2 inclined at different angles which remains immobile during the screen operation is mounted in the frame. Sieve 3 is stretched on the riddle. Flat springs 4, on which driving frame 5 rests, are mounted on the riddle. Attachable electromagnetic vibrator 6 is installed on the driving frame. It is also possible to use an inertial vibrator. The driving frame is combined to the

sieve by means of rigid pushing rods 7. The feed is in tank 8 with valve 9 which controls the size of the discharge hole. The oversize is collected to vessel 10, while the undersize to container 11.
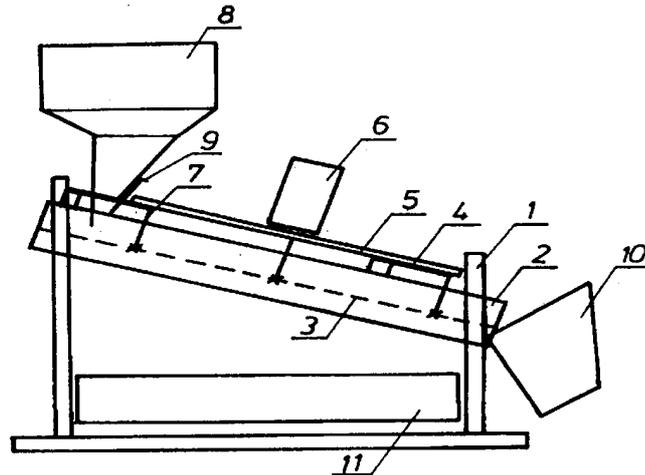
Fig. 8. Experimental rig for process investigations

RESULTS AND DISCUSSION

In this section some characteristic results of investigations for frame screen with a vibrating sieve were presented. These studies were carried out in the Institute of Chemical Engineering, Łódź Technical University in the 70's (Wodziński 1981). The authors of this paper intend to repeat the process investigations for the presented screen in order to verify them, and in particular to compare values characteristic for the screening process with those obtained in the present studies.

Below, diagrams presenting the following relations are shown:

$\eta = F(Q)$ – screening efficiency as a function of capacity for irregular particles – sand (Figs. 9 and 10), and for sharp-edged particles –agglomerates (Figs. 11 and 12).

The efficiency is meant here as the screening efficiency (undersize), i.e. the ratio of the amount of undersize which was screened off to that one which should be screened off during ideal screening to the amount of undersize in the feed (eq. 6).

$$\eta = \frac{m_d}{x \cdot m} \qquad (6)$$

where: m_d – mass of the screened material
x – undersize fraction in the feed
m – feed mass

Materials used in the experiments were dry, devoid of moisture. Both sand and agglomerates were screened, separated from impurities and fractionated in the whole range of particle size. The sand mixture contained particles of the size 0.1-10.0 mm, while marble agglomerates 0.1-5.0 mm.

Symbols used in the diagrams:

η– screening efficiency [–]

Q– screening capacity [kg/s]

α– angle of inclination of the sieve to level [^{o}]

l– mesh size [mm]

K– dynamic factor [–]
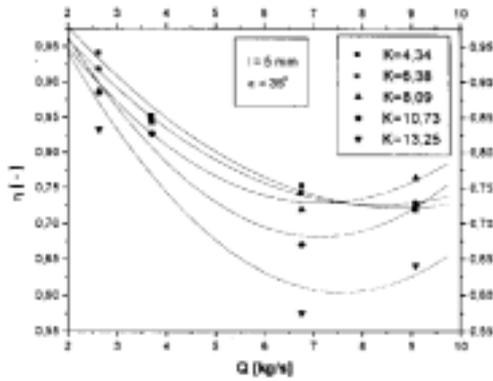
Fig. 9 Screening efficiency as a function of capacity for irregular particles
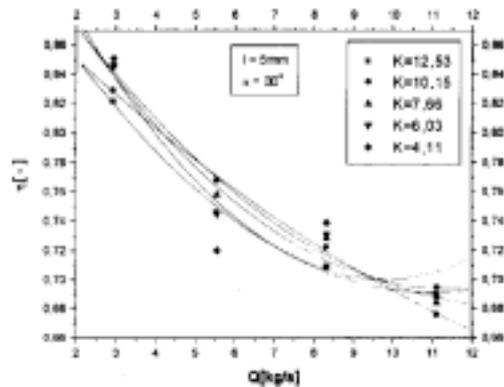
Fig. 10 Screening efficiency as a function of capacity for irregular particles
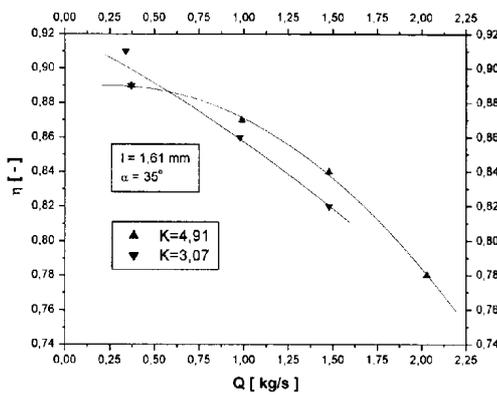
Fig. 11. Screening efficiency as a function of capacity for sharp-edged particles
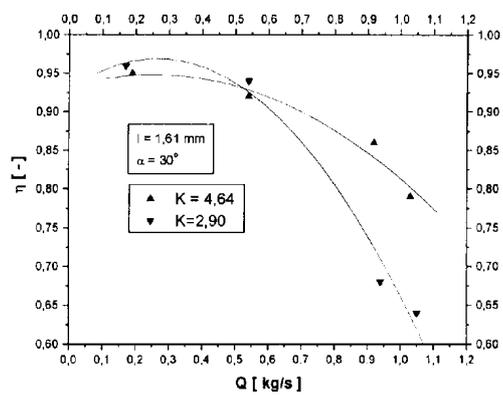
Fig. 12. Screening efficiency as a function of capacity for sharp-edged particles

CONCLUSIONS

Screens with driving sieves have the following characteristics:
1. High capacities of the screening process.
2. A possibility to choose the number of construction variants, especially in the case when different sieves inclined at different angles are used.
3. Self-cleaning of mesh by removal of particles which block it.
4. Simple servicing in the case when an electromagnetic vibrator is used as a drive.
5. Low energy demand of the screen, caused by much smaller vibrating masses (in relation to the screens with mobile riddles). This is connected also with an advantageous dynamics of the machine.

Due to a simple construction the frame screen discussed in this paper can be used in every industrial conditions. It can be made of generally available intermediate products. In this case there are no problems with high inertia forces transferred by the drive and suspension. There is no impact of dynamic vibrating masses on the base on which the machine is placed.

Screens with vibrating sieves are designed for fine screening in a wide range from 20-40 µm to about 10 mm and as such they can find application in many industrial branches.

REFERENCES

BANASZEWSKI T. (1990), *Przesiewacze,* Śląsk, Katowice.
BŁASIŃSKI H., WODZIŃSKI P., *Przesiewacze z sitami drgającymi,* Z.N. P.Ł., Inż. Chem., No. 5/1979.
SZTABA K. (1993), *Przesiewanie*, Śląsk, Wyd. Techniczne, Katowice.
WODZIŃSKI P. (1981), *Odsiewanie materiałów ziarnistych*, Z.N. P.Ł., No.394.
WODZIŃSKI P. (1997), *Przesiewanie i przesiewacze*, Monografie, Wyd. P.Ł., Łódź.

Przedmiotem zainteresowania autorów niniejszego artykułu są przesiewacze z sitami drgającymi. Są to maszyny różniące się tym od innych eksploatowanych w przemyśle przesiewaczy, że do drgań wzbudzane jest jedynie samo sito, a rzeszoto pozostaje nieruchome. W szczególności opisany jest przesiewacz z napędem ramowym, który został opracowany w Politechnice Łódzkiej. W pracy podane zostały przykładowe wyniki dotychczasowych badań procesowych tej maszyny. Obecnie autorzy poniższego artykułu prowadzą badania nad dynamiką ruchu oraz rozkładem amplitudy na sicie przesiewacza. Sposób wykonania opisywanej aparatury umożliwia zastosowanie wymiennie oprócz wibratora elektromagnetycznego również wibratorów rotacyjnych w związku czym może on być wykorzystywany w szerokim zakresie prac badawczych jak i przemysłowych. Przesiewacz badany jest wykonany w skali przemysłowej dla materiałów drobnouziarnionych.

J.K. PUTUBU[*], M.S. MOREY and S.R. GRANO[**]

A PULP-CHEMICAL STUDY OF SKARN ORE FEED BLENDS AT THE OK TEDI CONCENTRATOR, PAPUA NEW GUINEA

Parallel metallurgical and pulp chemical surveys have been performed at Ok Tedi Mining Ltd (Papua New Guinea) for skarn ore feed blends. Metallurgical results showed a variation in recovery at similar grade, suggesting uniform depression of activated minerals by a precipitate. Significant activation of pyrite was also indicated. This paper highlights results of pulp chemical surveys, which characterise the slurries in terms of oxygen demand (indicating sulfide reactivity) and pulp particle surface coatings. The surface analytical techniques of ethylene diamine tetra acetic acid (EDTA) extraction, X-ray photoelectron spectroscopy (XPS) and time of flight secondary ion mass spectrometry (ToF-SIMS) analyses were used to confirm Cu activation of pyrite, and the depression of chalcopyrite by hydroxy precipitates of Ca, Fe, Al and Si.

INTRODUCTION

The Ok Tedi copper-gold deposit is located at Mt. Fubilan in the Western Province of Papua New Guinea. The ore deposit is a porphyry-skarn intrusive system located within the raised sediments of the Hindenberg ranges in the Star Mountains of Papua New Guinea. Copper mineralisation resulted from the intrusion and alteration of monzonite and monzodiorite porphyry stocks. Subsequent leaching and redeposition of copper minerals resulted in a leached cap of significant gold overlaying a secondary enriched copper ore. Below this was the primary porphyry ore body. The current ore body consists of porphyry ores, which are effectively ringed by skarn ore bodies. The skarn ores exhibit high iron mineralisation, and higher copper and gold content than porphyry ores. The principal copper mineral is chalcopyrite, with minor bornite, chalcocite and covellite. Most gold occurs in association with

[*]Ok Tedi Mining Limited, P.O. Box 1, Tabubil, Western Province, Papua New Guinea.
[**]Ian Wark Research Institute, University of South Australia, Mawson Lakes Campus,
 Mawson Lakes, South Australia, Australia 5095.

copper, but is also intruded into pyrite systems. The copper-gold mineralisation typically consists of fine-medium-grained (< 100 μm) disseminated sulfides and gold. Table 1.1 shows the average ore processing characteristics at Ok Tedi, based on laboratory flotation tests (Lauder, 1997).

Table 1. Average ore processing characteristics from laboratory flotation database (Lauder, 1997). R.W.I. is the relative work index, and lime consumption was that required to achieve pH 11.5

Ore Type	R.W.I	Lime kg/t	Head Grade			Recovery (%)	
			% Cu	% ASCu	g/t Au	Cu	Au
Monzonite	11.7	1.60	0.96	0.07	0.60	87.6	75.2
Monzodiorite	11.5	2.01	0.57	0.05	0.56	80.2	70.6
Siltstone	14.1	1.94	0.66	0.07	0.53	75.6	61.9
Endoskarn	13.4	2.13	0.73	0.06	0.69	73.5	63.7
Magnetite skarn	10.8	1.86	2.45	0.18	2.72	72.9	64.3
Pyrite skarn	13.3	2.20	2.57	0.22	2.79	60.3	53.7
Calc-Silicate Skarn	13.3	2.40	1.72	0.20	1.97	67.2	61.2
Oxide Skarn	15.1	4.14	1.75	0.81	1.95	22.8	57.8

Ore for the remainder of mine life includes 60% porphyry sulfide-intrusive (0.6% Cu, 0.6g/t Au) and 35% sulfide skarn. The skarn ores represent 50% of copper and gold to mine life. The sulfide skarn includes 6% pyrite skarn, 17% magnetite skarn and 12% endoskarn. Oxide skarn ore is virtually depleted. However, oxide skarn was included in feed blends of reported surveys.

THE CONCENTRATOR

The Ok Tedi concentrator is located approximately one kilometre from the mine and consists of two parallel grinding and flotation circuits in mirror image. Modules 1 and 2 process ore at approximately 15 MTPA (2000 tph) per line. Both Modules consist of a SAG mill (13% ball charge of 120mm steel balls) followed by two parallel ball mills (32% load of 50mm steel balls) in closed circuit with ten D26B Krebs cyclones. Cyclone underflows are split to feed two flash flotation cells per ball mill. Flash flotation concentrates are fed to the final cleaner tank cells. Cyclone overflows become rougher feed at approximately 40% solids and P_{80} 150-200 microns.

The flotation circuit for each module consists of rougher-scavenger, cleaner, recleaner, column and tank cell. The rougher-scavenger flotation bank consists of 30 Outokumpu OK-38 m^3 cells, in parallel lines of 15. The flash cell concentrates, rougher concentrates from cells 1 to 3, column and recleaner concentrates, are combined to feed the final cleaner tank cell. Concentrate from rougher-scavenger

cells 4 to 9 is fed to the column cell, and concentrate from cells 10 to 15 (scavengers) is fed to the low grade concentrate regrind circuit. The regrind mills use 25mm grinding balls, and have a nominal cyclone overflow P_{80} of 40 microns.

The nominal rougher feed grades are 0.8% copper and 0.8g/t gold. Cytec S-7249 collector (a mixture of di-isobutyl di-thio phosphate and di-isobutyl mono-thio phosphate) is added (relative to copper in plant feed) to SAG mills at 3-4kg/tonne of Cu and also stage added to scavenger cell 9 tail at 1kg/tonne. Slaked lime is added to SAG feed, and is controlled to a rougher feed pH of 11.5. Approximately 25g/t OTX140 frother (an alcohol - glycol blend) is added to SAG mill feed.

EXPERIMENTAL

STRATEGY

Metallurgical surveys of the Ok Tedi concentrator were performed in conjunction with plant pulp chemical surveys. The pulp chemical surveys included 'probe' surveys of plant streams, examining Eh, pH, dissolved oxygen (D.O.) and temperature. Ethylene diamine tetra acetic acid (EDTA) extraction surveys of plant streams were also performed along with pulp solution analysis. The Ian Wark Research Institute (IWRI) performed particle surface analysis of selected stream samples. Particle size distributions and mineral liberation were examined by the IWRI using optical microscopy, and by JK Tech (University of Queensland) using Mineral Liberation Analysis (MLA). For surveyed pulps the feed P80 was shown to vary from 90 to 250 μm. However, copper minerals were liberated in all surveys.

PULP CHEMICAL SURVEY METHODS EH, PH, D.O. & TEMPERATURE

The Eh is a measure of the mixed potential generated by electrochemical interactions within the mineral pulp. It therefore may indicate the dominant electrochemical process within the pulp. The relative rate of pulp oxidation is expressed by the rate of oxygen consumption (rate of decrease in dissolved oxygen D.O.). Eh also varies in accordance with pulp D.O. levels. Furthermore, the electrochemical oxidation of collectors during adsorption onto value minerals is dependent on D.O., as oxygen reduction occurs during the electrochemical reaction. The optimum Eh for dithiophosphate or xanthate adsorption onto chalcopyrite is approximately 0.2 V SHE (Grano et al., 1991). The pulp pH is a measure of the alkalinity of the solution. All probe measurements were for a period of 2 minutes, and commenced approximately 15 seconds after sampling. Pulp D.O. was measured as % saturation.

EDTA EXTRACTION OF HYDROLYSED METAL IONS

EDTA (ethylene diamine tetra acetic acid) has been shown to solubilise oxidised metallic species, but not the metal sulfides (Rumball & Richmond, 1996).

Consequently, EDTA extraction followed by ICP analysis may give an indication of oxidation levels in a mineral pulp. The method includes extraction of a 0.01 dm^3 pulp sample, followed by conditioning with 0.09 dm^3, 3% EDTA (di sodium salt) for five minutes (with nitrogen purging). The sample is then filtered through 0.45 μm millepore. The filtrate is analysed by ICP, using EDTA standards. Species concentrations are expressed relative to the proportion of that element in the dry weight of the filter cake (Kant, Rao, & Finch, 1994).

XPS ANALYSIS

X-ray photoelectron spectroscopy (XPS) analysis was performed using a Physical Electronics X-ray Photoelectron Spectrometer, model 5600. XPS is an analytical technique involving an incident x-ray beam applied to the surface of solid samples. The x-ray photons expel inner shell electrons from surface atoms of the sample. The result is a spectrum of the kinetic energy of emitted electrons (x-axis, expressed as electron binding energy 'B.E.', which is characteristic of an element in a particular oxidation state) and the intensity of the electron beam (which is indicative of surface concentration). Therefore, surface concentrations of, for example, Cu(II) compared to Cu(I) may be ascertained. The penetration of an x-ray photon is considerably greater than that of an ion beam (used in ToF-SIMS). Consequently, XPS measures the oxidation state of elements over a number of atomic layers (approximately 5 to 10). Furthermore, the incident x-ray beam is not highly focused, but irradiates a surface area of approximately 1 cm^2. Therefore, XPS spectra provide an average measure of the atomic surface concentration and oxidation state of elements in atomic surface layers, with a small penetration of the bulk of the sample. XPS is the only technique, which gives the oxidation state of the elements in surface coatings on solids.

Sample preparation for analysis was according to the method of Smart (St.C. Smart, 1992) and included solution replacement at pulp pH (using NaOH), to remove some ultrafine particles.

ToF-SIMS ANALYSIS

Time of flight secondary ion mass spectrometry (ToF-SIMS) analyses were performed using a PHI TRIFT 2100 spectrometer equipped with gallium liquid metal ion gun (LMIG). This instrument allows spectroscopy for characterisation of chemical composition and imaging for mass spectra to be taken from the pre-selected areas (eg. particles). The system uses a pulsed primary ion beam to desorb and ionise species from a sample surface. Damage to the uppermost monolayer is minimised by applying extremely low primary ion fluxes. In order to maintain static conditions, typical analysis time ranged from 4 to 5 minutes with primary ion doses of around 3×10^{12} ions per cm^2.

Sample preparation for analysis was according to the method of Smart (St.C. Smart, 1992). As etching was not included in this work, particle surface coatings may

have been examined in the analyse s. Each sample was deposited onto a piece of indium from a water suspension and whilst still wet, introduced into the spectrometer preparation chamber. Prior to analysis the samples were outgassed under vacuum for approximately 12 hours.

The current work required identifying and quantifying individual surface species such as sulfur, copper, collector etc. Because of the surface heterogeneity, the analytical results can differ significantly between particles. Therefore, a sufficiently large number of grains must be analysed to allow detection and exclusion of particles, which are unreasonably different from others in the set (outliers). It also should be noted that SIMS spectral intensities are different for different chemical species/fragments. Therefore, spectra for different chemical fragments may not be compared directly. However, normalised elemental intensities for the same fragment, may be compared between spectra for the same particle type (eg. collector on chalcopyrite in concentrate compared to collector on chalcopyrite in tailing). Because normalisation in ToF-SIMS is relative to the substrate, peak intensities may not be compared directly between different substrates (eg. chalcopyrite compared to pyrite). However, intensity ratios may be used (eg. Cu to S) for comparing proportions of chemical species on different substrates.

RESULTS AND DISCUSSION

METALLURGICAL SURVEYS

The concentrator metallurgical balance is a fundamental indicator of plant performance and is therefore the primary reference. If the metallurgical balance suggests inadequate performance of a flotation unit, then pulp chemical data may be used to assist the interpretation of this phenomenon, and to provide a basis for possible remedial action. Metallurgical balances for plant surveys at Ok Tedi on 19/1/00, 15/3/00, 16/3/00, 17/3/00 and 21/3/00 are reported for the rougher–scavenger sections. Copper grade-recovery curves are shown in Figure 1. Comparison is made with 11/12/98 and 30/11/99 surveys because of the improved metallurgical performance shown in those surveys. The 11/12/98 survey was for monzonite/sulfide skarn feed and showed excellent plant performance.

Other data for rougher feed pulps of surveys is shown in the Table of Appendix 1. Figure 2 shows copper selectivity against iron. Flotation recovery by entrainment is approximated in Figure 2 by the average recovery of silicates for the March surveys. It is apparent from Figure 2 that an iron mineral (pyrite) was strongly activated to flotation. The poor copper grades of the 19/1/00 and 15/3/00 surveys were due to increased pyrite flotation. From Appendix 1 (point 3) the Cu:S ratio for rougher feed pulps of surveys are shown. It is apparent that for the survey of 12/11/98, the Cu:S ratio was much higher (at 0.4) than for other surveys. The implication is that there was little pyrite in the feed of the 11/12/98 survey.

K.J. Putubu, S.M. Morey, R.S., Grano
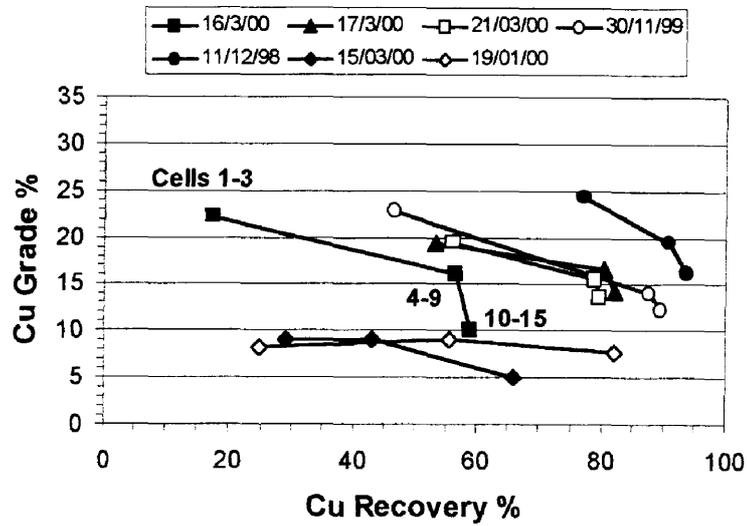
Fig. 1. Copper grade-recovery curves for rougher-scavenger surveys at Ok Tedi
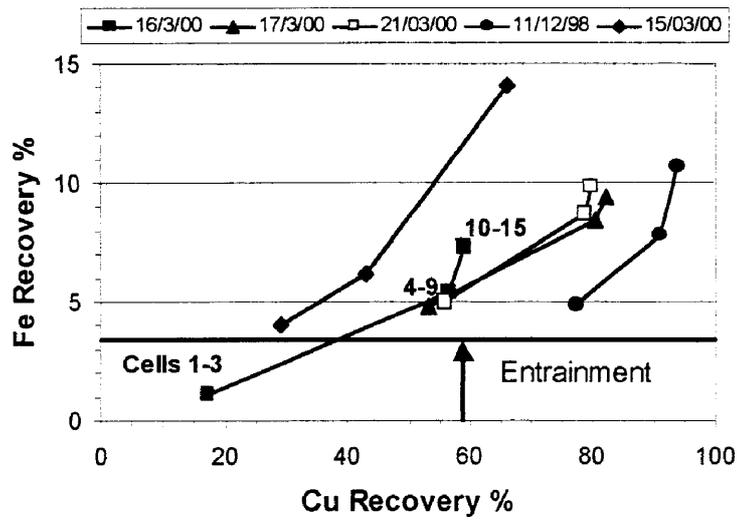
Fig.2. Cu-Fe selectivity curves for rougher-scavenger surveys at Ok Tedi

From Figure 1, it is apparent that the predominant metallurgical effect was a significant variation in chalcopyrite recovery at similar grade to other surveys. This suggests a general depression of all minerals in the Ok Tedi pulp.

From Figures 1 and 2 therefore, it is apparent that two pulp chemical phenomena are effecting a poor flotation performance of skarn blends.

These phenomena are :
1. The depression of chalcopyrite (and other mineral) flotation recovery, and
2. The inadvertent activation of pyrite.

Survey data indicates a correlation between feed tonnage rate (which correlates approximately with grind size) and recovery (see Appendix 1, points 3 and 4). This was despite optical microscopy and MLA analysis indicating liberation of chalcopyrite in all surveys. However, recovery by size analysis indicates significant losses of chalcopyrite in coarse fractions. The implication is that pulp depressant species were limiting the recovery of the more marginally floatable chalcopyrite particles in both the fine and coarse size fractions during the surveys.

PULP CHEMICAL SURVEYS

Two different pulp chemical surveys were performed in conjunction with each metallurgical survey. The first involved probe analysis of fresh plant pulp samples for readings of Eh, pH, dissolved oxygen (D.O.) and temperature. Figure 4 shows a selection of D.O. demand curves from the 22 plant streams analysed on survey days during January and March 2000. Some minor variability in results is indicated. However, the significant result is shown in a comparison of the two streams, which have been circled.
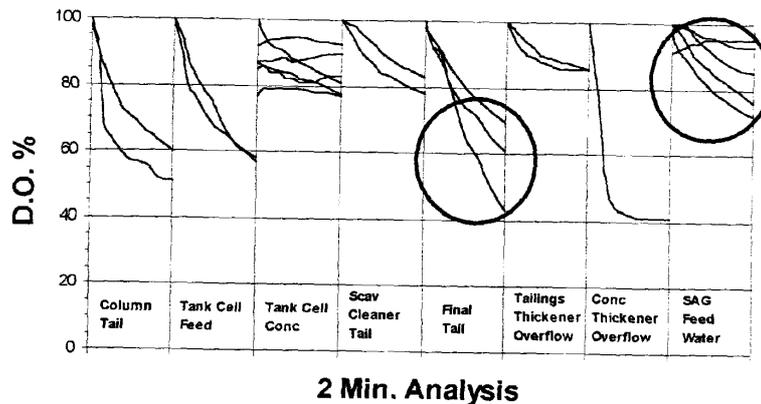
Fig. 3. Dissolved oxygen (D.O.) readings as % saturation taken over two minutes immediately after pulp sampling, during Ok Tedi surveys

Interpretation of the D.O. demand curves shown in Figure 3 is based on a comparison with the D.O. demand curves for water, such as that shown for SAG feed water in the figure. The D.O. demand for water generally shows a decrease in D.O. from saturation (100%) to approximately 80% of saturation over a two minute reading. With this as a 'baseline' curve indicating no significant D.O. demand, it is apparent from a comparison with the final tailing stream of the plant, that the final tailing stream consistently showed significant dissolved oxygen demand during

survey days. This suggests that the sulfide mineral particle surfaces (particularly pyrite) were not electrochemically passivated in the surveyed pulps.

The cessation of sulfide mineral particle oxidation may be caused by a build-up of an insulating surface layer of oxide, a phenomenon referred to as 'electrochemical passivation'. This is particularly important in relation to pyrite flotation. Passivated pyrite has a surface coverage of $Fe(OH)_3$. This is strongly hydrophilic and may counteract any adsorbed hydrophobic species such as collector-activator complexes, limiting its flotation. The implication of the significant D.O. demand of the concentrator tailing streams is that pyrite was not passivated during the surveys, and was therefore more susceptible to activation and flotation.

EDTA EXTRACTION AND SOLUTION ANALYSIS

EDTA sampling involved taking a 0.01 dm^3 syringe sample of pulp, which was conditioned in 0.09 dm^3 excess EDTA solution. The remainder of the pulp sample was filtered for water analysis. Concentration in the solution phase is then analyzed by ICP. EDTA extractable cations are expressed as a percentage of the same element in the conditioned solids (eg. % EDTA Cu). Table 2 shows a comparison of average % EDTA Cu for rougher feed pulps of Mount Isa Mines Copper, Northparkes Mines, and Ok Tedi. It is apparent from Table 2 that Ok Tedi surveyed pulps contained significantly higher concentrations of oxide copper. This suggests significant sulfide oxidation, and therefore, of acidity of the ore feed, along with potential for pyrite activation.

The difference between EDTA extractable cations, and cations in solution in the absence of EDTA, is a measure of the precipitation onto particle surfaces within the pulp. This precipitation may be a result of pulp oxidation and dissolution into the solution phase, followed by random precipitation onto particle surfaces. Alternatively, precipitation may be a result of surface oxidation of mineral particles and precipitation at the surface of those particles. This second type of precipitation is more mineral specific.

Table. 2. A comparison of rougher feed % EDTA Cu for three chalcopyrite concentrators

Concentrator	EDTA Cu, %
Mount Isa Mines	0.02
Northparks Mines	0.65
Ok Tedi Mining	4.50

Both cations and anions are included in the analysis of EDTA liquors. Anion concentrations may also increase in the solution phase when EDTA solubilizes the cation. This gives an indication of the type of precipitated salts that were present in the pulp. An example of the EDTA extractable cation data from surveys is shown for copper, in Figure 4. Sample points from pulp streams for Figure 4 are shown in Table 3.

Table 3. Sample points for Figure 4

Sample Number	Plant Stream	Sample Number	Plant Stream
1	SAG Discharge Screen U/S	12	Rou-Scav Cells 10-15 Concentrate
2	Ball Mill Discharge	13	Rou-Scav Cell 15 Tail
3	Primary Cyclone O/F	14	Final Tail
4	Flash Cell Concentrate	15	Scavenger-Cleaner Tail
5	Rougher Feed	16	Low Grade Regrind Discharge
6	Rougher Cell 1 Concentrate	17	Low Grade Regrind Cyclone O/F
7	Rougher Cell 1 Tail	18	Column Cell Tail
8	Rougher Cells 2-3 Concentrate	19	Tank Cell Feed
9	Rougher Cell 3 Tail	20	Tank Cell Concentrate
10	Rougher Cells 4-9 Concentrate	21	Tank Cell Tail
11	Rougher Cell 9 Tail		

Increased % EDTA Cu in tailings streams compared to preceding concentrate streams in Figure 4, suggests that $Cu(OH)_2$ is depressing chalcopyrite. This assumes that the majority of $Cu(OH)_2$ is associated with chalcopyrite surfaces (which was suggested by higher PPM values for concentrates of 19/1/00). This suggests that $Cu(OH)_2$ may be functioning as a flotation depressant in the pulp. However, the very high % EDTA Cu for tailings streams of the 23/3/00 survey (45% EDTA Cu) does not imply that 45% of the chalcopyrite particles in the tailing were oxide. Rather, the implication is that a significant quantity of the $Cu(OH)_2$ in this pulp was dispersed, being precipitated onto much more than just chalcopyrite surfaces. Significant surface exposure of $Cu(OH)_2$ was also indicated in the XPS analysis of rougher feed samples, shown below in Figure 6.
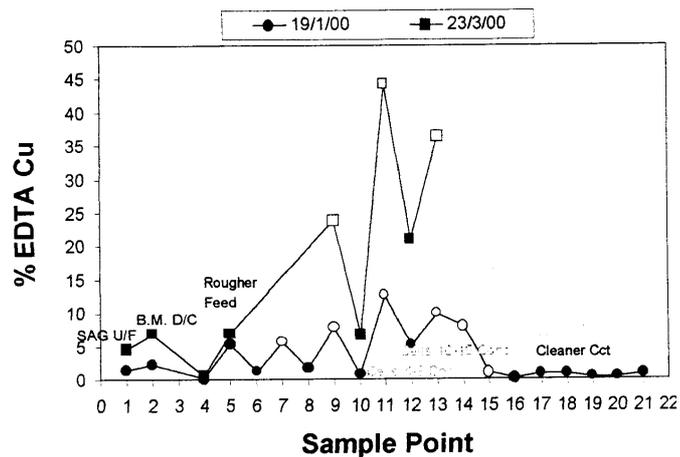
Fig. 4. Examples of EDTA extraction surveys, showing % EDTA Cu for plant streams. Tailings streams are shown in white

From EDTA and solution analysis, it was apparent that all $Cu(OH)_2$ was precipitated in the survey pulps. Approximately 80% of all EDTA extractable Ca was also precipitated. Sulphate levels in extracted solutions correlated approximately with Cu. However, for thermodynamic reasons, sulfate and calcium will have combined to form gypsum. However, there was approximately 10 times more EDTA extractable Ca in the pulps on average, compared to Cu, SO_4 or Fe, which were the other predominant oxide precipitates. Furthermore, concentration values for Ca were double for tailings samples, compared to the preceding concentrates. EDTA analysis therefore indicated Ca as a significant depressant of chalcopyrite flotation in surveyed pulps. During the time of the plant surveys, lime consumption was not recorded at Ok Tedi. However, it is known that lime usage increases with acidity of the feed ore (cf. Table 1) and varies from 2 to 5kg/t of feed ore. It may be noted that the natural pH of some of the feeds surveyed was approximately pH 4. A correlation between oxide skarn percentage in the feed blends and Ca levels in the pulp was found for surveyed pulps (see Appendix 1). However, insufficient data was available to show a correlation between Ca precipitation and decreased chalcopyrite recovery.

XPS ANALYSIS

XPS analysis was performed on rougher feed samples from Ok Tedi surveys of 17/1/00 and 19/1/00, and are shown in Figure 5. In both instances the plant flotation performance was poor (cf. Figure 1). Daily blend data (Appendix 1) shows a contribution of oxide copper from oxide skarn and sulfide skarn (magnetite) on 17/1/00. On the 19/1/00, the blend included 84% sulfide skarn (Magnetite) and 16% Endoskarn. On the 19/1/00, the feed acid soluble copper (ASCu) was 0.34%, which was the second highest ASCu value for all surveys (only 15/3/00 was worse, with 0.41%). EDTA analysis was also performed for 19/1/00 and showed 5.2% EDTA extractable Cu at rougher feed, which was comparable to March surveys using different ore blends (3.9 to 6.8% EDTA Cu in March).

XPS analysis confirmed the considerable surface exposure of Cu(II), which represents $Cu(OH)_2$ precipitation within the pulp, compared with Cu(I) which is found in $CuFeS_2$ and other copper sulfides. Figure 5 includes a spectrum for an MIM Cu chalcopyrite pulp (scavenger concentrate). This spectrum provides a comparison with an unoxidised chalcopyrite pulp, and highlights differences in the more oxidized Ok Tedi skarn ore feed. The spectra are charge corrected, based on charge shifting of C_{1s} peaks.

Figure 5 shows the spectral region for Cu_{2p} electron binding energies. The Cu_{2p} photoelectron spectrum includes two major peaks for the two spin states of the Cu_{2p} electrons. The major peak is for the $Cu_{2p3/2}$ electron and has a binding energy of 932.4 eV. The second peak is situated at a further 19.8 eV, for the $Cu_{2p1/2}$ electron. The Ok Tedi Cu_{2p} spectra show some differences to that of MIM Cu. As well as the two Cu peaks, a broad peak occurs between approximately 962 to 964 eV. This peak is an Auger peak for Ca, with a binding energy of 961.6 eV. This indicates the presence of

calcium precipitates from lime. In the Cu spectra, a broadening of the primary Cu_{2p} peak, and a broad multiple peak at slightly higher binding energy (known as 'satellites') are indicative of the presence of Cu(II). That is, $Cu(OH)_2$, was present in significant quantities on the surfaces of particles in Ok Tedi rougher feed magnetite skarn pulp, relative to Cu(I). Cu(I) was present as a component of Cu sulfides and possibly as adsorbed Cu on pyrite surfaces if the adsorption process occurred during grinding. A deconvolution of the major peak and satellites was performed (not shown). This indicated that on 17/1/00 and 19/1/00, on average approximately half of the Cu exposure was $Cu(OH)_2$. However, it should be noted that copper in the feed was only 2.6%, suggesting a relatively small proportion of the feed was $Cu(OH)_2$ precipitates. This was considerably less than the dispersion of other depressants such as Ca (cf. EDTA analysis).
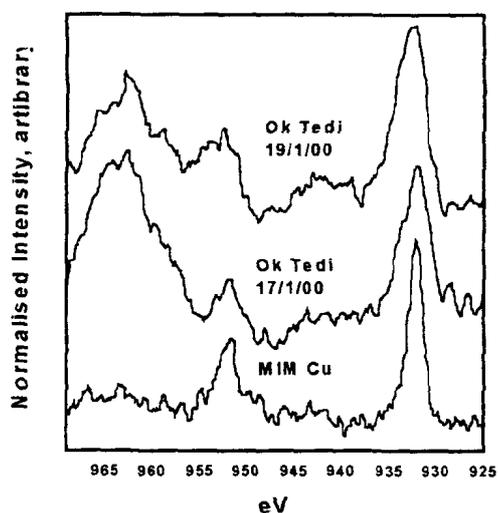
Fig. 5. XPS Cu_{2p} spectra for Ok Tedi rougher feed compared to MIM Cu

ToF-SIMS ANALYSIS

Time of Flight Secondary Ion Mass Spectrometry (ToF-SIMS) analyses were performed on final concentrate (tank cell) and final tailing samples from the 16/3/00 survey. Included in Figures 6 to 9 is a statistical analysis of 58 Cu sulfide particles and 58 pyrite particles. 30 Cu sulfide and 24 pyrite were analysed in the final tailing, and 28 Cu sulfide and 34 pyrite in the final concentrate. The normalised intensities for each surface species of interest have been averaged over the total number of particles of that type in the stream. Standard deviations were also calculated along with 95% confidence intervals for the normalised intensities, using 't' tests.
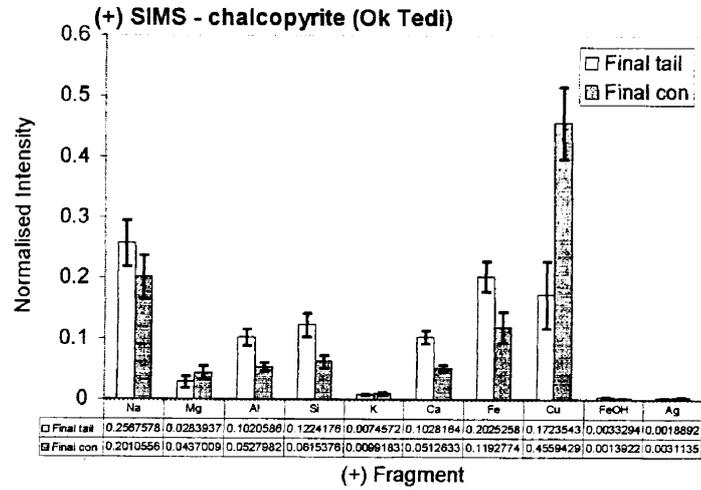
Fig. 6. (+) SIMS. Ok Tedi. Mass spectra for chalcopyrite in the final tail and final concentrate (confidence intervals calculated for P=95%)
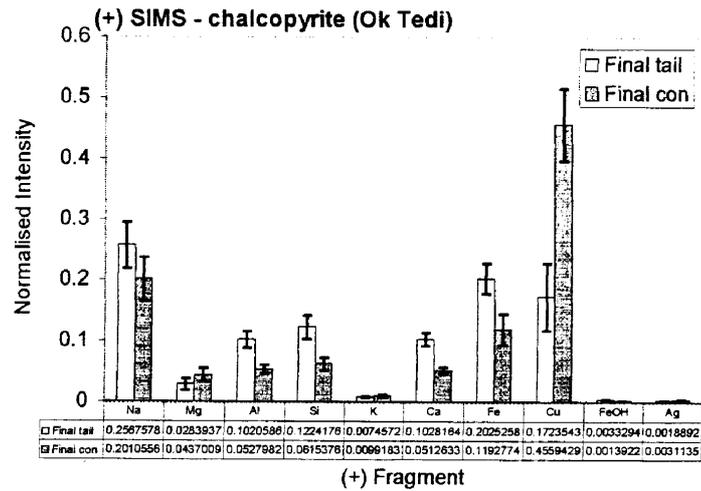
Fig. 7. (+) SIMS. Ok Tedi. Mass spectra for pyrite in the final tail and final concentrate (confidence intervals calculated for P=95%)

Statistically significant data are obtained from the averages of normalised intensities (shown in Figures 6 to 9), also from ratios of normalised intensities, and from a 'hydrophobicity index'. The hydrophobicity index has been a recent development at the IWRI and is proving a valuable tool in the interpretation of particle floatability (giving reason for particle location in a concentrate or tailing stream). The hydrophobicity index is a ratio of averaged normalised intensities for fragments representing hydrophobic surface species (CH and S, but not sulfate), and averaged normalised intensities for fragments representing hydrophilic surface

species (O and OH). The relative surface concentrations of these hydrophobic and hydrophilic indicators for the two samples analysed were calculated (each species is expressed as a proportion of total CH, S, O and OH). Expressed as ternary diagrams, the hydrophobicity index (not shown) clearly indicated that the balance between collector adsorption and oxidation products on particle surfaces was the primary determinant in particle floatability and hence recovery to concentrate. This confirmed the results of EDTA analysis, which indicated oxide precipitates were concentrated in tailing stream samples.

(-) SIMS - chalcopyrite (Ok Tedi)

	C	CH	O	OH	S	PO	PO2	PO3	SO3	DTP
Final tail	0.0433146	0.1255276	0.4941344	0.2461644	0.0817832	0.000658	0.0020382	0.0015217	0.0041315	0.0007263
Final con	0.0462257	0.1482589	0.3476777	0.2134038	0.2135713	0.0031786	0.012456	0.0082707	0.0035516	0.0034056

Fig. 8. (-) SIMS. Ok Tedi. Mass spectra for chalcopyrite in the final tail and final concentrate (confidence intervals calculated for P=95%)

(-) SIMS - pyrite (Ok Tedi)

	C	CH	O	OH	S	PO	PO2	PO3	SO3	DTP
Final tail	0.0294338	0.0877347	0.5864533	0.28444	0.008122	0.0001532	0.0012725	0.001582	0.0006383	0.0001701
Final con	0.0475497	0.1453037	0.4467514	0.261729	0.085703	0.0011508	0.0041118	0.0032037	0.0028563	0.0016405

Fig. 9. (-) SIMS. Ok Tedi. Mass spectra for pyrite in the final tail and final concentrate (confidence intervals calculated for P=95%)

ToF-SIMS normalised intensities give no indication of surface concentration. Therefore, data interpretation is based on comparisons. From the analysis of chalcopyrite particles in Figure 6, Ca and Fe along with Al and Si were shown to be more prevalent on tailings chalcopyrite particle surfaces compared to concentrate particles. All of these species showed approximately double the intensity on the final tailing chalcopyrite compared to the final concentrate.

On pyrite particles however (Figure 7), the increased normalised intensity for depressant species on tailings particles was 1.4 times for Ca, 1.1 times for Fe and 1.6 times for Al and Si. These ratios for pyrite differed to chalcopyrite, and suggest that these surface adsorbed species affected the pyrite and chalcopyrite hydrophobic/hydrophilic balance to different extents. Because chalcopyrite interacts with collector more strongly than pyrite (and will have very hydrophobic surface regions), it is probable that a higher surface concentration of hydrophilic precipitates was required to depress chalcopyrite particles, compared to pyrite. The greater surface concentration of calcium on final tailings chalcopyrite (and pyrite) compared to concentrate, confirmed EDTA extraction analysis, which indicated similar trends.

Another phenomenon indicated in the analysis of pyrite particles (Figure 7), was that Cu species had adsorbed onto pyrite particle surfaces, resulting in pyrite activation. The normalised intensity for Cu on pyrite in the concentrate was 7.3 times greater than for Cu on pyrite in the tailing (Figure 7). From Figure 9, the intensity of the 'CH' fragment on pyrite (collector) was 1.6 times greater on the concentrate compared to the tailing. This compares to 2.0 times the intensity for phosphate, also a collector fragment. This suggests that some adsorbed Cu on pyrite (possibly as Cu(I) sulfide), interacted with dithio phosphate collector. Copper and collector adsorption were therefore the most significant contributing factors to the flotation behaviour of pyrite in surveyed skarn pulps at Ok Tedi.

Physisorbed Cu(II) as hydrophilic $Cu(OH)_2$ may also have been present on the pyrite surface. However, no indication of a general depression of flotation by $Cu(OH)_2$ was observable from ToF-SIMS analysis, due to the dominance of the activating effect of Cu in conjunction with dithio phosphate collector.

SUMMARY AND CONCLUSIONS

A comparison of rougher-scavenger copper grade-recovery curves from metallurgical surveys of skarn feed blends at Ok Tedi, has indicated a variation in copper recovery with similar copper grade. This suggested a general depression of chalcopyrite and activated pyrite in the surveyed skarn pulps. Significant pyrite activation was shown. Feed tonnage (and by inference feed P80) was shown to correlate with decreased copper recovery. However, mineralogical analysis indicated adequate chalcopyrite liberation in all size fractions. Recovery by size analysis however, has indicated a depression of marginally floatable, liberated chalcopyrite in fine and coarse size fractions.

Pulp chemical surveys indicated dissolved oxygen (D.O.) demand was significant in concentrator pulps, and that pyrite surfaces were therefore not passivated as $Fe(OH)_3$. This implied that Cu activation and collector adsorption would have been enhanced on pulp pyrite surfaces. EDTA extraction analysis suggested $Cu(OH)_2$ and $Ca(OH)_2$ were flotation depressants in surveyed pulps. XPS analysis confirmed the presence of $Cu(OH)_2$ precipitates in rougher feed pulps. ToF-SIMS analysis, unequivocally showed that the significant pyrite flotation in surveyed pulps was due to the activation of pyrite by copper and collector. The so-called 'hydrophobicity index' of ToF-SIMS analysis indicated that ratio of oxy-hydroxide precipitates to collector on particle surfaces, determined the division of chalcopyrite particles between concentrate and tailings. ToF-SIMS analysis identified Ca, Fe, Al and Si as depressants of both chalcopyrite and pyrite. ToF-SIMS was technically unable to identify $Cu(OH)_2$ on activated particles.

At present, insufficient data is available to indicate any clear correlation between the identified pulp chemical depressant species and decreased chalcopyrite recovery in Ok Tedi skarn blend pulps. It is apparent that finer grinding, along with limitation of the acidic components of the feed blend, may result in improved recovery of chalcopyrite for skarn ore feed blends at Ok Tedi.

ACKNOWLEDGEMENTS

REFERENCES

PUTUBU, J. AMIRA P260C (Nov. '99) Ian Wark Research Institute, University of South Australia.

GRANO, S. R., GRIFFEN, L. K., JOHNSON, N. W., St.C. SMART, R., & RALSTON, J. (1991). *Treatment of naturally hydrophobic Gangue Minerals at the Copper Concentrator of Mt. Isa Mines Limited*. In Proceedings of the Fourth Mill Operators Conference, North West Tasmania: Aus. I.M.M, 121.

KANT, C., RAO, S. R., & FINCH, J. A. (1994*). Distribution of surface metal ions among the products of chalcopyrite flotation*. Minerals Engineering, 7(7), 905.

LAUDER, D., *Personal communications* (1997), Cited Orwe, D.D., (2000) M.App.Sc Thesis, University of South Australia.

RUMBALL, J. A., & RICHMOND, G. D. (1996). *Measurement of oxidation in a base metal flotation circuit by selective leaching with EDTA*. International Journal of Mineral Processing, 48, 1.(St.C. Smart, 1992).

SMART, St.C. R. (1992). *Protocols for Surface Analysis in Minerals Processing Chemical Technology,* University of South Australia.

APPENDIX 1

Data from Metallurgical and Pulp-Chemical Surveys

#	Category	Param	17/1/00	18/1/00	19/1/00	13/3/00	14/3/00	15/3/00	16/3/00	17/3/00	18/3/00	19/3/00	20/3/00	21/3/00	10/12/98	11/12/98	29/11/99	30/11/99
1	Feed	Cu %			2.61			0.81	0.74	0.97				1.45		2.59		1.50
		Au g/t						0.80	0.62	0.72				0.86		2.47		1.28
		S %						3.88	3.68	3.47				15.70		6.41		
		Fe %						13.30	12.27	13.28				21.03		47.89		
		SiO₂ %						46.80	49.39	47.21				34.08				
2	Cu:S	Ratio						0.21	0.20	0.28				0.09		0.40		
3	Ro-Scav	Rec.			82			66	60	82				80		94		90
4	Module Feed tph				1102				2074	742				1698		917		1079
5	Monzonite %					18.20	37.10	29.90	58.20	29.30	12.30	44.50	50.20	55.40		37.80	35.80	23.40
	(MP)	Cu %				0.28	0.62	0.69	0.70	0.52	0.52	0.50	0.52	0.68		0.82	0.60	0.68
	Acid Sol	Cu %				0.02	0.05	0.02	0.02	0.02	0.02	0.02	0.02	0.02		0.06	0.04	0.02
	Monxodiorite %					0.20	47.50	8.10	40.00	53.80	57.70	28.30	2.40			3.30		5.30
	(MD)	Cu %				0.50	0.50	0.47	0.38	0.38	0.38	0.38	0.38			0.53		0.57
	Acid Sol	Cu %				0.03	0.03	0.03	0.03	0.03	0.03	0.03	0.03			0.02		0.02
	Pyrite	Skn %															31.70	2.20
		Cu %															2.00	0.76
	Acid Sol	Cu %															0.24	0.08
	Sulfide	Skn %	98.60	100	68.20	2.60	12.80	16.40	0.20	12.80	12.00	24.40	45.20	35.40	100	58.90	32.50	66.80
		Cu %				1.02	0.99	2.77	3.90	0.80	3.90	2.47	1.97	1.94	1.86	1.86	1.96	2.00
	Acid Sol	Cu %	0.18	0.17	0.15	0.06	0.11	0.25	0.34	0.10	0.34	0.24	0.14	0.16	0.16	0.16	0.18	0.21
	Endoskarn %				31.80	64.60					1.50							
		Cu %			0.88						1.52							
	Acid Sol	Cu %			0.09	0.05					0.10							
	Siltstone %							32.30										
	(SLT)	Cu %						0.98										
	Acid Sol	Cu %						0.06										
	Oxide	Skn %	1.40			14.80	2.70	13.30	1.60	4.10	16.50	2.80	2.00	9.20				2.20
		Cu %				1.13	3.21	3.21	1.81	3.21	2.43	2.73	3.21	1.45				0.30
	Acid Sol	Cu %	2.13			2.13	2.13	2.13	2.13	2.13	1.54	2.13	2.13	0.89				0.02
6	Blend	ASCu %	0.21	0.17	0.13	0.13	0.35	0.10	0.35	0.06	0.12	0.32	0.14	0.12	0.15	0.16	0.12	0.15
	2 day average				0.15				0.23	0.21	0.09			0.13		0.14		0.15
7	Plant daily ASCu %				0.34				0.41	0.25	0.06			0.18		0.25		0.08
	Plant daily Cu %				2.24				1.05	1.08	0.63			1.05		2.80		1.08
8	EDTA Ex. Ro-Feed																	
	PPM	Cu			478				468.9	119.2				235.5				
	PPM	Fe			645				244.9	1026				488				
	PPM	S			343				209.5	148.1				260.6				
	PPM	Ca			3060				7442	4472				9353				

Dokonano równoległej oceny metalurgicznej i chemicznej mieszanki rud typu skarnowego w Ok. Tedi Mining Ltd. (Papua Nowa Gwinea). Wyniki metalurgiczne wskazują na zmienność uzysków przy zbliżonych zawartościach metalu w koncentratach, co wskazywałoby na jednakową depresję aktywowanych we flotacji minerałów. Przedmiotem artykułu jest ocena oddziaływań chemicznych w zawiesinie flotacyjnej w świetle zapotrzebowania na tlen decydujących o reaktywności minerałów siarczkowych. Badania powierzchniowe w oparciu o ekstrakcję przy użyciu kwasu wersenowego (EDTA), rentgenowskiej spektroskopii elektronowej oraz jonowej spektrometrii masowej (ToF-SIMS) potwierdziły aktywowanie pirytu miedzią oraz depresję chalkopirytu prze wytrącone wodorotlenki Ca, Fe, Al. i Si.

Kadry N. SEDIEK[*], Ashraf M. AMER[**]

SEDIMENTOLOGICAL AND TECHNOLOGICAL STUDIES OF ABU TARTUR BLACK SHALES, WESTERN DESERT, EGYPT

Newly conventional combination of sedimentological and technological studies aid in estimation of the resource potential of the Upper Cretaceous clays of Duwi Formation Abu Tartur plateau Western Desert, Egypt. This formation consists of interbedded black to Grey shale, phosphatic and glauconitic sandstones.

The granulometric, mineralogical, and geochemical analyses were carried out on the black clays, which provided detailed information about textural parameters, composition and paleoenvironment of deposition

The technological studies of black shale is new for its interesting enrichments in various rare metals as nickel , chromium and vanadium . This investigation is a laboratory study for extraction of vanadium from black shales by hydrochloric acid processing to produce leach solutions of vanadium, aluminum and magnesium chlorides. The effects of various factors affecting the leaching process such as temperature, acid concentration, particle size and stirring speed as well as the kinetics of the leaching process were studied.

The most favorable conditions for the extraction of the vanadium present in the black shale are temperature 100° C, acid concentration 6 M by weight, grain size 17 μm and leaching time 90 min.

Key words: black shale, paleoenvironment, vanadium, leaching.

INTRODUCTION

The black shale sample were collected from Abu Tartur plateau, Kharga oasis which is located at the intersection of longitude 30 05 E. and latitude 25 32 N. This area had attracted attention of many geologists since the discovery of great phosphate deposits in 1967. The stratigraphic position of the investigated deposits lies within upper and lower member of the Phosphate Formation (Said 1990). This formation underlies the Dakhla shale and overlies the Quseir Formation; lithologically it consists of phosphate beds interbedded with black and gray claystone, sandstone, siltstone and glaucony beds.

 *Alexandria University, Faculty of Science, Geology Department.
**Alexandria University, Faculty of Science, Environmental Science Department.

At the late time the government of the New Valley (El Kharga oasis) pay attention to exploit the wide extended clay deposits which exposed allover the oasis and extended even to El Dakhla oasis (El Kharga El Dakhla stretch). Among the clay deposits is the black shale, which have a considerable economic importance due to their special composition.

Black shales in Egypt are now known for their interesting enrichments in various metals especially rare vanadium (Melik 1971) and nickel (Amer 1994). No attempts havebeen made to process these black shales or to find a profitable use for them. The manufacture of vanadium alloys in Egypt depends mainly on imported vanadium. It is therefore claimed that the development of an indigenous source of vanadium to sustain self- sufficiency in vanadium. Attempts to utilize vanadiferous shales are mainly restricted to the leaching of vanadium by the stander roast-leach process (Sastry and Raju 1968, Bing and Thome 1978). A hydrometallurgical route has recently been proposed for the treatment and processing of vanadiferous shales. In this investigation black shale is leached with hydrochloric acid under mild condition whereby vanadium and iron dissolve. Separation of vanadium and iron can be achieved in economic scale using ion exchange (Martins at el. 1973 and Amer 1996).

MATERIAL AND METHODS

Twelve black shale samples were collected from the repeated black shale beds at Abu Tartur mine. Five-selected Sample were attained granulometric analysis, wet sieving was achieved by the use of pipette method (Lewis and McConchie 1993). Sand, silt, clay contents, sample nomenclature and four main statistical textural parameters Mz, σI, SkI and KG (Folk and Word 1957) were estimated (Tab. 1).

Table 1. Granulometric results, nomenclature and statistical textural parameters
of the studied black shale

Samp. No.	Rock Constituents			Nomen clature	Statistical Textural Parameters			
	Sand	Silt	Clay		Mz	σ I	Sk I	KG
b.c.9	0.60	76.40	23.00	Silt	5.46	1.30	0.06	0.59
b.c.7	0.50	59.66	39.84	Clay –silt	5.64	1.62	0.17	0.61
b.c.5	0.40	84.09	15.51	Silt	5.33	1.30	0.45	1.78
b.c.3	0.60	87.70	11.70	Silt	4.67	1.76	1.10	1.63
b.c.1	0.98	76.82	22.19	Silt	5.51	1.71	0.56	0.69

Clay mineral analysis had carried out by XRD method on six selected samples. A qualitative and quantitative estimation for clay mineral were made to the whole sample and to the separated clay fraction after various treatment (air dried, glycol

solvated and heating to 550 °C) in order to isolate the clay components. The resulted X-ray diffractograms were interpreted using Krotova and Kazakova method (1984).

Eight of the black shale samples were chemically analyzed at the Technical University of Berlin, Germany. Major elements were determined using energy dispersive X-ray florescence technique on fused pellets. Trace elements were also determined using pressed pellets and polyvinyl alchol as binding agents. Analytical results for selected and representative samples are listed in Table 2.

Table 2. Frequency distribution of the different minerals in the studied black shale

Samp. No.	Mineralogical composition							
	Q	Sm	I	S	K	F	J	Py
b.c.6	7.70	74.50	–	–	2.00	2.00	–	–
b.c.3	8.00	82.70	0.10	–	–	–	–	–
b.c.1	17.00	72.00	0.60	0.60	–	2.60	3.70	1.70

Q – Quartz   Sm – Smectite   I – Illite   S – Sederite
F – Feldspar   Py – Pyrite   J – Jarosite   K – Kaolinite

All leaching experiments were performed in 600-ml capacity glass beaker held in water bath controlled to ±1 °C using a thermostat/circulating pump. Using an impeller driven by a variable speed motor did the stirring of the liquid. The technique used in the present investigation has been described elsewhere (Amer 1996).

GRANULOMETRIC ANALYSIS

Wet sieving was used to analyze the black shales for define their textural composition. The obtained data and the resulted textural parameters are recorded in Table (1). It is appeared that the studied black shale lie belong silt and clay – silt according to (Picard 1971) .

Based on the illustrated data (Tab. 1) the studied sediments could be described as medium grained, poorly sorted, fine to strongly fine skewed silt.

Generally the fine clay fraction is very sensitive to depositional process, so the auther tried to use the obtained Statistical Textural Parameters (STP) and their binary relations to give an idea about the ancient environment and transportation mechanism.

Plotting the estimated values of C (the one percentile) and M (the Median 50 percentile) on C-M pattern proposed by (Passega 1964), illustrate that the studied black shale was deposited under turbidity current (Fig. 1). Moreover the binary plots (Stewart 1958), had cleared that, these samples lie in quiet water (slow suspension) condition.

Therfore the authers assumed that the studied black shale resemble the third main type of suspension which occur when turbid flows enter bodies of waters with no

significant density difference, such this situation the flow named hypopycal flow (Bates 1953, Tucker 1988). The fine material of black shale was settled out of suspension from admixture of water bodies most probably fluvio-marine environment.

(a) C – M. pattern (fter passega, 1957)

(b) Inclusive graphic standard deviation versus diameter
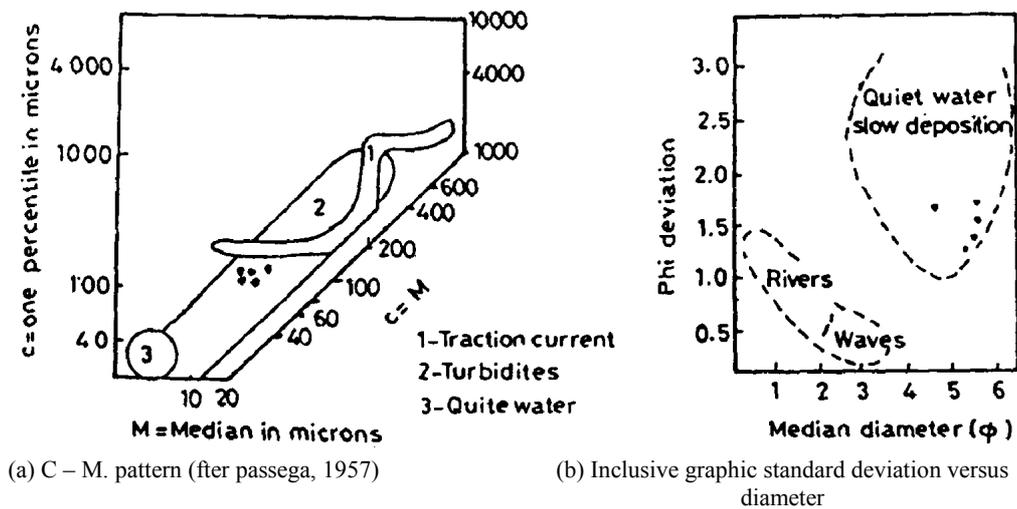
Fig. 1. Binary realationship of statistical textural parameter of Abu Tartur black shale

MINERALOGY

The results of X-ray diffraction analysis of Abu Tartur black shale are discussed below.

X-RAY ANALYSIS OF BULK SAMPLE

The bulk sample diffractograms revealed the presence of certain association as shown in Table 1. Quartz is present in moderate amount (7.7 to 17 %). Smectite is the dominant mineral (72 to 82.7 %), while feldspare forms small content (2.6 to 5.7), consequently kaolinite and illite as well as jarosite and pyrite occur as minor constituents (Tab. 2)

X- RAY ANALYSIS OF CLAY FRACTION

The X- ray diffractograms of the oriented clay fraction reveal the presence of high sharp peak 14.1 A and very weak 7.16 A peak on the untreated diffractogram. On the glycolated run the peak 14.1 shifts to larger spacing peak 17.9 A, while with heating to 550 C it collapsed and sharpened at 9.8 A peak (Fig. 2)

Using flow sheet for clay mineral identification (Starkey et.al. 1984, Krotova and Kazakova 1984) method, the clay fractions are composed of dominant smectite (montmorillonite) mineral with small amount of kaolinite-smectite interstratified layers.
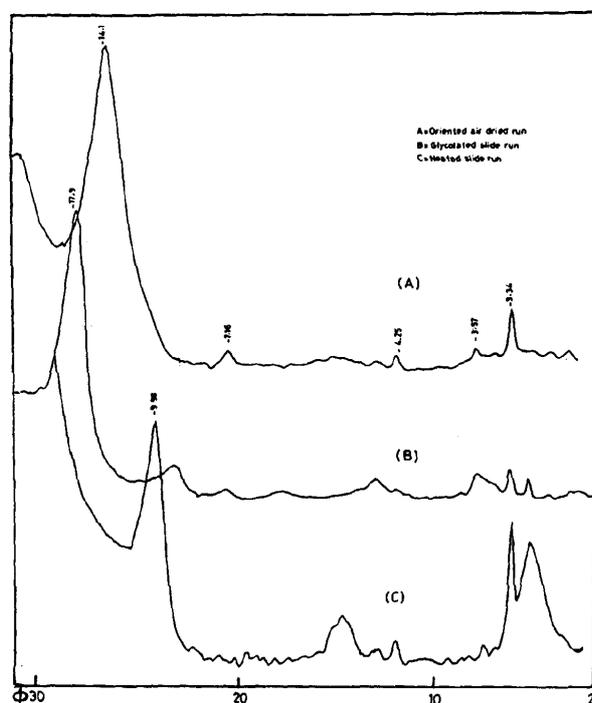
Fig. 2. Representative diffractogram of the clay fraction Abu Tartur black shale

The resulted clay mineralogy of the studied samples is taken as an indicator for paleoenvironmental interpretation where the abundance of smectite and low content of illite and kaolinite refer to deposition under fluvio-marine environments and the prevailed condition was of alkaline chemical affinity, at the same time the source rock had not attained intensive weathering.

GEOCHEMISTRY

The chemical analysis of eight selected samples is carried out in order to shed light on the chemical composition and their position relative to world types of black shale.

Table 3 A. Average content of the major elements of Abu Tartur black shale

Samp No.	Chemical Analysis									
	SiO_2	Al_2O_3	Fe_2O_3	CaO	MgO	Na_2O	K_2O	P_2O_5	TiO	SO_3^{2-}
9,10	58.09	19.80	5.92	1.50	2.11	0.72	0.90	1.69	1.07	2.37
5,6	58.32	16.66	8.45	1.02	1.20	0.35	0.79	2.48	1.25	1.99
3,4	59.40	18.19	4.93	0.57	2.18	0.32	0.78	1.38	1.30	2.54
1,2	59.09	16.48	3.38	2.47	1.46	1.19	0.59	1.16	0.81	1.86

Table 3 B. Average content of the trace elements of Abu Tartur black shale

SampNo.	Content in PPM									
	V	Sr	Cr	Ni	Co	Cu	Zn	Ba	Pb	Zr
9,10	425	180	300	89	60	35	88	150	219	230
5,6	490	190	190	80	48	35	79	140	190	220
3,4	430	170	185	43	49	30	72	149	185	200
1,2	260	199	180	33	40	32	62	113	113	180

Twenty major and trace elements were determined. Tables (3 A, 3 B) show the average content of these elements, it is obviously clear that the analyzed black shale samples are poor in Fe_2O_3, CaO, MgO, K_2O, Na_2O, while rich in Al_2O_3, P_2O_5, TiO and nearly with the same content of SiO_2 relative to the published contents of the world shales. On the other hand, they are rich in V, Cr, Co, and Pb, while poor in Sr, Ba and with similar values of Ni, Cu, and Zn comparatively to the Turkian and Wedepohl, 1961 and the data compiled from (Cullers and Stone 1991, Cullers, 1995).

The chemical analysis agreed with the results of clay mineralogy investigation where the low percent of K_2O reflects the absence or low content of illite mineral.

According to the geochemical classification which based on the log values of the ratios SiO_2/Al_2O_3 and Fe_2O_3/K_2O (Herron 1988), the Abu Tartur black shale are classified into iron–shale

Two main recommended ratios were used, which have intimate relation to environment (Roaldest 1978). These ratios are K_2O/Al_2O_3 and MgO/Al_2O_3, plotting their values on Roaldest diagram has cleared that the studied black shale lied in the area between marine and non-marine environment.

TECHNOLOGICAL STUDY

LEACHING ASPECTS

Temperature:	40 – 100 °C
Hydrochloric acid conc.	2 – 8 M
Grain size	17 – 80 μm
Stirring speed	250 – 1000 rpm/min.
Time of leaching	20 – 100 min.
Solide/liquid ratio	0.1

The dissolution of vanadium and iron using hydrochloric acid can be expressed by the following :

$$V_2O_3 + 6HCl \rightarrow 2VCl_3 + 3H_2O \qquad (1)$$

$$FeO(OH) + 3HCl \rightarrow FeCl_3 + 2H_2O \qquad (2)$$

$$Fe_2O_3 + 6HCl \rightarrow 2FeCl_3 + 3H_2O \qquad (3)$$
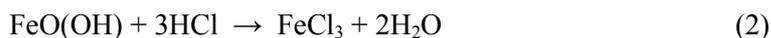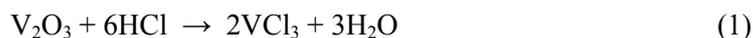
BEHAVIOUR OF VANADIUM

Effect of leaching time and temperature:

Results using 6 M HCl with grain size (17 μm) at 90 °C, stirring speed of 800 rpm/min are shown in figure 3. Vanadium extraction is highest ≥ 90%. The vanadium extraction increases with temperature. The activation energy for the leaching process is determined by an Arrhenius plot as shown in figure 4. The activation energy is calculated to be 18 kJ/mol which is indicative of a boundary layer diffusion control.
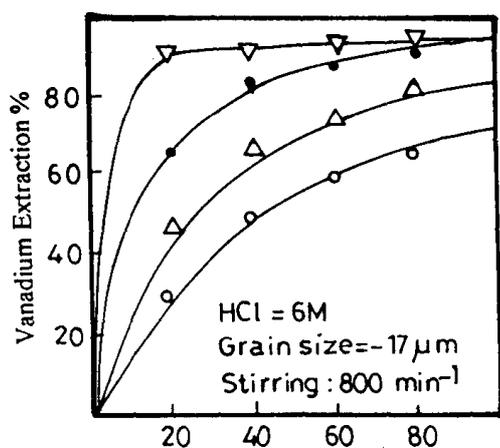
Fig. 3. Relation betwenn vanadium extraction   Fig. 4. Arrhenius plot for determining
and time at different temperatures   the activation energy

Effect of acid concentration:

Figure 5 shows the effect of HCl concentration in the range of 2-8 M. on leaching 17 μm. black shale deposits at rpm/800 min. agitation speed at 100 °C. It can be seen that the vanadium extraction increases with increasing acid concentration from 2-6 M.

Further increase of acid concentration has practically no effect on vanadium extraction. Chemical weathering affects the stability of silicate structures and probably accounts for enhanced extraction of vanadium. Increasing the temperature of acid results in a greater release of vanadium from its lattice position.

Effect of speed of agitation:

Figure 6 shows the effect of speed of agitation in the range of 250 – 1000 rpm/min using 6 M. HCl at 100 °C. It can be seen that, the rate of the reaction depends on the speed of agitation. As seen from figure 8, a plot of ln (1 - ά) versus time of the expremint at different agitation speeds yields a straight lines indicating that the leaching of black shale is a diffusion controlled process.
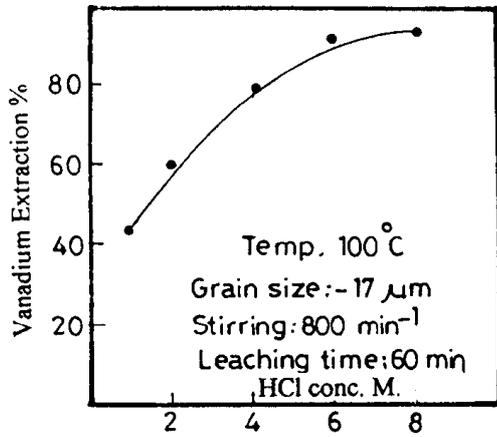
5. Effect of acid concentration
on vanadium extraction
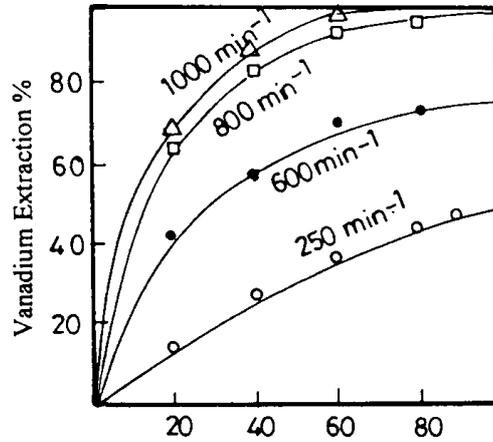
Fig. 6. Effect of speed agitation
on vanadium extraction
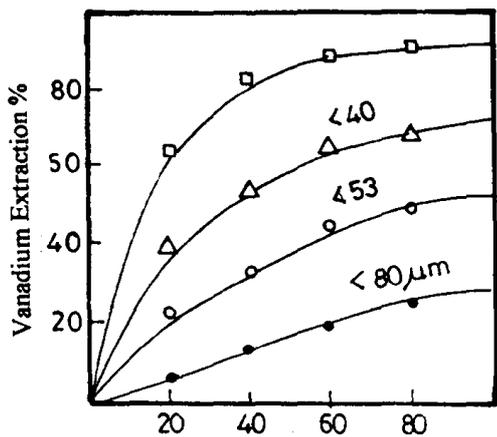
Fig. 7. Effect of particle size on vanadium
extraction
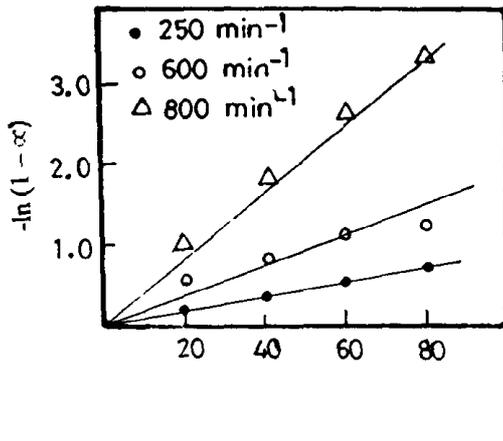
Fig. 8. Test of applicability of film diffusion
model to the experimental data

Effect of particle size:

Figure 7 shows the results obtained when particle size fraction with mean diameter of 17, 40, 53, and 82 μm were used. The apparent rate constants k were calculated according to the following equation (Fig. 8).

$$\ln(1 - \alpha) = kt$$

where: α − fraction reacted of vanadium from Abu Tartur black shale
k − reaction constant min.
t − leaching time min.

The external surface areas were calculated for different particle size using the following equation assuming spherical particles :

$$S = \frac{2\,m}{3\,p\,d}$$

where   S – external surface area for the particle – m²,
             m. –- the mass of the sample being leached – kg,
             p – the density of the sample – kg/m³,
             d – the particle mean diameter – μm.

The specific apparent constant k/s were calculated and are given in Table 4. It is clear that the smaller the particle size, the larger the specific apparent rate constant .It is known that the smaller the particle size , the thicker the boundary layer surrounding the particle. This further confirms that the controlling step is diffusion through the boundary layer.

Table 4. Rate constants for various particle sizes

D [μm]	S [m²]	k [min^{-1}]	k/S [(m² · min)$^{-1}$]
17	0.7	0.044	0.0629
40	0.33	0.017	0.0515
53	0.29	0.009	0.0310
80	0.25	0.004	0.0169
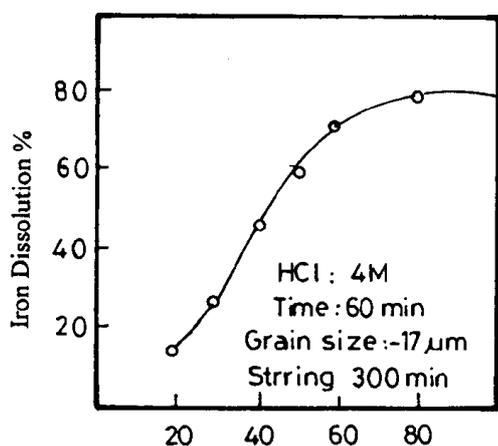
Fig. 9. Effect of temperature on
iron dissolution
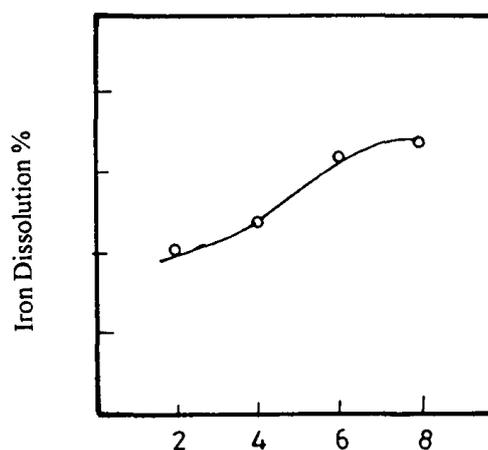
Fig. 10. Effect of hydrochloric acid concentration
on iron dissolution

BEHAVIOUR OF IRON DURING HYDROCHLORIC ACID PROCESSING

Figures (9, 10) show the behaviour of iron as a function of temperature and acid concentration. At low temperature 40 °C acid concentration is the dominating factor in deciding the percentage of metal extraction.

SEPARATION OF VANADIUM AND IRON BY ION EXCHANGE

Recovery of vanadium from acid leach solution by ion exchange is economically feasible. Pilot scale tests were made. The leach solution was heated to 50 °C and sodium chlorate was added to oxidize vanadium (V_2O_3) to vanadium (V_2O_5), which was then sorbed by the resin, changing its color to bright red. After washing with water, vanadium was eluted by sulfurous acid solutions, the elute was deep blue due to vanadium (VCl), and the resin turned lemon yellow. The strongly sorbed HSO_3^- was removed by 2 % solution of $NaClO_3$ acidified at pH 1.5 with H_2SO_4. The resin again turned golden brown color.

CONCLUSIONS

Generally the Abu Tartur black shale represented granulometrically as silt and clay –silt. Mineralogical data showed that the black were composed of non-clay mineral association as quartz, feldspare, jarosite and pyrite and clay mineral represented by frequent smectite and traces of illite and kaolinite-smectite interstratified layer.

Geochemical data suggested that the black shale classified as iron-shale. These shales were rich in major oxides as Al_2O_3, P_2O_5,TiO and poor in CaO, MgO, K_2O and Na_2O with similar SiO_2 content comparatively to the known world shale.

Based on the combined sedimentological data, the main characters of the paleoevironments could be interpreted; the source area of black shale had not attained intensive weathering and the resulted materials had carried by fluvial action, which finally interfered and admixed with marine environment to create alkaline, quiet and reduced conditions.

The technological work done indicates that a promising process might be devised for hydrochloric acid leaching of Abu Tartur black shales.

Vanadium extraction from shales is a function of temperature, acid concentration and a stirring speed as well as particle size of used black shale. The reaction rate is controlled by the diffusion of vanadium from silicate structure of black shale. The calculated activation energy is found to be 18 K/mol.

REFERENCES

AMER A.M. (1994*), Hydrometallurgical processing of Egyptian black shale of the Qusier-Safaga region,* Hydrometallurgy, Vol. 36, 95-107.

AMER A.M. (1996), *Aspects of the mineralogy and hydrometrallargy of some Egyptian serpentinite deposits*, Erzmetall, Vol. 49 N. 6, 373-378.

BATES C.C. (1953), *Rational theory of delta formation*, Bull. Amer. Ass.Petrol. Geol. Vol. 37, 2119-2162.

BING H., THOME, R. (1979), *Gwinnung von vanadin pentoxid aus Titanomagnetite*, Erzmetall. Vol. 31, 387-394.

CULLERS R.L , STONE J. (1991*), Chemical and mineralogical composition of the Pennsylvanian Fountan Formation*, Colorado, USA., Lithos**,** Vol. 27 115-131.

CULLERS R.L. (1995*), The controls on the major and trace – element evolution of shales, siltstone and sandstone of Ordovician to Tertiary age in the wet Mountains region,* Colorado, USA, Chem. Geol. Vol. 123, 107-132.

HERRON M.M. (1988), *Geochemical classification of terrigenous sands and shales from core or log data*, J. Sed. Petrol.,Vol**.** 58, 820-829.

FOLK R.L., WORD, W. (1957*), Brazos River bar: A study in the significance of grain size parameters*, J. Sed. Petrol. 27**,** 3-28.

KROTOVA G.E, V.E. KAZAKOVA (1984), *Directory for identification of clay minerals using X-ray diffraction method,* Univ.Patres Lomomba, Geol Depart. Moscow., No. 26, 52.

LEWIS D.G. McCONCHIE D. (1993), *Analytical sedimentology*, Chapman & Hall, New York. London.

MARTIN E., CLEMENT M. BAHR A. (1973), *Uber die sauer langung oolithishcer Eisenerze einschliesslich der selektiven gewinnung von einsen and vanadium*, Bd. 26 H.9.

MELIK E.K. (1971), *Geology and geochemistry of the black shales of the Qusier-Safaga region, Msc. Fac. Sci. Assuit Univ.*, Egypt.

PASSEGA R. (1964), *Grain-size representation by C-M patterns as a geological tool*, J. Sed. Petrol. 34, 840-847.

PICARD M.D (1971), *Classification of finr- grained sedimentary rocks*, J. Sed. Petrol.,Vol. 41, 179 –195.

ROALDEST E. (19780, *Mineralogical and chemical changes during weathering, transportation and sedimentation in different environments*, Ph. D.T hesis, Geol. Inst., Univ. Oslo, Norway.

SAID R. (1990), *The Geology of Egypt*, A.A.Balkema. Rotterdam Netherland, 734.

SASTRY A.R., RAJU C.V.R (1968), *Parameters of leaching in the soda roastring process for extraction of vanadium from titaniferous magnetit ores of Andhr.*, Chem Age. India, Vol.3, 195 -201.

STARKEY H.C., BLACKMAN P.D., HAUFF P.L. (1984*), The routine mineralogical analysis of clay – bearing samples,* U.S. Geol. Surv. Bull., p.p 1563.

STEWART H.B. Jr. (1958*), Sedimentary reflections on depositional environments in San Migue lagoon*, *Baja California, Mexico,* Bull. Amer. Ass. Petrol. Geol.,Vol.42, 2567-2618.

TEDESCO P.H. (1962), *Recovery of vanadium by ion exchange*, Univ.Nad . La plata, Publ. Fac. CIENC. Fisicomat. Vol. 8, No.2 ,37-56.

TEDESCO P.H., BIANCHI DE RUMI V.A.M. (1964), *Alkaline recovery of vanadium by ion exchange,* Afinidad, Vol. 21, No.230, 106-111.

TUCKER R. (1988), *Techniques in sedimentology*, Blackwell Scientific publications, pp. 394.

TUREKIEN K.K., WEDEPOHL K.H (1961), *Distribution of the elements in some major units of the earth, s crust.,* Bull. Geol. Soc.Amer., Vol .72,1 75-192.

Sediek N.K., Amer M.A., *Badania sedymentologiczne i technologiczne czarnych łupków ze złoża Abu Tartur w Zachodniej Pustyni w Egipcie*, Fizykochemiczne Problemy Mineralurgii, 35,2001, 141-152 (w jęz. ang.).

Badania sedymentologiczne i technologiczne miały za cel oszacowanie potencjalnych możliwości wykorzystania czarnych iłów ze złoża Abu Tartur leżącego na pustyni zachodniej w Egipcie. Złoże to zawiera czarny przechodzący w szary łupek, glaukonitowy i fosforanowy piaskowiec. Zostały przeprowadzone analizy granulometryczne, mineralogiczne i geochemiczne czarnych iłów. Wyniki analiz dostarczyły dokładne informacje o teksturze, składzie i paleosrodowisku złoża. Badania technologiczne czarnego łupka zostały przeprowadzone z uwagi na bogatą zawartość w nich metali rzadkich takich jak nikiel, chrom i wanad. Badano w skali laboratoryjnej, proces ekstrakcji wanadu kwasem solnym, otrzymując roztwór zawierający chlorki wanadu, glinu i magnezu. Wpływ różnych parametrów takich jak temperatura, stężenie kwasu solnego, uziarnienie nadawy, prędkość mieszania, na kinetykę procesu ługowania został przebadany. Najlepsze warunki ekstrakcji wanadu z czarnego łupka uzyskano stosując temperaturę 100°C, stężenie kwasu solnego 6M, granulację nadawy 17 μm i czas ługowania 90 minut

A. M. RAMADAN[*], A.M. SALEH[*], T.A. TAHA[*] and M.R. MOHARAM[*]

AN ATTEMPT TO IMPROVE MECHANICAL PROPERTIES OF BRICK PRODUCED FROM EL-MAGHARA COAL WASHING PLANT WASTE

Treatment of wastes became a vital demand to maintain the environment as clean as possible . The treatment of wastes and reuse of their constituents in industry will be helpful for this trend as well as for economy. Flotation technique is one of the important separation techniques that can be applied for treatment of wastes efficiently. The filter cake of El-Maghara coal washing plant was one of these wastes which contains a considerable amount of clay. This filter cake was treated in a previous work by flotation in order to clean it from the contained fine coal. The residual clay was tested as a raw material to produce brick models with acceptable mechanical properties. Improvement of the mechanical properties of such brick models by mixing such clay with sand is exactly the main objective of this work. The effect of different factors such as, weight percent of sand and its particle size on the mechanical properties of the brick models was investigated. It was found that 20 % and 60 % of sand sample characterized by size distribution of - 1500 + 0 µm and - 500 + 0 µm respectively are enough to achieve a considerable extent of improvement in the mechanical properties of the clay brick produced.

Key words: fine coal, clay, sand, brick, mechanical properties

INTRODUCTION

A serious consequence of coal mining and preparation is the significant amount of waste products which may lead to pollution of all three components of environment, namely, air, water and soil. Also, wet methods of coal beneficiation have contributed much to surface water pollution. Hence, treatment of plant process water and / or wastes and reuse of these wastes become necessary for preferable environment (Shan et.al 1990, Cellier,1990). Recently, a new strategy called wastless technology has been developed to prevent further environmental degradation (Cellier 1990). This approach

* Al-Azhar University, Fac. of Eng., Min. & Pet. Dept., Nasr City, Cairo, Egypt

aims to obtain the complete utilization of raw materials in order to decrease the amount of tailings and processing of these tailings to make the majority of its waste products acceptable for utilization in a manner both economically feasible and environmentally inoffensive. The coal fines of wastes were utilized by applying the technique that agglomerates it into a coarser more handleable size product which called coal brequitting technology. There are different technologies and attempts through the mineral processing literature concerned with the treatment of fine coal wastes and reuse of their constituents which can be helpful for both environment and economy (Lukc 1994, Tucker et.al1994). In earlier work (Ebied 1984), Fayoum clay powder was mixed with different amounts of sand and with sufficient amount of water and extruded into perforated briquettes. The results showed that a mixture of 70 % clay and 30 % sand (wt. %) was found to have a suitable ceramic properties. Another works (Elwan et. Al. 1999, Elwan et.al. 2001) dealing with mixing the by-pass cement dust as nonplasic material with clay for preparation of clay for brick industry. The results obtained showed that the substitution of 10 wt. % clay by cement dust increases the gas permeability of the fired bricks, which prevents the brick to bloat and also increases the crushing strength. Filter cake produced from El-Maghara coal washing plant, northern Sinai-Egypt, represents about 112,000 ton/year. Along the mine age which is about 35 years, a huge amount of filter cake will accumulate in the storage area near the mine. This kind of waste was found to contain more than 45 % of coal fines. It was suggested to recover this amount of fine coal by flotation technique. In a previous study (Ramadan et.al. 2000), an attempt was done to recover such high amount of coal fines by flotation technique. Promising results were obtained using kerosene as a collector with about 50 % yield. The residual clay was also tested as a raw material for producing brick models and acceptable results were recorded. Hence, a considerable amount of clay ,i.e, about 56,000 ton/year will be collected. The main objective of this work is to improve the mechanical properties of such brick models by mixing the residual clay after flotation process with different amounts of sand of different particle sizes.

MATERIAL AND METHODS

Filter cake produced from El-Maghara coal washing plant as tailing was used as a raw material for clay after its treatment by flotation to separate the involved coal fines. X ray analysis was done for such filter cake sample and the results are tabulated in table 1. The flotation tests were carried out in 8 liter Denver flotation cell. The applied optimum flotation conditions are shown in table 2.

The experimental procedure includes, 5 min conditioning, 5 min collector contact, 1 min frother contact and the flotation was continued until the bubbles got barren. Then, clay tailings were collected and kept for making brick models. The sand used was obtained from Sinai region and supplied by Manganese Sinai Co.. The chemical and sieve analyses of the sand sample are shown in tables 3 and 4.

Table 1. X ray analysis of filter cake sample

Constituent	Content %
SiO_2	26.10
TiO_2	1.5
Al_2O_3	13.36
Fe_2O_3	3.97
MnO	0.03
MgO	0.55
CaO	1.37
Na_2O	0.14
K_2O	0.92
P_2O_5	0.05
LOI	52.01
Total	100 %

Table 2. The optimum flotation conditions

Parameter	Dosage/value
Frother (pine oil)	60 mg/l
pH	6
Solid/liquid ratio	10 %
Gas flow rate	6 l/min.
Impeller speed	1000 rpm.

Table 3. Particle size distribution of sand sample

Particle size, μm	Wt., %
+ 1500	03.2
- 1500 + 1200	41.3
- 1200 + 750	30.2
- 750 + 500	13.1
- 500	12.2
Total	100

Table 4. Chemical analysis of sand sample

Constituent	Content, %
SiO_2	94.86
CaO	1.28
MgO	0.68
Fe_2O_3	0.33
TiO_2	0.73
Al_2O_3	2.12

The residual clay tailings were found to have about 78 % ash content. This means that a considerable amount of coal fines are still unrecovered. Also, it was found that the water reservation of such type of clay was about 33 %, which means that the porosity of such clay is very small. During the ignition of the native clay brick model the briquette bursts. This burst was attributed to the pressure exerted by the produced gases from the ignition of coal included in the clay. The amount of coal contained in the clay and the low porosity provided good support for such interpretation. To avoid the burst of briquette during the ignition as well as to improve its physical and mechanical properties, it is suggested to mix such clay with sand. This suggestion mainly aims to increase the porosity of clay to give a chance for the introduced gases during the ignition to escape. In this regard, a mixture of clay and sand were prepared at different weight percent, 20, 40, and 60 % of sand. First, the sand sample was used in the mixture as it is, i.e, - 1500 + 0 μm and second, the clay was mixed with the individual size fractions of sand, namely, - 1500 + 1200, - 1200 + 750, - 750 + 500, and - 500 + 0 μm at constant weight percent. Each mixture was mixed well with a suitable amount of water and the paste was hand formed in a wood briquette of 12.5 x 6 x 3 cm. The formed bricks were left to dry at room temperature in the laboratory atmosphere for one week and overnight at 100°C in a drier then, fired in a muffle furnace for 4 hours at 950°C. The physical properties (water absorption) and mechanical properties (Compressive strength) of the fired briquettes were measured to make sure that their specifications are compatible with the Egyptian standard specifications for brick industry (9).

RESULTS AND DISCUSSION

EFFECT OF APPLYING OPTIMUM CONDITIONS ON THE REMOVAL OF COAL FINES FROM THE FILTER CAKE

The optimum conditions indicated by Ramadan (Ramadan et. al. 2000) for the removal of coal fines from the filter cake were applied at different collector dosage in order to determine the optimum collector dosage for the separation process. These optimum conditions are shown in table 2 and the results obtained by applying them in flotation process are shown in figure 1. As can be seen from this figure the coal recovery increases by increasing the kerosene dosage. The increase of kerosene dosage more than 3 kg/t did not cause a considerable changes in coal recovery. On the other hand, the ash content changed in the range of 17 to 21 %. The best flotation recovery of fine coal is obtained at 3 kg/t of kerosene. This may be due to the best adsorption of kerosene on the coal surfaces which makes the coal surfaces more hydrophobic. This, in turn, may lead to strong attachment between coal surfaces and air bubbles. Under these conditions the removal of coal fines from the filter cake was found to increase. Hence, the main frame for the best operating conditions is completed by determining the suitable collector dosage.
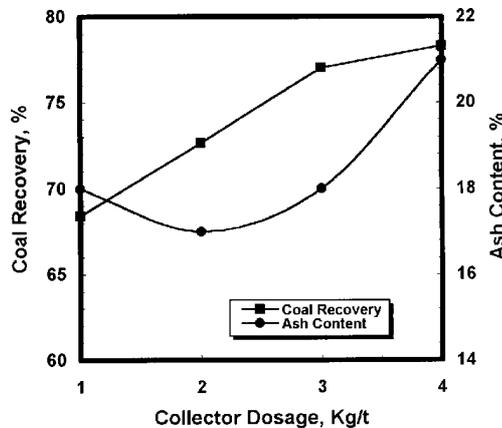
Fig. 1. Effect of collector dosage on the removal of coal fines from filter cake
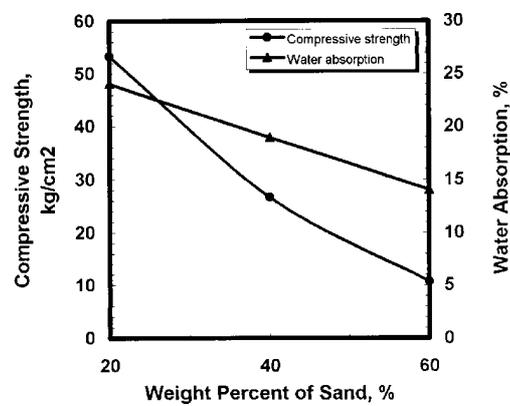
Figure 2. Effect of weight percent of sand (-1500 + 0 μm) on physical and mechanical properties of produced bricks

From the results obtained, it was found that the residual clay tailing have about 78 % ash content. This means that it still has about 20 % of coal fines. The water reservation of such clay was found to be about 33 % , i.e, it has very low porosity.

EFFECT OF WEIGHT PERCENT OF SAND (THE WHOLE SAMPLE)

To illustrate the effect of sand on physical and mechanical properties of clay bricks, different mixes were made by substituting clay by sand (20 %, 40 %, and 60 % by wt.) of - 1500 + 0 μm size range and the produced bricks were tested for compressive strength and water absorption determination. The results obtained are presented in figure 2. From this figure, it is clear that the compressive strength decreases by increasing the wt. % of sand in brick model. This may be attributed to the particle size distribution of sand sample. By increasing the wt. % of sand in brick model more than 20 % by wt., the voids between the coarse particles, which represent the highest content among the fractions indicated in table 3, will increase. The decrease of water absorption trend as shown in Fig. 2, may be taken as an evidence for such conclusion. These voids which created between the coarse particles may lead to the reduction in the compaction of the fired briquette. Also, these voids may promote the extensive cracking which results from the variation of thermal expansion between phases which, in turn, reduces the compressive strength of such brick models.

EFFECT OF SIZE FRACTION OF SAND

To indicate the effect of particle size of sand on the physical and mechanical properties of bricks produced from the clay tailings, each size fraction of sand was tested as nonplastic material with clay and mixed well at a typical value of 60 % sand

by weight. The results obtained are shown in Fig. 3. As shown from this figure, the decrease of particle size from 1350 μm to 975 μm did not cause any considerable changes in the compressive strength of the brick models. This may be attributed to the presence of coarse size fractions of sand which may lead to producing unsuitable brick models with regard to physical and mechanical properties. This result is mainly due to the reasons mentioned above about the worse side effect of the voids created between the coarse particles of sand. However, by decreasing the particle size fraction of sand less than 975 μm, the compressive strength of brick models was found to increase gradually until it reaches about 60 kg/cm^2 at 250 μm particle size. This may be attributed to the reduction of voids between particles as a result of presence of fine and unique size fraction of sand as nonplastic material with clay tailings. So, homogeneous and compacted brick models are produced with reasonable physical and mechanical properties. As a result of the homogeneity and compactness of the brick models, their porosity was found to be suitable for escaping the produced gases during ignition. The obtained results from the plotted data of water absorption may be a strong evidence for the mentioned interpretation.
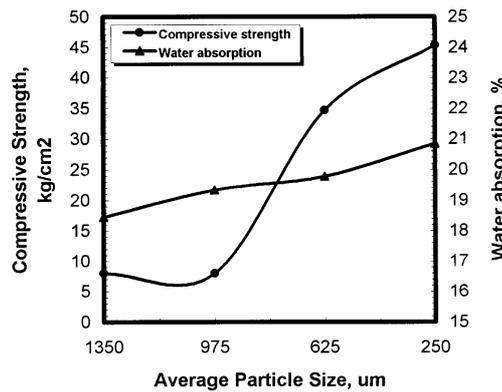
Fig. 3. Effect of particle size of sand on physical and mechanical properties of bricks
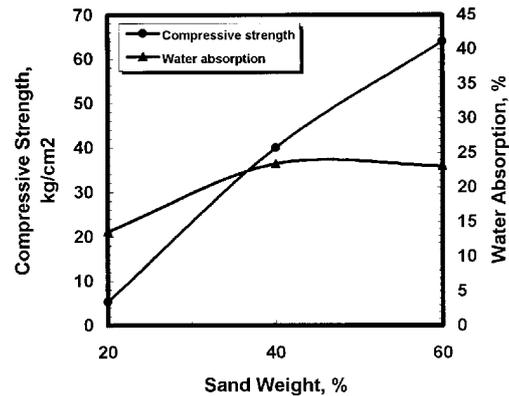
Fig. 4. Effect of weight percent of sand (for - 500 + 0 μm size fraction) on physical and mechanical properties of bricks

EFFECT OF WEIGHT % OF SAND FOR - 500 + 0 μm SIZE FRACTION

To illustrate the effect of wt. % of sand for - 500 + 0 μm size fraction, the data were plotted and indicated in figure 4. As shown from this figure, the compressive strength increases by increasing the wt. % of sand. On the other hand, the water absorption was also found to increase by increasing the wt. % of sand from 20 % to 40 %. However, by increasing the wt. % of sand higher than 40 % the water absorption was found to be nearly constant. This may be attributed to the large homogeneity between sand and clay which lead to severe cohesion between the particles of sand as

a result of the presence of clay which behaves as cementing material on the large surface area of sand particles. This cohesion may decrease the voids between sand particles to a great extent which, in turn, increases the compaction of fired brick models.

COMPARISON BETWEEN SPECIFICATIONS OF PRODUCED BRICK MODELS WITH THE EGYPTIAN STANDARD SPECIFICATIONS OF BRICK INDUSTRY

To make sure that the specifications of such brick models are suitable for brick industry the obtained optimum conditions were applied to produce brick models which have been tested for determining the water absorption and compressive strength in order to compare their specifications with the Egyptian standard specifications. The results obtained are tabulated in table 5. From these results, it is clear that the brick models produced in this work are compatible well with the Egyptian standard specifications for brick industry (Barakat 1984).

Table 5. Specifications of brick model

Test	Egyptian standard	Brick model specifications
Water absorption %	not more than 30	23 % by wt.
Compression resistance	not less than 20 kg/cm^2	62 kg/cm^2

CONCLUSIONS

An adequate physical and mechanical properties could be produced by substituting clay by sand. The weight percentage of sand depends on the particle size of sand sample. Throughout this study, it was found that 20 % and 60 % of sand sample which is characterized by size distribution of - 1500 + 0 and - 500 + 0 μm respectively is enough to give a considerable improvement of clay brick produced. The results of the study may be applied for exploiting the clay of northern Sinai whether from the filter cake of El-Maghara coal washing plant or from natural clays which are found in the same area for brick making. This, no doubt, will take part in the development of this area.

REFERENCES

BARAKAT M. A.(1984) *Building materials and standard measuring tests,* Dar El-Ratib Co. Publishers, Cairo, Red-lay bricks, Chapt. 9, pp 262-283.

CELLIER F., (1990), Improvement in the quality of water at the freyming washery by means of a rapid clarifier, *Proceeding of the 11th Inter. Coal prep. Congress*, Tokyo, Japan, pp. 212 - 215.

EBIED E. A., (1984), Evaluation and Studies of some local raw materials and its capability for production of some building materials, M.sc. thesis, Faculty of science, Cairo University.

ELWAN M., ABDEL- AZIZ D., and EL-DIDAMONY H., (1999), Effect of by - pass cement dust on the properties of clay bricks", *Ceramic Silikaty*, 43 (3), p. 109 – 114.

ELWAN, VI. NI., El- ALFI E.A. and EL - DIDAMONY H.,(2001) Effect of by-pass cement dust as nonplastic material on clay bricks, *7th Inter. Conference in Min., Pet., and Metall., Eng.* (MPM), Min., and Metall. Eng. Dept., Faculty of Eng., Assuit University, Assuit, Egypt, pp. 333 - 342.

LUKAC J.(1994), Briquitting of hard brown coal without binding agent, *Proceeding of 12th Inter. Coal Prep. Congress*, Cracow, Poland, pp. 581 - 586.

RAMADANA.M., SALEH A.M., and MOHARAM M.R.,(2000) Waste treatment of El-Maghara coal washing plant by flotation for beneficial reuse of its constituents in industry, *8th International Mineral Processing Symposium*, Antalya, Turkey, Oct. 16 - 18.

SHAN Z., YAN X., ZHANG C., PI P., XE X., (1990), New approach to clean - coal dewatering and waste water purification, *Proceeding of the 11th Inter. Coal Prep. Congress*, Tokyo, Japan, pp. 199 – 204.

TUCKER P.V., BOSWORTH G.B. and KALB G.W., (1994), New developments in coal briquitting Technology, *Proceeding of 12th Inter. Coal Prep. Congress*, Cracow, Poland, pp. 587 – 598.

Ramadan M.A., Saleh M.A. Taha A.T. Moharam M.R., *Uwagi nad poprawą mechanicznych właściwości cegieł produkowanych z odpadów węlowych z zakładu El-Maghara*, Fizykochemiczne Problemy Mineralurgii, 35, 2001, 153-160 (w jęz. ang.).

Poprawa mechanicznych właściwości cegieł wykonanych z mułu węglowego przez dodanie piasku, stanowiła główny cel badań. Wpływ takich parametrów jak zawartość piasku, skład ziarnowy na właściwości mechaniczne produkowanych cegieł był badany. Zostało ustalone, że obecność 20% piasku o uziarnieniu –1500 μm oraz 60% piasku o uziarnieniu –500 μm pozwala na wyraźną poprawę mechanicznych właściwości produkowanych cegieł.

Çetin HOŞTEN[*]

MICRO-FLOATABILITY OF RUTILE AND ZIRCON WITH SOAP AND AMINE TYPE COLLECTORS

Single-mineral floatability of pure, heavy sand rutile and zircon minerals using sodium oleate and hydrogenated tallow amine acetate as collectors was studied by a micro-flotation device over a wide pH range from 2 to 12, at three levels of the collectors and two levels of a polypropylene glycol type frother. Rutile yielded a peak foatability at pH 6 with sodium oleate, and floated reasonably well over a wide pH range from 2 to 8 with the amine collector. An abrupt deterioration of the floatability of rutile was observed at pH>8. The maximal floatability range for zircon was from pH 6 to 10, followed by a sharp decrease at pH>10, with both of the collectors. The floatability of zircon decreased sharply with decreasing pH in the acidic medium, below pH 6. The results were discussed in view of collector species distribution as a function of pH to suggest adsorption mechanisms for the collectors. The upper critical flotation pH values for the minerals seemed to be sufficiently distinct to suggest a potential for the differential flotation of the minerals in the alkaline medium with both of the collectors tested.

Key words:flotation, rutile, zircon, sodium oleate, tallow amine acetate

INTRODUCTION

Rutile (TiO_2) and zircon ($ZrO_2.SiO_2$) are among the valuable constituents of heavy mineral sand deposits and contribute heavily to the economic viability of a majority of existing plant operations. Natural rutile is the favored feedstock mineral for the production of white TiO_2 pigment through the chloride process (Stanaway, 1994), and mainly used in the coatings, plastics and paper industries (Pearson, 1999). Zircon is sourced as a by-product of titanium minerals production from heavy mineral sand deposits. The most important market for zircon is as an opacifier for ceramic tiles and sanitarywares in the form of zircon flour (micronized to 100% finer than 6μm). The other major applications for zircon are as a ground product in the manufacture of frit (micronized to 95% finer than 45μm), as a component of refractories, particularly in glass furnaces, and as a moulding sand in the foundry industry (Pearson, 1999).

[*]Department of Mining Engineering, Middle East Technical University, Ankara, Turkey.

Conventional rutile and zircon sand production begins with dredge mining of heavy mineral deposits, followed by gravity concentration, mostly through the use of Humphrey's spirals. The gravity concentrate is then dried and subjected to a series of magnetic and high-tension separations for commercial production of titanium minerals (rutile, ilmenite) and staurolite (or garnet) sands. The tailing from the dry process, enriched in zircon and silica sand, undergoes a wet upgrading by spirals and shaking tables to reject the silica sand and other Al_2O_3-containing minerals such as kyanite and sillimanite. The zircon gravity concentrate, typically containing 95% zircon, is then dried (or calcined at 500-700°C) for subsequent upgrading by dry separation equipment such as high-tension rolls, induced roll magnets, and electrostatic plate separators to produce a concentrate having a grade of +97% $ZrO_2.SiO_2$.

The conventional processing methods work efficiently for particles coarser than 75μm. Significant loss of productivity occurs in finer sizes, and the separation process becomes uneconomical below 45μm particle size. Commercial rutile and zircon concentrates have tight specifications for the inclusion of the other mineral. In many applications, the TiO_2 content in zircon concentrate should not be higher than 2%. Likewise, for premium-quality zircon the TiO_2 content is limited to no more than 0.2%. Such levels of purity cannot be obtained even with the advanced fine-particle gravity separation at sizes below 45μm. The froth flotation process remains as a sensible research alternative for the selective separation of zircon from titanium-bearing minerals (rutile and ilmenite), contained in the fine-sized tailings of conventional mineral sands treatment operations.

There exist a limited number of studies reported in the literature with regard to flotation characteristics of zircon and rutile. Flotability of pure zircon and rutile minerals with sodium oleate as collector was studied by Madhavan et al. (1965) as a function of pH. They found that the lower critical pH value for the flotation of zircon was 1.5 and that of rutile 2.6, which indicated the possibility of separation of zircon and rutile in the acidic medium.The upper critical pH values were so close (10.5 and 10.6, respectively) that differential flotation of the two minerals did not seem to be possible in the alkaline medium. They also reported that zircon, when once coated with sodium oleate, did not desorb either at higher or lower pH, whereas sodium oleate seemed to be a desorbing collector from the rutile surface either below the lower critical pH or above the higher critical pH. Plaksin et al. (1967) reported similar findings for the flotation of zircon with sodium oleate alone, indicating its ready flotation in neutral, slightly acidic, and slightly alkaline media. They did not find any significant adverse effect of a triatomic phenol depressant (pyrogallol) on zircon flotability. Sodium sulhide and caustic soda were found to desorb sodium oleate from zircon surface (Pol'kin et al., 1967). Li and Box (1995) examined selective flotation of zircon and rutile under hot soap (sodium oleate) conditions, and achieved high zircon recoveries (97-98%) in the 8.5 to 11.2 pH range, at a conditioning temperature of 90°C, giving the lowest TiO_2 grade (2.4%). Paves and Peres (1993) reported that a

commercial hydroxamate collector could readily float both zircon and rutile in the wide pH ranges 2.5 to 9 and 3 to 8, respectively, while sodium metasilicate was reported to effectively depress both minerals. Modified phosphoric acid ester and styryl phosphonic acid collectors were also tested for the flotation of rutile in slightly acidic media from some hard-rock rutile ores (Bulatovic and Wyslouzıl, 1999; Liu and Peng, 1999).

Probably the first major commercial flotation of zircon from heavy mineral sands has been considered for Sierra-Leone Operations with the intention of the separation of zircon from rutile at sizes finer than 100 mesh. In one proposed scheme, zircon was floated using a cationic amine collector at pH 2.5. Sodium flouride was used to activate the zircon, and starch was used to depress the titanium oxides. In an alternative scheme, quartz was floated with amine at pH 10 while the titanium oxides were again depressed by starch. The pH was then lowered to 2.5 and amine was used to float the zircon after activation with sodium fluoride (Davies et al., 1994).

It is apparent from the literature that there exists a need for an efficient industrial flotation scheme for separation of fine-grained zircon from titanium-bearing minerals in order to reprocess accumulated tailings of conventional dry processes and/or to devise new processing schemes to replace the conventinal methods so as to improve overall recovery. This need calls for a fundamental understanding of the flotation properties and surface characteristics of zircon and titanium-bearing minerals (mainly rutile and ilmenite), as well as those of some other mineral constituents associated with these minerals, in the light of recent advances in froth flotation science.

As a part of ongoing extensive research on the flotation behavior of zircon, rutile, and ilmenite, this paper presents some initial findings with regard to single-mineral micro-flotability of zircon and rutile in the presence of sodium oleate or hydrogenated tallow amine acetate, over a wide pH range from 2 to 12.

MATERIALS AND EXPERIMENTAL METHODS

MİNERAL SAMPLES

The zircon mineral sample used in this reseach was obtained from DuPont's Starke, Florida Operations. Already calcined at about 550°C in a rotary kiln partly for improving its appearance (color), the sample was designated as Premium Zircon Sand, and contained 67.22% ZrO_2, 31.11% SiO_2, and 0.11% TiO_2.

The rutile mineral sample was also obtained from DuPont. As-received sample was further purified by a high-intensity, dry magnetic separator (Permroll) so as to remove iron-bearing impurities. The purified sample, after repeated washing with distilled water, assayed 96.66% TiO_2, 0.48% SiO_2, 0.39% ZrO_2, and 0.32% Fe_2O_3.

Both mineral samples were wet screened with distilled water to yield 150x200 mesh (106x75 μm) size fractions for micro-flotation tests. These sized test samples were pretreated with 10% HCl solution, and then washed repeatedly with distilled

water to clean the mineral surfaces, and dried at 60°C for use in the micro-flotation tests.

Zeta-potential measurements with the same samples in our earlier studies revealed that the iso-electric points of the rutile and zircon occured at pH 3.5 and 4.4, respectively (Köse et al., 2000; Muratoğlu et al., 2000).

REAGENTS

Sodium oleate (Na-Ol), manufactered in our laboratory, and a commercial (Akzo Nobel) sample of hydrogenated tallow amine acetate, HTAA (RNH_3Ac, where R is 96% C_{18}), were used as collectors. A stock solution of 0.1M total oleate concentration was prepared by neutralization of analytical-grade oleic acid with NaOH in distilled water. For preparing the amine stock solution, 0.1g solid prills (MW: 331g) of the amine collector was dissolved in distilled water in a 250-ml volumetric flask that was placed in a water bath maintained at 70°C. A desired concentration of collector solutions were freshly prepared by subsequent dilutions from the stock solutions.

Dilute solutions of HCl and NaOH were used as pH regulators. The polypropylene glycol type frother Dowfroth 400 was used as a frother at two concentrations, 50 ppm and 100 ppm.

MİCRO-FLOTATİON TESTS

The microflotation tests were performed in an automated shaking test-tube instrument, the EMDEE Microflot Agitator (Chudacek, 1991). A sample mass of 0.4g was conditioned in 70ml of the test solution in a centrifuge test-tube for a required time, using gentle magnetic stirrer agitation. The stirrer bar was then removed, the tube was stoppered and vigorously agitated in the Microflot agitator for 20 cycles. During agitation a mineralized froth was formed, which was then removed using a pipette. The froth fraction was dried overnight, and weighed to yield flotation recovery in the single-mineral floation system of this study.

In the conditioning stage, the mineral test sample was first stirred in distilled water for 5 minutes, and then the pulp pH was adjusted by the addition of HCl or NaOH solutions. A predetermined amount of collector solution was added into the pulp to obtain the desired concentration, and the pulp was further conditioned for five minutes. Then, the frother solution was introduced into the gently stirred pulp in the test tube, and the tube was immediately placed in the agitator. Each test was repeated twice. All tests were carried out at room temperature.

Micro-flotation tests were conducted at three levels of the collector concentration and two levels of the frother concentration in a wide pH range from 2 to 12, with increments of two pH units. Additional tests were made at pH 11 for some critical conditions.

RESULTS

Micro-flotation recoveries (micro-floatabilities) of pure minerals, rutile and zircon, are plotted in Figs. 1 and 2, respectively, as a function of pH, at three levels of Na-Ol concentration and two levels of frother concentration.
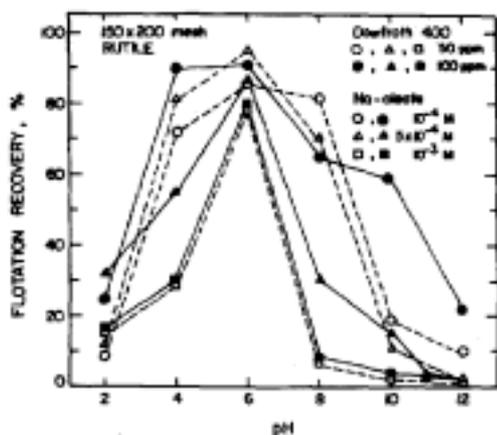
Fig. 1. Floatability of rutile with sodium oleate as a function of pH
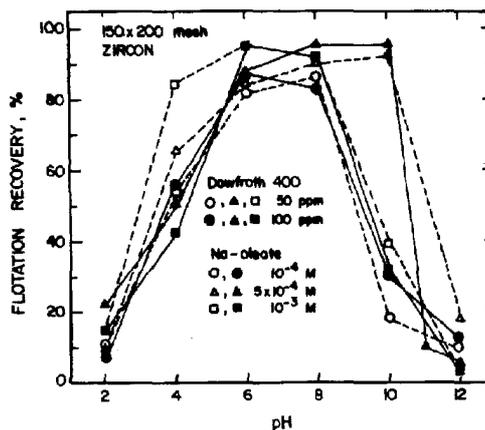
Fig. 2. Floatability of zircon with sodium oleate as a function of pH

Peak recoveries of rutile were achieved at pH 6 with Na-Ol for all the concentration levels tested, irrespective of the frother concentration. The floatability of rutile, however, decreased significantly with increasing and decreasing pH around 6; the decrease in the floatability being sharper with increasing concentration of the collector Na-Ol. The lower and the upper critical pH values for rutile flotation appeared to depend also on the Na-Ol concentration. The frother concentration, tested at two levels, did not lead to any significant change in the overall flotation trend. Among the conditions tested with Na-Ol, the best flotability for the rutile was determined for the case of $5x10^{-4}$M Na-Ol, 100 ppm frother, and pH 6.

Optimal floatability pH range of the zircon sample with Na-Ol was relatively wider than that of the rutile. Peak recoveries, being a function of the Na-Ol concentration, were achieved at pH values from 6 to10. The best floatability for the zircon was determined for the case of $5x10^{-4}$M Na-Ol, 100 ppm frother, and pH 10. The decrease in the zircon floatability was much sharper in the strongly alkaline range than the acidic range.

Floatabilities of the rutile and zircon samples with the amine type collector, hydrogenated tallow amine acetate (HTAA), are plotted as a function of pH in Figs. 3 and 4, respectively. The pH range of maximum flotation of rutile was somewhat more sensitive to the frother concentration than that of zircon. Flotation recoveries around 90% were observed in the pH range 6 to 8 for rutile, and 6 to 10 for zircon.

Floatability of both minerals decreased sharply in the alkaline region above their respective critical pH values, pH 8 for rutile and pH 10 for zircon. In the acidic region, rutile indicated a higher degree of floatability than zircon.
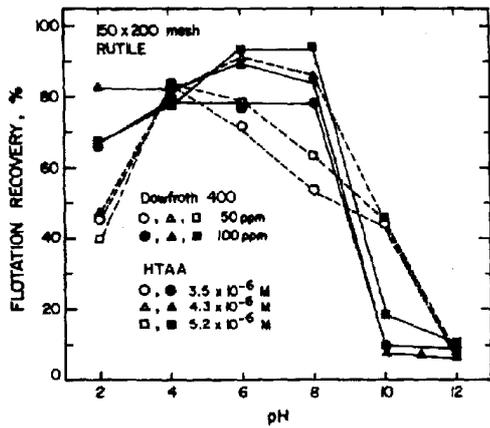
Fig. 3. Floatability of rutile with amine as a function of pH
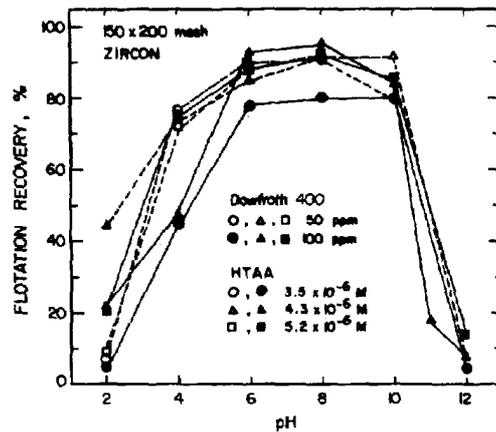
Fig. 4. Floatability of zircon with amine as a function of pH
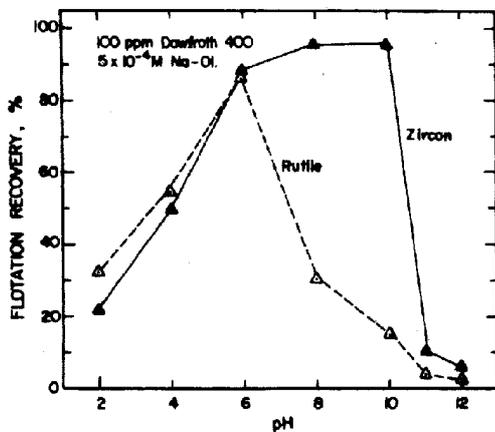
Fig. 5. Floatability of rutile and zircon with sodium oleate as a function of pH.
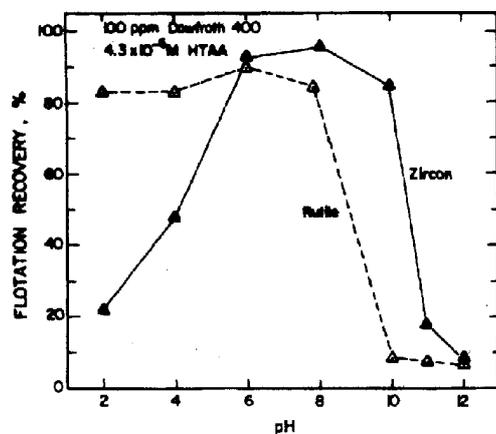
Fig. 6. Floatability of rutile and zircon with amine as a function of pH.

A comparison of the floatability plots of the rutile and zircon mineral samples with the two collectors, Na-Ol and HTAA, are presented in Figs. 5 and 6, respectively. These figures reveal that pH 10 is critical for the likely differential flotation of the two minerals with both of the collectors. A second critical pH for the possible differential flotation seemed to be pH 2 with the use of HTAA.

DISCUSSION

Even though the differential flotation from a mixture of rutile and zircon had not been tested at the time of writing, it is apparent from the present study that the selectivity between these minerals should be achieved in the alkaline medium with sodium oleate or HTAA as collector since there seems to be sufficient differences in the upper critical pH values of the minerals in both collector systems.

In sodium oleate-mineral systems, each mineral has a critical oleate concentration for flotation; and the type of collector adsorption (physical, chemical, or a combination) is governed by the solution pH and oleate concentration (Drzymala and Lekki, 1992). According to the data on oleate species distribution as a function of pH (Pugh and Stenius, 1985; Drzymala, 1985), the molecular precipitated oleic acid is the predominant species at low pH (<5); monomer oleate ion and oleate dimers predominate in the alkaline range pH> 8.There also exist relatively low concentrations of the intermediate ion-molecular species,$(RCOO)_2H^-$, at pH 8. At pH>5 and <7.5, molecular and ionic oleate species co-exist in relatively more abundant concentrations.

In view of the oleate species distribution data and the negative zeta potential of the mineral particles, the maximal flotation of rutile at pH 6 in the present study can be attributed to adsorption of molecular precipitated oleic acid (RCOOH) and oleate ion (RCOO$^-$). Even though the mechanism of adsorption is still unclear, it has been generally agreed that the initial adsorption step involves the chemisorption of the oleate ion bound to the lattice cation so as to create optimal conditions for the physical adsorption of other collector species. Abramov (2000) proposed that effective flotation takes place only when there is an optimal ratio of chemisorbed and physisorbed collector species, while the former provides hydrohopization of the surface and the latter ensures kinetic functions (effective film rupture) of air bubble-particle attachment.

In the case of the oleate/zircon system, the maximal floatability starts at pH 6 but, in contrast to the rutile system, extends further into the alkaline region (pH 10), and drops sharply above pH 10. The co-existing collector species in the mid-pH range 6 to 10 are predominantly monomer and dimer oleate species, and, in relatively much lower concentration, the ion-molecular species. Although the ion-molecular species has been claimed to promote the co-adsorption and flotation with other collector species (Ananthapadmanabhan and Somasundaran, 1981), this species cannot be held responsible for the floatability of the mineral samples in the present study since its effect as such is absent in the case of rutile. It is very likely that specific adsorption of monomer and dimer oleate species led to flotation in the mid-pH range. The predominant species in the strongly alkaline range (pH>10), where a sharp decrease in the zircon floatability was observed, are also monomer or dimer oleate species. This sharp floatability decrease in the strongly alkaline range can be plausibly attributed to overwhelming competition of OH$^-$ ions for surface sites against the chemisorbing anionic monomer or dimer oleate species.

The striking difference between the upper critical pH of flotation of rutile (pH 6) and that of zircon (pH 10) should be explicable by the differences in their crystal chemistry and surface properties. Flotation in chemisorption systems of oxides and silicates is said to be related directly to the formation of hydroxy complexes of metal ions (or their reduced species) comprising the mineral (Fuerstenau and Palmer, 1976). It seems, therefore, plausible to suppose that the difference in the upper critical pH of the two minerals arises from the differences in their extent of surface hydroxylation and the stability of the water of hydration around the particle surfaces, with which the collector species compete.

In the case of the amine system, the difference in the upper critical pH values of the two minerals was diminished. The critical pH for zircon was again 10, as in the oleate system, but that of rutile shifted to pH 8. According to the amine species distribution diagram (Pugh, 1986), the quantities of ionic amine (aminium ion) and the ion-molecular complex $RNH_2.RNH_3^+$ are maximum at around pH 10, and both decrease rapidly with increasing pH. Most researchers are in agreement that amines are physisorbing collectors for oxide and silicate mineral surfaces. Physical adsorption of the aminium ion and a synergistic co-adsorption of neutral amine molecules and/or the ion-molecular complex are believed to be the major mechanism of the surface hydrophobization. The sharp cessation of flotation at high pH values in amine systems has been attributed to diminishing ionic amine concentration and, at the same time, to competion from the increasing Na^+ concentration from the added NaOH.

The upper critical pH of flotation (pH 10) for the silicate mineral zircon of the present study coincides with the maximum flotation pH of quartz with amines, reported in an earlier study (Bleier et al., 1976). It seems reasonable to suppose that the difference in the upper critical pH values of the rutile and zircon is mainly due to the silica tetrahedra in the structure of the latter mineral so that its surface behaves as if it were a mixed oxide made up of silica and metal oxide. The silica part controls the floatability in the pH range 8 to 10.

CONCLUSIONS

Sodium oleate and hydrogenated tallow amine acetate were efficient collectors for rutile and zircon. Zircon floated better over a relatively wider near-neutral and basic pH range than rutile with both of the collectors, probably due to its mixed metal oxide-silica surface structure. Rutile floated reasonably well in the pH range 2 to 8 with the amine collector, but yielded a peak floatability at pH 6 with the oleate. The upper critical pH values of flotation were:10 for zircon with both of the collectors; 6 for the rutile/oleate system, and 8 for the rutile/amine system. Differential flotation of the two minerals seems possible at pH 10. Further research has been undertaken to float minerals from their mixtures in the absence and presence of an efficient depressant.

ACKNOWLEDGEMENT

REFERENCES

ABRAMOV A.A. (2000). *Physico-chemical fundamentals of nonsulphide minerals flotation.* In: Mineral Processing on the Verge of the 21st Century, Ed. G. Özbayoğlu et al., Balkema, Rotterdam, 189-201.

ANANTHAPADMANABHAN K.P., SOMASUNDARAN P. (1981). *Oleate chemistry and hematite flotation.* In: Proceedings of Interfacial Phenomena in Mineral Procesing, the Engineering Foundation Conference, 207-227.

BLEIER A., GODDARD E.D., KULKARNI R.D. (1976). *The structural effects of amine collectors on the flotation of quartz.* In: Flotation, A.M. Gaudin Memorial Volume, Ed. M.C. Fuerstenau, V.1,AIME, New York, 117-147.

BULATOVIC S., WYSLOUZIL D.M. (1999). *Process development for treatment of complex perovskite, ilmenite and rutile ores.* Minerals Engineering, 12(12), 1407-1417.

CHUDACEK M.W. (1991). *EMDEE Microflot flotability test.* Int. J. Mineral Processing, 33, 383-396.

DAVIES J.P, WONDAY S., KEILI A.K., (1994). *Development and operation of zircon flotation at Sierra Rutile Limited.* In: Proceedings of 10th Industrial Minerals International Congress, 160-172.

DRZYMALA J. (1985). *Chemical Equilibria in the oleic acid-water-NaCl system.* J. Colloid and Interface Science, 108, 257-263.

DRZYMALA J., LEKKI J., (1992). *A contribution to understanding oleate flotation of minerals.* In: The Proceedings of the 4th Int. Miner. Process. Symposium, Antalya, Turkey, Ed. G. Özbayoğlu, V.1, 213-224.

FUERSTENAU M.C., PALMER B.R. (1976). *Anionic flotation of oxides and silicates.* In: Flotation, A.M. Gaudin Memorial Volume, Ed. M.C. Fuerstenau, V.1, AIME, New York, 148-196.

KÖSE M, HOŞTEN Ç., TOPKAYA Y., AKSER M. (2000). *Selective flotation of ilmenite from ilmenite-rutile mixtures.* In: Mineral Processing on the Verge of the 21st Century, Ed. G. Özbayoğlu et al., Balkema, Rotterdam, 253-256.

LI, C., BOX, J. (1995). *Floatability and adsorption characteristics of zircon and rutile in hot soap flotation.* In: Proceedings of the 19th IMPC, V.3, 129-133.

LIU Q., PENG Y. (1999). *The development of a composite collector for the flotation of rutile.* Minerals Engineering, 12(12), 1419-1430.

MADHAVAN T.R, KARVE V.M., SOMNAY J.Y. (1965). *Selective flotation of beach sand sillimanite, zircon and rutile.* Mining Magazine, 113(3), 202-207.

MURATOĞLU R.A., HOŞTEN Ç., TOPKAYA Y., AKSER M. (2000). *Floatability of zircon with sodium oleate.* In: Proceedings of the 21st IMPC, Rome, Ed. P. Massacci, Elsevier, Amsterdam, B8b-109-115.

PAVEZ 0., PERES A.E.C. (1993). *Flotation of monazite-zircon-rutile with sodium oleate and hydroxamates.* In: Proceedings of 18th IMPC, Sydney, 1007-1012.

PEARSON K. (1999). *A zircon market insight,* Industrial Minerals, May, 25-35.

PEARSON K. (1999). *A TiO$_2$ industry focus.* Industrial Minerals, July, 56-69.

PLAKSIN I.N., TIKHONOV S.A, UFIMTSEVA G.S. (1967). *Pyrogallol as aregulator in non-sulphide mineral flotation.* In: Flotation Properties of Rare Metal Mineral, Ed. I.N. Plaksin, Primary Sources, New York, 29-37.

POL'KIN S.I., ILIE P., SOLNYSHKIN V.I., ZAKHAROV A.E. (1967). *Selective desorption of sodium oleate from pyrochlore, zircon, and monazite by sodium sulfide.* In: Flotation Properties of Rare Metal Mineral, Ed. I.N. Plaksin, Primary Sources, New York, 46-56.

PUGH R.J., STENIUS P. (1985). *Solution chemistry studies and flotation behaviour of apatite, calcite and fluorite minerals with sodium oleate collector.* Int. J. Mineral Processing, 15, 193-218.

PUGH R.J. (1986). *The role of the solution chemistry of dodecylamine and oleic acid as collectors in the flotation of fluoride.* Int. J. Mineral Processing, 18, 19-41.

STANAWAY K.J. (1994). *Overview of titanium dioxide feedstocks.* Mining Engineering, December, 1367-1370.

Hosten C., *Mikroflotacja rutylu i cyrkonu z udziałem mydeł i aminowych kolektorów*, Fizykochemiczne Problemy Mineralurgii 35, 2001, 161-170 (w jęz. ang.)

Flotowalność czystych minerałów rutylu i cyrkonu badano przy pomocy testów mikroflotacyjnych. Kolektorami w procesie flotacji były oleinian sadu i octan talowej aminy. Badania flotacyjne prowadzono w zakresie pH od 2 do 12, stosując trzy różne stężenia kolektora i dwa stężenia odczynnika pianotwórczego (glikol polipropylenowy). Rutyl wykazywał maksimum flotowalności przy pH 6, przy użyciu jako kolektora oleinianu sodu. Stosując kolektor aminowy dobre wyniki flotacji rutylu uzyskano w zakresie pH od 2 do 8. Wyraźny spadek flotowalności obserwowano przy pH>8. Maksymalna flotowalność cyrkonu, przy użyciu obu kolektorów, była w zakresie pH 6-10. Flotowalność cyrkonu malała szybko przy pH>10. Równie, wyraźny spadek flotowalności cyrkonu obserwowano w środowisku kwaśnym pH poniżej 6. Otrzymane wyniki z flotacji zostaly przedyskutowane w oparciu o prawdopodobne mechanizmy adsorpcji badanych kolektorów do powierzchni minerałów. Różnice w flotacji minerałów w obszarze alkalicznym sugeruja możliwość separcji tych minerałów przy zastosowaniu badanych kolektorów flotacyjnych.

N. Emre ALTUN[*], Cahit HİÇYILMAZ[*]

EVALUATION OF ÇORUM ALPAGUT WASTE LIGNITE FINES

The fine fraction having 71.2 % -0.1mm particles in the Çorum Alpagut Lignite Mine of Turkish Coal Enterprises not only causes economical losses, but also is an important environmental hazard source since this fraction is pumped and accumulated in the slime ponds around the region. The amount collected in those ponds can be neither marketed nor removed away. Consequently, the fine fraction problem in Çorum Alpagut Dodurga Lignite Mine appears to be the most important disadvantage for the plant. To overcome this problem, this fine fraction coal which comprises of approximately 20 % of the total washed coal, should be concentrated to obtain a marketable product with acceptable calorific and ash values. For this purpose concentration experiments including Humphrey Spiral and Shaking Table have been carried out with these fine fractions taken from the cyclones and thickener that are currently in operation in the coal washery of the plant. As a result of those studies, all the concentration methods have proved to be effective, producing a concentrate with a considerable calorific value increase and an acceptable ash percentage. The combustion kinetics and properties of those fractions have also been determined by thermogravimetric methods and the results of the concentration studies have been supported with the combustion kinetic values of fractions and their products.

INTRODUCTION

The tailing ponds of coal washeries is one of the major sources of environmental pollution for the surroundings. In addition to this, large areas that can be utilized for agricultural or similar activities, become useless. All these facts make those ponds one of the most critical problems for the coal washing industry all around the world (Kirnarsky et al. 1998).

One of the plants which faces such a problem is TKİ Alpagut-Dodurga Coal Washery located in Dodurga-Çorum which meets the industrial and domestic demands of the region. This plant is run by Park Company and works on the basis of Drewboy Bath and Heavy Medium Cyclones cleaning with a capacity of 100 tons/hour (Figure 1). The plant produces four different products with sizes of 50-150mm, 18-50mm, 10-

*Middle East Technical University, Mining Engineering Department, Ankara, TURKEY

18 mm and 0-10mm. In addition to the Heavy Medium Cyclone, two more cyclones, namely Coarse and Fine Circuit Cyclones are also in operation in the flowsheet. These cyclones are not used for cleaning but to assist the dewatering operation by decreasing the amounts that will go to the thickener.
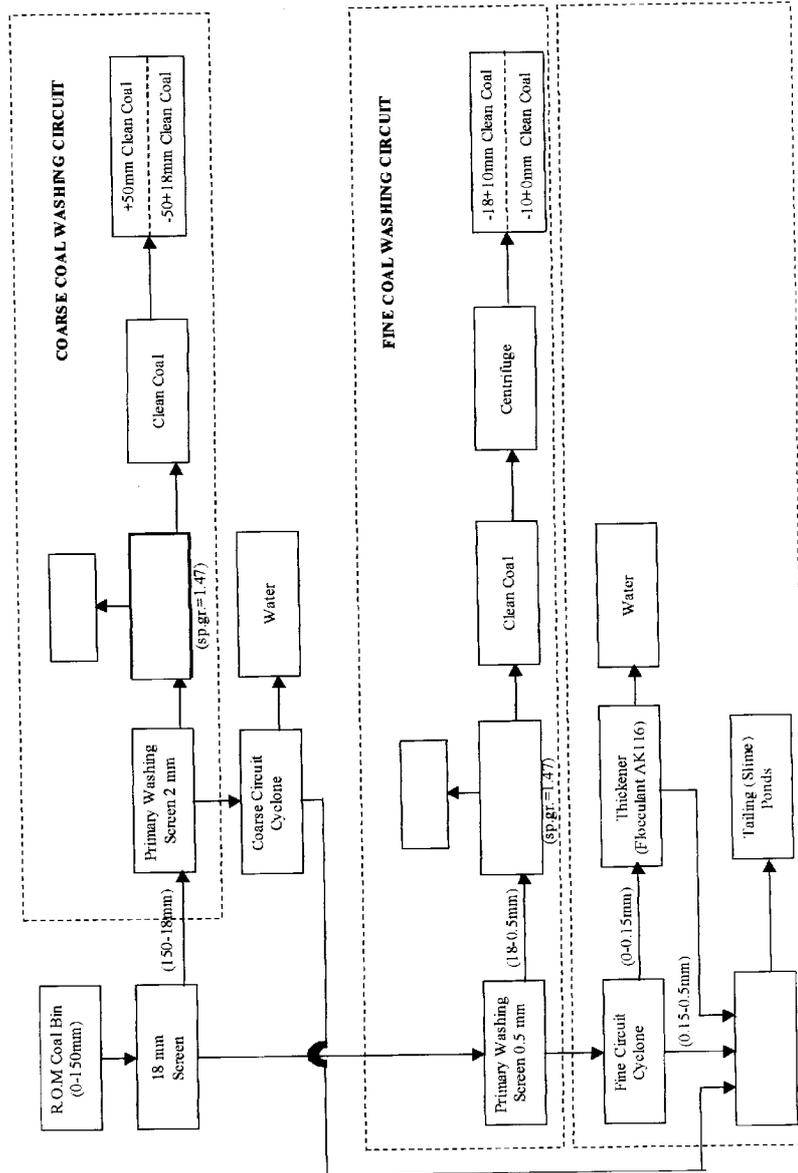
Fig. 1. Simplified flowsheet of TKI Alpagut Dodurga Lignites Coal Washery

The underflows of those cyclones are separated as the tailing fraction and pumped to the tailing ponds around the region. The amount lost as tailing fraction is dramatically high and reaches about 20 % of the total production. The existing ponds will be full and out of use soon due to this great amount removed, so new available areas are required immediately. Also the amount of 20% is an important amount that accounts as a defficiency for the plant. Consequently, the fine fraction of TKİ Alpagut-Dodurga Lignites is not only an environmental hazard source, but also an economically lost potential.

Decreasing the amount of tailings will solve both the tailing pond and economic problems. Therefore, in this study the possibility of obtaining a concentrate from the tailings fraction of the Alpagut Washery by gravitational concentration methods and the characteristics and kinetics of the products are searched.

MATERIAL AND METHODS

For the concentration applications, the fine fraction having 71.2 % -0.1mm slime, separately taken from the fine circuit cyclone, coarse circuit cyclone and thickener of TKİ Alpagut-Dodurga Lignites coal washery, have been used.

These separately taken fractions were first dewatared and dried completely both to take samples for thermogravimetric analysis and calorimetry measurements and to obtain uniform amounts for each experiment. The concentration experiments were carried out using a laboratory Wilfley type shaking table with dimensions of 123-64cm and 5 turn Humphrey Spiral 24 AM CC with feeds whose pulp densities were about 30 %. For the combustion characteristics and kinetics of the samples, the thermogravimetric analysis were performed by placing approximately 26 mg samples in a Polymer Laboratories 1500 PL/TG analyser. During the thermogravimetric analysis, the samples were combusted at a range of 20-900°C at a heating rate of 10°C/min by supplying a constant airflow of 15ml/min. The calorific values of each sample and the products were determined by using a Parr Oxygen Bomb Calorimeter. Prior to the experiments, the TG analyser was calibrated for the qualitative estimation of the weight changes during combustions.

RESULTS AND DISCUSSION

HUMPHREYS SPIRAL EXPERIMENTS

Humphreys Spiral experiments have been carried out individually by using feeds taken from the underflows of fine circuit and coarse circuit cyclones and thickener. Since the pulp density of about 30 % has proved to be effective for coal washing operations with Humphreys Spiral, this value is preserved for all feeds. The ash percentages and calorific values of the feeds before the concentration are given in Table 1.

Table 1. The Ash and Calorific Values of Feeds

Feed Source	Ash (%)	Calorific Value (kcal/kg)
Fine Circuit Cyclone	36.36	3358
Coarse Circuit Cyclone	32.62	3932
Thickener	53.77	2209

After the experiments, two products namely, concentrate and tailing have been obtained for the thermogravimetric analysis and calorific value determination. It has been observed that the ash percentage of the concentrates obtained from the underflow of fine and coarse circuit have decreased from 36.36 % to 28.26 % and 32.62 % to 25.14 % respectively (Table 1&2, Figure 2&3). Furthermore, the calorific values of those feeds have also increased. On the other hand, the ash percentage of the concentrate of the thickener feed decreased slightly (Table 1&2, Figure 4). In addition to this, the changes in the calorific value of the thickener feed was not as great as the differences obtained in the underflows of the cyclones neither (Table 1&2).
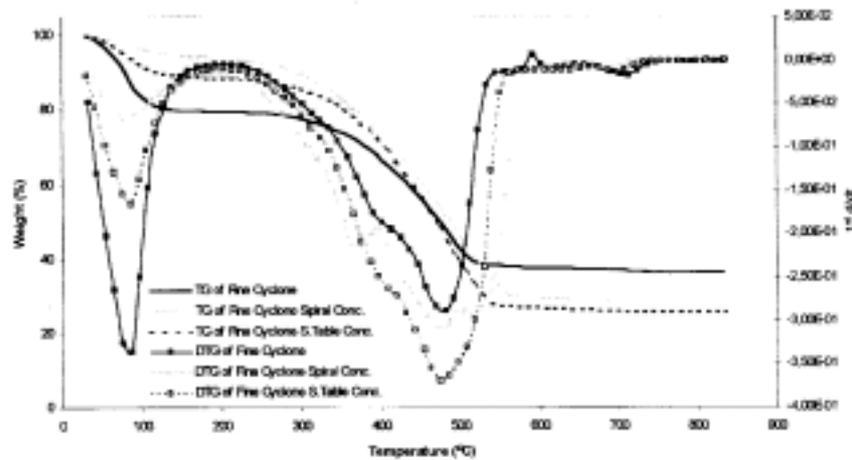
Fig. 2. TG and DTG curves of fine cyclone circuit underflow and fine cyclone circuit underflow concentrate by humphreys spiral and shaking table

Table 2. The Ash and Calorific Values of the Concentrates of Humphreys Spiral

Concentrate Type	Ash (%)	Calorific Value (kcal/kg)
Fine Circuit Cyclone Conc.	28.26	4081
Coarse Circuit Cyclone Conc.	25.14	4137
Thickener Conc.	49.12	2301
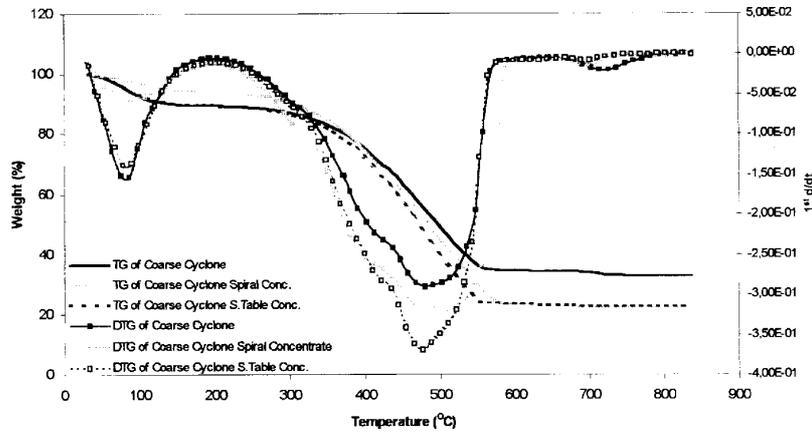
Fig. 3. TG and DTG curves of coarse cyclone circuit underflow and coarse cyclone circuit underflow
concentrate by humphreys spiral and shaking table

Similar to the concentrate, in the tailings portion there has been not only an important increase in the ash values of the fine and coarse circuit cyclones, but also a noticable decrease in their calorific values (Table 1&3). However, the ash percentage of the tailing of the thickener feed has slightly increased. Also important decreases in the calorific values was not achieved in the thickener tailing (Table 1&3).

Table 3. The Ash and Calorific Values of the Tailings of Humphreys Spiral

Tailing Type	Ash (%)	Calorific Value (kcal/kg)
Fine Circuit Cyclone Tailing	53.18	1929
Coarse Circuit Cyclone Tailing	43.03	3002
Thickener Tailing	56.11	1822

It can be concluded that Humphreys Spiral proved to be effective and efficient for the concentration of the fine and coarse cyclone circuit underflows, whereas the same success could not be obtained for the thickener feed. The reason for those two different concentration results is the occurrence of AK116 flocculant in the thickener, which is used in great amounts to increase the settling rate of coal particles before pumping to the ponds. Under the effect of AK116, the coal particles in the thickener feed are tightly agglomerated and this is the major reason of the unsuccessful results obtained.

SHAKING TABLE EXPERIMENTS

Shaking Table experiments have also been carried out by the same principle; individually by using feeds taken from the underflows of fine and coarse circuit cyclones and thickener with approximately the same pulp density of 30 %. Like the Humphreys Spiral experiments, high decreases in the ash values of concentrates of the underflows of the fine and coarse circuit cyclones occurred. The ash percentage of the concentrates obtained from the feeds of fine and coarse circuit tailings have decreased from 36.36 % to 25.41 % and 32.62 % to 22.44 % respectively (Table 1&4, Figure 2&3). Furthermore, the calorific values of those feeds have also increased parallel to the decreases in the ash percentages (Table 1&4). On the other hand, the ash percentage of the feed of the thickener decreased slightly (Table 1&4, Figure 4) and the increase in the calorific value was not so high either.
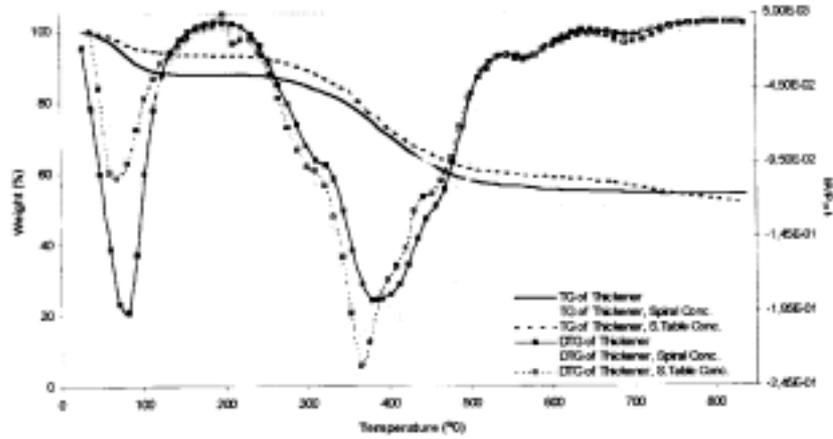
Fig. 4. TG and DTG curves of thickener feed and thickener concentrate by humphreys spiral and shaking table

Table 4. The Ash and Calorific Values of the Concentrates of Shaking Table

Concentrate Type	Ash (%)	Calorific Value (kcal/kg)
Fine Circuit Cyclone Conc.	25.41	4364
Coarse Circuit Cyclone Conc.	22.44	4480
Thickener Conc.	51.22	2242

The trend was similar for the ash percentages and the calorific values of the tailing portions of the fine and coarse circuit cyclones feeds. The ash values increased from 36.36 % to 68.32 % and 32.62 % to 64.59 %, respectively and important decreases occurred in the calorific values (Table1&5). However, the ash percentage of the tailing of the thickener feed has increased slightly again (Table 1&5).

Table 5. The Ash and Calorific Values of the Tailings of Shaking table

Concentrate Type	Ash (%)	Calorific Value (kcal/kg)
Fine Circuit Cyclone Tailing	68.32	1504
Coarse Circuit Cyclone Tailing	64.59	2059
Thickener Tailing	54.18	1907

As well as Humphreys Spiral concentration, experiments with Shaking Table showed that the concentration of the fine and coarse cyclone circuit underflows is possible whereas the flocculant effect in the thickener is the major obstacle against the concentration process due to the particle agglomeration.

KINETIC ANALYSIS

Not only the combustion process of a lignite but also its modelling is extremely complicated since several components are simultaneously oxidized during the reaction (Hiçyılmaz et al. 2000). For the kinetic modelling of the combustion of TKİ Alpagut Dodurga Lignite slime fraction samples, Arrhenius Type kinetic model is utilized for analyzing the thermogravimetric data obtained at the end of TG experiments. According to this model:

$$\frac{dw}{dt} = Ar \exp\left(\frac{-E}{RT}\right) w^n \tag{1}$$

where $\dfrac{dw}{dt}$ is the rate of weight change of the reacting material, Ar is the Arrhenius Constant, E is the activation energy, T is the temperature, R is the gas constant, and n is the reaction order.

For analysing the TG/DTG data, the model assumes that the rate of weight loss of the total sample is dependent only on the rate constant, the weight of the sample remaining and the temperature with assumed unity reaction order. So, the equation takes the following form;

$$\frac{1}{w}\left(\frac{dw}{dt}\right) = Ar \exp\left(\frac{-E}{RT}\right) \tag{2}$$

and when the logarithm of both sides is taken, the equation becomes;

$$\log\left[\frac{1}{w}\left(\frac{dw}{dt}\right)\right] = \log Ar - \frac{E}{2.303\,RT} \tag{3}$$

When $\log\left[\dfrac{1}{w}\left(\dfrac{dw}{dt}\right)\right]$ is plotted against $\dfrac{1}{T}$, the straight line will be obtained having a slope of $\dfrac{-E}{2.303\,R}$ and an intercept of Arrhenius Constant (Kök et al. 1997).

The individual activation energies for each reaction region can be notionally attributed to different reaction mechanisms, but they do not give any indication of the contribution of each region to the overall reactivity of the coal. Therefore, the concept of weighted mean activation energy, E_{wm}, was applied to determine the overall reactivity of coal (Cumming 1984);

$$E_{wm} \;=\; F_1 E_1 \;+\; F_2 E_2 \;+\; F_3 E_3 \;+......+\; F_n E_n \tag{4}$$

where F_1, F_2, …….,F_n are the mass fractions of the combustible content of the sample burned during each region of Arrhenius linearity, and E_1, E_2,……E_n are the individual apparent activation energies obtained over each region of Arrhenius linearity. Figure 5 shows the log (1/w)(dw/dt) vs 1000(1/T) curve for the fine circuit cyclone underflow and the application of weighted mean activation energy concept with respect to the reaction regions.
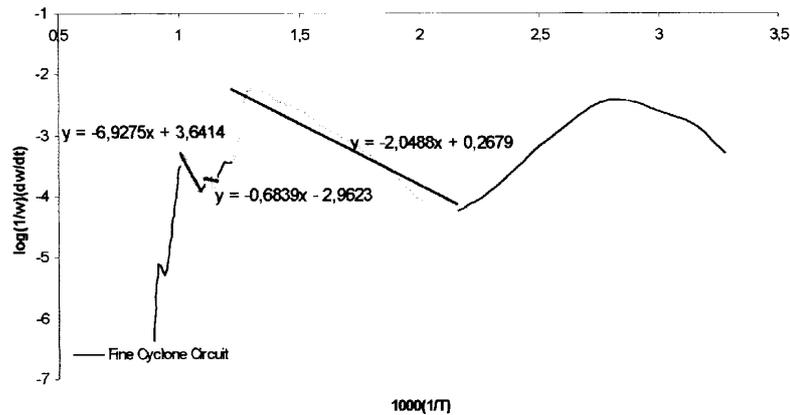
Fig. 5. log(1/w)(dw/dt) vs 1000(1/T) curve of fine circuit cyclone
undreflow and the combustion regions

The Activation Energy concept is a measure of the degree of easiness of a coal to begin the reaction and combust completely. In Table 7, the activation energies of the feeds and concentrates and therefore the effect of concentration processes on the activation energies of the samples are seen.

The declines in the activation energies of the concentrates of fine and coarse circuit feeds show that, the concentration processes carried out with those samples are

effective due to the removal of the mineral constiuents and the results obtained in the kinetic analysis is parallel to those of thermogravimetric analysis. However the decrease in the activation energy of the concentrate of thickener feed is not so high. This is again due to the defficiency of the concentration processes which is caused by the existence of high amounts of AK116 flocculant. The results of the thermogravimetric and kinetic analysis have the same trend, in other words, the activation energies obtained support the success of the concentration processes with the fine and coarse cyclone circuit feeds whereas, the negative effect of flocculant on the concentration of the thickener sample is again seen.

Table 7. Activation energies of the samples

Type of Sample	Concentration Method	Act.Energy (kj/mol)
Fine Cyclone Circuit	-	17.4
Fine Cyclone Circuit Concentrate	Humphreys Spiral	15.2
Fine Cyclone Circuit Concentrate	Shaking Table	14.9
Coarse Cyclone Circuit	-	17.0
Coarse Cyclone Circuit Concentrate	Humphreys Spiral	14.8
Coarse Cyclone Circuit Concentrate	Shaking Table	14.6
Thickener	-	21.9
Thickener Concentrate	Humphreys Spiral	20.8
Thickener Concentrate	Shaking Table	21.2

CONCLUSION AND RECCOMENDATIONS

According to this study, aiming the utilization of the fine fraction as well as a reduction in the amount of tailings of Alpagut Dodurga Coal Washery, the following conclusions and reccomendations are derived:
1. The Humphreys Spiral and Shaking Table concentration processes are observed to be effective on the concentration of fine and coarse cyclone circuit underflows and resulted in high decreases in ash percentage and activation energies whereas important increases in the calorific values are obtained in the concentrates of those.
2. The same processes were not able to produce concentrates with efficient ash and activation energy decrease and calorific value increase in the sample taken from the thickener. This is due to the agglomeration of fine coal particles related to the existence of AK116 flocculant in high amounts.
3. The fine fraction of the TKİ Dodurga Alpagut Lignites Coal Washery can be concentrated with gravitational concentration methods and at the end of the experiments, it has been determined that approximately 60 % of this fine fraction

can be recovered as concentrate. This means that the amount sent to tailing ponds can be decreased down to 8 % which will solve the tailing ponds problem with a great extent. The efficiency of the concentration processes can also be increased by systematic trials and variations in the operating variables of the concentration equipment. However, the absence of AK116 is a must for a successful operation.

4. The slime problem in the region will be decreased greatly in case the required modifications are performed in the flowsheet of the washery and concentration is realized. Therefore, the tailing (slime) pond problem and the usage of AK116 and its cost will be reduced.

5. If concentration is realized in the region, the fraction obtained as concentrate may be too fine for household heating or industrial purposes, but briquetting of this portion can be performed after finding out the optimum briquetting conditions, and the market problem may be overcome by this way.

REFERENCES

CUMMING, J.W. (1984) *Reactivity assesment of coals via a weighted mean activation energy.* Fuel, 63: 1436-1440.

HIÇYILMAZ, C & ALTUN N.E. (2000) *Focusing on the combustion properties of binder added coal.* Mineral Processing on the Verge of the 21st Century, Antalya, Turkey: 441-446, Rotterdam: Balkema.

KIRNARSKY, A. & SBITNEV, M. (1998). *Development of spiral separation technology for coal slimes treatment.* Proceedings of the 5th international symposium on environmental issues and waste management in energy and mineral production, Ankara, Turkey: 659-662. Rotterdam: Balkema.

KÖK, V.M., ÖZBAŞ, E. & HIÇYILMAz, C. (1997) *Effect of Particle size on the thermal and combustion properties of coal.* Thermochimica Acta, 302: 125-130.

Altun N.E., Hicyilmaz C., *Zagospodarowanie odpadowych pyłów węgla brunatnego z kopalni Corum Alpagut, Turcja*, Fizykochemiczne Problemy Mineralurgii 35 (2001), 171-180 (w jęz. ang.)

Drobna klasa ziarnowa odpadowych pyłów węgla brunatnego z kopalni Corum Alpagut w Turcji, zawiera 71,2% ziaren o wymiarze mniejszym niż 0,1 mm. Materiał ten powoduje określone straty ekonomiczne oraz stwarza potencjalne niebezpieczeństwo dla środowiska naturalnego. Materiał gromadzony jest w stawach osadowych w rejonie kopalni. Materiał zgromadzony w stawach osadowych nie może być sprzedany ani ponownie zawrócony do przeróbki. Drobna klasa ziarnowa odpadowych pyłów węglowych stanowi poważny problem dla zakładu. W celu rozwiązania tego problemu, należy przerobić drobną klasę ziarnową o zawartości około 20% węgla, na produkt handlowy o odpowiedniej zawartości węgla i popiołu. Dla realizacji tego celu zastosowano spiralę Humphrey'a i stół koncentracyjny. Materiał użyty do badań pochodził z cyklonu i osadnika z obiegu wodno-mułowego kopalni., Zastosowane metody koncentracji pozwoliły uzyskać produkt o odpowiedniej kaloryczności i niskiej zawartości popiołu. Kinetyki spalania otrzymanych produktów były określane metodami termograwitacyjnych.

Tadeusz BIESZCZAD[*], Stanisława SANAK-RYDLEWSKA[**]

ELECTROWINNING OF COPPER AND LEAD FROM AMMONIUM ACETATE SOLUTIONS

This paper presents the results of laboratory studies on electrowinning of copper and lead from spent leachate obtained by leaching of copper concentrates with ammonium acetate solutions. The effect of electrolyte composition and the electrolysis current density on the process efficiency was investigated. The electrolyte was also pre-treated with ammonia before it was electrolysed under the same above-mentioned conditions.

1. INTRODUCTION

In pyrometallurgical processing of copper concentrates, the relatively high content of lead in the concentrate, reaching up to 2.5%, poses a problem. Lead is concentrated mainly in by-products of pyrometallurgical processes, such as dust and sludge formed during removal of dust from metallurgical gases. There are two approaches to the problem of lead accompanying copper production: efficient capture of lead-containing waste from the pyrometallurgical production of black copper and its further processing to recover metallic lead, and reduction of lead content in copper concentrate (most often by hydrometallurgical methods) used as furnace feed material. Lead content in the concentrate can be reduced below 1% by leaching with concentrated ammonium acetate (Sanak-Rydlewska S., Bieszczad T., 2000, Sanak-Rydlewska S., 2000).

Electrolysis is one method for regenerating leachate. An advantage of this method is that some components can be removed from the system without introducing new ones (Bieszczad T., 1998). Whether a metal can be removed by electrowinning depends primarily on the standard potential of its electrode reaction. The metals easiest to recover are those with positive standard potentials (noble metals). More difficult to recover are metals whose standard potentials are negative, because gaseous

---

*Jagiellonian University, Krakow, Poland
**University of Mining and Metallurgy, Krakow, Poland

hydrogen may develop together with metal deposition. In most cases, however, hydrogen evolution can be avoided owing to the high overpotential of hydrogen evolution on solid electrodes. In practice, the least noble metal that can be deposited by electrolysis in aqueous solutions is manganese, whose standard potential is −1.18 V. Less noble metals can be deposited in the form of amalgams at the mercury electrode or by electrolysis conducted in molten salts.

The best known and most widely applied electrolytic processes are electrorefining of copper and silver, and zinc production. About 53% of the zinc produced worldwide (and in Poland) is obtained by electrolysis (Gupta C.K., 1990). Electrowinning of copper is a final unit operation in the hydrometallurgical method for copper production (Łętowski F., 1976; Kozłowska-Kołodziej B., 1978; Kołodziej B., 1996). The method involving copper leaching-electrowinning is commercially used by many companies (Kuhn A.T., 1971). Electrolysis is conducted in solutions containing 20-70 g/dm^3 Cu^{2+} and similar amounts of sulphuric acid. In these processes the cathodes are made of copper whereas the anodes are made of lead-antimony (6-16%)-silver (0-1%) alloy. A method for obtaining copper from lean deposits that is gaining importance involves direct extraction from the deposit, followed by electrowinning (SX-EW-solvent extraction-electrowinnig) (Suttil K.R., 1993). Electrolysis done in a double membrane electrolysis cell (DMEC process) makes it possible to obtain cobalt and nickel from scrap metals. (Redden L.D., 1992). Electrolysis is also used in both electrorefining and electrowinning of lead from leachate produced by leaching spent lead batteries and other lead-containing materials (Kołodziej B, 1999). A breakthrough in regenerating solutions with very low metal contents can be the use of electrodes made of carbon fibre fabric. (Przyłuski J., 1994).

Electrowinning of metals (mainly copper) from the ammoniated solutions is much less frequent. This problem has been addressed in several papers (Marczenko N.A., 1957; Komkin W.D., 1960; Goerlich Z., 1972) examining the effect of cathodic current density, ammonia and copper ion concentrations, temperature and hydrodynamic conditions on the efficiency of electrowinning and the quality of deposits.

The use of state-of-the-art electrochemical processes in cells of unconventional design seems to be the future for precious metals recovery and waste utilization (combined with hydrometallurgy).

2. INVESTIGATION METHODS

The measurements were performed in a rectangular Plexiglass vessel containing two identical acid-resistant-steel electrodes with an active surface of 50 cm^2 each, placed of 0.5 cm apart. The electrodes were connected to a 5351-type (UNITRA UNIMA) stabilised power supply that ensured pre-set current throughout the measurement. In each of the measurements, 100 cm^3 of electrolyte were used, flowing through the electrolytic cell at a constant rate of 75 cm^3/min, forced by a peristaltic

pump. During the measurements the potentials were controlled between the cathode and anode, and between the cathode and the silver-silver chloride electrode connected via a 40% ammonium acetate salt bridge. In the study, 10% and 40% ammonium acetate solutions were used, which contained about 2 g/dm^3 Cu^{2+} and 0.2 g/dm^3 Pb^{2+}; 5 g/dm^3 Cu^{2+} and 0.5 g/dm^3 Pb^{2+}; and 10 g/dm^3 Cu^{2+} and 1 g/dm^3 Pb^{2+}. The selected electrolyte concentrations correspond roughly to those obtained after leaching of copper concentrate with ammonium acetate. The electrolysis was conducted at room temperature at three different currents: 50 mA, 100 mA and 500 mA. Leachate samples were analysed for Cu and Pb content by the ICP method.

3. ANALYSIS OF ELECTRODE REACTIONS

In the constant-current electrolysis, forced reactions occur on the cathode and anode. A general principle is that the first ions discharged at the cathode are those with the highest cathodic reduction potential. On the anode, anions with the lowest anodic oxidation potential are discharged first, followed by ions of successively higher potential. The problem of determining the product of electrode reactions is solved by calculating reduction and oxidation potentials for all ions present in the solution, according to the following equations:

$$P_k = E_{el} - \eta_k = E^0 + (2.303RT/nF)\log a_k - \eta_k \tag{1}$$

$$P_a = E_{el}' + \eta_a = E^{'0} + (2.303RT/nF)\log a_a + \eta_a \tag{2}$$

where: P_k, P_a – anodic oxidation and cathodic reduction potentials, E_{el}, E_{el}' – half-cell potentials, $E^0, E^{'0}$ – standard half-cell potentials, η_k, η_a – cathodic and anodic process overpotentials, a_k, a_a – cation and anion activities, and F - faraday.

The electrolysed solutions contained the following cations and anions: NH_4^+, Cu^{2+}, Pb^{2+}, H^+, CH_3COO^- and OH^- Their approximate decomposition potentials can be calculated from the equations specified above.

Among the cations, ammonia ions have the highest concentration in the solution. No data exist in the literature on cathodic reduction of NH_4^+ ion, but the simplest electrode reaction has been assumed, according to the equation:

$$2NH_4^+ + 2e \rightarrow 2NH_{3(g)} + H_{2(g)}. \tag{3}$$
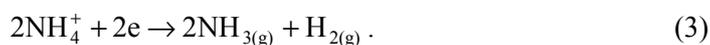
On the basis of the thermodynamic data of this reaction, ΔG^0 and then the standard potential E^0 can be calculated. The calculated standard potential is – 0.651 V. The potential of ammonium ion decomposition can be evaluated by this equation:

$$P_{NH_4^+} = -0.651 + 0.059 \log[NH_4^+] - \eta_{NH_3} - \eta_{H_2}. \tag{4}$$

The calculated electrode potential (the first two terms of equation (4)) is -0.644 V for the 10% ammonium acetate solution and -0.609 V for the 40% solution. The hydrogen evolution overpotential in acid (pH of the studied solutions is about 5) is about 0.5 V on the iron electrode (about 0.6 V on copper electrode); no data are available on the overpotential for ammonium evolution. With the overpotential for ammonia evolution equal to zero, the potential of NH_4^+ decomposition will be below -1 V.

Cu^{2+} ions are reduced at the cathode according to the reaction:

$$Cu^{2+} + 2e \rightarrow Cu. \tag{5}$$

The standard potential of this reaction is $+0.337$ V. The electrode potential calculated for the Cu^{2+} concentration of 2 g/dm^3 is $+0.293$ V, and $+0.313$ V for the concentration of 10 g/dm^3. These potentials will decrease as copper ions are removed in the course of electrolysis. It is difficult to estimate the overpotential of copper ion deposition on iron and metallic copper. It depends on many factors, of which the most important is cathodic current density. At low current densities the overpotential of deposition of metal ions on the parent metals is low. Because of this, one can expect that the potential of copper ion deposition will be close to the cathode equilibrium potential in a given solution. In ammoniated solutions the electrode reaction occurs according to the equation

$$[Cu(NH_3)_4]^{2+} + 2e \rightarrow Cu_{(s)} + NH_{3(g)} \tag{6}$$

the standard potential of which is $E^o = -0.5$ V [Milazzo G., 1963].

Pb^{2+} ions will be reduced at the cathode according to the equation:

$$Pb^{2+} + 2e \rightarrow Pb \tag{7}$$

The standard potential of this reaction is -0.126 V. By assuming, as previously, low overpotential of lead deposition, the potential of Pb^{2+} decomposition in a solution with a concentration of 0.2 g/dm^3 is close to -0.215 V, and -0.194 V for a solution with a concentration of 1 g/dm^3.

Cathodic reduction of hydrogen ions in acid solutions (the pH of the studied solution is about 5) occurs according to the reaction:

$$2H^+ + 2e \rightarrow H_2. \tag{8}$$

The potential of the hydrogen electrode depends on the pH of the solution and is – 0.295 V for pH = 5. The overpotential of hydrogen evolution on the iron electrode (in acid solution) is high and amounts to about 0.5 V, hence the hydrogen evolution potential in this system is – 0.795 V.

Even a rough estimate of the discharge potentials of cations present in the studied system demonstrates that the copper deposition reaction has the highest potential and will take place first. Theoretically, deposition of lead should begin when the electrode potential, which decreases as the copper ion concentration drops, has reached the value – 0.214 V (for Pb^{2+} concentration of 1 g/dm^3), which corresponds to very low Cu^{2+} concentrations of about 10^{-10} g/dm^3. Actually, electrolysis of lead begins much earlier. When conducting a constant-current electrolysis one should remember that cation and anion discharge overpotentials are strongly affected by the current density, although in a different fashion, and concurrent deposition of several ions may occur.

Apart from cathodic reactions, anodic oxidation takes place. Water decomposition with oxygen evolution

$$2H_2O \rightarrow O_2 + 4H^+ + 4e \qquad E^0 = 0.401\,V \qquad (9)$$

anodic oxidation of acetate ion [Isaacs N. S., 1974]

$$2CH_3COO^- \rightarrow C_2H_6 + 2CO_2 + 2e \qquad E^0 = -0.364\,V \qquad (10)$$
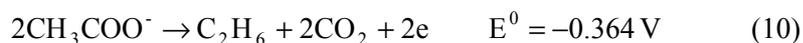
and oxidation of Pb^{2+} ions

$$Pb^{2+} + 2H_2O \rightarrow PbO_2 + 4H^+ + 2e \qquad E^o = -0.5\,V \qquad (11)$$

should also be considered in the studied system.

As the overpotential for oxygen evolution on iron is about 0.25 V, the oxygen evolution potential in this system will be about 1.18 V (assuming that the solution has pH of 5).

Assuming that the overpotentials for evolution of ethane and CO_2 are similar to that of oxygen (no data are available), the decomposition potential of the acetate ion would be about 0.1 V. This means that on the anode, the water decomposition reaction will proceed, accompanied by oxygen evolution.

The oxidation potential for reaction (11) in a solution with pH = 5 and lead content of 0.2 g/dm^3 is 0.954 V, and it rises with the decrease in Pb^{2+} ion concentration. The potential thus calculated should be increased to include the overpotential for PbO_2 deposition – there are, however, no literature data about this reaction. Under the conditions of the studied electrolysis, no deposition of solid PbO_2 on the anode was observed, but evolution of gaseous products could be seen. Consequently, the overpotential for PbO_2 deposition on the steel anode must be higher than 0.02 V.

4. DECOMPOSITION VOLTAGE

Knowledge of the decomposition potentials for various electrolytes as determined from I = f(V) dependencies allows prediction of the sequence in which these ions will undergo electrode reactions.

Current as a function of the voltage applied was measured for 10% and 40% ammonium acetate solutions containing 5 g/dm^3 Cu^{2+} or Pb^{2+}, as well as solutions containing both ions at the same time but in a concentration ratio of 10 to 1. Voltage was applied to the cell electrodes from a UNITRA UNIMA type 5352 M power supplier and the current was measured with an HC–81 ammeter. The dependence of the current response to the applied potential is shown in Fig. 1. The curves are almost independent of the ammonium acetate and the presence of the other ions at a 10 times lower concentration. Only two curves are shown – one characteristic of copper ions, the other of lead ions. The discharge potentials of copper and lead ions are −1.20 V and −1.63 V, respectively.
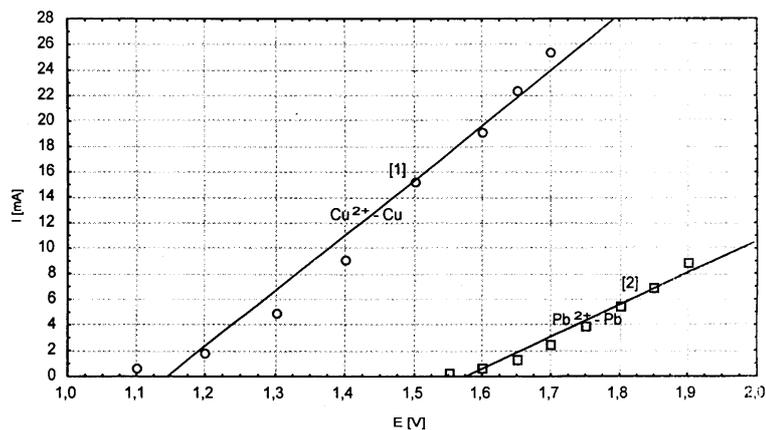
Fig. 1. Current – voltage dependence 1 – 40% solution CH_3COONH_4 + 5g/dm^3 $Cu(CH_3COO)_2$
2 – 40% solution $CH_3COOONH_4$ + 5g/dm^3 $Pb(CH_3COO)_2$

5. MEASUREMENT RESULTS AND INTERPRETATION

After one hour's leaching of copper concentrate with ammonia acetate, the solutions contained about 2 g/dm^3 Cu^{2+} and about 0.2 g/dm^3 Pb^{2+}. As concentrated ammonia acetate solutions have a high buffer capacity for lead (II), the same solution can be used several times for leaching [Bieszczad T., unpublished data]. Solutions of such high concentrations must not go into the wastewater. A method of solving this problem is electrowinning of metals from the leachate. This paper presents the results for solutions whose composition is similar to spent leaching solutions.

5.1. ELECTROWINNING OF COPPER AND LEAD FROM PURE ACETATE SOLUTIONS

The solutions to be used in electrolysis were made by dissolving appropriate amounts of copper (II) and lead (II) acetates in 10% or 40% ammonium acetate solution. In each case the Cu^{2+} concentration was 10 times higher than the Pb^{2+} concentration (roughly corresponding to the composition of spent solution after leaching of copper concentrate).

5.1.1. ELECTROLYSIS OF 10% CH_3COONH_4 SOLUTIONS

The results of electrolysis conducted in a 10% ammonium acetate solution containing about 2.5 g/dm^3 Cu^{2+} and about 0.25 g/dm^3 Pb^{2+} are shown in Table 1.

Table 1. Results of electrolysis conducted in a 10% ammonium acetate solution containing about 2.5 g/dm^3 Cu^{2+} and about 0.25 g/dm^3 Pb^{2+}

No.	I [A]	t [min]	$c_{Cu^{2+}}$ [g/dm^3]	$c_{Pb^{2+}}$ [g/dm^3]	E_{K-A} [V]	E_K vs. ref. el. [V]	Current efficiency [%]
1	0.025	0 200	2.501 0.686	0.248 0.053	1.7–2.0	– 0.38 to – 0.65	~ 92
2	0.1	0 100	2.501 0.939	0.248 0.076	1.9–2.1	– 0.52 to – 0.67	~ 89
3	0.5	0 30	2.683 1.493	0.270 0.119	2.6–2.8	– 1.18 to – 1.29	~ 40

The symbols used in the table are defined as follows: I - current of electrolysis (A), t – time elapsed prior to sampling (min), $c_{Cu^{2+}}$, $c_{Pb^{2+}}$ - analytically determined concentrations of Cu^{2+} and Pb^{2+} (g/dm^3), E_{K-A} - potentials of the cathode and anode (V), E_K vs. ref. el. – potential of cathode vs. the saturated silver-silver chloride electrode (V), current efficiencies calculated for electrowinning of copper (%).

The approximate current efficiencies, computed from the obtained results, depend on the electrolysis current. The highest efficiencies were obtained for the lowest currents. In all electrolyses, lead deposited along with copper and its concentration in the solution was markedly lower. The amount of deposited lead increased with the decrease in the electrolysis current. In the studied system, one should consider the possibility of unfavourable secondary chemical dissolution of deposited metallic lead and copper by ammonium acetate. This process will be affected mostly by the quality of the formed deposits, temperature and hydrodynamic conditions in the system. In the first electrolysis, a fairly compact deposit, resembling slightly soiled copper, formed on the cathode. In the next electrolysis, the deposit was brown, whereas in the last one the deposit was dark and spongy with a highly developed surface. In the electrolysis conducted at the highest current density, hydrogen evolved on the cathode, which

explains the low current efficiency and the structure of the deposit. In all cases oxygen evolved at the anode.

In planning circulation and the use of leaching electrolytes in a closed cycle, one should be prepared for its enrichment in copper and lead ions. The data for solutions with higher Cu and Pb content are given in Table 2.

Table 2. Results of electrolysis conducted in a 10% ammonium acetate solution with increased content of copper and lead

No.	I [A]	t [min]	$c_{Cu^{2+}}$ [g/dm^3]	$c_{Pb^{2+}}$ [g/dm^3]	$E_{K–A}$ [V]	E_K vs. ref. el. [V]	Current efficiency [%]
4	0.5	0 50	5.275 1.075	0.591 0.084	2.6	– 1.10 to – 1.02	~ 85
5	0.5	0 100	10.626 1.242	1.263 0.102	2.6	– 1.04 to – 1,02	~ 95

The electrolyses were performed at current of 0.5 A because of much higher concentrations of electrodeposited ions. The current densities produced under such conditions are much higher and increase with the concentration of copper and lead in the solution. The electrolysis voltage and the potential of the cathode vs. the saturated silver-silver chloride electrode are similar and almost independent of the ion concentration in the solution. On the cathode a black powdery deposit is formed, easily peeling off the electrode, and probably a very small amount of hydrogen evolves.

Electrolyses of solutions with the lowest concentrations of copper and lead were also performed with the distance between the electrodes increased to 2 cm. This change slightly improved the current efficiency of the process at the highest current density, whereas the other parameters of the process and the cathodic deposit remained the same as in the system with the electrodes spaced 0.5 cm apart.

5.1.2. ELECTROLYSIS OF 40% CH$_3$COONH$_4$ SOLUTIONS

The measurements were conducted in a 40% ammonium acetate solution, with the other conditions remaining unchanged. The results for the lowest concentrations of copper and lead ions at various electrolysis currents are given in Table 3.
The electrolysis voltage and the potential of the cathode vs. the saturated silver-silver chloride electrode are similar to those in the electrolysis done in a 10% CH$_3$COONH$_4$ solution. The current efficiencies are also similar – the highest value was observed for the lowest current density and amounted to 95%. The greatest changes in the lead concentration in the solution were obtained for the lowest electrolysis currents.

The results of measurements for higher concentrations of copper and lead at electrolysis current of 0.5 A are given in Table 4.

Table 3. Results of electrolysis conducted in a 40% ammonium acetate solution containing
about 2.5 g/dm^3 Cu^{2+} and about 0.25 g/dm^3 Pb^{2+}

No.	I [A]	t [min]	$c_{Cu^{2+}}$ [g/dm^3]	$c_{Pb^{2+}}$ [g/dm^3]	$E_{K–A}$ [V]	E_K vs. ref. el. [V]	Current efficiency [%]
6	0.05	0 / 200	2.962 / 1.020	0.287 / 0.059	1.9–2.1	– 0.52 to – 0.85	~ 98
7	0.1	0 / 100	2.962 / 1.281	0.287 / 0.080	2.1	– 0.91 to – 0.87	~ 85
8	0.5	0 / 30	3.040 / 1.980	0.280 / 0.155	2.8–2.6	– 1.28 to – 1.09	~ 36

Table 4. Results of electrolysis conducted in a 40% ammonium acetate solution with increased
content of copper and lead

No.	I [A]	t [min]	$c_{Cu^{2+}}$ [g/dm^3]	$c_{Pb^{2+}}$ [g/dm^3]	$E_{K–A}$ [V]	E_K vs. ref. el. [V]	Current efficiency [%]
9	0.5	0 / 50	5.301 / 1.891	0.614 / 0.198	2.6	– 1.12 to – 1.09	~ 69
10	0.5	0 / 100	12.758 / 4.022	1.531 / 0.354	2.6	– 1.00 to – 1.07	~ 88

The cathode deposits formed in both electrolyses are spongy, brittle and black, and easily peel off the electrode. After electrolysis with higher metal content, small grains of metallic copper were easily discernible in the deposit.

5.2. ELECTROWINNING OF COPPER AND LEAD FROM AMMONIATED SOLUTIONS

The solutions used in earlier experiments were treated with ammonia following the same procedure in each case: 5 cm^3 of concentrated ammonia water was added to 100 cm^3 of a 10% or 40% CH$_3$COONH$_4$ solution with an appropriate Cu^{2+} and Pb^{2+} content, the solution was filtered off, and 100 cm^3 of the filtered solution was taken for electrolysis. The treatment with ammonia had two goals: to complex copper ions and to partially precipitate lead by increasing the pH of the solution. The first objective was reached; the solution turned deep blue, a colour characteristic of tetra-ammino copper complexes. Analyses showed that the high stability of the acetate complexes of lead prevented precipitation of the sparingly soluble lead (II) hydroxide. The results of electrolyses conducted in ammoniated solutions, shown in the tables below, were obtained under conditions analogous to those specified earlier.

5.2.1. ELECTROLYSIS OF 10% CH$_3$COONH$_4$ + NH$_3$ SOLUTIONS

The results of measurements done in ammoniated 10% ammonium acetate solutions at various currents of electrolysis are given in Table 5.

Table 5. Results of electrolysis conducted in an ammoniated 10% ammonium acetate solution containing about 2.5 g/dm^3 Cu^{2+} and about 0.25 g/dm^3 Pb^{2+}

No.	I [A]	t [min]	$c_{Cu^{2+}}$ [g/dm^3]	$c_{Pb^{2+}}$ [g/dm^3]	E_{K-A} [V]	E_K vs. ref. el. [V]	Current efficiency [%]
11	0.05	0 200	2.466 1.040	0.222 0.035	1.5–1.6	−0.51 to −0.62	~ 72
12	0.1	0 100	2.466 1.054	0.222 0.041	1.9–2.1	−0.62 to −0.83	~ 71
13	0.5	0 30	2.407 1.334	0.214 0.062	2.4	−1.27 to −1.09	~ 36

The voltage of electrolysis and of the cathode vs. the saturated silver-silver chloride electrode are similar to those in electrolyses without ammonia (Table 1), whereas the current efficiencies are lower at low current densities. For currents of 0.05 A and 0.1 A the copper deposit produced on the cathode was glossy and relatively compact, whereas at 0.5 A the cathode was covered with a spongy deposit. One should note the high depletion of lead ions in ammoniated solution.

The results of electrolyses of solutions with higher copper and lead concentrations are shown in Table 6.

Table 6. Results of electrolysis conducted in ammoniated 10% ammonium acetate with increased content of copper and lead

No.	I [A]	t [min]	$c_{Cu^{2+}}$ [g/dm^3]	$c_{Pb^{2+}}$ [g/dm^3]	E_{K-A} [V]	E_K vs. ref. el. [V]	Current efficiency [%]
14	0.5	0 50	4.828 1.633	0.437 0.136	2.3	−1.19 to −1.24	~ 65
15	0.5	0 100	10.313 1.532	1.219 0.075	2.6	−1.03 to −1.00	~ 89

The obtained current efficiencies are lower than those obtained in corresponding non-ammoniated solutions. In both cases, simultaneous evolution of gaseous hydrogen on the cathode was noted. The black deposit forming on the cathode easily peeled off the electrode, and at higher concentrations it became greasy.

5.2.2. ELECTROLYSIS OF 40% CH$_3$COONH$_4$ + NH$_3$ SOLUTIONS

The results of measurements conducted in ammoniated solutions at various currents of electrolysis are shown in Table 7.

Table 7. Results of electrolysis conducted in an ammoniated 40% ammonium acetate solution containing about 2.5 g/dm^3 Cu^{2+} and about 0.25 g/dm^3 Pb^{2+}

No.	I [A]	t [min]	$c_{Cu^{2+}}$ [g/dm^3]	$c_{Pb^{2+}}$ [g/dm^3]	E_{K-A} [V]	E_K vs. ref. el. [V]	Current efficiency [%]
16	0.05	0 200	2.533 0.847	0.198 0.027	1.6–2.6	– 0.58 to – 0.90	~ 85
17	0.1	0 100	2.533 1.250	0.198 0.063	2.0–2.1	– 0.57 to – 0.98	~ 65
18	0.5	0 30	2.533 1.680	0.198 0.125	2.4	– 1.15 to – 1.24	~ 29

The highest current efficiencies and the highest depletion of lead ions were noted for the lowest current densities. Irrespective of the current value, a black, spongy, easily peeling deposit is formed at the cathode

Table 8 presents the results of electrolysis of ammoniated solutions with higher concentrations of copper and lead.

Table 8. Results of electrolysis conducted in an ammoniated 40% ammonium acetate with increased content of copper and lead

No.	I [A]	t [min]	$c_{Cu^{2+}}$ [g/dm^3]	$c_{Pb^{2+}}$ [g/dm^3]	E_{K-A} [V]	E_K vs. Ref. el. [V]	Current efficiency [%]
19	0.5	0 50	5.327 2.171	0.628 0.196	2.5–2.6	– 1.19 to – 1.13	~ 64
20	0.5	0 100	10.130 2.841	1.265 0.332	2.6	– 1.33 to – 1.28	~ 74

The obtained current efficiencies are not high, a results of the noticeable evolution of gaseous hydrogen. Under conditions of electrolysis No. 19, the deposit formed on the cathode was similar to deposits obtained in earlier electrolyses, whereas during the electrolysis of the solution with the highest metal content, a black, greasy deposit formed on the cathode.

6. SUMMARY

The electrolysis of solutions with low content of metals has drawn interest due to its possible application to industrial fluid and wastewater treatment. In this study electrolysis was used to investigate regeneration of concentrated ammonium acetate solutions formed as a result of leaching of lead from copper concentrate.

Theoretical calculations and the experimental values of decomposition potentials show that in the system under study, copper and lead are co-deposited on the cathode, with gaseous hydrogen being also evolved at high current densities.

The current efficiency of the process, calculated relative to copper, is almost independent of the ammonium acetate concentration and of whether or not the solution is ammoniated. The current efficiency decreases (for the same composition) with the increase in current density, and increases with an increase in copper and lead.

The lower the cathodic current density, the higher the changes in lead ion concentration. Greater changes are noted in ammoniated solutions.

The voltages of electrolysis and the potentials of the cathode vs. the saturated silver-silver chloride electrode increase with the increase in current density, and are independent of the ammonium acetate concentration.

The cathodic current density and electrolyte composition affect the quality of the cathodic deposit. Deposits obtained at low current densities are more compact, whereas those obtained at higher current densities are spongy and easily peel off the electrode.

BIBLIOGRAPHY

BIESZCZAD T., SANAK-RYDLEWSKA S., (1998), Zeszyty Naukowe Politechniki Śląskiej No. 1399 „Górnictwo" z. 245, Gliwice, pp. 65-75.

BIESZCZAD T., SANAK-RYDLEWSKA S., unpublished data.

GOERLICH Z., PETLICKI J., (1972), Zeszyty Naukowe UJ, Prace Chem., 312, 18, 295 .

GUPTA C.K., MUKHERJEE T.K., (1990), *Hydrometallurgy in extraction processes,* CRC Press, vol. II, 185.

ISAACS N. S., (1974), *Fizyczna chemia organiczna.* PWN, W-wa, pp. 259 – 260.

KOŁODZIEJ B., (1996), *Seminarium „Hydrometalurgia – cechy i możliwości metody",* Wrocław, p. 49.

KOŁODZIEJ B., (1999), IV Seminarium „Hydrometalurgia ołowiu", Lubin, p. 47.

KOMKIN W.D., PIERCOVSKIJ M.Ł., (1960), Zh. Prikl. Chim., 33, 1215.

KOZŁOWSKA-KOŁODZIEJ B., (1978), Rudy Metale, 8, 23, 392.

KUHN A.T., (1971), *Industrial electrochemical processes,* Elsevier Publishing Company, Amsterdam – London – New York.

ŁĘTOWSKI F., KOŁODZIEJ B., CZERNECKI M., JĘDRACZEK A., ADAMSKI Z., (1976), Hydrometallurgy, 29, 36.

MARCZENKO N.A., (1957), Zh. Prikl. Chim., 30, 248.

MILAZZO G., (1963), Electrochemistry, Esevier Publ. Comp.

PRZYŁUSKI J., DARKOWSKI A., GABRYSZEWSKI M., (1994), Int. Conf. Recycl. Met. Proc., 397.

REDDEN L.D., GREAWES J.N., (1992), Hydrometallurgy, 29, 547.

SANAK-RYDLEWSKA S., BIESZCZAD T., (2000), 5th Conference on Environment and Mineral Processing, Part II, 22.06 – 24.06, Ostrawa, Czech Republic.

SANAK-RYDLEWSKA S., BIESZCZAD T., MAŁYSA E., KONOPKA E., (2000), Zeszyty Naukowe Politechniki Śląskiej No. 1479 „Górnictwo" z. 245, pp.159-164.

SUTTIL K.R., (1993), *SX Copper Burns Bright.* Eng. Min. J., 12, 194, 24.

W artykule przedstawiono wyniki badań laboratoryjnych nad procesem elektrowydzielania miedzi i ołowiu z roztworów modelowych, o składzie podobnym do tego, jakie uzyskuje się w procesie ługowania koncentratów miedziowych roztworami octanu amonowego. Dla roztworów modelowych przebadano wpływ składu roztworu elektrolitu i wielkości prądu elektrolizy na wydajność procesu. Zastosowano również wstępną obróbkę elektrolitu amoniakiem, po której poddano roztwór elektrolizie w takich samych warunkach, jakie stosowano dla roztworów bez dodatku amoniaku.

Z przeprowadzonych obliczeń teoretycznych i z wyznaczonych doświadczalnie napięć rozkładowych wynika, że w badanym układzie na katodzie zachodzi reakcja współwydzielania miedzi i ołowiu a przy wysokich prądach także gazowego wodoru. Wydajność prądowa procesu, liczona w stosunku do miedzi, prawie nie zależy od stężenia octanu amonowego i od tego czy roztwór poddawany procesowi elektrolizy zawierał amoniak, czy nie. Wydajność maleje (przy stałym składzie roztworu) ze wzrostem prądu elektrolizy, natomiast rośnie ze wzrostem stężenia miedzi i ołowiu w elektrolicie. Zmiany stężenia jonów ołowiu są tym większe im mniejszy jest prąd elektrolizy. Większe zmiany stężeń ołowiu występują w roztworach amoniakalnych. Napięcia elektrolizy, jak i potencjały katody względem nasyconej elektrody chlorosrebrowej, rosną ze wzrostem prądu elektrolizy, natomiast nie zależą od stężenia octanu amonowego.

Przy niskich wartościach prądu otrzymuje się osady bardziej zwarte a przy wyższych, gąbczaste, łatwo odpadające od elektrody. Ponieważ otrzymane osady w procesie elektrolizy stanowią mieszaninę miedzi i ołowiu, w przyszłości będą przedmiotem badań nad ich rozdziałem, w celu odzyskania czystych metali.

Teofil JESIONOWSKI[*], Andrzej KRYSZTAFKIEWICZ [*] and Aleksandra DEC[**]

MODIFIED TITANIUM WHITE - CHARACTERISTICS AND APPLICATION

In the studies, type R-211 was used, produced by Chemical Works, Police S.A. (Poland). Surface modification of titanium white was performed in order to alter its physicochemical character. In this aim, silane coupling agents were used, carrying methacryloxy, vinyl and amine groups.

Basic characteristics of the titanium white included estimation of bulk density, water, dibuthyl phthalate and paraffin oil absorbing capacities. Moreover, studies were conducted to define morphology, surface structure and dispersion of TiO_2, as affected by the type of applied modifier. The parameters were examined using scanning electron microscopy (SEM). Using dynamic light scattering (DLS) effects of the applied modifiers were tested on tendency to form particle agglomerates. Significant changes were observed in the tendency to form primary and secondary agglomerate structures, particularly upon modification with U-15D aminosilane. The fillers permitted to improve physicochemical and utility properties of the façade acrylic paints.

Key words: titanium dioxide, surface modification, acrylic paint

INTRODUCTION

Titanium dioxide (titanium white) is a natural product, which enters into the composition of ilmenite, $FeTiO_3$. In the nature, it exists in three polymorphic varieties: anatase, rutile, and brookite, which differ in arrangement of elementary particles.

Titanium dioxide is obtained from natural raw materials, such as rock ilmenites, ilmenite sands, leucoxen, or from enriched ores, like enriched ilmenites, titanium slags, or synthetic rutiles. Titanium pigments are produced by two distinct technologies: the sulphate technology and the chloride technology (Wypych, 1999).

Titanium whites are the most frequently applied white pigments, commonly used in the paint, plastic, rubber, paper, ceramic, cosmetic and textile industries.

*Poznan University of Technology, Institute of Chemical Technology and Engineering,
pl. M. Sklodowskiej-Curie 2, 60-965 Poznan, Poland, e-mail: Teofil.Jesionowski@put.poznan.pl,
phone:+48(61)6653626, fax:+48(61)6653649
**PPW Lakma S.A., Frysztacka 173 St., 43-400 Cieszyn, Poland

Moreover, titanium white is used as a polymer filler in, i.a., PVC, polyolefines, polystyrene and many other (Spychaj et al.,1993). Dispersion of pigments and fillers in the vehicle significantly affects the quality and properties of the obtained paints and coats. Dispersion of a pigment (e.g., of titanium white) in the vehicle involves decomposition of the agglomerate structures and their dispersion in the form of primary particles. In the process the size of agglomerates gradually decreases while the total surface of the pigment gradually increases. When pigment dispersion is completed, the wetted particles may show a tendency for re-agglomeration (flocculation). For this reason, it is important to maintain a stable balance between deflocculation and flocculation (Kobayashi, 1997).

Pigment dispersion affects coat properties, such as its lustre, coating power, rheological properties and its stability during storage (Gesenhues, 1999). Fine dispersion of its particles is indispensable for an even distribution of the pigment in a coat and, thus, for the most economic use of the pigment. The smaller is the size of dispersed particles, the more homogeneous is distribution of the pigment (Brown et al.,1997). The raw materials are selected and the formulations are determined depending upon the purpose of the dispersion paints (for interior or exterior use).

Titanium white is subjected to surface processing in order to improve its insufficient refractoriness to weather conditions, its whiteness and dispersion. The processing includes mainly a stabilisation (Sales et al., 1998; Pownceby et al., 1999), involving introduction of other elements to its crystallic lattice, and surface modification (Esumi et al., 1998, 1999; Innocenzi et al., 2000; Shirai et al., 1999), aimed at altering its physicochemical properties. The most frequently applied modifiers include silane, titanate, and zirconate coupling agents, as well as fatty acids and their derivatives and surfactants.

EXPERIMENTAL DETAILS

MATERIALS

Titanium dioxide (R-211) was obtained by the sulfate technology in the Chemical Works "Police" S.A. (Poland). Principal physicochemical data of the pigment are shown in Table 1. The data of Table 1 allowed to conclude that a standard titanium white was used, of typical pH and oil absorption number. 3-Methacryloxypropyltrimethoxysilane (U-511), vinyltrimethoxysilane (U-611) and N-2-aminoethyl-3-aminopropyltrimethoxysilane (U-15D) produced by UniSil Co. Tarnów (Poland) were used as modifiers.

METHODS

MODIFICATION PROCESS

Modification of the surface of TiO_2 was carried out in a mixer. For modification, solutions of appropriate silane were prepared, while solutions of the silane coupling agents were prepared in a mixture of water and methanol (4:1 v/v). Solutions

containing 0.5 weight parts of these compounds in appropriate solvents per 100 weight parts of the modified titanium dioxide were used. The amount of solutions of modifying compounds was always selected in such a way as to ensure optimum wettability of the surface of TiO_2. After mixing, the solvent was removed by evaporation and the modified powders were dried at $110^{\circ}C$.

Table 1. Principal properties of the applied titanium white

Physicochemical variable	Titanium white R-211
Density [g/cm^3]	3.9
Content of titanium dioxide [% w/w]	at least 92
-including rutile	at least 98.5
Content of volatile substances at $105^{\circ}C$ [% w/w]	max. 0.5
Content of water soluble materials [% w/w]	max. 0.5
Residue on a sieve of 45 μm. mesh [% w/w]	max. 0.02
Brightness	95.0
Shade in a white paste	7.0
Relative scattering ability	94
Ability to tone down the shade	1800
Shade in a gray paste	2.5
pH in water suspension	7.8
Oil absorption number [g/100g pigment]	28
Specific resistance of water extract [Ohm x cm]	at least 8,000

PHYSICOCHEMICAL PROPERTIES EXAMINATION

Following the modification, the titanium dioxide was subjected to physicochemical tests, the bulk density as well as water, dibutyl phthalate and paraffin oil absorption capacity was estimated. The end point of water absorption capacity was noted when an excess of a single drop induced an evident liquefaction of the paste being formed. The end point of dibutyl phtahalate or paraffin oil absorption capacities was registered when an excess of a single phthalate or oil drop altered abruptly the consistency of the paste which adhered to a glass plate.

Studies on morphology and microstructure were performed in order to obtain data on dispersion, particle shape and morphology of the granules, structure of individual particles and on TiO_2 aggregation and agglomeration type. The researches were conducted using scanning electron microscopy (SEM). The observations were performed using the Phillips SEM 515 microscope.

Size distributions of TiO_2 particles were estimated using a ZetaPlus instrument (Brookhaven Instruments Inc., USA), by dynamic light scattering method.

APPLICATION OF MODIFIED TITANIUM WHITE

Titanium white was applied as a pigment in acrylic dispersion paints. Two types on acrylic paints were selected, listed in Table 2.

Table 2. Systems of acrylic dispersion paints for studies on application of samples of titanium dioxide

1. AKRYL LAKMA Acrylic dispersion paint, white, water soluble, for facade use	Amount [wt%]
Acrylic-styrene dispersion (acrylic-styrene polymer, 50 wt% in water)	20-25
Carbonate fillers	30-35
Titanium white R-211 unmodified or modified	15-17
Dispersing agents, wetting agents, densifiers	23-35
2. AKRYBET Acrylic dispersion paint, white, organic solvent soluble, for exterior use	Amount [wt%]
Acryl resin in a solvent (whitespirit)	20-25
Carbonate fillers	30-35
Titanium white R-211 unmodified or modified	15-17
Dispersing agents, wetting agents, densifiers	23-35

Titanium whites were introduced to paints for interior or exterior use.

RESULTS AND DISCUSSION

The conducted studies on TiO_2 surface modification using silane coupling agents aimed at altering the hydrophilic/hydrophobic character of the surface. Basic physicochemical parameters of unmodified and the modified titanium white are presented in Table 3. Only insignificant alterations in the surface character were noted in the surface modified pigments.

Table 3. Physicochemical parameters of unmodified and modified titanium dioxide.

Bulk density [g/dm^3]	Water absorbing capacity [cm^3/100g]	Dibutyl phthalate absorbing capacity [cm^3/100g]	Paraffin oil absorbing capacity [cm^3/100g]
TiO_2 - unmodified			
651	150	100	200
TiO_2 + U-611			
778	100	150	250
TiO_2 + U-511			
756	100	200	250
TiO_2 + U-15D			
732	150	100	200

An increased capacity to absorb water by TiO_2 surface could be noted only after modification of the surface with U-15D aminosilane. Since surface of the so modified titanium white carries amine groups which can interact by hydrogen bonds with water molecules, the surface exhibits a slightly hydrophilic character.

The use for modification of silane coupling agents was followed by a slight increase in bulk densities of the titanium white samples. The electron micrograph of the unmodified sample of titanium white, R-211, is presented in Fig.1a while the appropriate particle size distribution of the titanium pigment sample is shown in Fig.1b.

Aggregates		Agglomerates	
Diameter d (nm)	Intensity G(d)	Diameter d (nm)	Intensity G(d)
19.8	17	45.5	8
22.0	38	50.5	48
24.4	55	56.1	100
27.0	37	62.2	90
30.0	11	69.0	52

| a) | b) |
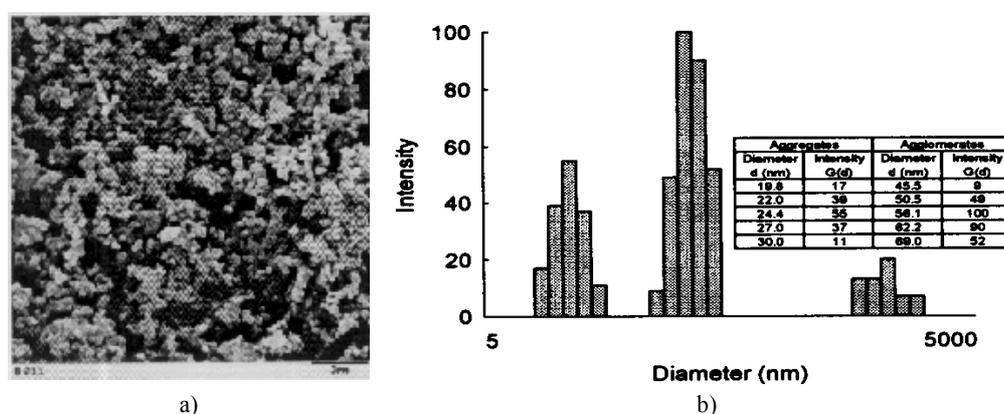
Fig. 1.a) SEM and b) particle size distribution of unmodified TiO_2

In the electron micrograph (Fig.1a), a slight tendency of the unmodified white particles was noted for agglomerate formation. The sample was not uniform, which was confirmed by the particle size distribution, containing three bands (Fig.1b). The first two bands corresponded to particles of less than 100 nm in diameter and showed distinct intensity. The particles of 19.8 to 30.0 nm in diameter formed a low intensity band (maximum intensity of 55 corresponded to particles of 24.4 nm in diameter). On the other hand, particles of diameters in the 45.5 to 69.0 nm range formed an intense band (maximum intensity of 100 corresponded to particles of 56.1 nm in diameter). The particle size distribution contained also a very narrow, intense band corresponding to particles of 195.5 to 296.5 nm in diameter (maximum intensity of 20 corresponded to particles of 240.8 nm in diameter). The distribution of unmodified titanium white particles into the three bands of various intensities proved the relatively high heterogeneity of the pigment. The effective particle diameter was 45.5 nm.

Particle size distribution for the titanium white modified with 0.5 weight parts of U-611 vinylsilane is shown in Fig.2. The distribution contained only two bands of particles of similar intensities, which indicated a greater homogeneity of the modified, as compared to the unmodified, titanium white particles. The band of higher intensity

was formed by particles of 34.6 to 44.5 nm in diameter (maximum intensity of 100 corresponded to particles of 39.3 nm in diameter). On the other hand, the particles of 121.8 to 166.8 nm in diameter formed the less intense band (maximum intensity of 94 corresponded to particles of 147.1 nm in diameter). The effective particle diameter was 63.5 nm.
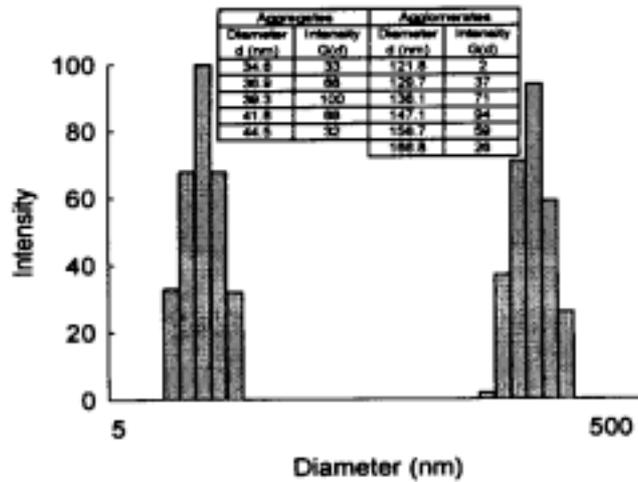
Fig. 2. Particle size distribution of TiO_2 modified with U-611 silane

Following modification of titanium white with methacryloxysilane A-174, the particle size distribution (Fig.3a) presented presence of even four bands of distinct intensities. This proved a deteriorated homogeneity of titanium white, linked to strong adhesive interactions of methacryloxy groups, which induced formation of larger particle clumps (Fig.3b).

a)   b)
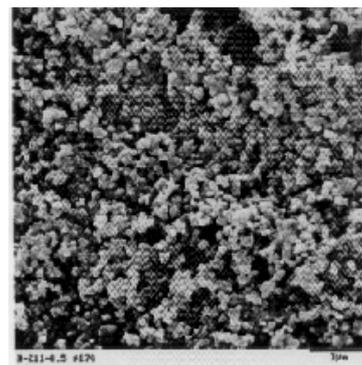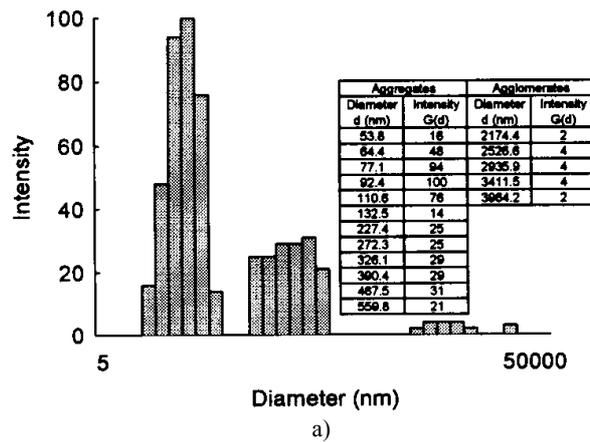
Fig. 3. a) Particle size distribution and b) SEM of TiO_2 modified with A-174 silane

The band of the highest intensity was shifted toward particles of a greater diameter and was formed by particles of 53.8 to 132.5 nm in diameter (maximum intensity of 100 corresponded to particles of 92.4 nm in diameter). Particle accumulations of higher diameters and of a low intensity fitted the diameter range of 224.4 to 559.8 nm (maximum intensity of 31 corresponded to particles of 467.5 nm in diameter). The particle agglomerate range contained two bands of a very low intensity: one fitting the range of 2,174.4 to 3,964.2 nm (maximum intensity of 4 corresponded to the particle diameter of 2,935.9 nm) and the other of intensity of 3 corresponding to particles of the high diameter of 6,974.4 nm. The effective particle diameter increased to 125.3 nm.

In the size distribution curve (Fig.4) after modification of titanium white using U-15D aminosilane formed two intense bands in the range of 6.0 to 38.0 nm (intensity of 100 corresponded to the particle diameter of 29.9 nm). The effective particle diameter was as low as 15.7 nm.

Aggregates		Agglomerates	
Diameter d (nm)	Intensity G(d)	Diameter d (nm)	Intensity G(d)
1.0	3	20.8	8
1.1	6	23.4	58
1.3	5	26.5	91
1.4	3	29.9	100
6.2	8	33.7	55
7.0	27	38.1	21
7.9	63		
8.9	76		
10.0	62		
11.3	20		
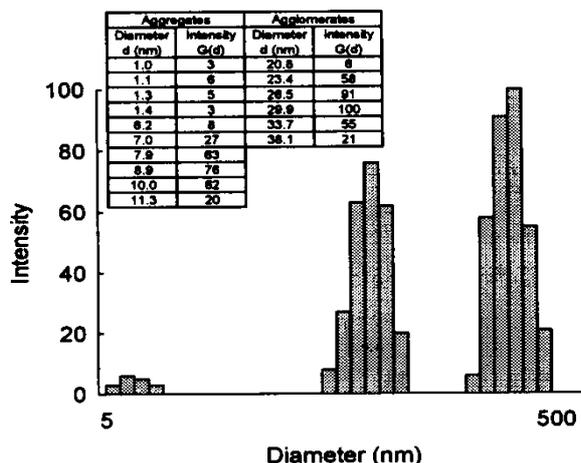
Fig. 4. Particle size distribution of TiO$_2$ modified with U-15D silane

Results of studies on application of the unmodified titanium white, R-211, and the respective modified titanium white in acrylic paints: ACRYL LAKMA facade paint and AKRYBET paint for exterior use are presented in Table 4 and Table 5.

As evident from the Tables data, densities of the facade paints fitted the required density range of 1.43 to 1.55 g/cm^3. Similarly the densities of the paints for exterior use were consistent with the required range of 1.35 to 1.50 g/cm^3. Moreover, also the other parameters, like viscosity, drying time, and resistance to scrubbing corresponded to those of the best standard types of paints based on titanium white. A test was also made of grinding the paints in a grindometer. The paints which contained aminosilane modified titanium white yielded results inconsistent with the requirements (particles of around 100 μm in size). In the remaining cases grinding yielded a very good result (particles of around 50 μm in size).

Table 4. Parameters of AKRYL LAKMA acrylic dispersion white, water soluble paint for facade use

Parameter	Norm requirements [PN-91/B-10102]	AKRYL LAKMA	AKRYL LAKMA containing			
			R-211	R-211+A-174	R-211+U-611	R-211+U-15D
Density, [g/cm^3]	1.45-1.55 [≤ 1.6]	1.48	1.46	1.47	1.43	1.46
Viscosity, KW10 estimated by time of dripping, [s]	Drips after 17-24″	Drips after 17″	Drips immediately	Drips immediately	Drips immediately	Drips immediately
Drying time, (20°C, 58% air humidity) 1° [min.] 5° [min.]	- [≤ 3h]	13′ 20′	17' 23'	18' 29'	16' 22'	17' 23'
Resistance to wet scrubbing	[≥ 1500 advances]	No base exposure after 10,000 advances	No base exposure after 10,000 advances	No base exposure after 10,000 advances	No base exposure after 10,000 advances	No base exposure after 10,000 advances
Quality coating of white paint	≤ III	III	II	II	II	II

Table 5. Parameters of AKRYBET acrylic white, organic solvent soluble paint for exterior use

Parameter	Norm requirements [PN-91/B-10102]	AKRYBET	AKRYBET containing			
			R-211	R-211+A-174	R-211+U-611	R-211+U-15D
Density, [g/cm³]	1.35-1.50 [≤ 1.6]	1.39	1.38	1.36	1.37	1.38
Viscosity, KW4 estimated by time of dripping, [s]	Drips after 50 to 150″	Drips after 136"	Drips after 111"	Drips after 124"	Drips after 99"	Drips after 107"
Drying time, (20°C, 58% air humidity) 1° [min.] 5° [min.]	- [≤ 3h]	30' 35'	32' 43'	24' 42'	57' 73'	37' 57'
Resistance to wet scrubbing	[≥ 1500 advances]	No base exposure after 10,000 advances	No base exposure after 10,000 advances	No base exposure after 10,000 advances	No base exposure after 10,000 advances	No base exposure after 10,000 advances
Quality coating of white paint	≤ III	III	III	III	III	III

CONCLUSIONS

♦ Following modification of titanium white with TiO_2 methacryloxysilane, a deteriorated homogeneity of was observed. This proved a homogeneity of TiO_2 linked to strong adhesive interactions of methacryloxy groups, which induced formation of larger particle clumps.

♦ Modified titanium whites used in paints for exterior use and facade paints augment quality of the paints and, in particular, their resistance and utility parameters.

REFERENCES

BROWN R.F.G., CARR C. and TAYLOR M.E., 1997, *Effect of pigment volume concentration and latex particle size on pigment distribution,* Progress in Organic Coatings, 30, 185.

ESUMI K., HAYASHI H., KOIDE Y., SUHARA T. and FUKUI H., 1998, *Adsorption of metal ion and aromatic compounds by anionic surfactants-coated particles of titanium dioxide*, Colloids Surf. A., 144, 201.

ESUMI K., SAKAI K., TORIGOE K., SUHARA T. and FUKUI H., 1999, *Simultaneous adsorption of sodium dodecyl sulphate and poly(vinyl pyrrolidone) on titanium dioxide with quaternary ammonium* groups, Colloids Surf. A., 155, 413.

INNOCEZI P., BRUSATIN G., GUGLIELMI M., SOGNORINI R., BOZIO R. and MOGGINI M., 2000, *3-(Glycidoxypropyl)-trimethoxysilane-TiO₂ organic-inorganic materials for optical limiting,* J. Non-Crystalline Solids, 265, 68.

KOBAYASHI T., 1997, *Pigment dispersion in water-reducible* paints, Progress in Organic Coatings, 28, 79.

POWNCEBY M.I. and FISHER-WHITE M.J., 1999, *Phase equilibria in the system Fe_2O_3-MgO-TiO₂ between 1173 and 1473 K, and Fe^{2+}-Mg mixing properties of ilmenite, ferrous-pseudobrookite and ulvöspinel solid solutions*, Contrib. Mineral Petrol., 135, 198.

SALES M., VILA J. and ALARCON J., 1998, *Effect of NiO and/or TiO_2 mullite formation and microstructure from gels*, J. Mater Sci., 33, 4435.

SHIRAI Y., KAWATSURA K. and TSUBOKAWA N., 1999, *Graft polymerization of vinyl monomers from initiating groups introduced onto polymethylsiloxane-coated titanium dioxide modified with alcoholic hydroxyl groups*, Progres in Organic Coatings, 36, 217.

SPYCHAJ S., SPYCHAJ T. and Osinska A, 1993, *Powierzchniowa modyfikacja chemiczna proszkowych napełniaczy mineralnych, Część III. Dwutlenek tytanu,* Chemik, 46, 120.

WYPYCH G., 1999, "Handbook of fillers", ChemTec Publishing, Toronto, pp.154-163.

Jesionowski T., Krysztafkiewicz A., Dec A., Modyfikowane biele tytanowe charakterystyka i zastosowanie, Fizykochemiczne Problemy Mineralurgii, 35, 195-205 (w jęz. ang.)

W badaniach wykorzystano biel tytanową marki R-211 produkowaną przez Zakłady Chemiczne Police S.A.. Modyfikację powierzchni bieli tytanowej prowadzono w celu zmiany jej charakteru fizykochemicznego. W tym celu do modyfikacji zastosowano silanowe związki wiążące z następującymi grupami funkcyjnymi: metakryloksy, winylową oraz aminową.

W celu otrzymania podstawowej charakterystyki bieli tytanowej oznaczano jej: gęstość nasypową, chłonności – wody, ftalanu dibutylu oraz oleju parafinowego. Ponadto przeprowadzono badania mające na celu określenie morfologii, budowy powierzchni i dyspersji cząstek ditlenku tytanu w zależności od rodzaju modyfikatora. Oceny dokonano przy zastosowaniu skaningowej mikroskopii elektronowej (SEM). Techniką dynamicznego rozpraszania światła (DLS) badano wpływ użytych modyfikatorów na tendencję do tworzenia aglomeratów cząstek.

Modyfikowane i niemodyfikowane biele tytanowe zastosowano jako pigmenty w farbach akrylowych.

Stwierdzono, że winylosilan w największym stopniu hydrofobizuje powierzchnię bieli tytanowej, natomiast aminosilan podwyższa hydrofilowość tej powierzchni. Modyfikowane biele tytanowe przyczyniają się ponadto do poprawy parametrów fizykochemicznych i użytkowych fasadowych farb akrylowych.